How adaptive strategies of cooperation and cheating define the population dynamics of mitochondrial mutations

By

Bryan L. Gitschlag

Dissertation

Submitted to the Faculty of the

Graduate School of Vanderbilt University

in partial fulfillment of the requirements

for the degree of

DOCTOR OF PHILOSOPHY

in

Biological Sciences

September 30, 2021
Nashville, Tennessee

Approved:

Maulik R. Patel, Ph.D.

Seth R. Bordenstein, Ph.D.

Lauren Parker Jackson, Ph.D.

Jared T. Nordman, Ph.D.

David C. Samuels, Ph.D.

This work is dedicated to future generations of curious minds and to the giants of science on whose shoulders this work is honored to stand

Acknowledgments

This work would not have been possible without the love, support, and encouragement from numerous people. I owe a debt of gratitude to Abu Sayeed, Jonathan Evans, and Travis Kallman. While serving with them in the military, they challenged me to think deeply on matters of philosophy, religion, science, and our place in the cosmos, which played an instrumental role in my progress toward studying evolutionary biology. I likewise wish to acknowledge the prominent skeptic and stage magician Matt Dillahunty for similar reasons. I owe another debt of gratitude to my academic advisor, Dr. Maulik R. Patel, who accomplished an inspiring balance between pushing me to meet high expectations, showing patience and compassion, being available at times that I had questions or needed advice, and being an all-around good friend in addition to a stellar colleague and role model. I would like to thank the other members of the Patel Laboratory, past and present, for the many opportunities to be challenged and to break bread. I thank my family for their love, encouragement and support as well. I would not have made it this far without them, in more ways than one. Last but most certainly not least, I would especially like to thank my partner, the love of my life, Parker, with whom it seems as though I have experienced enough adventures for a dozen lifetimes. His compassion, empathy, and ability to challenge me and introduce me to new experiences are truly without limit and have greatly contributed to the completion of this document. Thank you all.

This work was generously supported primarily through an NIH research project grant (R01 GM123260), the Ruth L. Kirschstein National Research Service Award Individual Predoctoral Fellowship grant (1F31GM125344), a Vanderbilt University Medical Center Diabetes Research and Training Center Pilot and Feasibility Grant, Vanderbilt University startup funds for the Patel Laboratory, and the NIH-sponsored Cellular, Biochemical and Molecular Sciences Training Program grant (5T32GM008554-18).

Table of contents

List of Figures

Appendices

List of Tables

Chapter 1

Introduction: the evolutionary adaptive strategies of cooperation and cheating define the population dynamics of mitochondrial mutations, but how?

"Seen in the light of evolution, biology is, perhaps, intellectually the most satisfying and inspiring science. Without that light it becomes a pile of sundry facts—some of them interesting or curious but making no meaningful picture as a whole."

–Theodosius Dobzhansky, *Nothing in Biology Makes Sense Except in the Light of Evolution* (1973)

Understanding biological systems through an evolutionary framework

Evolution is the story of how life came to be what it is today. Living things owe their diversity and complexity, as well as their heritable structural and functional characteristics, to a long history of descent with modification. Accordingly, fundamental insights into the structure and behavior of biological systems ought to be accessible through a better understanding of the evolutionary processes shaping them. In recent years, research findings across numerous areas of molecular and cell biology have greatly underscored this idea that understanding the evolution of a system provides valuable insight into its organization and behavior. In particular, eukaryotic organisms exhibit a number of vital functions that are taxonomically widely conserved despite the fact that they involve rapidly-evolving genes. Examples include genes involved in meiosis (Anderson et al., 2009), the maintenance of centromeric chromatin (Henikoff et al., 2001), and the maintenance of telomeric integrity (Lee et al., 2017). The seemingly paradoxical high rate of evolution among genes involved in widely-conserved biological processes has led scientists to infer that the

maintenance of these functions requires recurrent adaptive innovation (Lee et al., 2017, McLaughlin and Malik, 2017).

Why might adaptive innovations be continually necessary to maintain a widely-conserved biological function? One proposed explanation for this apparent paradox involves the co-evolution between entities with opposing adaptive interests. Some stretches of hereditary information propagate at the expense of others, without benefiting—and sometimes even while harming—the fitness of their host genomes, hence the term "selfish genetic elements" (Agren and Clark, 2018, Werren et al., 1988). By negatively impacting their hosts, selfish genetic elements can introduce an additional layer of selective pressure, whereby selection for host fitness is expected to result in the evolution of mechanisms that suppress the propagation of selfish genetic elements. This recurrence of adaptation and counter-adaptation can give rise to an evolutionary arms race consisting of a quasi-steady-state of reciprocally antagonistic co-evolution, formalized as the "Red Queen" hypothesis (McLaughlin and Malik, 2017, Van Valen, 1973), named in honor of Lewis Carroll's *Through the Looking Glass*, wherein the Red Queen famously says, "it takes all the running you can do, to keep in the same place." Red Queen interactions are especially well-known in the context of the co-evolution between pathogens and host immunity, although they also characterize the co-evolution between endogenous selfish genetic elements and their host genomes (McLaughlin and Malik, 2017). One category of selfish genetic elements, meiotic drive genes, facilitate their own transmission by undermining the fitness of gametes lacking them (Bravo Nunez et al., 2018, Hammond et al., 2012, Hu et al., 2017, Larracuente and Presgraves, 2012, Schimenti, 2000). Accumulating evidence in recent years has implicated meiotic drive genes in infertility (Zanders and Unckless, 2019), suggesting that understanding the causes of infertility may require a greater understanding of not only beneficial genes but also selfish genetic elements, as well as the co-evolution between beneficial and selfish genetic elements.

In addition to individual genes, a number of microbial symbionts can likewise facilitate their own transmission across generations at the expense of the fitness of hosts, constituting another widely-studied category of selfish entities. The bacterial genus *Wolbachia* includes some especially widespread examples, having been estimated to inhabit close to two thirds of all insect species (Hilgenboecker et al., 2008). As intracellular bacterial symbionts, *Wolbachia* are typically inherited maternally, entering the next generation through host eggs (Werren et al., 2008), while males can be understood as evolutionary "dead ends." Accordingly, *Wolbachia* have evolved ways to propagate by boosting the production of female hosts, which come at the expense of male fitness, hence their categorization as reproductive parasites. Methods of reproductive parasitism include the killing or feminization of male progeny, the production of female progeny from unfertilized eggs, and incompatibility between sperm and eggs when they come from hosts that are not infected by the same type of *Wolbachia*, a phenomenon known as cytoplasmic incompatibility (Werren et al., 2008). However, by impacting host fitness, reproductive parasites introduce pressures that can select for the evolution of host resistance, potentially giving rise to "Red Queen" dynamics as in the case of genetic conflicts within a genome or the co-evolution of pathogens and host immunity. Interestingly, host suppression of the male-killing phenotype has been reported to coincide with an alternate form of reproductive parasitism, namely cytoplasmic incompatibility (Hornett et al., 2008, Jaenike, 2007), which raises the possibility that different forms of reproductive parasitism may share a similar molecular basis. More recent work using flies has zeroed in on a small number of genes thought to underlie the male-killing and cytoplasmic incompatibility phenotypes (LePage et al., 2017, Perlmutter et al., 2019, Perlmutter et al., 2020), providing promising candidates for insights into the molecular details of these forms of parasitism. Moreover, given their stable presence in mosquitos and their ability to interfere with transmission of mosquito-borne pathogens (Dutra et al., 2016, Walker et al., 2011, Walker et al., 2021), *Wolbachia* infection has shown potential as a means to curb the spread of mosquito-borne infections, which claim more than a million human lives per year (Caraballo and King, 2014).

Understanding the interactions between selfish symbionts and their hosts, and the evolutionary processes shaping these interactions, are therefore highly consequential, for example by leading to potential life-saving applications in the fight against infectious disease.

In this work, I focus on how the biology of the mitochondrial genome is likewise informed by evolutionary principles. In particular, in this chapter I discuss evidence that the population dynamics of mitochondrial mutations are characterized by two opposing evolutionary adaptive strategies, namely cooperation and cheating. In the chapters that follow, I identify an ideal model system for studying the dynamics of cheating among mitochondrial genomes, by showing that a mutant mitochondrial genome variant in an experimentally tractable animal species—the genome variant *uaDf5* in the roundworm *Caenorhabditis elegans*—behaves as a selfish mitochondrial genome, propagating within hosts and across generations at the expense of host fitness. I then cover experimental work to investigate the mechanistic basis for the cheating behavior of this mutant genome. Next, I describe experiments that I designed to quantitatively measure the different levels of natural selection acting on this genome, including the positive ("selfish") selection favoring the proliferation of the mutant genome within individual hosts, as well as the negative selection that occurs due to the impact of this genome on host fitness. By applying these experiments to different conditions and host genotypes, I proceed to characterize how the host organism interfaces with its environment to shape the population dynamics of the selfish mitochondrial genome, with a particular focus on the important environmental variable of dietary nutrient supply. Finally, I address the general applicability of my findings by expanding the scope of these experiments to include other mutant mitochondrial genome variants. By elucidating mechanisms and conditions underlying the cheating behavior of a selfish mitochondrial genome, this work advances our understanding of interactions at the foundation of the eukaryotic cell in light of how these interactions are shaped by evolutionary processes.

Transitions in individuality: cooperation and cheating in the evolution of complexity

Life is generally organized into a hierarchy of cooperative collectives: multiple genes make up a genome; different genomes collectively form the eukaryotic cell; individual cells give rise to colonies of cells, multicellular organisms, and symbiosis between multicellular organisms and their resident microbial communities; likewise, multicellular organisms are often organized into larger, more complex groups, such as societies. New levels of organization emerge when natural selection favors cooperation and minimization of conflict between previously-autonomous replicating entities, giving rise to a unified collective that replicates and undergoes selection as a higher-level "individual," a process known as an evolutionary transition in individuality (Hammerschmidt et al., 2021, Michod, 2006, Michod and Roze, 1997, Szathmary, 2015, West et al., 2015). Cooperation is thus an adaptive strategy—a behavior that affects fitness due to the interactions between entities—that plays a central role in the evolution of larger, more complex life forms (Fisher and Regenberg, 2019, Gulli et al., 2019, Michod et al., 2006, West et al., 2015, Hammerschmidt et al., 2014). However, because cooperators incur the near-term cost of contributing to the fitness of partners, albeit for long-term collective benefit, cooperation creates conditions that can select for the emergence of selfish, "cheater" entities, which show up at multiple levels in the hierarchy of biological organization.

What defines "cheating" in the context of evolutionary theory? Like cooperation, cheating can be thought of as an adaptive strategy, in that it represents a category of interactions that affect the fitness of the interactors. However, cheating can be defined in direct contrast to cooperation, since it involves taking advantage of a cooperative relationship. Formally, cheating can be defined as occurring when a cooperative partner benefits the fitness of another entity (the "cheater"), at the expense of its own fitness, particularly when these effects arise from a cooperative behavior being directed toward some entity other than the "intended" recipient (Ghoul et al., 2014). In this context,

the “intended” recipient of a costly cooperative act is the recipient needed to facilitate the payoff that ensures the evolutionary success of the cooperative behavior. In other words, cheaters reap the benefit of belonging to a cooperative relationship without incurring the cost of reciprocating. Cheaters can thus be viewed as a form of parasite, at least in cases where parasitism involves betraying an otherwise-cooperative relationship. As mentioned in the previous section, meiotic drive genes represent a type of cheater at the molecular scale, facilitating their own transmission at the expense of other genes by compromising the fitness of gametes within the organism that lack the meiotic drive genes, examples of which have been identified across diverse taxa including plants, fungi, and animals (Bravo Nunez et al., 2018, Hammond et al., 2012, Hu et al., 2017, Larracuente and Presgraves, 2012, Schimenti, 2000). Cancer is characterized by unchecked cell proliferation and the monopolization of resources at the expense of other cells within the body, constituting a form of cheating at the cellular level (Aktipis et al., 2015). Cheating behaviors likewise occur in many species of social animals (Riehl and Frederickson, 2016).

By benefiting from the contributions of cooperators without reciprocating, cheaters gain a fitness advantage (Aktipis et al., 2015, Dobata et al., 2009, Ghoul et al., 2014, Strassmann et al., 2000). This advantage can break down at higher levels of biological organization, though, which rely on cooperation at lower levels (Aktipis et al., 2015, de Vargas Roditi et al., 2013, Fiegna and Velicer, 2003, Moreno-Fenoll et al., 2017, Rainey and Rainey, 2003, Wenseleers and Ratnieks, 2004). Hence, natural selection can simultaneously favor different traits across the levels of the biological hierarchy, a phenomenon known as multilevel selection (de Vargas Roditi et al., 2013, Hammerschmidt et al., 2014, Shaffer et al., 2016, Takeuchi and Kaneko, 2019, Wilson and Wilson, 2007). Multilevel selection thus provides an explanation for the paradoxical coexistence between selfish and cooperative entities within hierarchically structured populations—that is, populations structured in a manner such that replication and natural selection occur at different levels, simultaneously favoring cheating at one level but cooperation at another.

Mitochondria: symbionts at the root of eukaryotic evolution

The eukaryotic cell, which comprises protozoans, plants, fungi, and animals, is itself the product of one of the major cooperative transitions described in the previous section. Approximately two billion years ago, a symbiotic relationship began when a bacterial cell was engulfed by a larger Archaeal cell (Lang et al., 1999, Sagan, 1967, Wang and Wu, 2015). Rather than being digested, the occupant became a metabolic asset, enabling the host cell to relocate the electrochemical gradient for energy production from its cell membrane down to a sub-cellular compartment. This internalization of the bioenergetic membrane is hypothesized to overcome the surface-area-to-volume constraint that energy production imposes on cell size, purportedly enabling these organisms to evolve larger, more complex cells (Lane, 2014).

In addition to cell size, mitochondria and their symbiotic interactions with the host have evidently shaped the evolution of biological complexity in other ways. These effects stem from the fact that mitochondria retain their own genomes, owing to their heritage as once free-living bacteria. Over the course of evolutionary history, mitochondrial DNA (mtDNA) has become greatly pared down in size, albeit to varying degrees across taxa, with many genes having been translocated to the nucleus (Adams and Palmer, 2003). Several hypotheses have been proposed to explain the migration of genes from the mitochondrial to the host genome, most of which invoke adaptive benefits associated with being encoded in the nucleus. One such hypothesis proposes that moving genes to the nucleus helps prevent the irreversible accumulation of deleterious mutations, a phenomenon typical of asexual genomes (Muller's Ratchet), or otherwise facilitates the spread of beneficial mutations, due to the ability of nuclear genes to more readily segregate and recombine during meiosis (Blanchard and Lynch, 2000). Another hypothesis suggests that the transfer of genes to the nucleus could be adaptive by exposing the genes to a lower relative mutation rate (Berg and Kurland, 2000, Brandvain and Wade, 2009). Another interesting

possibility invokes the proliferation of mutant mtDNA variants. In particular, if a mitochondrial gene becomes inserted into the nuclear DNA, then a mutant mtDNA variant with a deletion of the same gene can presumably proliferate to fixation (100 percent frequency), due to a replication advantage associated with the loss of the gene, for example, with the host remaining viable as long as the nuclear copy of the gene remains functional (Berg and Kurland, 2000). Incidentally, reasons for the selfish proliferation of deleteriously mutated mtDNA represent the primary focus of my work, described in the following chapters. Despite having lost many genes to the nucleus, however, mitochondria continue to retain their own genomes, for which numerous explanatory hypotheses have also been put forth. For example, the hydrophobicity of mtDNA-encoded proteins, which function as subunits in the membrane-bound enzyme complexes of the electron transport chain (ETC), may interfere with the ability to send these proteins to the mitochondria if synthesized elsewhere. In support of this idea, mtDNA-encoded proteins in cultured cells were observed to be mistargeted to the endoplasmic reticulum if synthesized in the cytoplasm (Bjorkholm et al., 2015). Another hypothesis suggests that encoding and expressing some of the core ETC components in close proximity to the ETC, rather than in the nucleus, allows for more finely-tuned regulation of gene expression in response to local cues, such as the redox status of the gene products (Allen, 1993, Allen, 2015). In any case, the fact that many mitochondrial proteins have become encoded in the nucleus, while others are still mtDNA-encoded, means that energy production via the ETC requires numerous cooperative interactions between the mitochondrial and host genomes.

Due to some key differences between the mitochondrial and nuclear genomes, their interactions and co-evolution are thought to largely underlie the complexity of eukaryotic organisms. In contrast to the nuclear genome, for example, mtDNA is present at high copy number, with a single animal cell containing hundreds to thousands of individual mtDNA molecules (O'Hara et al., 2019, Robin and Wong, 1988, Shay et al., 1990). Cells therefore frequently contain a mixed population

(heteroplasmy) of mtDNA sequence variants due to the occasional mutations. Moreover, whereas the nuclear genome undergoes one round of replication per cell-division cycle to ensure that the daughter cells each receive one copy, mtDNA replicates throughout the cell cycle (Bogenhagen and Clayton, 1977, Chatre and Ricchetti, 2013, Newlon and Fangman, 1975, Sasaki et al., 2017, Sena et al., 1975). This relaxed replication enables the relative prevalence of heteroplasmic mutant mtDNA to vary between hosts, as well as over time within a host. When present at low levels, even a mutation that severely disrupts the function of mtDNA-encoded genes has negligible effects due to the substantially larger population of metabolically competent ("wildtype") mtDNA copies. However, if the mutant genomes rise to sufficiently high allele frequency within their host, they can pass a critical frequency threshold whereupon they overwhelm the ability of the cell to maintain metabolic integrity, at which point the previously negligible mutation becomes pathogenic (Stewart and Chinnery, 2015, Wallace and Chalkia, 2013). Remarkably, even otherwise neutral mtDNA variants can have harmful effects when coexisting in a heteroplasmic state (Sharpley et al., 2012), suggesting that heteroplasmy can be inherently deleterious. Although the basis for this is not known, the dependence of ETC function on mito-nuclear interactions has been suggested to make it highly sensitive to variation in mtDNA sequence (Sharpley et al., 2012). Consistent with a deleterious effect of heteroplasmy, theoretical modeling studies have shown that a widespread feature of sexual reproduction, namely gametic asymmetry accompanied by uniparental inheritance of mitochondria, can evolve in response to the selection pressure to minimize the heteroplasmic mixing of mtDNA or otherwise facilitate co-adaptation with the host genome (Christie et al., 2015, Hadjivasiliou et al., 2012, Radzvilavicius, 2021). Theoretical modeling also implicates mtDNA mutations in the evolution of animal reproductive development, since setting aside a dedicated germline during early development—as opposed to producing gametes via the later differentiation of somatic tissue—reduces the requirement for ongoing mtDNA replication, thereby limiting the accumulation of mtDNA mutations and preserving metabolic integrity (Radzvilavicius et al., 2016). The mitochondrial genome has even been

implicated in the evolution of new species, since mito-nuclear incompatibility has been identified as a causal factor in reproductive isolation between geographically separated animal populations (Lamelza and Ailion, 2017). Given these considerations, the mitochondrial genome and its relationship with its host is thus understood to be at the root of many aspects of evolution in eukaryotic organisms.

Cooperation and cheating among mitochondria

Mitochondria cooperate with each other and with their host by supplying important genes for energy production. In return, the nuclear genome supplies the proteins and building blocks needed to replicate mtDNA. If a mutation disrupts the normal contribution that mtDNA makes toward energy production, then the mutant mtDNA could be described as a selfish genetic element, as long as it continues to replicate. Like other examples of biological cheaters described previously, selfish mitochondrial genomes benefit at the expense of a cooperative partner. Since these costs and benefits can be defined in terms of fitness effects, selfish mitochondrial genomes can be thought of as those that undergo positive selection within their hosts—or otherwise persist, evading extinction from the population—while simultaneously undergoing negative selection due to imposing a fitness cost on their hosts. Mutant mitochondrial genomes matching this description are taxonomically widespread, having been identified across various species of plants, fungi, and animals (Havird et al., 2019, Klucnika and Ma, 2019). In yeast, for example, the selfish proliferation of mutant mtDNA results in a commonly observed colony-growth defect, earning such colonies the term “petite” mutants (MacAlpine et al., 2001, Jasmin and Zeyl, 2014, Harrison et al., 2014). Interestingly, the study of petite colonies in yeast is what led to the realization in the early 1950s that the cytoplasm contains its own genetic material (Chen and Clark-Walker, 2000). In animals, selfish mitochondrial genomes have been identified both in the laboratory and in wild

populations. One well-known selfish mtDNA variant, termed *nad5*Δ due to a deletion in the coding region of the ETC gene *ND5*, was found in wild populations of *Caenorhabditis briggsae* (Clark et al., 2012, Phillips et al., 2015). The *nad5*Δ mtDNA has a transmission advantage over wildtype mtDNA, despite being associated with deleterious fitness consequences (Estes et al., 2011). Interestingly, this mutation has been found in geographically diverse populations of *C. briggsae* (Clark et al., 2012, Howe and Denver, 2008), suggesting that selfish mtDNA may be able to persist across evolutionary time-scales. Mutations that confer a selfish transmission advantage at the expense of host fitness have also been observed to occur spontaneously in laboratory populations of *C. elegans* (Dubie et al., 2020, Konrad et al., 2017). Importantly, the vast majority of the mtDNA content within an adult hermaphroditic member of *C. elegans* is confined to the maternal germline (Bratic et al., 2009, Tsang and Lemire, 2002a), which is precisely where mtDNA molecules are poised to compete for transmission to the next generation, due to maternal inheritance. Taken together, these findings provide evidence that cheating may represent a common evolutionary strategy among mitochondrial genomes.

If mutant mtDNA levels can vary over time within and between hosts due to relaxed replication—that is, since mtDNA replication is not tightly coupled to the cell cycle—why would a combination of random genetic drift and selection for host fitness fail to eliminate the mtDNA mutation? The simple explanation is that the levels of mutant mtDNA do not merely fluctuate within their hosts stochastically through genetic drift, but rather that mutant mtDNA can preferentially proliferate within hosts. The combination of high intracellular mtDNA copy number and relaxed replication can evidently give rise to mtDNA variants whose effects result in increasingly greater numbers of the mutant mtDNA copies. But how does this occur? Multiple studies have focused on the proliferation of deleterious mtDNA mutations, especially in the context of human disease (Diaz et al., 2002, Dunbar et al., 1995, Durham et al., 2007, Grandhi et al., 2017, Herbst et al., 2013, Holt et al., 1997, Larsson et al., 1990, Moraes et al., 1999, Moraes et al., 1995, Picard et al., 2014,

Samuels et al., 2013, Santra et al., 2004, Trifunov et al., 2018, Yoneda et al., 1992). Apart from documenting the phenomenon of mutant mtDNA proliferation, these studies tend to focus on two notable explanatory themes. One such theme invokes a replication advantage that is intrinsic to the mutant genome, such as the shorter replication time of a smaller molecule due to a deletion of a part of the genome (Diaz et al., 2002, Moraes et al., 1999). Another intrinsic replication advantage may occur when a mutation introduces additional origin-of-replication sites (Holt et al., 1997), potentially resulting in a higher rate of replication events.

Although mutant mtDNA variants with an intrinsic replication advantage could be viewed as selfish genetic elements in the sense that they outcompete wildtype mtDNA, they represent only a subset of selfish mitochondrial genomes. This is because any effect on their host would merely result from—rather than being coupled to—their proliferation. In other words, since the benefit of cheating arises from the costly contributions of a cooperative partner (Ghoul et al., 2014), mutants whose proliferative advantage depends on the behavior of the host genome could be expected to represent another general category of mitochondrial cheaters. Consequently, mitochondrial genomes might cheat even if they carry no intrinsically advantageous mutations, as long as they affect mitochondrial function in a manner that preferentially leads to their own replication. Incidentally, mutant mitochondrial genomes whose proliferation is linked to their impact on mitochondrial function and mito-nuclear interactions represents a second explanatory theme appearing in these studies. Indeed, early research on mtDNA heteroplasmy dynamics revealed that the proliferative advantage of a mutant genome can depend on host genotype (Dunbar et al., 1995). More recent research has revealed that rising levels of mutant mtDNA can cause abrupt, large-scale changes in host gene expression (Picard et al., 2014). Taken together, these findings suggest that the host genome may be able to respond to the presence of mutant mtDNA in a manner that influences the proliferation of the mutant genome. Consistent with this idea, numerous studies have identified compensatory replication, whereby the cell synthesizes more

mtDNA in an attempt to rescue mitochondrial function, as a likely albeit inadvertent driver of a vicious cycle of mutant genome proliferation, at least in somatic tissue (Capps et al., 2003, Durham et al., 2007, Herbst et al., 2013, Trifunov et al., 2018).

Despite these advances, research on the topic has yielded little in the way of mechanistic detail, at least with respect to the proliferation of selfish mtDNA in the maternal germline and across generations. Two recent studies in fruit flies have shed some important light on this issue, however, one focusing on selective mtDNA replication and the other on selective elimination. In particular, one study found that the abundance of the enzyme responsible for catalyzing mtDNA synthesis, POLG, determines not only the total mtDNA copy number, but also the frequency of a deleterious mutant genome across successive generations (Chiang et al., 2019). Why might one genome variant preferentially benefit depending on the levels of an enzyme that replicates both the mutant and wildtype genomes? One possibility involves selective protein synthesis on the outer mitochondrial membrane. The protein PINK1 accumulates on the outer membrane of dysfunctional mitochondria, inhibiting protein synthesis locally and selectively, preventing the proliferation of a deleterious mutant mtDNA (Zhang et al., 2019). Since the enzyme POLG is encoded in the nucleus and imported into the mitochondria, one attractive explanation for these findings is that when POLG is in short supply, mutant genomes preferentially suffer due to the reduced protein synthesis, and hence a scarcity of replication machinery, at the site of mitochondria containing the mutant genome. Although this would explain why the mutant genome preferentially suffers from lower POLG levels, it remains unclear why the mutant genome actually manages to outcompete the wildtype genome when POLG levels are high (Chiang et al., 2019). A second study in flies focused on the selective elimination of mutant mtDNA. To preserve metabolic integrity, the cell is equipped with molecular machinery for isolating, and subsequently digesting, fragments of the mitochondrial network where mitochondrial function is severely compromised. In the maternal germline of heteroplasmic flies, where mutant mtDNA runs the risk

of infiltrating the next generation, fragmentation of the mitochondrial network was observed to aid in the selective elimination of the mutant genome (Lieber et al., 2019). According to these findings, mutant mitochondrial genomes may selfishly propagate across generations by perturbing mitochondrial function in a manner that triggers a positive feedback-loop of mtDNA replication, or in a manner that interferes with the host's ability to sequester and degrade dysfunctional mitochondria, or both.

Selfish mitochondrial genomes can outcompete cooperative genomes within hosts, while the cooperative genomes simultaneously retain an advantage at the level of selection for host fitness. By what mechanism(s) does a mitochondrial genome preferentially proliferate despite carrying a mutation that is costly to host fitness? Moreover, what conditions and mechanisms shape the outcome of competition between the cooperative and selfish mitochondrial genomes, particularly when both the within-host and between-host levels of selection are taken into consideration? I sought to address these questions using an experimentally tractable model of a selfish mitochondrial genome, described below and in the chapters that follow.

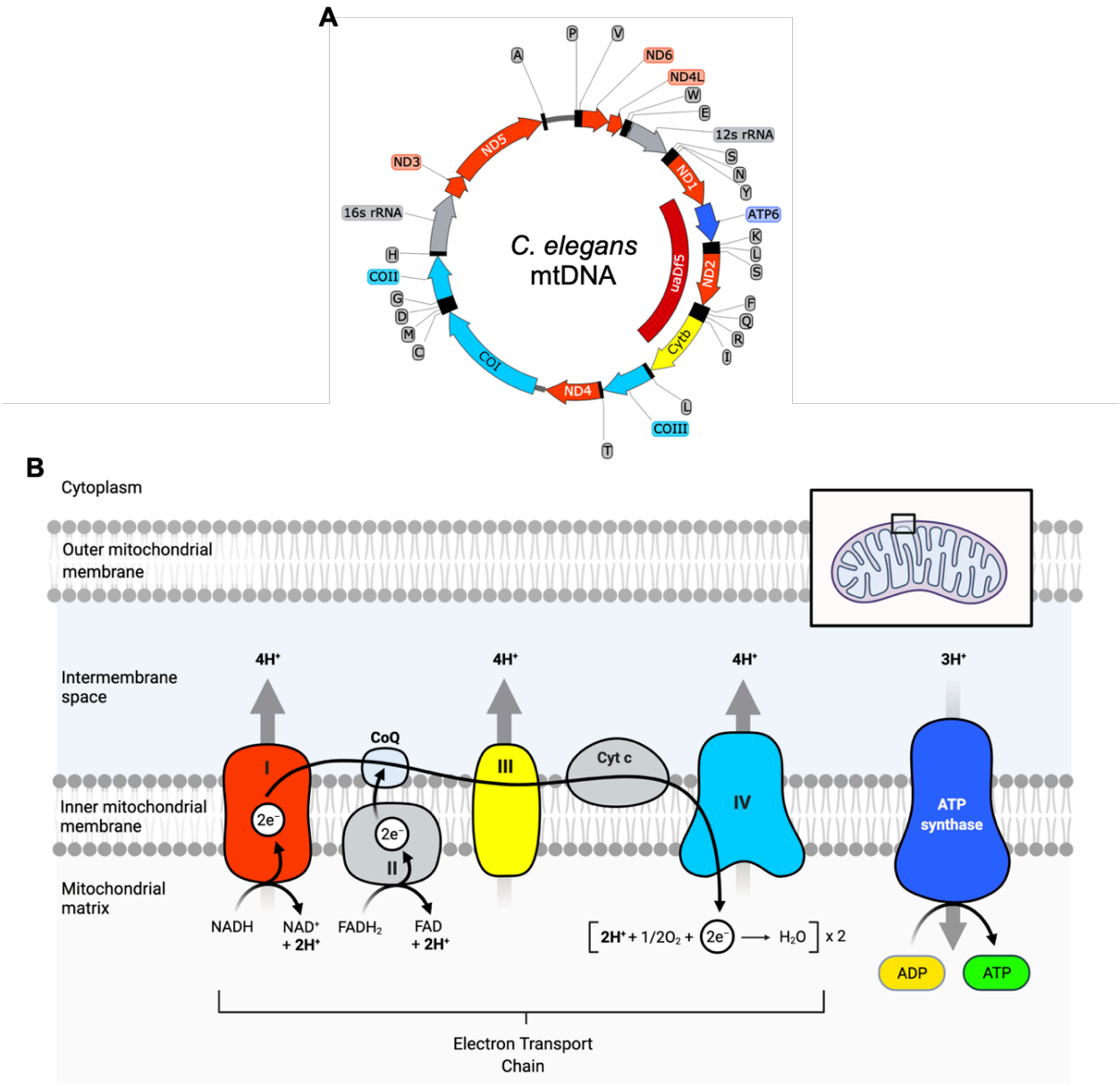

Figure 1-1. Map of *Caenorhabditis elegans* mitochondrial genome and diagram of its role in energy production

(A) Mitochondrial genome map in *C. elegans*. Genes are color-coded according to electron transport chain (ETC) complex: respiratory complex I (light red), complex III (yellow), complex IV (light blue), complex V (dark blue), ribosomal RNA (gray), tRNA (black), non-coding regions (thin line). The size and location of the *uaDf5* deletion is represented by the dark red bar. Image created using SnapGene® software (from Insightful Science; available at snapgene.com).
(B) Diagram illustrating the contribution of the mitochondrial genome toward energy production via the ETC. For reference, the ETC diagram shown here can be viewed as an enlargement of the small box on the mitochondrion illustrated in the inset (upper right corner). Complexes are color-coded according to the locations of proteins encoded by the similarly color-coded genes in panel (A). The proteins comprising complex II and Cytochrome C (Cyt c), shown in gray, are exclusively encoded in the nuclear genome. Complexes I, III, IV, and V are multi-protein complexes that each consist of protein subunits encoded by

both the mitochondrial and nuclear genomes (individual protein subunits of each complex are not shown). Complex I transfers two electrons from the oxidation of each molecule of NADH (a product of glucose and fatty acid breakdown and the Krebs Cycle) to a molecule of Coenzyme Q (CoQ) and utilizes energy from transferring the electrons to pump four protons to the intermembrane space. Complex II transfers two electrons from the oxidation of $FADH_2$ (a product of fatty acid breakdown and the Krebs Cycle) to CoQ. Complex III transfers one of the two electrons from the net oxidation of CoQ to each of two Cytochrome C molecules, using the energy from electron transfer to pump another four protons to the intermembrane space. Complex IV combines electrons from the oxidation of Cytochrome C and protons from the mitochondrial matrix with oxygen, creating water and pumping another four protons (per oxygen molecule consumed) to the intermembrane space. Complex V provides a path for the flow of protons down their concentration gradient, across the inner membrane and back into the mitochondrial matrix. The flow of protons fuels the production of energy in a form that the cell can use for vital functions such as DNA replication, RNA and protein synthesis, and other biochemical reactions requiring energy consumption. Specifically, for approximately every three protons that pass through complex V, one inorganic phosphate ion is combined with one molecule of adenosine diphosphate (ADP) to synthesize adenosine triphosphate (ATP). Image adapted from “Electron Transport Chain,” by BioRender.com (2021). Retrieved from https://app.biorender.com/biorender-templates

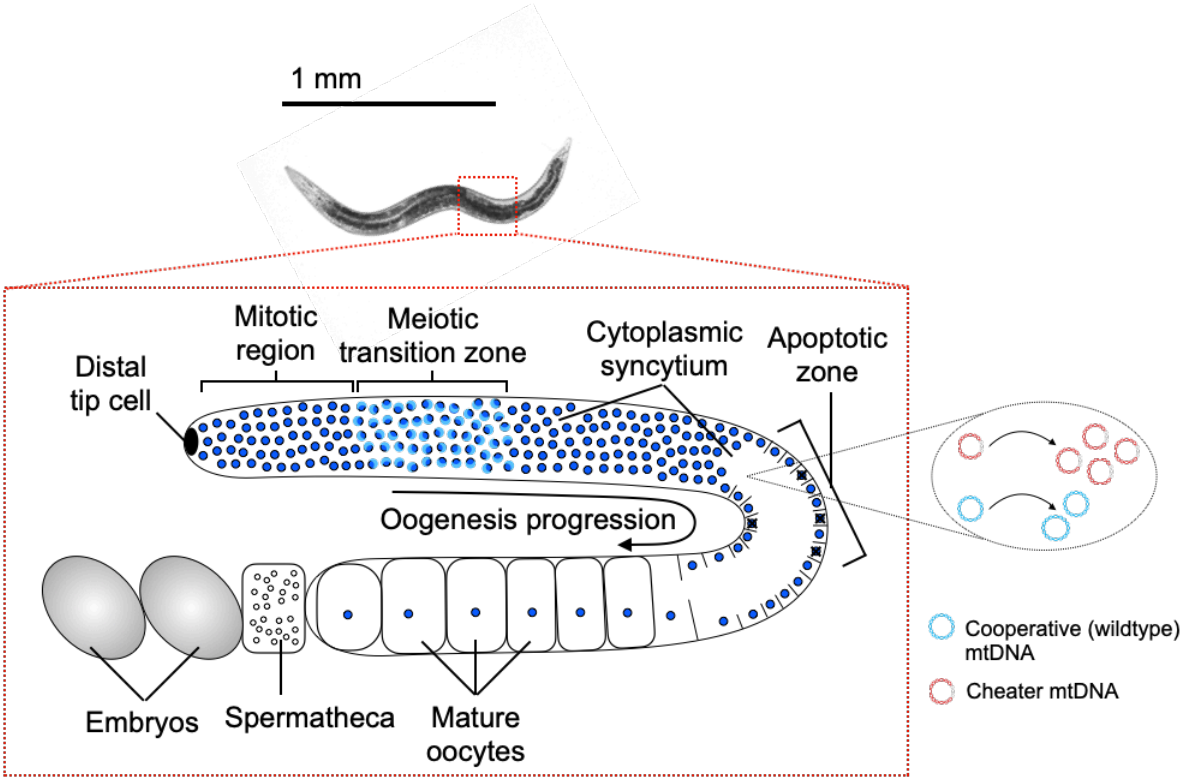

Figure 1-2. Microscope image and illustrated reproductive system of a heteroplasmic adult *Caenorhabditis elegans* hermaphrodite

The reproductive anatomy in adult *C. elegans* (box with red dotted outline) consists of a population of cell nuclei that exist within a contiguous syncytium of shared cytoplasm until late oocyte maturation (Waters and Reinke, 2011). Germline cells (dark blue circles) proliferate by mitosis and flow away from the distal tip cell (DTC, black oval). Mitotic proliferation is sustained via a chemical signal produced by the DTC and transmitted through the GLP-1/Notch receptor expressed by the germline cells. As distance from the DTC increases, the loss of signaling through the GLP-1/Notch receptor halts mitotic proliferation and induces the cells to center meiosis (dark blue circles with light blue crescents). Many germline cells undergo apoptosis (black x-marks) and export their organelles into the common cytoplasmic syncytium, possibly functioning as nurse cells for the remaining cells that are destined to become mature oocytes (Raiders et al., 2018). At the proximal end of the germline, oocytes are fertilized by sperm produced in the spermatheca and subsequently undergo embryonic development. The vast majority of mtDNA replication within the animal occurs in conjunction with germline development (see Chapter 6, Figure 6-6) (Bratic et al., 2009, Tsang and Lemire, 2002a). Moreover, due to maternal inheritance, the germline syncytium houses the population of mtDNA variants that compete for transmission to the next generation, providing a level of selection (within-host or sub-organismal selection) at which mtDNA mutants can “cheat” by outcompeting wildtype genomes (right side, dotted oval). This occurs at the expense of host fitness, resulting in another level of selection (organismal selection) at which wildtype mtDNA retains a fitness advantage over the cheater mtDNA. Germline illustration reproduced from Pereira et al., 2021.

Caenorhabditis elegans is an ideal model organism for studying the mechanisms and population dynamics of selfish mitochondrial genomes

To elucidate mechanisms and conditions that shape the evolutionary dynamics of cheater genomes, it is imperative to identify a system that is both experimentally tractable and that hosts such a genome. The roundworm species *C. elegans* ideally fits this description for a number of reasons. In addition to being the first multicellular organism to have its genome fully sequenced (Consortium, 1998), *C. elegans* was the first animal species in which double-stranded RNA was observed to robustly target gene expression (Fire et al., 1998). These considerations, together with a short generation time of around 3 days, make *C. elegans* highly amenable to genetic manipulations. Moreover, the mitochondrial genome and its role in energy metabolism in *C. elegans* (Figure 1-1) is remarkably similar across animal species. Of the 37 mtDNA-encoded genes in mammals, 36 are also encoded in *C. elegans* mtDNA, including 2 ribosomal RNA genes, 22 transfer RNA genes, and 12 of the 13 protein-coding genes found in mammalian mtDNA (Okimoto et al., 1992). Also like mammalian mtDNA, *C. elegans* mtDNA is uniparentally inherited, entering the embryo from the maternal germline (Al Rawi et al., 2011). However, unlike mammals and many other animal taxa, the vast majority—upwards of 90 percent—of the total mtDNA content within the adult hermaphroditic *C. elegans* is confined to the maternal germline (Bratic et al., 2009, Tsang and Lemire, 2002a), which exists as a contiguous syncytial cytoplasm shared by the germline stem-cell population (Figure 1-2 and reviewed by Waters and Reinke, 2011). The vast majority of overall population dynamics of mitochondrial mutations in *C. elegans* thus reflects two primary factors: selection for host fitness and the biology of the female germline, where mtDNA molecules compete for transmission to the next generation. Accordingly, *C. elegans* is especially ideal for efforts to characterize the conflicting multilevel selection dynamics between cheater proliferation and impact on host fitness. Finally, a deleterious but stably persisting mitochondrial genome, namely the mutant mtDNA variant *uaDf5* (Figure 1-1A, dark red bar), has

been identified in a laboratory strain of *C. elegans* (Tsang and Lemire, 2002b). This mutant genome rises in frequency, especially in animals that inherit the mutant genome at low initial frequency, and can persist across hundreds of generations without being eliminated by drift or negative selection (Tsang and Lemire, 2002b), despite being associated with a variety of deleterious fitness consequences (Liau et al., 2007). These findings suggest that the *uaDf5* variant may behave as a cheater, a hypothesis that I address in the following chapter. If *uaDf5* indeed behaves as a bona fide selfish mitochondrial genome, then its stable presence in a laboratory strain of *C. elegans*, combined with the versatile experimental toolkit available for doing genetics and cell biology with *C. elegans*, position this genome as an ideal model for investigating the mechanisms and conditions underlying the cheating behavior of a selfish mitochondrial genome.

The evolutionary adaptive strategies of cooperation and cheating define the population dynamics of mitochondrial mutations, but how? This question of "how," with particular focus on the less-understood behavior of cheating, remains the focus of my work using heteroplasmic *C. elegans*, described in the chapters that follow.

Part I

Establishing a bona fide selfish mitochondrial genome

Chapter 2

The mutant variant *uaDf5* in *Caenorhabditis elegans* is a bona fide selfish mitochondrial genome

Adapted in part from:

Gitschlag, B. L., Kirby, C. S., Samuels, D. C., Gangula, R. D., Mallal, S. A., & Patel, M. R. 2016. Homeostatic Responses Regulate Selfish Mitochondrial Genome Dynamics in *C. elegans*. *Cell Metabolism*, 24, 91-103

Gitschlag, B. L., Tate, A. T., Patel, M. R. 2020. Nutrient status shapes selfish mitochondrial genome dynamics across different levels of selection. *eLife*, 9:e56686

Introduction

Because the eukaryotic cell is predicated on a mutualistic symbiotic relationship, the successful transmission of hereditary information across generations in eukaryotic organisms requires cooperation between two genomes of separate ancestry: the mitochondrial and host (nuclear) genomes. However, since cooperation requires contributing to the fitness of a partner, albeit for collective benefit, cooperators remain vulnerable to an alternative adaptive strategy, namely defection or cheating, whereby entities can reap the benefits of having cooperative partners without incurring the cost of reciprocating (Ghoul et al., 2014). Mutations in mitochondrial DNA (mtDNA) can thus give rise to cheater genomes, provided the mutant mtDNA can experience its own fitness gain at the expense of the host, which requires natural selection to act on mtDNA both within and between hosts. Indeed, selection can act on the mitochondrial genome at multiple levels of scale within the hierarchy of biological organization, particularly when different mtDNA sequence variants coexist within individual hosts, a state known as heteroplasmy. For example, individual mtDNA molecules can undergo selection within an organelle due to an intrinsic

replication advantage (Holt et al., 2014), such as when a mutant mtDNA variant contains multiple origins of replication. Selection can also occur between organelles, whereby the host cell may selectively target individual mitochondria for replication or degradation (Lieber et al., 2019, Zhang et al., 2019). Selection can also act on mtDNA between cells within a multicellular host (Shidara et al., 2005), and finally between host organisms due to the effect of mtDNA mutations on overall host fitness. Moreover, since the high mtDNA copy number within a typical eukaryotic cell can presumably shield the host against the deleterious effects of the occasional mtDNA mutation, mutant genomes that impose pathogenic phenotypic consequences tend to be those that propagate to high numbers within a host in spite of their fitness cost (Stewart and Chinnery, 2015). Accordingly, the population dynamics of mitochondrial mutations can often be characterized by the multilevel selection effects of cooperation and cheating.

In order to elucidate the mechanisms and conditions that shape the outcome of competition between cooperating and cheating genomes, I first sought to identify a bona fide selfish mitochondrial genome within an experimentally tractable model organism. The ability to track shifts in mitochondrial mutant frequency across an organism's lifespan within a short time—together with the large sample sizes and versatile genetic toolkit available—make the hermaphroditic roundworm *Caenorhabditis elegans* ideally suited for this type of work. The vast majority of mitochondrial content in the adult *C. elegans* hermaphrodite is confined to the maternal germline (Bratic et al., 2009, Tsang and Lemire, 2002a), which exists as a contiguous syncytium of cytoplasm shared among a common pool of organelles and nuclei until the final stages of oocyte maturation (Pazdernik and Schedl, 2013). Selection within a host thus predominantly reflects the biology of the female germline, where mtDNA variants compete for transmission to the next generation. Accordingly, here I focus on selection for mitochondrial genotype at the within-host (sub-organismal) level as a largely single phenomenon, in addition to selection for mitochondrial genotype at the organismal level. By focusing on selection for mitochondrial

genotype overall, I bypass the challenges of studying selection among organelles, which undergo dynamic fusion and fission and hence do not persist as discrete units.

Previous studies have identified a *C. elegans* strain harboring a heteroplasmic mutant mtDNA variant labeled *uaDf5* (hereinafter referred to as ΔmtDNA, denoting a deletion-bearing genome). This genome contains a 3.1-kilobase deletion that removes four protein-coding genes and seven tRNA genes (see Chapter 1, Figure 1-1) (Tsang and Lemire, 2002b). Due to the loss of essential metabolic proteins, as well as RNA components important for protein synthesis in mitochondria, individuals carrying only ΔmtDNA are not expected to be viable. Indeed, animals homoplasmic for ΔmtDNA have not been reported (Tsang and Lemire, 2002b, Liau et al., 2007). Remarkably, however, animals that have lost ΔmtDNA had also not been previously observed prior to my work, even after passaging over hundreds of generations (Tsang and Lemire, 2002b, Liau et al., 2007). Moreover, ΔmtDNA levels have been reported to steadily increase in individuals, particularly those that inherit it at a low frequency (Tsang and Lemire, 2002b). This tendency to propagate evidently comes at a cost to host fitness, as ΔmtDNA has also been associated with reductions in lifespan, egg-laying rate, and sperm motility (Liau et al., 2007). Together, these previous findings raise the interesting possibility that ΔmtDNA behaves as a selfish genetic element.

Determining whether ΔmtDNA behaves as a genuine selfish mitochondrial genome requires addressing two key questions. First, does ΔmtDNA propagate across generations at the expense of host fitness? The defining characteristic of a biological cheater is to benefit at the expense of a cooperative partner, particularly when the benefit and expense arise from a cooperative behavior being directed at the cheater rather than the “intended” recipient (Ghoul et al., 2014). Mitochondrial genomes typically cooperate with each other and with the host genome by contributing to energy production, while the host genome cooperates by supplying proteins and building blocks needed for replication of mtDNA. Selfish or cheater variants would therefore

propagate via the misdirection of resources. In other words, they propagate using resources that are normally—but in the case of cheaters, are not—invested in sustaining an mtDNA population that positively contributes to energy production and overall host fitness. Alternatively, a mutant mtDNA variant could conceivably propagate out of necessity, by continuing to make an essential contribution toward host fitness, while still carrying a mutation that negatively affects host fitness. This possibility raises the second key question that must be addressed: does ΔmtDNA propagate for reasons other than a cheating behavior? Here, I address both questions by first showing that ΔmtDNA proliferates in spite of being costly for host fitness, in agreement with previous research on this genome variant. I then address alternatives to the "cheating" hypothesis, by showing that the sustained propagation of ΔmtDNA observed in heteroplasmic animals can neither be attributed to necessity nor to the intrinsic replication advantage of the smaller genome size.

Methods

Animal husbandry. *C. elegans* strains used in this study were maintained on 60-mm standard nematode growth medium (NGM) plates seeded with live OP50-strain *E. coli* bacteria as a food source, unless otherwise indicated. Nematode strains were incubated at 20˚C. Age-matched nematodes were used in all experiment samples except when tracking heteroplasmy levels across generations. Three *C. elegans* strains were used in this study: the *uaDf5* heteroplasmy crossed into a wildtype nuclear background (the Bristol strain), the *mpt2* heteroplasmy crossed into a wildtype nuclear background (the Bristol strain), and the Bristol strain as a wildtype control.

Lysate preparation. To prepare nematodes for genotyping and quantification of ΔmtDNA frequency, nematodes were transferred to sterile PCR tubes or 96-well PCR plates containing lysis buffer with 100 µg/mL proteinase K. Lysis buffer consisted of 50 mM KCl, 10 mM Tris pH

8.3, 2.5 mM $MgCl_2$, 0.45% Tween 20, 0.45% NP-40 (IGEPAL), and 0.01% gelatin, in deionized water. Volume of lysis buffer varied by worm count: 10 µL for individual nematodes and 50 µL for pooled nematodes used for tracking heteroplasmy levels across generations. Each tube or plate was then incubated at -80˚C for 10 minutes to rupture nematode cuticles, followed by lysis incubation at 60˚C for 60 minutes (90 minutes for pooled nematodes), and then at 95˚C for 15 minutes to inactivate the proteinase K. Nematode lysates were then stored at -20˚C.

Detecting presence of the ∆mtDNA variant. To confirm the presence of heteroplasmic ∆mtDNA and wildtype mtDNA, worms were first lysed as described above. Next, the presence of ∆mtDNA and wildtype mtDNA copies was confirmed by PCR using the ∆mtDNA-specific forward primer 5'-CCATCCGTGCTAGAAGACAA-3' with the wildtype-specific forward primer 5'-TTGGTGTTACAGGGGCAACA-3' (specific to a site within the region spanning the deletion), and reverse primer 5'-CTTCTACAGTGCATTGACCTAGTC-3', which is common to both ∆mtDNA and wildtype mtDNA.

Quantifying ∆mtDNA levels. Levels of ∆mtDNA were quantified using droplet digital PCR (ddPCR). Nematodes were lysed as described above, then diluted in nuclease-free water, with a dilution factor varying depending on nematode concentration: 200x for individual nematodes and 20,000x for pooled nematodes used for tracking heteroplasmy levels across generations. Next, either 2 µL or 5 µL of each dilute nematode lysate was combined with 0.25 µL of a 10-µM dilution of each primer needed for amplifying wildtype mtDNA, mutant mtDNA, or both, as necessary. The following primers were used for ddPCR amplification.

For amplifying wildtype mtDNA (paired with primers for amplifying *uaDf5*):

Forward primer: 5'-GTCCTTGTGGAATGGTTGAATTTAC-3'

Reverse primer: 5'-GTACTTAATCACGCTACAGCAGC-3'

For amplifying *uaDf5*:

Forward primer: 5'-CCATCCGTGCTAGAAGACAAAG-3'

Reverse primer: 5'-CTACAGTGCATTGACCTAGTCATC-3'

For amplifying wildtype mtDNA (paired with primers for amplifying *mpt2*):

Forward primer: 5'-GGATTAATTTTCTCAAGGGGTGCTG-3'

Reverse primer: 5'-CTTTTTCAAAGACGAAAACTGTAACC-3'

For amplifying *mpt2*:

Forward primer: 5'-GAAGAAGGTGGTAGCCTTGAGGAC-3'

Reverse primer: 5'-CGTATAAGAAAAGTCTTGGGATGTTAAG-3'

Mixtures of dilute nematode lysate and primer were combined with 12.5 µL of Bio-Rad QX200™ ddPCR EvaGreen Supermix and nuclease-free water to a volume of 25 µL in Eppendorf™ 96-well twin.tec™ PCR plates. Droplet generation and PCR amplification were performed according to manufacturer protocol with an annealing temperature of 58˚C (*uaDf5*) or 55˚C (*mpt2*). Wildtype and ΔmtDNA primers were combined in the same reaction, and each droplet was scored as containing either wildtype or mutant template using the 2-dimensional (518 nm and 554 nm dual-wavelength) clustering plot option in the Bio-Rad QuantaSoft™ program.

Measuring ΔmtDNA across development (Figure 2-2). Three individual age-synchronized parents were selected according to initial ΔmtDNA frequency (parents with low, middle, and high frequency, determined by ddPCR as described above). In particular, one age-matched (L4-stage) nematode was picked at random under a dissecting microscope from each of three lines respectively maintained under artificial selection for low (<50 percent), medium (50-70 percent), and high (>70 percent) ΔmtDNA frequency. Each of animal was placed onto a fresh NGM plate seeded with live OP50 *E. coli* and incubated for 2 days at 20˚C. Each day-2 adult was then transferred to a fresh food plate every 4 hours and allowed to lay embryos. At each 4-hour time

point, approximately one third of the embryos produced were individually lysed. After three 4-hour transfers, for a total of 12 hours, the adults were individually lysed. A 12-hour time window for embryo production was chosen in order to generate a sufficient offspring count to allow for the establishment of single-brood frequency distributions of ΔmtDNA. The 12-hour time window was divided into 4-hour segments in order to maintain age-synchronicity, as each larva was lysed within 4 hours of being laid for the duration of the entire 12-hour period. After 2 days at 20˚C, approximately one third of the L4-stage larvae were individually lysed in the same 4-hour intervals to maintain age synchronicity. After an additional 2 days at 20˚C, the remaining third of offspring were individually lysed in 4-hour intervals once again, as they reached the same age at which their respective parents were lysed. The ΔmtDNA frequency of each individual was determined using ddPCR as described above and a ΔmtDNA frequency distribution was plotted for each offspring life stage.

Detecting the effect of ΔmtDNA on aerobic respiration. Basal and maximum oxygen consumption rates were measured using the Seahorse XFe96 Analyzer in the High-Throughput Screening Facility at Vanderbilt University. One day before experimentation, each well of a 96-well sensor cartridge that comes as part of the Seahorse XFe96 FluxPak was incubated with 200 µL of the Seahorse XF Calibrant Solution. On the day of the experiment, 10-20 L4-stage larval animals were randomly sampled from either a stock population stably maintaining ΔmtDNA in the range of 50-80 percent (mean heteroplasmic frequency is approximately 60 percent), or from a wildtype control (Bristol strain). The animals were placed into each well of the cell culture microplate. Wells contained either M9 buffer or 10 µM FCCP. After calibration, 16 measurements were performed at room temperature. Measurements 12 through 16 were averaged and normalized to the number of worms per well.

Detecting the effect of ∆mtDNA on fertility. To assay fertility, day-2 adult nematodes were individually transferred onto NGM plates seeded with live OP50 *E. coli* and incubated at 20˚C for 4 hours. I randomly selected 12 heteroplasmic adults carrying ∆mtDNA above the mean heteroplasmic frequency of 60 percent (within the range of 60 to 80 percent), and another 12 heteroplasmic adults carrying ∆mtDNA below 60 percent (between 40 and 60 percent), plus 8 homoplasmic (wildtype) adults as controls, and compared fertility between these groups. The adults were then individually lysed as described above and ∆mtDNA frequency was determined using ddPCR as described previously. Fertility was scored as the average number of viable progeny produced per hour during the 4-hour window, where viable progeny were identified as those that had progressed from embryos to larvae within 24 hours of being laid.

Detecting the effect of ∆mtDNA on development. The impact of ∆mtDNA levels on development was assayed by comparing ∆mtDNA frequency with developmental stage for each nematode in a population of age-synchronized larvae. To age-synchronize larvae, multiple mature heteroplasmic adults carrying ∆mtDNA in the Bristol nuclear background were transferred to an NGM plate seeded with live OP50 *E. coli* and allowed to lay eggs at 20˚C for 2 hours. Adults were then removed from the plate. After 48 hours, each nematode was individually lysed and its respective larval stage (L2, L3, or L4) was annotated. None of the nematodes had yet reached adulthood at this point. Embryos that failed to transition to larvae were discarded. The ∆mtDNA frequency of each larval nematode was determined using ddPCR.

Sequencing non-∆mtDNA. Non-∆mtDNA was amplified as three overlapping PCR products. The coordinates of the PCR products and the primers utilized are as follows:

1-5132bp

Forward primer: 5’-CAGTAAATAGTTTAATAAAAATATAGCATTTGGGTTG-3’

Reverse primer: 5’-CCGTGGCAATATAACCTAGATGTTCTACC-3’

4997-13311bp

Forward primer: 5’-TTGGTGTTACAGGGGCAACA-3’

Reverse primer: 5’-GTATGCAAAACATATATTTTTATTAAACTAAAATCCC-3’

12691-423bp

Forward primer: 5’-GTGGATTAATTTTCTCAAGGGGTGCTG-3’

Reverse primer: 5’-CCTAAATATCTTCTATAAGTTAATACTGTGGGAG-3’

The following primers were used to sequence the above PCR products:

1-5132bp PCR product

Forward primer 1: 5’-GTGTTTTTTGTTTTAGCTGTTTTAAGTAGG-3’

Forward primer 2: 5’-GTGTTTTTCTGTTATTTCAAGAATCCTGGG-3’

Forward primer 3: 5’-GGAGGCTGAGTAGTAACTGAGAACCC-3’

Forward primer 4: 5’-CTTTTATTACTCTATATGAGCGTC-3’

Forward primer 5: 5’-CCATCCGTGCTAGAAGACAA-3’

Forward primer 6: 5’-GCTGCTGTAGCGTGATTAAGTACTTTG-3’

Forward primer 7: 5’-GTTCTAGGTTAAATCCTGCTCGTTTTTG-3’

Forward primer 8: 5’-GAGTCTTTTAATTGGATTGTTTTGGGAG-3’

Reverse primer 1: 5’-CCTAAATATCTTCTATAAGTTAATACTGTGGGAG-3’

Reverse primer 2: 5’-CGCACTGTTAAAGCAAGTGGACGAG-3’

Reverse primer 3: 5’-CCGTGGCAATATAACCTAGATGTTCTACC-3’

4997-13311bp PCR product

Forward primer 1: 5’-TTGGTGTTACAGGGGCAACA-3’

Forward primer 2: 5’-GACTAGGTCAATGCACTGTAGAAGACCC-3’

Forward primer 3: 5'-TCATCATCTGGGGTTGGAATTTGC-3'

Forward primer 4: 5'-CCTAAAGCTCATGTAGAGGCTCCTAC-3'

Forward primer 5: 5'-GAAATGTAGGGTTTTCAGCACCATTAGTC-3'

Forward primer 6: 5'-CAGCAGGGTTAAGATCTATCTTAGGTGG-3'

Forward primer 7: 5'-GGTGGGTTGACAGGTGTTGTATTATC-3'

Forward primer 8: 5'-GTCTGTAAGGTTCATACCCTTGAGGTGG-3'

Forward primer 9: 5'-CTAGATCAATTAAGTTTAGGTGAACCACG-3'

Forward primer 10: 5'-GGTGGAATTAGTGTTTGGCTTATACCCAC-3'

Forward primer 11: 5'-GGTGAGGTCTTTGGTTCATAGTAGAAC-3'

Forward primer 12: 5'-GTGGATTAATTTTCTCAAGGGGTGCTG-3'

Reverse primer 1: 5'-CGAATTTAAACCCGTCTATAACG-3'

Reverse primer 2: 5'-GCCCAAGCATGAATAACATCAGCAGATG-3'

Reverse primer 3: 5'-CTAGCGTAAACACTAAAACTATTAATAGCAC-3'

Reverse primer 4: 5'-CTCTAAACGTTACCAAAAAAAGAATAAACG-3'

Reverse primer 5: 5'-GTATGCAAAACATATATTTTTATTAAACTAAAATCCC-3'

Reverse primer 6: 5'-CTTCTACAGTGCATTGACCTAGTC-3'

12691-423bp PCR product

Forward primer 1: 5'-GTGGATTAATTTTCTCAAGGGGTGCTG-3'

Reverse primer 1: 5'-CCACTGCTTAAAAATAAGGTGTACCCC-3'

Reverse primer 2: 5'-CCTAAATATCTTCTATAAGTTAATACTGTGGGAG-3'

Reverse primer 3: 5'-CAACCCAAATGCTATATTTTTATTAAACTATTTACTG-3'

Selection for loss of ΔmtDNA. Every generation, 8-16 individual animals were grown in isolation and PCR was performed on these single individuals after they produced progeny, to qualitatively determine ΔmtDNA levels. Next, 8-16 individuals from the plate with the lowest apparent ΔmtDNA

levels were transferred to fresh food plates to establish the subsequent generation, and the process was repeated until ΔmtDNA was no longer detected by PCR.

Tracking heteroplasmy levels across generations. To track the frequency of heteroplasmic mtDNA mutations across multiple generations, populations of nematodes carrying one of two ΔmtDNA variants (*uaDf5* or *mpt2*) were maintained on 10-cm NGM plates seeded with OP50 *E. coli*. Every 3 days, nematodes were washed off the plates using sterile M9 buffer into a sterile 1.7 mL collection tube. Approximately 500 nematodes of mixed ages from each line were transferred to a fresh food plate, marking the start of a subsequent generation. An additional 500 nematodes were lysed together in a single pooled lysate. These lines were propagated as "non-competing" control lines in an organismal-competition experiment to measure the impact of ΔmtDNA on host fitness (see Chapters 5 and 7). Heteroplasmy levels were quantified using ddPCR as described.

Tracking heteroplasmic mutant mtDNA levels across development (Figure 2-6D and 2-6E). Frequency of *uaDf5* and *mpt2* were measured longitudinally across development among multiple isolated single-parent broods. Multiple L4-stage (late larval) heteroplasmic animals were picked at random under a dissecting microscope from a stock population carrying *uaDf5* or *mpt2* in the Bristol strain (wildtype) nuclear background. These larvae were transferred to a fresh food plate and incubated for 2 days at 20˚C. The day-2 adults were then segregated onto individual plates and incubated for 4 hours at 20˚C to produce age-synchronized progeny. Each parent was then individually removed and lysed. Three embryos from each parent were also lysed at the same time, in one pooled lysate per three same-parent embryos. After 4 days, three adult progeny per brood were pooled and lysed as they reached day 2 of adulthood. Progeny from each time-point were lysed in pools of three, across multiple independent broods, to minimize the effect of random drift. Frequency *uaDf5* and *mpt2* were determined using ddPCR as described above.

Results

∆mtDNA proliferates at the expense of host fitness. Using a multiplex droplet digital PCR (ddPCR) approach to quantify mitochondrial genotype (Figure 2-1), I found that ∆mtDNA frequency rises across organismal development in a manner that depends on the initially inherited frequency of ∆mtDNA (Figure 2-2), consistent with earlier work (Tsang and Lemire, 2002b). The apparent upper limit of sub-organismal (within-host) ∆mtDNA proliferation is consistent with the phenomenon of frequency-dependent selection, a common feature of cheater entities (Dobata and Tsuji, 2013, Dugatkin et al., 2005, Pruitt and Riechert, 2009, Riehl and Frederickson, 2016, Ross-Gillespie et al., 2007). Another important feature of cheaters is that their selection advantage tends to break down at higher levels of selection, where fitness depends on cooperation at lower levels (Aktipis et al., 2015, de Vargas Roditi et al., 2013, Fiegna and Velicer, 2003, Moreno-Fenoll et al., 2017, Rainey and Rainey, 2003, Wenseleers and Ratnieks, 2004). Indeed, consistent with a disadvantage at a higher level of selection, I observe numerous indicators that ∆mtDNA undermines overall host fitness. These include reduced aerobic respiration (Figure 2-3A), in spite of elevated overall mitochondrial mass and the activation of mitochondrial stress-response mechanisms (see Chapter 4) (Gitschlag et al., 2016, Lin et al., 2016). Other indicators that ∆mtDNA impacts host fitness include reduced fertility (Figure 2-3B) and slowed larval development (Figure 2-3C) in heteroplasmic animals. Consistent with prior research, these results confirm that ∆mtDNA bears key hallmarks of a biological cheater.

Alternate hypothesis: ∆mtDNA propagates by necessity. One explanation for the stable maintenance of ∆mtDNA over many generations is balanced heteroplasmy, in which two mtDNA haplotypes possess lethal but non-overlapping mutations. In this scenario, neither mtDNA variant can be lost because neither mtDNA is capable of fully supporting viability. On the contrary, the intact region of ∆mtDNA would genetically complement the mutated region of the other mtDNA

variant, and vice versa. Host survival would therefore select for persistence of the heteroplasmic state. To test this hypothesis, the non-ΔmtDNA variant in heteroplasmic animals was sequenced. Using primers specific to a sequence located inside the deleted region (and thus absent from ΔmtDNA), the entire genic region of non-ΔmtDNA can be amplified as two large PCR products (Figure 2-4). Under the "balanced heteroplasmy" hypothesis, the non-ΔmtDNA genome is not a fully metabolically competent (wildtype) genome, but rather contains additional deleterious mutations affecting loci that remain intact in ΔmtDNA. However, sequencing revealed that the non-ΔmtDNA in heteroplasmic animals is wildtype. Next, to sequence an approximately 500-basepair, highly AT-rich, non-coding region that was not captured within the two PCR products, the non-coding region was amplified by itself using primers that are common to both genomes. Sequencing of this region did not reveal any apparent heteroplasmic mutations, which would have been expected if there were any mutations specific to the non-ΔmtDNA variant. Thus, the sequencing data do not support balanced heteroplasmy as an explanation for ΔmtDNA persistence, since the non-ΔmtDNA is wildtype, suggesting that ΔmtDNA is not critical for host viability.

The sequencing data are instead consistent with ΔmtDNA behaving as a selfish genetic element. I reasoned that if ΔmtDNA is not critical for viability, then I should be able to recover healthy individuals that have lost it. To test this hypothesis, I conducted an artificial selection experiment in which I selected for individuals with progressively lower ΔmtDNA levels across multiple generations (Figure 2-5A, red boxes). Under this artificial selection regime, I was able to recover healthy individuals that did not have detectable levels of ΔmtDNA by PCR (Figure 2-5B), suggesting that these individuals have lost ΔmtDNA. To confirm complete loss of ΔmtDNA, I used ddPCR to assay for the presence of ΔmtDNA in lysates obtained from the eighth and final generation of the artificial selection experiment. Since ddPCR relies on performing thousands of independent PCR amplifications in parallel across a population of droplets, which are designed

to segregate the template DNA molecules into an average of one template per droplet (Hindson et al., 2011), it provides a highly sensitive way to detect rare variants, up to single-molecule resolution. I observed complete loss of ΔmtDNA using ddPCR (Figure 2-5C). Together with the sequencing results, my observation that ΔmtDNA can be eliminated rules out balanced heteroplasmy as an explanation for ΔmtDNA maintenance. Instead, together with my previous observations, I conclude that ΔmtDNA not only propagates at the expense of host fitness but is also superfluous for host viability, consistent with the "cheater" hypothesis of ΔmtDNA propagation.

Alternate hypothesis: ΔmtDNA has an intrinsic replicative advantage. One attractive hypothesis for maintenance of mutant mtDNA with large deletions like ΔmtDNA invokes a replicative advantage over wildtype mtDNA due to their smaller genome size (Wallace, 1992). The replicative advantage of a smaller genome has been shown under limited physiological contexts (Moraes et al., 1999, Diaz et al., 2002); nevertheless, this advantage could potentially enable the proliferative dynamics that I observe with ΔmtDNA. If this hypothesis were correct, I would expect to see different dynamics in mitochondrial genomes harboring smaller deletions, where the mutant and wildtype genomes are closer in size. However, the mutant mtDNA variant *mpt2* (Figure 2-6A), which carries a deletion of only 245 basepairs, persists at similarly high frequency across multiple generations (Figure 2-6B and 2-6C), despite differing in size from the wildtype genome by less than 2 percent. Moreover, *mpt2* and *uaDf5* similarly proliferate across development, with each mutant genome increasing as a percentage of total mtDNA from embryo to adulthood (Figure 2-6D and 2-6E). While not ruling out a replicative advantage, these data suggest that other mechanisms likely contribute to the proliferative success of ΔmtDNA.

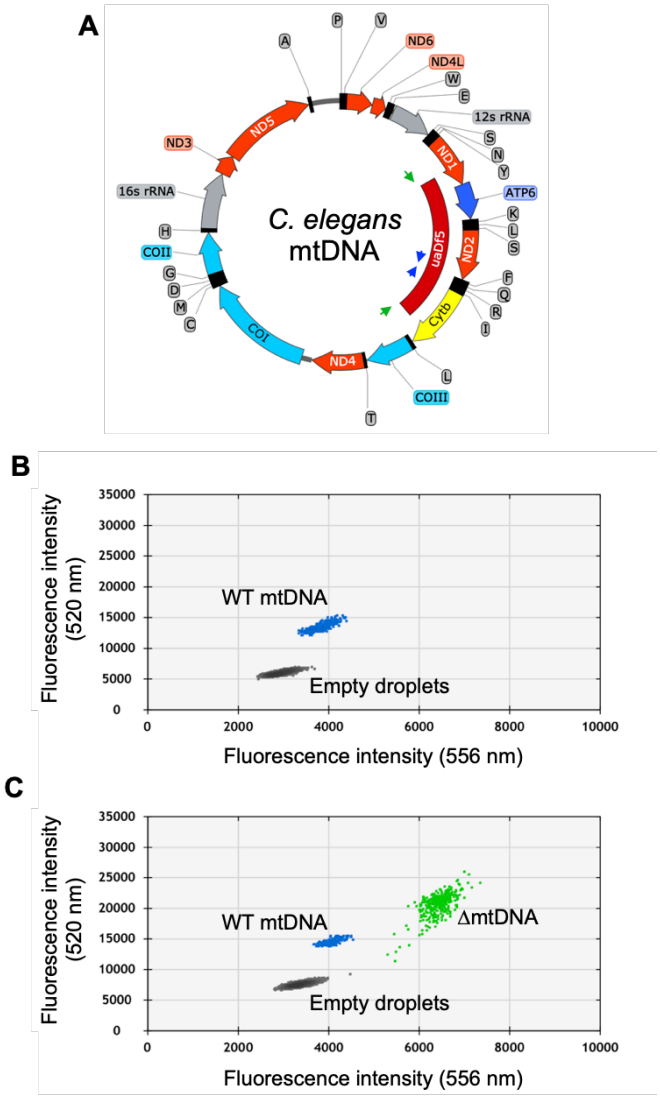

Figure 2-1. Quantification of mtDNA copy number and ΔmtDNA frequency by droplet digital PCR

(A) Map of mtDNA showing the *uaDf5* deletion (ΔmtDNA) and the strategy for oligonucleotide primer design for the multiplex quantification of ΔmtDNA and wildtype mtDNA simultaneously within the same reaction. Due to the deletion size, primers flanking the *uaDf5* deletion (green arrows) amplify a PCR product off of the ΔmtDNA but not wildtype mtDNA template (see panel B). Likewise, primers complementary to a sequence within the region spanning the *uaDf5* deletion (blue arrows) amplify a PCR product off of the wildtype mtDNA but not ΔmtDNA template.
(B-C) Sample droplet digital PCR data plots showing mtDNA copy number in lysates from homoplasmic wildtype (B) and heteroplasmic (C) nematodes. Mutant frequency is determined from ΔmtDNA copy number over total copy number.

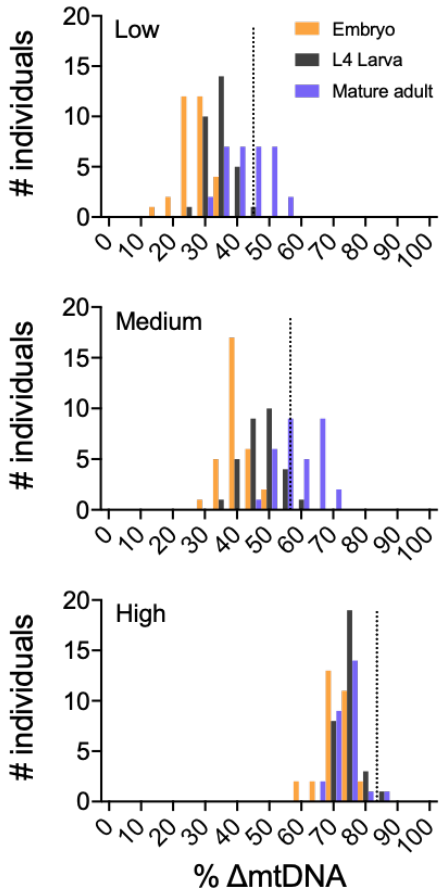

Figure 2-2. Proliferation to, and maintenance of, high ΔmtDNA frequency

ΔmtDNA frequency across developmental stages of single broods from low (top, N=94), intermediate (middle, N=93), or high (bottom, N=88) parental ΔmtDNA frequency (dotted lines). Mature adults were lysed at day 2 of adulthood, the same age at which the parents were lysed. Animals in this experiment were maintained on a diet of live OP50 *E. coli* at 20˚C.

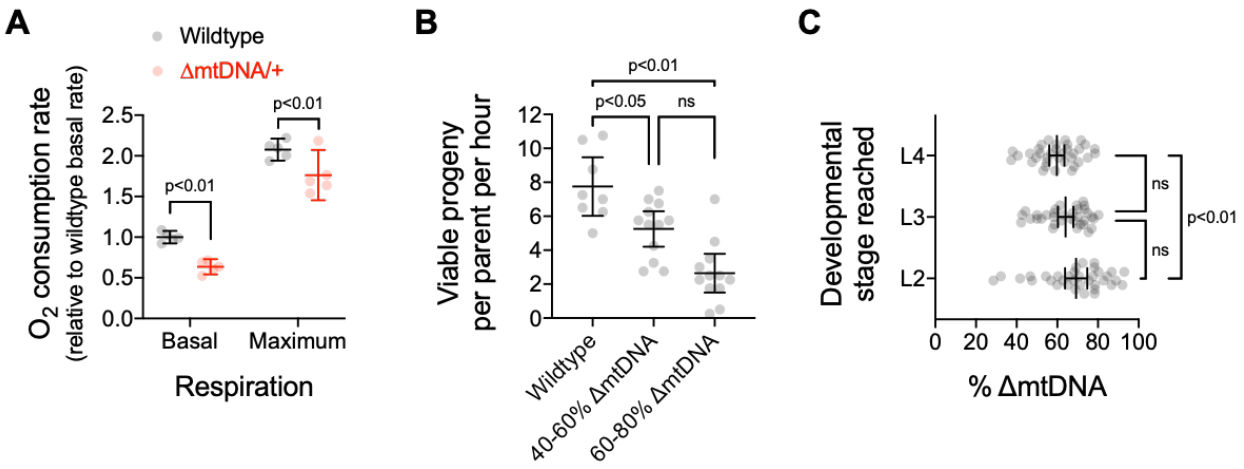

Figure 2-3. Evidence of organismal fitness consequences associated with ΔmtDNA

(A) Basal and maximum aerobic respiration in age-synchronized L4 animals. Two-way ANOVA with Sidak's multiple comparisons test.
(B) Peak fecundity (viable progeny per hour per parent at day 2 of adulthood) binned according to the low end of the ΔmtDNA frequency distribution (below the mean heteroplasmic ΔmtDNA frequency of 60 percent, N=12) or the high end (above 60 percent, N=12), with wildtype controls (N=8). Brown-Forsythe and Welch ANOVA with Dunnett's T3 multiple comparisons test.
(C) Larval stage reached within 48 hours starting from age-synchronized embryos, plotted as a function of ΔmtDNA frequency. N=35 nematodes per larval stage. Brown-Forsythe and Welch ANOVA with Dunnett's T3 multiple comparisons test.
All experiments featured in this figure used nematodes that were maintained on a diet of live OP50 *E. coli* at 20˚C. Error bars represent 95% confidence intervals.

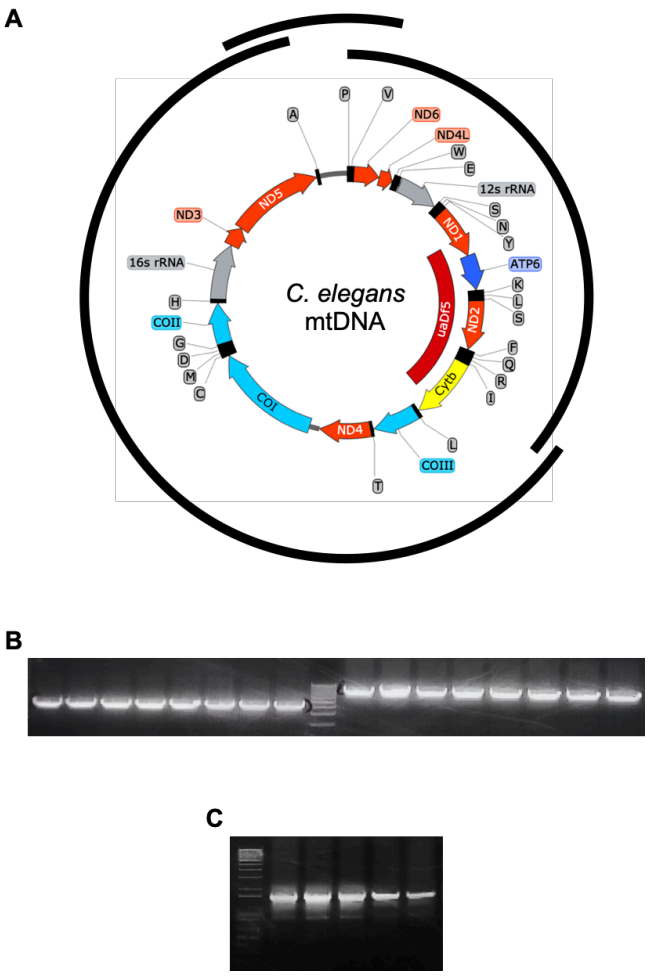

Figure 2-4. PCR products used for sequencing non-ΔmtDNA genome, mapped to *C. elegans* reference mtDNA

(A) Three overlapping PCR products were amplified from *C. elegans* mtDNA. The reverse primer used for generating the PCR product spanning base-pair positions 1 through 5,132 is specific to a region within the *uaDf5* deletion in ΔmtDNA, as is the forward primer used for generating the PCR product spanning base-pair positions 4,997 through 13,311. Additional primers were used for sequencing all three PCR products (see **Methods**).
(B) Gel image of products amplified by PCR across the protein-coding mtDNA regions (the two larger black bars in panel A).
(C) Gel image of product amplified by PCR across the major non-coding (D-Loop) region (the smallest black bar in panel A).

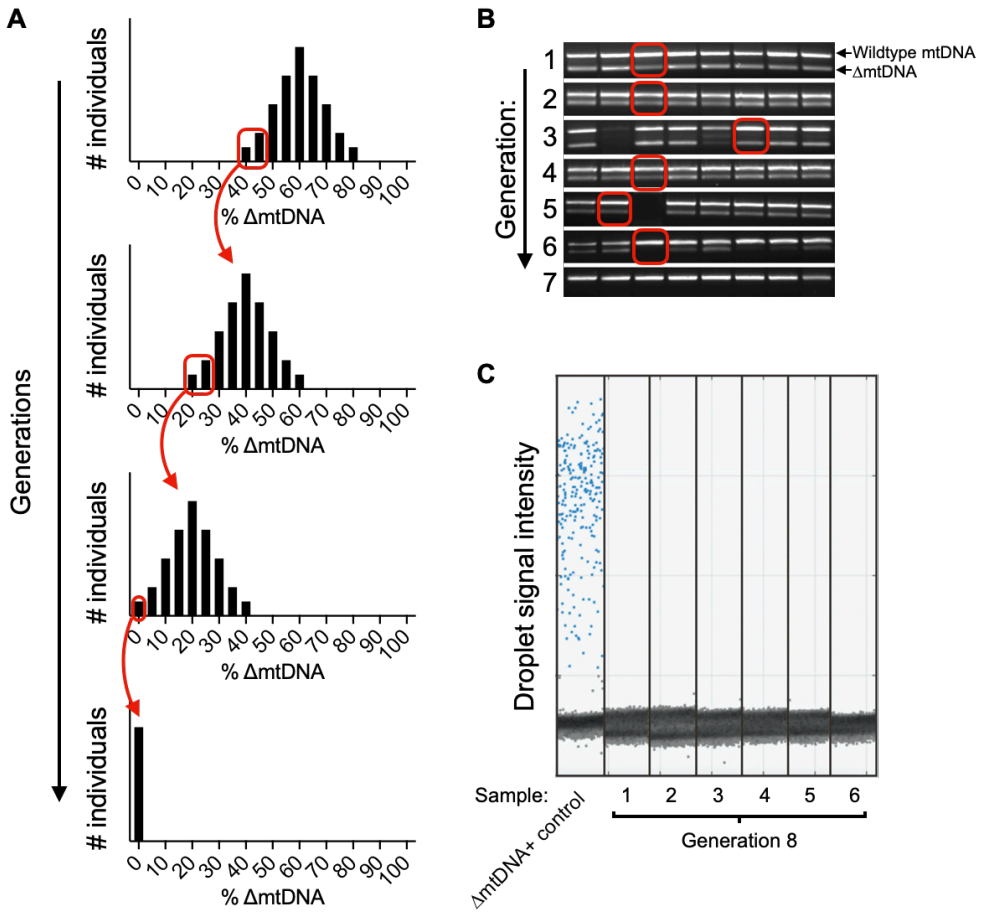

Figure 2-5. ΔmtDNA can be forced out from a stably persisting heteroplasmy in *C. elegans*

(A) Schematic illustrating the selection strategy to force loss of ΔmtDNA from a heteroplasmic *C. elegans* line. Each generation, the progeny of individuals with the lowest ΔmtDNA levels were selected for subsequent propagation.
(B) Single-worm PCR of ΔmtDNA and wildtype mtDNA. Successive propagation of individual worms with low ΔmtDNA levels (red boxes) results in complete loss of ΔmtDNA from the population over multiple generations.
(C) ddPCR data from single worms (one per sample column) confirming complete loss of ΔmtDNA. Positive droplets containing ΔmtDNA-specific PCR product exhibit increased fluorescence intensity (blue) compared to negative droplets that contain no ΔmtDNA (gray). For each droplet, the droplet reader detects droplet size, shape, and fluorescence intensity, and automatically distinguishes positive from negative droplets on the basis of these criteria. Left-most sample column is a ΔmtDNA-positive control.

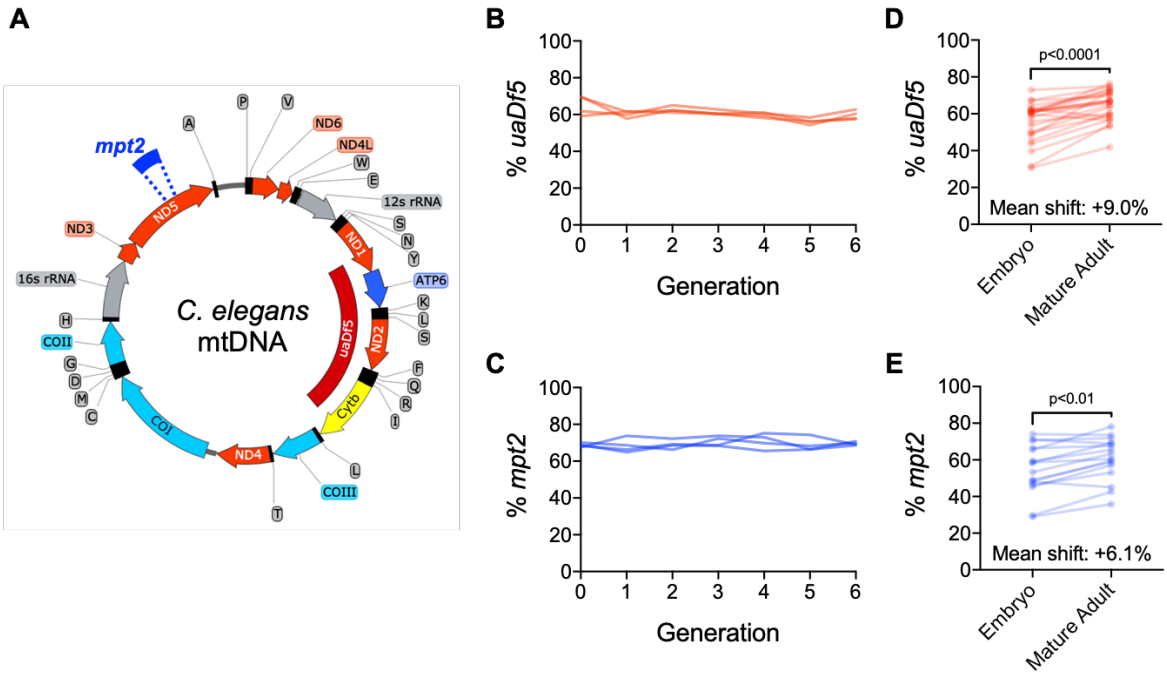

Figure 2-6. Tracking frequency of two ΔmtDNA variants, *uaDf5* and *mpt2*, across multiple generations and animal development

(A) *C. elegans* mtDNA map, including sizes and locations of the two mutations featured in this study: *uaDf5* (dark red bar) and *mpt2* (dark blue bar).
(B) Frequency of ΔmtDNA variant *uaDf5* across six generations among four independent heteroplasmic populations (each red line represents a separate replicate population).
(C) Frequency of ΔmtDNA variant *mpt2* across six generations among four independent heteroplasmic populations (each blue line represents a separate replicate population).
(D) Comparison of *uaDf5* frequency between embryonic stage and mature adulthood across multiple independent cohorts. Each line connecting an embryo with an adult data point represents animals belonging to the same brood, sampled sequentially at embryonic and mature adult timepoints. Data shown here represents a sub-sample from among the "embryo" and "mature adult" time-points in Figure 5-1A, selected to match the range of starting (embryonic) frequencies of *mpt2* in panel (E) by omitting cohorts with starting *uaDf5* frequencies that do not overlap with that of *mpt2*. Because the magnitude of mutant mtDNA proliferation depends on initial frequency (Figure 2-2), *uaDf5* and *mpt2* proliferation across animal development were compared among similar frequency ranges, omitting cohorts with non-overlapping initial mutant frequencies.
(E) Comparison of *mpt2* frequency between embryonic stage and mature adulthood across multiple independent replicate populations (blue lines), similar to panel (C). Data shown here represents a sub-sample of data from the experiment featured in Figure 7-2E but with *mpt2* frequency shown for embryos (omitted in Figure 7-2E) instead of parents (shown in Figure 7-2E).

Discussion

The central challenge to understanding the complex population dynamics of mutant mtDNA arises from key differences between the mitochondrial and nuclear genomes that can be attributed to the endosymbiotic origins of mitochondria. For example, because mtDNA is a high-copy-number genome, new mutations coexist with wildtype mtDNA in a heteroplasmic state. Moreover, in contrast to the host genome, mtDNA undergoes relaxed replication that is not tightly coupled to the cell cycle (Bogenhagen and Clayton, 1977, Chatre and Ricchetti, 2013, Newlon and Fangman, 1975, Sasaki et al., 2017, Sena et al., 1975), enabling mutant mtDNA levels to vary over time and between hosts. Mitochondrial mutations whose effects enable the mutant genome to proliferate at the expense of host fitness are precisely the mutant variants expected to reach high enough levels to give rise to disease phenotypes. Accordingly, elucidating the mechanistic basis for the evolutionary adaptive strategy of cheating and the conditions that shape cheater fitness would yield valuable insight into an integral feature of cell biology and biomedical science, namely the population dynamics of mitochondrial mutations and their role in disease.

What mechanisms and conditions underlie selfish mitochondrial genome dynamics? I sought to address this question here by identifying a bona fide selfish mitochondrial genome within an experimentally tractable model organism, namely the *uaDf5* genome (ΔmtDNA) in the nematode *C. elegans*. To accomplish this, I developed a multiplex ddPCR protocol to quantitatively measure mutant mtDNA frequency. I then used this approach, in conjunction with assays of mitochondrial respiration and overall organismal fitness, to confirm that a promising candidate genome proliferates across development at the expense of host fitness. Interestingly, although host stress-response mechanisms have been implicated in ΔmtDNA propagation (see Chapter 4) (Gitschlag et al., 2016, Lin et al., 2016), such mechanisms do not appear to protect the host from the fitness cost incurred by harboring ΔmtDNA. On the contrary, I observed several indicators that ΔmtDNA

imposes a host fitness cost, consistent with multilevel selection and in agreement with prior studies of this genome (Gitschlag et al., 2016, Liau et al., 2007, Lin et al., 2016). These indicators include reductions in mitochondrial respiration, fertility, and rate of larval development, underscoring the notion that ∆mtDNA propagates at the expense of host fitness.

Finally, I sought to follow up on the putative selfish proliferation of ∆mtDNA by addressing alternatives to the "cheater" hypothesis. In particular, in addition to propagating at the expense of host fitness, I found that ∆mtDNA does not persist out of necessity for host viability, nor can the persistence of high mutant mtDNA levels simply be attributed to the replication advantage of smaller genomes. Based on these observations, I conclude that there are other mechanisms at work and that the ∆mtDNA variant *uaDf5* in *C. elegans* is an ideal model genome for follow-up work to mechanistically characterize the complex population dynamics of a selfish mitochondrial genome, which will be the focus of subsequent chapters.

Acknowledgments

The *uaDf5* heteroplasmic strain was kindly provided by the Caenorhabditis Genetics Center (CGC). I would like to recognize O. Thompson and R. Waterston at University of Washington for identifying the *mpt2* deletion from the Million Mutation Project worm collection. I would like to thank Harmit Malik of the Howard Hughes Medical Institute and the Fred Hutchinson Cancer Research Center for valuable advice and support, and Ann T. Tate of Vanderbilt University for valuable guidance on experimental design. Quantification of mtDNA copy number and ∆mtDNA frequency was accomplished with the help of the Simon A. Mallal Laboratory at Vanderbilt University Medical Center, and I especially thank Rama Gangula of the Mallal Laboratory for training on the use of the droplet digital PCR technology.

Funding for this work was provided by a Helen Hay Whitney Foundation Fellowship, by grants from the Mathers Foundation and the Howard Hughes Medical Institute to the Harmit Malik Laboratory, startup funds from Vanderbilt University for the Maulik R. Patel Laboratory, the NIH-sponsored Cellular, Biochemical and Molecular Sciences Training Program (5T32GM008554-18), the Ruth L. Kirschstein National Research Service Award Individual Predoctoral Fellowship (1F31GM125344), and the NIH-funded Tennessee Center for AIDS Research (P30 AI110527) to the Mallal Laboratory.

Part II

Mechanistic basis for the cheating behavior of a selfish mitochondrial genome

Chapter 3

The mitochondrial genome *uaDf5* cheats by exploiting the regulation of mtDNA copy number

Adapted in part from Gitschlag, B. L., Kirby, C. S., Samuels, D. C., Gangula, R. D., Mallal, S. A., & Patel, M. R. 2016. Homeostatic Responses Regulate Selfish Mitochondrial Genome Dynamics in *C. elegans*. *Cell Metabolism*, 24, 91-103

Introduction

Selfish mitochondrial genomes are common, having been identified and studied across a diversity of organisms, including plants, fungi, and animals (Havird et al., 2019, Klucnika and Ma, 2019, Taylor et al., 2002). In yeast, for example, selfish mitochondrial DNA (mtDNA) variants arise at high rates and result in the formation of "petite" colonies (Bernardi, 2005, Williamson, 2002). Despite harboring major deletions and rearrangements, and causing severe growth defects, many of these mutant mtDNA variants are able to outcompete wildtype mtDNA and are hence dubbed "hypersuppressive" mtDNA (MacAlpine et al., 2001, Jasmin and Zeyl, 2014, Harrison et al., 2014). Selfish mtDNA has also been extensively documented in animals. In natural populations of the nematode species *Caenorhabditis briggsae*, for example, a mutant mtDNA variant has been found to have a transmission advantage over wildtype mtDNA (Clark et al., 2012, Phillips et al., 2015), despite being associated with deleterious fitness effects (Estes et al., 2011). Interestingly, phylogenetic analysis suggests that this mutation arose prior to a dispersal of *C. briggsae* into geographically diverse populations (Howe and Denver, 2008), suggesting that selfish mitochondrial genomes might be capable of stably persisting on evolutionary time-scales.

What accounts for these competitive dynamics among deleteriously mutated mtDNA molecules? In some cases, the proliferation of mutant mtDNA variants has been attributed to an intrinsic replication advantage, such as the presence of multiple origins of replication (Holt et al., 2014) or the faster replication rate of smaller genomes (Diaz et al., 2002). However informative, a focus on the intrinsic properties of the mutant mtDNA itself runs the risk of missing important ways in which mitochondrial mutations might propagate. After all, since the eukaryotic cell—and by extension, the propagation of its genetic material—is predicated on mutualistic interactions between the mitochondrial and host genomes, a mutant mtDNA variant could conceivably propagate without any intrinsic replication advantage, by affecting other aspects of cell biology.

In Chapter 2, I established that the deleteriously mutated mtDNA (∆mtDNA) variant called *uaDf5* is a genuine selfish genetic element in *C. elegans*. In particular, I showed that ∆mtDNA outcompetes wildtype mtDNA to become the predominant allelic variant, accounting for upward of 60 percent of the total mtDNA within heteroplasmic hosts, despite being unnecessary for host viability. Moreover, the proliferation of ∆mtDNA is associated with numerous indicators of deleterious host fitness effects and may not be merely attributable to an intrinsic replication advantage, given that mutant mtDNA variants much closer in size to wildtype mtDNA can also maintain a sizeable allelic majority within their heteroplasmic hosts. Here, I sought to follow up on these findings by identifying a mechanistic basis for how ∆mtDNA proliferates within hosts. Using droplet digital PCR (ddPCR) to quantify mtDNA copy-number dynamics, I show that the variation in copy number between hosts is far greater for ∆mtDNA than for wildtype mtDNA, suggesting that ∆mtDNA "hitchhikes" to high frequency by evading the homeostatic regulation of mtDNA copy number. Drawing from the literature, I then discuss a theoretical model for mtDNA copy-number regulation that provides a promising explanation for how ∆mtDNA evades this regulation.

Methods

Animal husbandry. The *C. elegans* strain used in this study consisted of the heteroplasmic ΔmtDNA variant *uaDf5* crossed into a transgenic line expressing the *zcIs9* [*hsp-60p*::GFP + *lin-15*(+)] fluorescent reporter in an otherwise wildtype nuclear background (the Bristol strain). The *C. elegans* were maintained on 60-mm standard nematode growth medium (NGM) plates seeded with live OP50-strain *E. coli* bacteria as a food source. Nematodes were incubated at 20˚C.

Lysate preparation. To prepare nematode lysates for quantification of ΔmtDNA frequency, mature day-4 adult nematodes were transferred to sterile PCR tubes or 96-well PCR plates containing 50 µL lysis buffer with 100 µg/mL proteinase K. Lysis buffer consisted of 50 mM KCl, 10 mM Tris pH 8.3, 2.5 mM $MgCl_2$, 0.45% Tween 20, 0.45% NP-40 (IGEPAL), and 0.01% gelatin, in deionized water. Each tube or plate was then incubated at -80˚C for 10 minutes to rupture nematode cuticles, followed by lysis incubation at 60˚C for 60 minutes, and then at 95˚C for 15 minutes to inactivate the proteinase K. Nematode lysates were then stored at -20˚C.

Quantifying mutant and wildtype mtDNA levels. Quantification of ΔmtDNA and wildtype mtDNA copy number was achieved using droplet digital PCR (ddPCR). Individual hermaphrodite worms heteroplasmic for ΔmtDNA were each randomly selected from a stock population at the fourth and final (L4) larval stage and transferred to NGM plates seeded with OP50 *E. coli* as a food source. At 96 hours post-transfer, the hermaphrodites were lysed as day 4-adults. Lysates were diluted 1:100 in nuclease-free water for amplifying mtDNA and 1:5 for amplifying nuclear DNA. Next, 2 µL of each dilute lysate was combined with 0.25 µL of a 10-µM dilution of one of the following primer pairs as needed for amplifying mtDNA or nuclear DNA.

Wildtype-specific primers for amplifying wildtype mtDNA:

Forward primer: 5'-GTGATGCAGAGATGTTTATTGAAGC-3'

Reverse primer: 5'-CACTCTGGAACAATATGAACTGGC-3'

Common primers for amplifying both ΔmtDNA and wildtype mtDNA:

Forward primer: 5'-GCGGTATCGTAAGAAAATCAAAATATGG-3'

Reverse primer: 5'-CTTTGTCTTCTAGCACGGATGG-3'

Actin-specific primers for amplifying nuclear DNA:

Forward primer: 5'-CAACACTGTTCTTTCCGGAGG-3'

Reverse primer: 5'-GTGATTTCCTTCTGCATACGATC-3'

Mixtures of dilute lysate and primer were combined with 12.5 µL of Bio-Rad QX200™ ddPCR EvaGreen Supermix and nuclease-free water to a volume of 25 µL in Eppendorf™ 96-well twin.tec™ PCR plates. Droplet generation and PCR amplification were performed according to manufacturer protocol with an annealing temperature of 55˚C. Template copy number was quantified using the Bio-Rad QuantaSoft™ program and determined as the number of PCR-positive droplets per sample on a 1-dimensional (518 nm wavelength) amplitude plot. Copy number of each mtDNA variant was normalized to nuclear DNA copy number (amplified using the actin-specific primers) to control for variation in cell-count between lysates.

Results

Although ΔmtDNA levels are variable between individuals, they can reach high frequency in individuals, accounting for approximately 60 percent of the total mtDNA within a heteroplasmic population (see Chapter 2). However, ΔmtDNA tends to rise across development (see Chapter 2, Figure 2-2). Indeed, here I observe that ΔmtDNA typically comprises 50-80 percent of overall

mtDNA present in day-4 adults (Figure 3-1). To ascertain mechanisms that facilitate ΔmtDNA proliferation, I next examined how levels of ΔmtDNA relate to those of wildtype mtDNA. One simple "direct competition" model suggests that wildtype mtDNA levels should be inversely proportional to ΔmtDNA levels, while total mtDNA levels remain consistent. Alternatively, the copy number of wildtype mtDNA is maintained independent of ΔmtDNA levels.

Here I sought to distinguish between these possibilities. Using ddPCR, I quantified mtDNA copy number across 60 individual day-4 adults that were heteroplasmic for ΔmtDNA. Replication of mtDNA in *C. elegans* does not start until the L4 larval stage, after which it greatly increases during maturation and in the first few days of adulthood, reaching steady-state levels by day 4 (Bratic et al., 2009). Copy number measurements in day-4 adults thus predominantly reflect germline mtDNA, since more than 90 percent of the total mtDNA content in an adult hermaphrodite is contained within the female germline (Bratic et al., 2009, Tsang and Lemire, 2002a). The "direct competition" model predicts relatively constant levels of total mtDNA amongst individuals, with a trade-off between the amount of ΔmtDNA and wildtype mtDNA. In contrast, my results show that wildtype mtDNA levels are maintained within a relatively consistent range compared to the mutant genome, whose copy number is significantly more variable (Figure 3-2). In conclusion, my data are consistent with the hypothesis that wildtype mtDNA levels, but not total mtDNA levels, are well regulated.

One attractive hypothesis for the regulation of mtDNA copy number involves the coupling of mitochondrial function to mtDNA replication. To maintain an optimal mtDNA population for meeting its energy demands, the cell could be expected to resume replicating additional mtDNA copies until some output of mitochondrial function reaches a certain threshold. Consequently, any mutated mtDNA copies that do not contribute to such a functional output would fail to be "counted," enabling them to "hitchhike" to higher levels as the cell blindly replicates both mutant and wildtype

genomes until sufficient wildtype levels are reached. This model, dubbed the “maintenance of wild-type” hypothesis (Capps et al., 2003), predicts that the host would be able to maintain wildtype mtDNA copy number within a narrow range at the expense of generating unregulated numbers of mutant mtDNA, with wildtype mtDNA levels dropping off substantially only at extremely high mutant frequency (Figure 3-3A). The copy-number dynamics that I observe in animals carrying ΔmtDNA is remarkably consistent with theoretical prediction based on this model, especially when mutant and wildtype copy number are visualized as a function of mutant frequency (Figure 3-3B). Based on these data, I conclude that ΔmtDNA proliferates at the expense of host fitness, at least in part, by escaping a mechanism of mtDNA copy-number regulation.

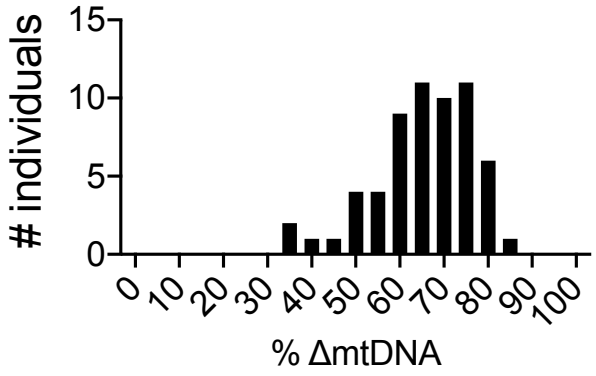

Figure 3-1. ∆mtDNA frequency distribution in day-4 adults

Histogram showing ∆mtDNA frequency distribution in day-4 adult individuals (N=60) from a population stably maintaining ∆mtDNA, determined using ddPCR.

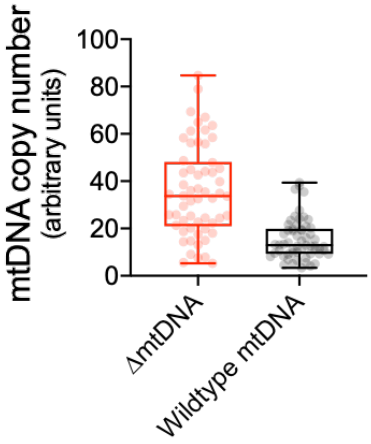

Figure 3-2. ΔmtDNA and wildtype mtDNA copy number from heteroplasmic animals

Wider variation in ΔmtDNA relative to wildtype copy number ($p<0.0001$) suggests that wildtype mtDNA, but not ΔmtDNA, is subject to homeostatic copy-number control. Data points show mtDNA copy number from single individuals (N=60). Box and whisker plot shows the median, lower and upper quartile (boxes), and minimum and maximum (error bars) mtDNA copy number. F test for differences of variance.

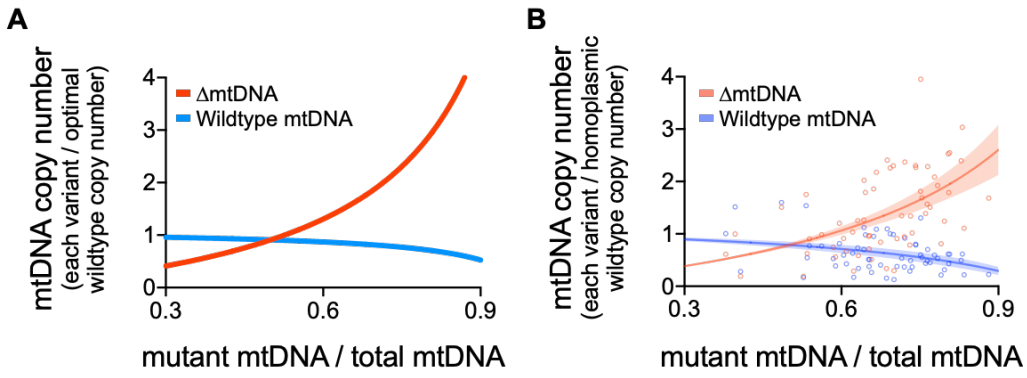

Figure 3-3. Theoretical prediction and empirical data corresponding to a model of mtDNA copy-number regulation

(A) Theoretical prediction of mutant and wildtype mtDNA copy number as a function of mutant mtDNA frequency, according to the "maintenance of wild-type" hypothesis (Capps et al., 2003). According to this model, selfish mutant mtDNA exploits copy-number regulation to "hitchhike" to high frequency, as wildtype mtDNA copy number remains relatively constant, only substantially dropping off at very high mutant mtDNA frequency.
(B) Wildtype mtDNA (blue) and ΔmtDNA (red) copy-number values from individual day-4 adult worms represented in Figure 3-2 (N=60), normalized to mean mtDNA copy number in homoplasmic-wildtype animals and plotted as a function of ΔmtDNA frequency. Shaded regions represent 95% confidence interval.

Discussion

In contrast to the nucleus, which regulates gene expression by controlling the production of RNA, protein, or both, mitochondria permit a third layer of gene regulation: the ability to replicate additional copies of the mitochondrial genome itself as necessary. Because aerobic respiration depends on the expression of mtDNA-encoded proteins, mtDNA copy number can serve as a useful proxy indicator of metabolic capacity. Furthermore, altered mtDNA copy number is implicated in numerous human diseases and prognosis (Clay Montier et al., 2009, Reznik et al., 2016). The maintenance of mtDNA copy number is therefore a subject of great research interest, with several models having been proposed. One study found that mtDNA levels in cultured human cells depend on the number of origins of replication, with replication favoring mutant molecules that contain a larger number of replication origins (Tang et al., 2000a). Conversely, comparison of mutant and wildtype mtDNA content in cultured cells revealed that total mtDNA mass was constant even when mutant and wildtype genomes differed in size and in number of replication origins, suggesting a possible role for the availability of nucleotides in regulating mtDNA copy number (Tang et al., 2000b). More recently, computational modeling and experimental observation support the previously mentioned “maintenance of wild-type” model, whereby the cell induces mtDNA replication to establish optimal mtDNA levels, which can lead to unregulated proliferation of mutant genomes in the context of a heteroplasmy (Chinnery and Samuels, 1999, Capps et al., 2003, Durham et al., 2007, Tam et al., 2015).

My investigation of mtDNA copy-number dynamics in heteroplasmic *C. elegans* shows regulation of wildtype mtDNA levels but “runaway” dynamics of ΔmtDNA levels. These findings are most consistent with the “maintenance of wild-type” model, which requires a feedback mechanism whereby mtDNA replication is inversely related to wildtype mtDNA levels, allowing cells to maintain mtDNA at optimal levels (Figure 3-4). When mutant mtDNA variants fail to support

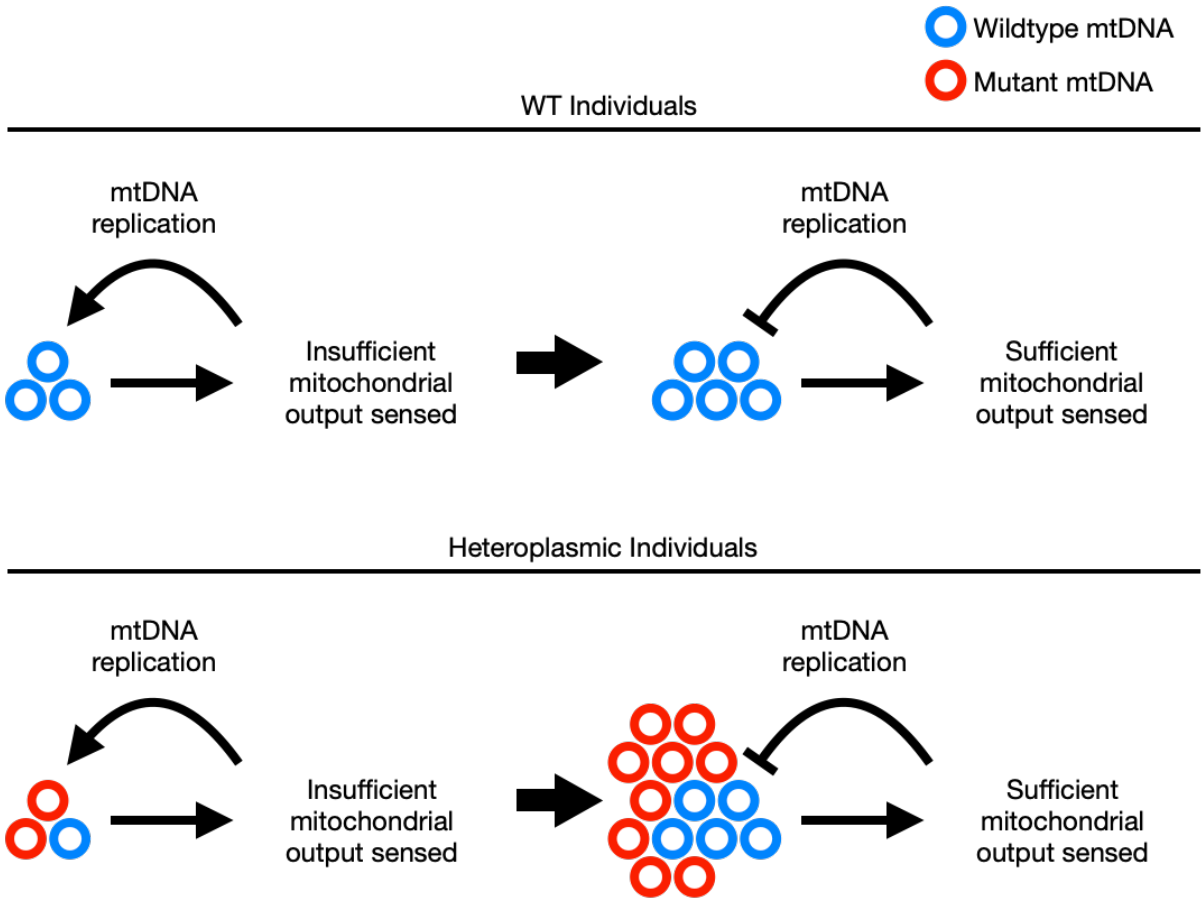

Figure 3-4. "Maintenance of wild-type" model of mtDNA copy-number regulation

In wildtype individuals (top), an output of mtDNA is sensed, triggering feedback inhibition of replication when mtDNA copy number reaches a minimum threshold. In heteroplasmic animals (bottom), mutant mtDNA copies that fail to contribute the same output are invisible to the mechanism of feedback inhibition. The mutant copies therefore hitchhike to higher levels as the cell undergoes further mtDNA replication until sufficient wildtype mtDNA levels are achieved. This model predicts that wildtype mtDNA copy-number homeostasis is achieved at the cost of unregulated mutant levels.

normal mitochondrial function, insufficient levels of wildtype mtDNA in a heteroplasmy elicit mtDNA replication. However, replication of mutant genomes can also occur, requiring additional rounds of replication to establish the optimal wildtype mtDNA levels, leading to more mutant copies. This negative feedback model of copy-number homeostasis predicts "runaway" dynamics of mutant mtDNA like those observed for ∆mtDNA. Based on these data, ∆mtDNA can be viewed as taking advantage of homeostatic mtDNA copy-number control to hitchhike to high frequency. Similar over-proliferation of mtDNA is observed in individuals with heteroplasmic mtDNA diseases (Durham et al., 2007). Taken together, these data suggest that exploitation of homeostatic mtDNA copy-number control by mutant mtDNA might be a conserved and widespread "cheating" strategy. To my knowledge, this is the first study to show that this strategy can operate in the germline to potentially influence inheritance of mtDNA heteroplasmy.

What is the mitochondrial output that is sensed to achieve mtDNA copy-number regulation? Given its central role in cellular energy production, the mitochondrial genome could conceivably undergo replication in response to energy depletion, such as low ATP levels, high ADP or AMP levels, or both (see Chapter 1, Figure 1-1, for an illustration of the mitochondrial genome and its role in energy production). Accordingly, mutations that compromise its contribution toward energy production might predispose the mutated genome to compensatory replication as the host seeks to rescue energy production. Consistent with this idea, the protein CLK-1 (the *C. elegans* homolog of human COQ7) has previously been shown *in vitro* to bind a DNA sequence corresponding to one of the origins of replication in mtDNA in a manner that is inhibited by ADP (Gorbunova and Seluanov, 2002). More recent work has shown that deletion of the gene *clk-1* is associated with an approximately 30-percent increase in mtDNA copy number (Cristina et al., 2009, Kirby and Patel, 2021). Interestingly, pharmacological rescue of coenzyme Q synthesis (a key function of COQ7) was observed to reverse several phenotypic effects of *clk-1* deletion, but not the elevation in mtDNA copy number (Kirby and Patel, 2021). Taken together, these findings suggest that CLK-

1 may be involved in the regulation of mtDNA copy number by binding mtDNA and inhibiting replication when local energy levels are high, while dissociating from mtDNA to permit replication when energy is depleted. This model predicts that in heteroplasmic animals carrying a deleterious mtDNA mutation, CLK-1 should bind to the wildtype genome at higher rates than the mutant genome. Moreover, this model also predicts that the mutant genome should lose some of its proliferative advantage over the wildtype genome in heteroplasmic animals upon deletion of *clk-1*. Testing these predictions in future research could yield valuable insights on the nature of mtDNA copy-number homeostasis and its role in the dynamics of selfish mitochondrial genomes.

Acknowledgments

The *uaDf5* heteroplasmic strain was kindly provided by the Caenorhabditis Genetics Center (CGC). I would like to thank Harmit Malik of the Howard Hughes Medical Institute and the Fred Hutchinson Cancer Research Center, and David C. Samuels of Vanderbilt University Medical Center, for valuable advice and support. Quantification of mtDNA copy number and ΔmtDNA frequency was conducted with the help of the Simon A. Mallal Laboratory at Vanderbilt University Medical Center, and I especially thank Rama Gangula of the Mallal Laboratory for training on the use of the droplet digital PCR technology.

Funding for this work was provided by a Helen Hay Whitney Foundation Fellowship, by grants from the Mathers Foundation and the Howard Hughes Medical Institute to the Harmit Malik Laboratory, startup funds from Vanderbilt University for the Maulik R. Patel Laboratory, the NIH-sponsored Cellular, Biochemical and Molecular Sciences Training Program (5T32GM008554-18), and the NIH-funded Tennessee Center for AIDS Research (P30 AI110527) to the Mallal Laboratory.

Chapter 4

The mitochondrial genome *uaDf5* selfishly propagates by exploiting a key stress-tolerance mechanism of the host

Adapted in part from Gitschlag, B. L., Kirby, C. S., Samuels, D. C., Gangula, R. D., Mallal, S. A., & Patel, M. R. 2016. Homeostatic Responses Regulate Selfish Mitochondrial Genome Dynamics in *C. elegans*. *Cell Metabolism*, 24, 91-103

Introduction

Cooperative interactions facilitate the evolution of biological complexity. Unfortunately, cooperation also opens up opportunities for the emergence of selfish, "cheater" entities that can benefit from the cooperative contributions of others without incurring the cost of reciprocating, resulting in cheaters having a fitness advantage over cooperators. How, then, does cooperation frequently persist as a successful evolutionary strategy under the threat of cheating? One common method for maintaining the fitness of cooperators involves the direct targeting of cheaters, often termed "enforcement" or "policing" behaviors. Policing is taxonomically widespread, with examples ranging from bacteria to animals (Manhes and Velicer, 2011, Ratnieks et al., 2006, Riehl and Frederickson, 2016). Perhaps the most well-documented examples can be found in the social insects, where reproduction by members of the worker castes can be viewed as a form of selfishness, by redirecting colony resources away from the care of the queen and her progeny (Wenseleers and Ratnieks, 2004). In many social insects, including various species of bees, wasps, and ants, the reproduction of workers is suppressed by nestmates via aggression, mutilation, or the removal or consumption of worker progeny, collectively categorized under the label of "worker policing" (Ratnieks et al., 2006). Given the existence of mechanisms that enforce

cooperation, the adaptive fitness of cheaters might be expected to select for the ability to evade such policing.

Just as cooperation is present between different genomes within the eukaryotic cell, so too is a well-characterized policing mechanism. Severe mitochondrial dysfunction is often characterized by a loss of the membrane electrochemical potential that ordinarily fuels aerobic energy production (see Chapter 1, Figure 1-1B). During a loss of membrane potential, the protein PINK1 localizes to the outer membrane of the defective mitochondria, which recruits the protein Parkin to the outer mitochondrial membrane as well (Matsuda et al., 2010, Narendra et al., 2012). Parkin functions as an E3 ubiquitin ligase—an enzyme that tags mitochondria with the protein ubiquitin—resulting in the degradation of the damaged mitochondria in a mitochondria-specific form of autophagy, termed "mitophagy" (Matsuda et al., 2010, Narendra et al., 2008, Narendra et al., 2012). Although PINK1/Parkin-dependent mitophagy is triggered by the loss of mitochondrial membrane potential and not necessarily by mitochondrial DNA (mtDNA) mutations per se, mutant mtDNA should nevertheless be selectively targeted for elimination if they harbor mutations that compromise membrane potential. Consistent with this idea, PINK1/Parkin-dependent mitophagy has been shown to select against deleteriously mutated mtDNA in cell culture (Suen et al., 2010), *Drosophila* muscle tissue (Kandul et al., 2016), and *Caenorhabditis elegans* (Valenci et al., 2015). Interestingly, previous work also relates PINK1 and Parkin to the regulation of mitochondrial morphology. In particular, promoting mitochondrial fission has been reported to ameliorate deleterious phenotypes associated with mutations in the PINK1/Parkin pathway (Liu et al., 2011, Poole et al., 2008). The ability of the host to fragment its mitochondrial network can therefore at least partly compensate for the loss of PINK1/Parkin function. Consistent with this possibility, mitophagy can occur in a PINK1/Parkin-independent manner (Allen et al., 2013, Di Rita et al., 2018, Hibshman et al., 2018). Moreover, inducing mitochondrial fragmentation—by disrupting the opposing process of mitochondrial fusion through knockdown of the *mitofusin* gene—was

observed to result in selection against mutant mtDNA in *Drosophila*, in a manner similar to PINK1 overexpression (Kandul et al., 2016). Together, these studies suggest that the ability to isolate and degrade dysfunctional, mutant-bearing mitochondria represents a general form of policing against selfish mtDNA.

Despite the presence of a policing mechanism encoded by the host genome, the selfish mitochondrial genome (∆mtDNA) still maintains a proliferative advantage over wildtype mtDNA in heteroplasmic *C. elegans* (see Chapter 2). This suggests that ∆mtDNA may evade the PINK1/Parkin pathway. To explore this possibility, I sought to further characterize the effects of ∆mtDNA on mitochondrial function as well as its interactions with the host genome. One likely explanation for the evasion of mitophagy by ∆mtDNA involves the activation of additional responses to mitochondrial dysfunction. In addition to mitophagy, the cell is also equipped with mechanisms that seek to rescue mitochondrial function without having to eliminate the dysfunctional mitochondria (Eckl et al., 2021). Here, I adapt a previous study (Gitschlag et al., 2016) to report that ∆mtDNA perturbs mitochondrial function in a manner that elicits the activation of one such mechanism, the mitochondrial unfolded protein response (UPR^{mt}). Interestingly, I find that ∆mtDNA proliferates in a manner that depends at least partly on UPR^{mt} activation, since ∆mtDNA levels decline in hosts with compromised ability to activate UPR^{mt}. As predicted, this decline is dependent on the gene *pdr-1*, which encodes the *C. elegans* homolog of Parkin. Taken together, my findings indicate that in addition to the evasion of mtDNA copy-number control (see Chapter 3), ∆mtDNA also propagates by activating and subsequently exploiting UPR^{mt}, which protects ∆mtDNA from a cellular policing mechanism.

Methods

Animal husbandry. The *C. elegans* strains used in this study were maintained on 60-mm standard nematode growth medium (NGM) plates seeded with live OP50-strain *E. coli* bacteria as a food source. Nematodes were incubated at 20˚C. Genotypes used in this study include mutant alleles *pdr-1*(gk448); *atfs-1*(tm4525); *atfs-1*(et15); and the ∆mtDNA variant *uaDf5*. Transgenic lines used here include *zcIs9* [*hsp-60p*::GFP + *lin-15*(+)], *zcIs17* [*ges-1*::GFP^{mt}], and *zcIs18* [*ges-1*::GFP^{cyt}].

Lysate preparation. To prepare nematode lysates for genotyping and quantification of ∆mtDNA frequency, mature day-4 adult nematodes were transferred to sterile PCR tubes or 96-well PCR plates containing 50 µL lysis buffer with 100 µg/mL proteinase K. Lysis buffer consisted of 50 mM KCl, 10 mM Tris pH 8.3, 2.5 mM $MgCl_2$, 0.45% Tween 20, 0.45% NP-40 (IGEPAL), and 0.01% gelatin, in deionized water. Each tube or plate was then incubated at -80˚C for 10 minutes to rupture nematode cuticles, followed by lysis incubation at 60˚C for 60 minutes and then at 95˚C for 15 minutes to inactivate the proteinase K. Nematode lysates were then stored at -20˚C.

Genetic crosses. To evaluate mitochondrial function and UPR^{mt} activation in the presence of ∆mtDNA, the fluorescent UPR^{mt} reporter *hsp-60p*::GFP, mitochondria-targeted GFP, and cytosolic GFP were each introduced to the ∆mtDNA heteroplasmic line by classical genetic crosses. To investigate the roles of UPR^{mt} and mitophagy in the propagation of ∆mtDNA, the mutant alleles *pdr-1*(gk448), *atfs-1*(tm4525), and *atfs-1*(et15), were each introduced to the ∆mtDNA heteroplasmic line by classical genetic crosses. Males for these crosses were generated by heat-shocking at 30˚C for six hours. Presence or absence of fluorescent reporters in F2 progeny was confirmed by fluorescence microscopy. The gain-of-function allele *atfs-1*(et15) was crossed into the UPR^{mt} reporter *hsp-60p*::GFP and the presence of the gain-of-function mutation was confirmed

by increased fluorescence intensity of the reporter due to the constitutive activation of UPR^{mt} in these animals. Loss-of-function alleles were detected in F2 progeny using the following primers.

atfs-1(tm4525):

Forward: 5'-GAAACCGCCTCCTTTCGCCTTTTG-3'

Interior reverse: 5'-GACTTCATCGTCGTCCATGGGTACG-3'

Exterior reverse: 5'-TCTCCAATTTTGTTAACTTCCAGCAGCC-3'

pdr-1(gk448):

Exterior forward: 5'-GAATCATGTTGAAAATGTGACGCGAG-3'

Interior forward: 5'-CTGACACCTGCAACGTAGGTCAAG-3'

Reverse: 5'-GATTTGACTAGAACAGAGGTTGACGAG-3'

Quantifying mutant and wildtype mtDNA. Quantification of ΔmtDNA and wildtype mtDNA was achieved using droplet digital PCR (ddPCR). As detailed in Chapter 3, individual hermaphrodite worms heteroplasmic for ΔmtDNA were each randomly selected from a stock population at the fourth and final (L4) larval stage and transferred to NGM plates seeded with OP50 *E. coli* as a food source. At 96 hours post-transfer, day-4 adult hermaphrodites were lysed as described previously (see **Lysate preparation**). Lysates were diluted 1:100 in nuclease-free water for amplifying mtDNA and 1:5 for amplifying nuclear DNA. Next, 2 µL of each dilute lysate was combined with 0.25 µL of a 10-µM dilution of one of the following primer pairs as needed for amplifying mtDNA or nuclear DNA.

Primers for amplifying wildtype mtDNA:

Forward primer: 5'-GTGATGCAGAGATGTTTATTGAAGC-3'

Reverse primer: 5'-CACTCTGGAACAATATGAACTGGC-3'

Common primers for amplifying both ΔmtDNA and wildtype mtDNA:

Forward primer: 5'-GCGGTATCGTAAGAAAATCAAAATATGG-3'

Reverse primer: 5'-CTTTGTCTTCTAGCACGGATGG-3'

Actin-specific primers for amplifying nuclear DNA:

Forward primer: 5'-CAACACTGTTCTTTCCGGAGG-3'

Reverse primer: 5'-GTGATTTCCTTCTGCATACGATC-3'

Mixtures of dilute lysate and primer were combined with 12.5 µL of Bio-Rad QX200™ ddPCR EvaGreen Supermix and nuclease-free water to a volume of 25 µL in Eppendorf™ 96-well twin.tec™ PCR plates. Droplet generation and PCR amplification were performed according to manufacturer protocol with an annealing temperature of 55˚C. Template copy number was quantified using the Bio-Rad QuantaSoft™ program and determined as the number of PCR-positive droplets per sample on a 1-dimensional (518 nm wavelength) amplitude plot. Frequency of ΔmtDNA was determined as the percentage of total mtDNA in heteroplasmic animals.

Quantification of gene expression. Gene expression was quantified using a commercial cDNA synthesis kit from Thermo Scientific and ddPCR. Lysates were prepared by transferring 10 adult worms to 10 µL lysis buffer with 20 mg/mL proteinase K. The lysates were incubated at 65˚C for 10 minutes, 85˚C for 1 minute, and 4˚C for 2 minutes. RNA transcripts in the worm lysates were immediately converted to cDNA. To accomplish this, 2 µL worm lysate was incubated at 37˚C for 2 minutes with 0.5 µL double-stranded DNase (dsDNase), 0.5 µL 10x dsDNase buffer, and 2 µL H_2O. Following dsDNase incubation, lysates were combined with 0.5 µL oligo d(T) primer, 0.5 µL 10 mM dNTP, 1.5 µL H_2O, 2 µL 5x reverse transcriptase buffer, 0.5 µL Maxima H Minus reverse transcriptase, and incubated at 25˚C for 10 minutes and 55˚C for 30 minutes, followed by a 5 minute heat-inactivation at 85˚C and 2 minutes at 4˚C. The cDNA was then diluted to 50 µL with nuclease-free H_2O and stored at -80˚C. Copy number of cDNA was quantified using ddPCR, as described above, using the following primers.

Actin:

Forward: 5’-CAACACTGTTCTTTCCGGAGG-3’

Reverse 5’-GTGATTTCCTTCTGCATACGATC-3’

nuo-2:

Forward: 5’-GACGAACACAAACGTGAACGGTTGG-3’

Reverse: 5’-GGCACTCGGCTGCATACTTTCC-3’

ND4:

Forward: 5’-ATTTCCAATTTATTTTTTACATCTTTGATTACC-3’

Reverse: 5’-CCCGCTGTGCCTAATTTTAATAG-3’

Cytochrome b:

Forward: 5’-GAGGTTTTGGTGTTACAGGGGCAAC-3’

Reverse: 5’-GCATCTTTACCTAAGTACTCAGGTC-3’

ND1:

Forward: 5’-GCCATCCGTGCTAGAAGACAAAG-3’

Reverse: 5’-CCTCTAACTAACTCCCTTTCACCTTCAG-3’

CO2:

Forward: 5’-CTAGATCAATTAAGTTTAGGTGAACCACG-3’

Reverse: 5’-CCAAGCATGAATAACATCAGCAGATG-3’

hsp-60:

Forward: 5’-CTTGAGCCATCGTCGATTATTGATG-3’

Reverse: 5’-CATCTTGGAGAGCTGTGCGAACC-3’

hsp-6:

Forward: 5’-GAAGATACGAAGACCCAGAGGTTC-3’

Reverse: 5’-GAACGAATGCTCCAACCTGAGATG-3’

Fluorescence microscopy. Fluorescence images of worms were captured using Zeiss Axio Zoom V16 stereo zoom microscope. The fluorescence intensities were quantified using ImageJ. 25 animals were used to calculate average fluorescence intensity for each group. To correlate *hsp-60p*::GFP fluorescence with ΔmtDNA levels, worms heteroplasmic for ΔmtDNA and expressing the *hsp-60p*::GFP reporter were individually picked as day-4 adults and immobilized on unseeded NGM plates treated with 250 µL of 10 mM levamisole. Worms were individually imaged, followed by lysis and ddPCR quantification of mtDNA heteroplasmy as described previously (see **Quantifying mutant and wildtype mtDNA**).

Mitochondrial staining. 250 µL of 10 µM TMRE dye was added to NGM plates seeded with OP50 *E. coli* as a food source and allowed to dry. Adult animals were grown on these plates for overnight. These animals were picked onto new food plates without the TMRE dye and imaged one hour later. Same protocol was followed to stain animals with Mitotracker Green FM using a dye concentration of 50 µM.

Targeting gene expression. RNA interference (RNAi) was used to knock down gene expression. RNAi was induced using feeder plates. Cultures consisting of 2 mL LB and 10 µL ampicillin were inoculated with bacteria harboring the ZC376.7 (*atfs-1*) ORF plasmid clone and incubated on a shaker at 37˚C overnight. Next, 750 µL of each overnight culture was transferred to a flask containing 75 mL LB and 375 µL ampicillin. The 75 mL culture was incubated on a shaker at 37˚C for 4-6 hours, until $OD_{550\text{-}600} > 0.8$. An additional 75 mL LB was added to the culture along with 375 µL ampicillin and 600 µL of 1 M isopropyl β-D-1-thiogalactopyranoside (IPTG) to induce expression of the small interfering RNA (siRNA). Cultures were incubated an additional 3.5-4 hours on a shaker at 37˚C and centrifuged at 3900 rpm for 6 minutes. After discarding the supernatant, the resulting pellets were resuspended in 6 mL M9 buffer with 8 mM IPTG and 250 µL of resuspension was pipetted onto unseeded NGM plates. Once dry, RNAi feeder plates were stored at 4˚C. Control

plates were prepared using the same protocol with bacteria harboring an empty (no siRNA) vector. Worms were transferred at the L4 larval stage to empty vector control plates and RNAi plates and stored at 20˚C. Additional L4 worms were selected from the F1 generation, aged to day-4 adults on fresh RNAi plates, and lysed as described above. For multigenerational RNAi, L4 worms were transferred to fresh RNAi and empty vector control plates every 2-3 days and lysed after seven generations.

Fitness assays. Three adults picked from a population of animals growing on RNAi plates since the L4 larval stage were allowed to lay eggs for 3 hours on corresponding fresh RNAi plates. The number of unhatched and hatched embryos were counted one day later to determine the percentage of unhatched embryos. After an additional two days, the total number of larvae and adults were counted to determine the fraction of animals that experienced delayed growth. Subsequently, all animals were transferred to fresh RNAi plates every other day until day 4 of adulthood. The number of total dead animals were counted until day 4 of adulthood to determine the percentage of dead animals.

Western blot analysis. One hundred adult worms were lysed in 10 µL of 2X SDS sample buffer and boiled for 10 minutes, followed by SDS PAGE gel and transfer to membrane. Mouse monoclonal anti-beta-actin (Santa Cruz Biotechnology catalog # sc-47778) or mouse monoclonal anti-GFP (Santa Cruz Biotechnology catalog # sc-9996) were used at 1:500 dilution overnight at 4˚C as primary antibodies. Horseradish peroxidase (HRP)-conjugated goat anti-mouse antibody (Santa Cruz Biotechnology catalog # sc-2005) was used at 1:5000 dilution for 90 minutes at room temperature as the secondary antibody. SuperSignal™ West Pico Chemiluminescent Substrate (Thermo Fisher) was used for detecting HRP.

Results

Mitochondrial transcriptional imbalance in heteroplasmic animals. Since heteroplasmic animals carry ΔmtDNA in addition to wildtype mtDNA, I first determined whether ΔmtDNA contributed to the mtDNA transcripts. Since some genes are deleted from ΔmtDNA, I reasoned that expression of all genes from the wildtype mtDNA but only some from ΔmtDNA would result in a stoichiometric imbalance in mtDNA-encoded transcript levels (see schematic Figure 4-1A). Cytochrome b and *ND1*, genes deleted in ΔmtDNA, were expressed at similar levels in homoplasmic wildtype animals as in heteroplasmic animals (Figure 4-1B). Expression levels of actin as well as a nuclear-encoded electron transport chain subunit, *nuo-2*, were also unaltered in the heteroplasmic animals (Figure 4-1B). However, compared to homoplasmic wildtype animals, the genes *CO2* and *ND4*, which are encoded in both ΔmtDNA and the wildtype genome, were significantly elevated in the heteroplasmic animals (Figure 4-1B). This implies that the mutant genomes are transcriptionally active and their expression contributes to substantial transcriptional imbalances in mtDNA-encoded genes.

Mitochondrial perturbations in heteroplasmic animals. Organismal fitness is significantly affected by the presence of ΔmtDNA (see Chapter 2). At the molecular level, I observe overexpression of ΔmtDNA-encoded transcripts, resulting in transcriptional imbalance. Given these effects, I sought to determine whether ΔmtDNA imposes cellular consequences. Mitochondrially targeted green fluorescence protein (GFP^{mt}) has previously been used as a model matrix protein to assess mitochondrial protein homeostasis, or proteostasis (Yoneda et al., 2004, Benedetti et al., 2006). If heteroplasmic animals have altered proteostasis, it might result in decreased fluorescence intensity of the mitochondrially targeted GFP. Indeed, GFP^{mt} fluorescence is significantly diminished in heteroplasmic animals that express GFP^{mt} in the intestinal cells under the control of the *ges-1* promoter (Figure 4-1C) (Benedetti et al., 2006). In contrast, no such

decrease is observed in the fluorescence of cytoplasmic GFP (GFP^{cyt}) in heteroplasmic animals (Figure 4-1C). Together, these data suggest that the fluorescence of mitochondrially targeted GFP, but not cytoplasmic GFP, is specifically affected in animals carrying ΔmtDNA. Consistent with fluorescence data, western blot analysis also shows decreased GFP^{mt} protein levels in heteroplasmic animals (Figure 4-1D). This decrease in mitochondrial GFP does not seem to be due to a decrease in overall mitochondrial mass. On the contrary, I observe increased mitochondrial signal in animals stained with the fluorescent dye MitoTracker Green FM, which localizes to mitochondria independently of the membrane electrochemical potential (Figure 4-1E) (Dingley et al., 2014, Hicks et al., 2012). The signal intensity of tetramethyl rhodamine ethyl ester (TMRE), which localizes to mitochondria in a membrane potential-dependent manner (Dingley et al., 2014, Yoneda et al., 2004, Billing et al., 2011, Palikaras et al., 2015), is also higher in heteroplasmic animals compared to wildtype controls (Figure 4-1F). These data suggest an increase in mitochondrial organelle mass in the heteroplasmic animals, correlating with an increase in total mtDNA copy number. These data also suggest that the decreased GFP^{mt} levels and fluorescence in heteroplasmic animals are due to alterations in mitochondrial proteostasis rather than due to decreased mitochondrial organelle mass. This altered proteostasis might reflect decreased GFP^{mt} import efficiency into mitochondria, or a compromised protein-folding environment inside the mitochondrial matrix, or both. Either scenario might result in a loss of fluorescence signal due to the degradation of misfolded protein. Taken together, my findings suggest that mitochondrial gene expression and protein quality control are severely affected by the presence of ΔmtDNA.

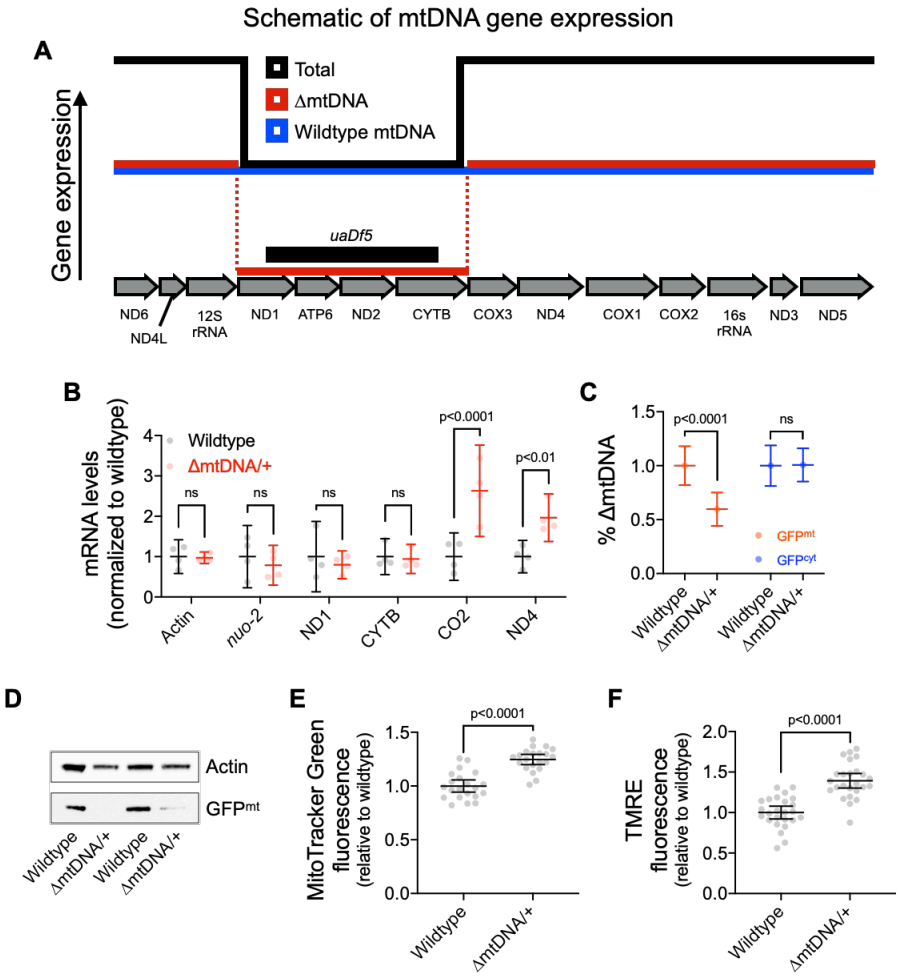

Figure 4-1. Mitochondrial perturbations associated with ΔmtDNA

(A) Schematic showing expected expression of mtDNA-encoded transcripts in heteroplasmic individuals. The presence of ΔmtDNA is expected to result in stoichiometric imbalance of gene expression, as the expression of ΔmtDNA and wildtype mtDNA copies (red and blue lines, respectively) combine to generate total expression (black line) at elevated levels for genes located outside the deletion but at normal wildtype levels for genes missing from ΔmtDNA.
(B) Animals heteroplasmic for ΔmtDNA exhibit expression levels similar to that of wildtype animals for mtDNA-encoded genes affected by the deletion (*CYTB* and *ND1*), as well as a nuclear-encoded mitochondrial gene (*NUO-2*) and actin. However, ΔmtDNA results in overexpression for mtDNA-encoded genes located outside the *uaDf5* deletion in ΔmtDNA (*CO2* and *ND4*). All transcript levels are normalized to wildtype. N=4 biological replicates consisting of 10 mature adult nematodes per replicate. Two-way ANOVA with Sidak's multiple comparisons test.
(C) Mitochondrially targeted GFP (GFP^{mt}), but not cytosolic GFP (GFP^{cyt}), is significantly reduced in ΔmtDNA-carrying heteroplasmic individuals. Mann-Whitney tests with Bonferroni correction.
(D) Western blot analysis of wildtype and ΔmtDNA-carrying heteroplasmic animals expressing GFP^{mt} reveals reduced levels in heteroplasmic individuals relative to actin. Data are shown from two biological replicates each for wildtype and heteroplasmic strains.
(E) Fluorescence increase in heteroplasmic animals stained with mitochondrial membrane potential-independent dye MitoTracker Green FM. N=21. Mann-Whitney test.
(F) Fluorescence increase in heteroplasmic animals stained with mitochondrial membrane potential-dependent dye TMRE. N=25. Mann-Whitney test.
Error bars represent 95% confidence intervals.

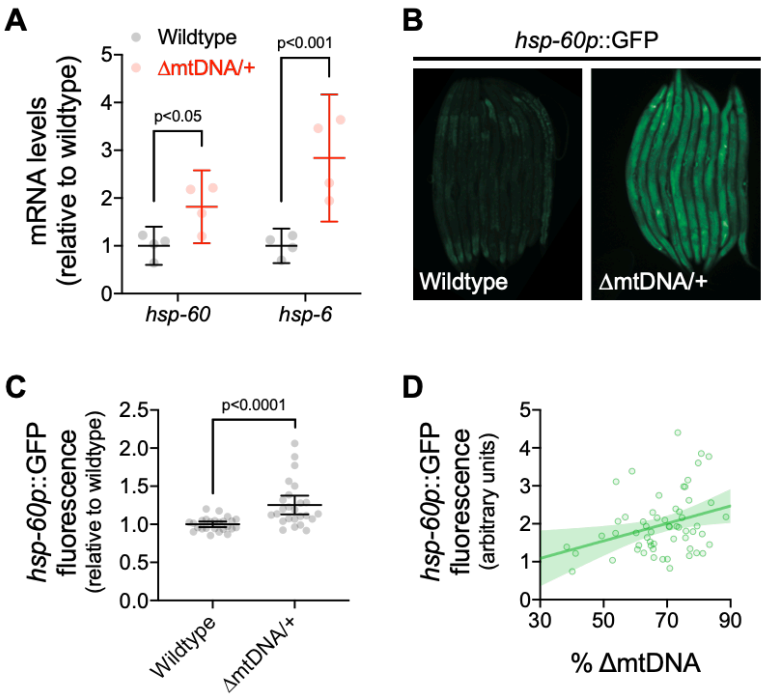

Figure 4-2. UPR^{mt} is activated in heteroplasmic animals carrying ΔmtDNA

(A) Transcription of two UPR^{mt}-activated molecular chaperones, *hsp-60* and *hsp-6*, is increased in individuals with ΔmtDNA compared to wildtype individuals. N=4 biological replicates consisting of 10 mature adult nematodes per replicate. Two-way ANOVA with Holm-Sidak's multiple comparisons test.
(B) Visual comparison of GFP fluorescence between heteroplasmic and wildtype animals, each expressing *hsp-60p*::GFP.
(C) Quantification of fluorescence between wildtype homoplasmic and heteroplasmic animals shows increased activation of the UPR^{mt} marker *hsp-60p*::GFP in the presence of ΔmtDNA. Each data point is from a single individual picked randomly from a population. N=25. Mann-Whitney test.
(D) Positive relationship between ΔmtDNA frequency and *hsp-60p*::GFP fluorescence (trendline) indicates that UPR^{mt} activation increases at higher ΔmtDNA frequency. Each data point corresponds to a single individual (N=60), using animals represented in Figures 3-2 and 3-3. Shaded region represents 95% confidence range.
Error bars represent 95% confidence intervals.

High levels of ΔmtDNA activate the mitochondrial unfolded protein response. The mitochondrial unfolded protein response (UPR^{mt}) has emerged as an important protective stress response that is activated under a variety of conditions that affect mitochondrial proteostasis (Houtkooper et al., 2013, Yoneda et al., 2004, Haynes and Ron, 2010, Runkel et al., 2013, Baker et al., 2012). This homeostatic response involves expression of hundreds of target genes including chaperones and proteases that eliminate misfolded and nonfunctional complexes inside mitochondria (Nargund et al., 2015, Nargund et al., 2012). To determine whether UPR^{mt} is induced in the heteroplasmic animals, I quantified *hsp-6* and *hsp-60* transcript levels using ddPCR. These genes encode mitochondrial chaperone proteins whose expression is upregulated upon UPR^{mt} activation (Yoneda et al., 2004, Nargund et al., 2012). I observe significant increases in *hsp-6* and *hsp-60* transcript levels in heteroplasmic animals (Figure 4-2A). I was able to further confirm UPR^{mt} activation using a transgenic fluorescent reporter in which the *hsp-60* promoter drives GFP expression (Figure 4-2B and 4-2C) (Yoneda et al., 2004). These data suggest that UPR^{mt} might be appreciably induced in animals that carry ΔmtDNA above a certain frequency threshold. Consistent with this notion, I was able to observe a weak but positive relationship between UPR^{mt} activation and ΔmtDNA frequency (Figure 4-2D). Taken together, these results indicate that presence of the selfish mtDNA induces UPR^{mt}.

UPR^{mt} modulates ΔmtDNA levels. UPR^{mt} plays a physiologically protective role under conditions that affect mitochondrial function (Nargund et al., 2012, Baker et al., 2012, Runkel et al., 2013). Might the protective role for UPR^{mt} inadvertently create the conditions that allow ΔmtDNA to thrive? According to this hypothesis, I predicted that loss of UPR^{mt} would result in a decrease in ΔmtDNA levels. To test this hypothesis, I knocked down the expression of *atfs-1*, a gene that encodes a transcription factor central to UPR^{mt} activation (Nargund et al., 2012). As predicted, targeting *atfs-1* expression resulted in a significant decrease in ΔmtDNA frequency (Figure 4-3A). I similarly observe a decrease in ΔmtDNA levels in *atfs-1* loss-of-function mutants (Figure 4-3B). Moreover,

wildtype mtDNA levels are well regulated in *atfs-1* loss-of-function mutants, thus ruling out loss of mtDNA copy-number control as a potential explanation for the decrease in ΔmtDNA levels (Figure 4-3C and 4-3D, compare to Chapter 3, Figures 3-2 and 3-3). These data are consistent with the hypothesis that loss of UPR^{mt} exposes ΔmtDNA to more stringent selection.

If UPR^{mt} enables ΔmtDNA propagation, then restoring *atfs-1* should allow ΔmtDNA levels to recover after a period of *atfs-1* knockdown. Indeed, ΔmtDNA levels recover within a single generation when *atfs-1* expression is restored in ΔmtDNA animals after several generations under *atfs-1* knockdown conditions (Figure 4-4A). These data suggest that UPR^{mt} is required for ΔmtDNA to attain high levels. I next tested if the converse was also true—that is, whether forcing the constitutive activation of UPR^{mt} decreases selection against ΔmtDNA, thereby driving ΔmtDNA to higher frequency. For this, I used an *atfs-1* gain-of-function allele to constitutively activate UPR^{mt} (Rauthan et al., 2013). I did not observe any significant increase in the ΔmtDNA levels in animals heterozygous for the *atfs-1* gain-of-function allele (Figure 4-4B). However, given that the starting ΔmtDNA levels in my heteroplasmic strain were already high (nearly 80 percent ΔmtDNA), I speculated that they might not be able to further increase due to an upper threshold effect. It is also possible that given the induction of UPR^{mt} in individuals with high ΔmtDNA levels, the *atfs-1* gain-of-function allele might not induce significant further UPR^{mt} activation in these animals. To overcome these limitations, I tested whether ΔmtDNA levels can rise in *atfs-1* gain-of-function heterozygotes in a population with lower starting ΔmtDNA frequency (approximately 30 percent ΔmtDNA). In this case, I observed a significant increase in ΔmtDNA frequency in *atfs-1* gain-of-function heterozygotes relative to animals homozygous for wildtype *atfs-1* (Figure 4-4C). Together, these results show that *atfs-1* can modulate ΔmtDNA levels.

Loss of UPR^{mt} does not select against ΔmtDNA at the organismal level. Organismal selection provides one potential explanation for the observed decrease in ΔmtDNA frequency upon loss of

atfs-1. Perhaps loss of *atfs-1* combines with high ΔmtDNA levels to more strongly impact host fitness. Consistent with this idea, the knockdown of *atfs-1* expression enhances developmental delay in animals exposed to the oxidative stress-inducing drug paraquat (Runkel et al., 2013). Mutations in *isp-1* and *clk-1*, known to cause mitochondrial stress, similarly compromise development under *atfs-1* knockdown conditions (Nargund et al., 2012). I sought to determine whether knockdown of *atfs-1* causes developmental delay in animals carrying ΔmtDNA. While I observe a mild developmental delay in heteroplasmic animals, consistent with prior observation (see Chapter 2), it is not enhanced by *atfs-1* knockdown (Figure 4-5A). Likewise, I did not observe appreciable levels of embryonic lethality in heteroplasmic animals raised under *atfs-1* RNAi conditions (Figure 4-5B). The absence of an *atfs-1* knockdown-dependent effect on reproductive fitness suggests that selection against ΔmtDNA is unlikely to occur at the organismal level.

UPR^{mt} modulates ΔmtDNA levels via mitophagy. Organelle-level selection provides an alternate possibility for the observed decrease in ΔmtDNA levels upon loss of *atfs-1*. According to this hypothesis, ΔmtDNA might be more susceptible to mitophagy in the absence of UPR^{mt}. Mitophagy is initiated by the accumulation of PINK-1 on the outer membranes of dysfunctional mitochondria, which in turn recruits Parkin to mediate mitophagy (Matsuda et al., 2010, Randow and Youle, 2014). If mitophagy mediates the decrease in ΔmtDNA levels upon loss of UPR^{mt}, then ΔmtDNA levels can be predicted to recover in animals defective for UPR^{mt} if mitophagy is also compromised. In order to test this prediction, I quantified ΔmtDNA levels in *atfs-1*;*pdr-1* double-mutants (Figure 4-6A and 4-6B). I observed significant recovery of ΔmtDNA levels in *atfs-1*;*pdr-1* double-mutant animals compared to *atfs-1* single-mutants. Relative to the wildtype nuclear background, the highest ΔmtDNA levels were in *pdr-1* single-mutants (Figure 4-6B), in agreement with the idea that mitophagy limits the proliferation of ΔmtDNA. In summary, my findings indicate that UPR^{mt} facilitates high levels of ΔmtDNA by protecting the mutant genome from mitophagy, with loss of UPR^{mt} exposing the mutant genome to increased mitophagy.

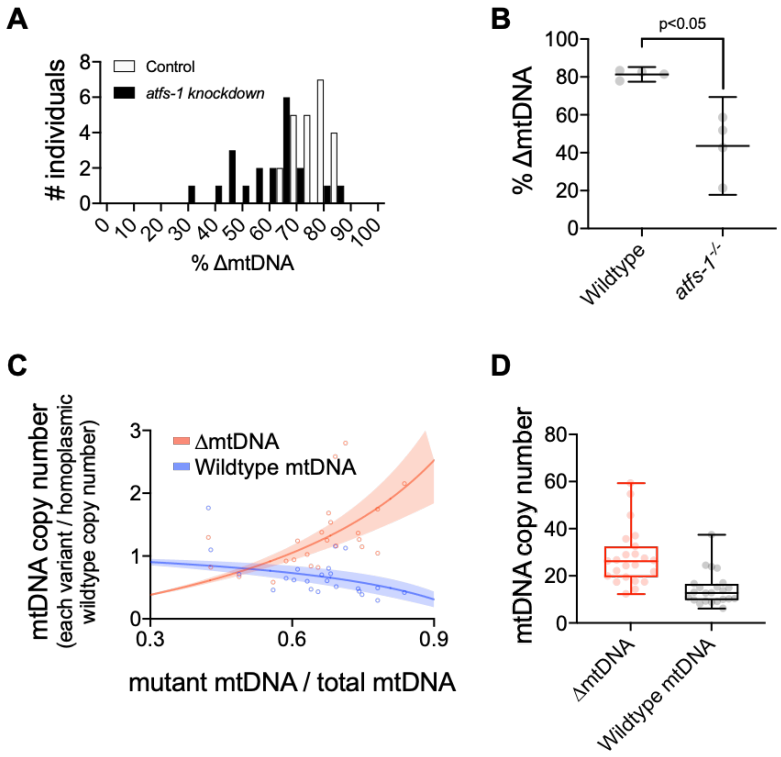

Figure 4-3. Loss of UPR^{mt} activation results in decreased ΔmtDNA levels but does not affect mtDNA copy-number control

(A) Histograms showing ΔmtDNA frequency distributions of heteroplasmic animals grown under RNAi-mediated knockdown of *atfs-1* (N=20), required for UPR^{mt} activation, versus heteroplasmic animals grown on control (empty vector) conditions (N=23).
(B) ΔmtDNA frequency decreases in *atfs-1* loss-of-function mutants compared to ΔmtDNA frequency in hosts expressing wildtype *atfs-1*. N=4. Mann-Whitney test.
(C) Wildtype mtDNA (blue) and ΔmtDNA (red) copy-number values from individual day-4 adult *atfs-1* mutants (N=23, normalized to mean mtDNA copy number in homoplasmic animals and plotted as a function of ΔmtDNA frequency. N=23. Shaded regions represent 95% confidence interval.
(D) Wider variation in ΔmtDNA relative to wildtype copy number ($p<0.05$) in *atfs-1* mutants suggests that copy-number regulation persists in animals with defective UPR^{mt}. Box and whisker plot shows the median, lower and upper quartile (boxes), and minimum and maximum (error bars) mtDNA copy number. F test for differences of variance.
Error bars represent 95% confidence intervals.

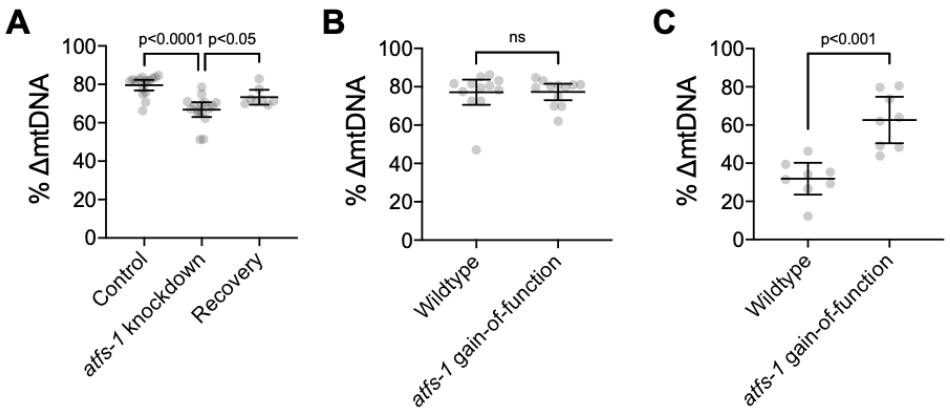

Figure 4-4. Persistence of ΔmtDNA at high frequency depends in part on UPR^{mt} activation

(A) Growth under RNAi-mediated knockdown of *atfs-1* across seven generations reduces average ΔmtDNA frequency (N=16). However, restoration of *atfs-1* expression by removing animals from *atfs-1* knockdown and returning them to control conditions results in recovery of elevated ΔmtDNA frequency in a single generation (N=8). One-way ANOVA with Dunnett's multiple comparisons test.
(B) When starting ΔmtDNA frequency is high (75-80 percent), constitutive UPR^{mt} activation in individuals heterozygous for an *atfs-1* gain-of-function allele causes no further rise in average ΔmtDNA frequency (N=12). Mann-Whitney test.
(C) In contrast to when ΔmtDNA frequency is already high, ΔmtDNA frequency rises dramatically when the *atfs-1* gain-of-function allele is crossed into a strain harboring relatively low (approximately 30 percent) ΔmtDNA frequency (N=8). Mann-Whitney test.
Error bars represent 95% confidence intervals.

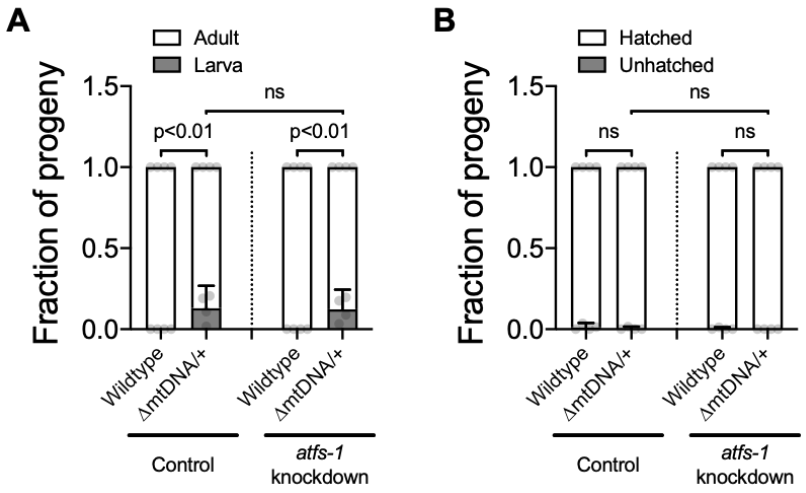

Figure 4-5. Knockdown of UPR^{mt} does not significantly alter the reproductive fitness cost associated with ΔmtDNA

(A) Heteroplasmic individuals exhibit delayed growth: as 100 percent of progeny from wildtype parents reach adulthood in three days, approximately 10 percent of heteroplasmic progeny remain in the larval stage. Knockdown of *atfs-1* showed no effect on development in homoplasmic wildtype animals and did not further enhance the developmental delay in *uaDf5* heteroplasmic animals. N=4 replicate experiments. Two-way ANOVA with Sidak's multiple comparisons test.
(B) No significant difference was observed between heteroplasmic and wildtype animals, or between *atfs-1* knockdown and control conditions, on the percentage of embryos that remain unhatched after one day. N=4 replicate experiments. Two-way ANOVA with Sidak's multiple comparisons test.

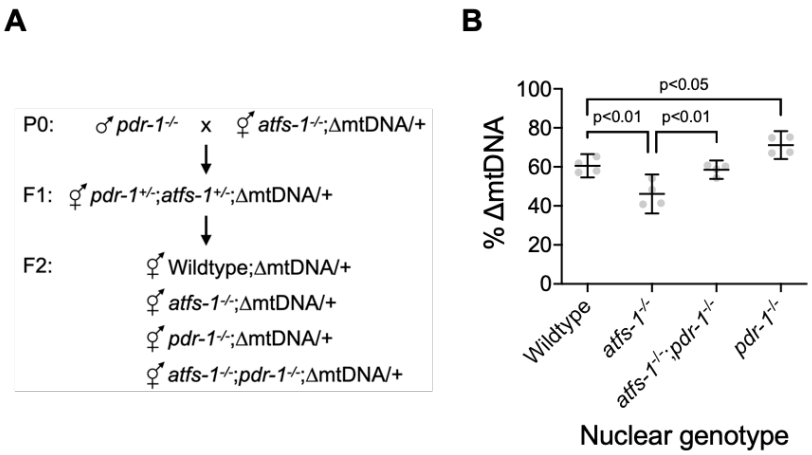

Figure 4-6. Loss of the mitophagy-promoting E3 ubiquitin ligase gene *pdr-1* rescues ΔmtDNA proliferation in UPR^{mt}-defective hosts

(A) Crossing scheme employed to isolate ΔmtDNA animals in wildtype, *atfs-1* mutant, *pdr-1* mutant, and *atfs-1*;*pdr-1* double-mutant backgrounds.
(B) ΔmtDNA in *atfs-1* mutants is restored to high frequency in *atfs-1*;*pdr-1* double-mutants. ΔmtDNA reaches highest levels in *pdr-1* single-mutants. N=4 biological replicates consisting of 10 mature adult animals each. One-way ANOVA with Sidak's multiple comparisons test.
Error bars represent 95% confidence intervals.

Discussion

∆mtDNA activates the mitochondrial unfolded protein response. In this study, I observed UPR^{mt} activation in animals with high ∆mtDNA levels, as determined by measuring transcript levels for two mitochondrial chaperone proteins, HSP-6 and HSP-60, as well as by measuring the fluorescence of a GFP reporter of *hsp-60* expression. How does ∆mtDNA induce UPR^{mt}? Defective protein handling inside mitochondria is believed to trigger UPR^{mt} (Yoneda et al., 2004, Houtkooper et al., 2013, Mouchiroud et al., 2013). Here, I observe overexpression of genes that are encoded in both ∆mtDNA and wildtype mtDNA. However, it is unclear whether the overexpression of these genes at the transcriptional level actually translates to more protein, since ∆mtDNA also lacks several tRNA genes, which could compromise protein synthesis. On the other hand, the dynamics of mitochondrial fusion and fission could redistribute the tRNA molecules encoded by the wildtype genome, potentially giving ∆mtDNA access to all the molecular machinery necessary for protein synthesis. If these transcripts are translated, they might overwhelm the protein-handling environment in the mitochondria. Alternatively, they might result in formation of stoichiometrically imbalanced non-functional electron transport chain complexes. In any case, I observe a decrease in mitochondrially targeted GFP in ∆mtDNA animals, consistent with the hypothesis that either protein import into mitochondria or protein folding inside the mitochondrial matrix is compromised. Future experiments aimed at characterizing the details of the protein-handling environment in heteroplasmic animals will help determine the mechanistic basis of UPR^{mt} induction.

UPR^{mt} activation relies on decreased import efficiency of ATFS-1 into mitochondria. Active protein import into mitochondria is known to rely on the mitochondrial membrane potential. In heteroplasmic animals, although I see UPR^{mt} induction and a role for ATFS-1 in modulating ∆mtDNA levels, mitochondrial membrane potential is likely not compromised. Indeed, I actually see an increase in staining of heteroplasmic animals with TMRE, a mitochondrial membrane

potential-dependent dye. This increase might not be reflective of an actual increase in mitochondrial membrane potential but probably results from an overall increase in mitochondrial organelle mass, since I also observe an increase in staining with MitoTracker Green FM, a dye that localizes to mitochondria independently of the membrane potential. Overall, these data suggest a different molecular basis for decreased ATFS-1 import efficiency than decreased mitochondrial membrane potential.

The mitochondrial unfolded protein response promotes ΔmtDNA proliferation. Mitochondrial stress is known to promote longevity (Dillin et al., 2002, Rea et al., 2007). Additional work has implicated UPR^{mt} in this extension in lifespan (Durieux et al., 2011, Houtkooper et al., 2013). Given the role of UPR^{mt} in alleviating proteotoxic stress in mitochondria (Schulz and Haynes, 2015), it has been proposed to protect mitochondria from age-related decline in proteostasis (Taylor and Dillin, 2011, Jensen and Jasper, 2014). Here I show that UPR^{mt} is activated in the context of high ΔmtDNA frequency, representing an attempt by the cell to rescue mitochondrial function in the presence of ΔmtDNA. However, I also observe UPR^{mt} activation to favor elevated ΔmtDNA levels. The longevity-promoting protective role of this pathway can therefore be viewed as a double-edged sword, by creating the conditions that promote ΔmtDNA proliferation to the detriment of the host. Consistent with this interpretation, heteroplasmic animals expressing an *atfs-1* gain-of-function mutation, which constitutively activates UPR^{mt}, exhibit reduced metabolic activity compared to heteroplasmic animals with wildtype *atfs-1* (Lin et al., 2016).

Why does loss of UPR^{mt} result in reduced ΔmtDNA levels? I suggest that UPR^{mt} protects ΔmtDNA against selection, with loss of UPR^{mt} sensitizing the cell and exposing ΔmtDNA to selection. Selection can operate at the organismal level, arising from a reduction in fitness of animals with high ΔmtDNA levels when UPR^{mt} is compromised. Although I observe a slight developmental delay in animals carrying ΔmtDNA, this delay is not enhanced by *atfs-1* knockdown, nor did I observe

increased rates of non-viable embryos. These data suggest that UPR^{mt} protects ΔmtDNA against selection, perhaps at the organelle level. Under this hypothesis, mitochondria harboring high levels of ΔmtDNA might be more susceptible to mitophagy in the absence of UPR^{mt}. In support of this hypothesis, I observe recovery of ΔmtDNA levels in *atfs-1*;*pdr-1* double-mutants, which are defective for both UPR^{mt} and mitophagy. Interestingly, *pdr-1* mutants exhibit ΔmtDNA levels higher than either the wildtype controls or the double-mutants, consistent with the previously published data that loss of *pdr-1* results in elevated ΔmtDNA frequency (Valenci et al., 2015). Furthermore, overexpression of Parkin is reported to result in selection against mutant mtDNA in cultured mammalian cells (Suen et al., 2010). My observation that ΔmtDNA levels recover in *atfs-1*;*pdr-1* double-mutants suggests that UPR^{mt} protects selfish mtDNA from negative selection at the sub-cellular level.

The ability of UPR^{mt} to relax selection against ΔmtDNA does not, in and of itself, explain the preferential proliferation of ΔmtDNA, particularly when UPR^{mt} activation is restored ("recovery" condition in Figure 4-4A), or when UPR^{mt} is constitutively active (Figure 4-4C), or in *pdr-1* single-mutants with intact UPR^{mt} (Figure 4-6B). However, recall that ΔmtDNA evades the ability of the host to regulate its mtDNA copy number (see Chapter 3). Taken together with the observation that Parkin mediates selection against ΔmtDNA (Figure 4-6), I conclude that ΔmtDNA is exposed to a combination of sub-organismal (within-host) mechanisms, both favoring and disfavoring ΔmtDNA in different ways. Accordingly, the relaxed selection against ΔmtDNA in *atfs-1* mutants may be sufficient to explain ΔmtDNA proliferation, as long as mtDNA copy-number control, and thus ΔmtDNA-biased replication, are not abolished by loss of *atfs-1* (Figure 4-3C and 4-3D). On one hand, these findings do not rule out other possible mechanisms by which *atfs-1* might promote ΔmtDNA propagation. Indeed, other work suggests that mitochondrial biogenesis and organelle fusion-fission dynamics may influence ΔmtDNA levels in an *atfs-1*-dependent manner (Lin et al., 2016). On the other hand, the frequency of mutant mtDNA in *Drosophila* was found to vary

depending on the expression-levels of genes essential for mtDNA synthesis (Chiang et al., 2019) or mitochondrial fusion (Kandul et al., 2016). Given that these processes are regulated by numerous upstream pathways, especially those involved in responding to physiological stress (van der Bliek et al., 2017), the influence of *atfs-1* on ∆mtDNA levels may represent a specific example of a more general phenomenon. In other words, mutant mitochondrial genomes might generally behave selfishly by exploiting their hosts' attempts to preserve metabolic function and to alleviate the stress caused by the mutation.

Generalizability of these findings. As with the "maintenance of wild-type" model of mtDNA copy-number control, successful proliferation of mutant mtDNA via UPR^{mt} activation does not invoke an intrinsic replicative advantage of the mutant genome. In both cases, the proliferation of mutant mitochondrial genomes is linked to a deleterious effect on mitochondrial function, underscoring their behavior as selfish genomes. Also in common with the "maintenance of wild-type" model of mtDNA copy-number control is the evasion by ∆mtDNA of a mechanism that would otherwise limit the proliferation of mutant mitochondrial genomes. In the case of mtDNA copy-number control, ∆mtDNA evades the ability of the cell to inhibit mtDNA synthesis, whereas in the case of UPR^{mt}, ∆mtDNA evades the targeted degradation of dysfunctional mitochondria and their resident genomes. Consequently, an array of mtDNA mutations of varying sizes, including small deletions and point mutations, could be predicted to proliferate selfishly as long as they similarly induce UPR^{mt}, compromise the accurate sensing of mtDNA levels, or both.

Exploitation of homeostatic processes might also underlie persistence of naturally occurring selfish mtDNA. Many natural isolates of *C. briggsae* are heteroplasmic for mutant mtDNA (*nad5*Δ mtDNA) with an approximately 900-basepair deletion that disrupts an essential gene (Howe and Denver, 2008). This *nad5*Δ mtDNA is widespread in *C. briggsae* natural populations despite its deleterious organismal effects (Estes et al., 2011). This mutant variant has also been shown to have a strong

drive to increase in frequency when bottlenecked through small populations (Clark et al., 2012). It will be interesting to determine in the future whether homeostatic mtDNA copy-number control or UPR^{mt} activation contribute to persistence of *nad5*Δ mtDNA in *C. briggsae*.

Although UPR^{mt} is less characterized in mammals, previous reporting suggests that the mechanism by which UPR^{mt} modulates heteroplasmy levels in *C. elegans* reported here may be widely conserved. Specifically, the accumulation of unfolded protein was shown to result in the up-regulation of the chaperone HSPD1 (HSP-60) and the mitochondrial protease CLPP in mammalian cells (Zhao et al., 2002). More recently, the mammalian protein ATF5 has been identified as a candidate regulator of UPR^{mt} in mammals and was shown to mimic *atfs-1* function by activating UPR^{mt} in *C. elegans* (Fiorese et al., 2016), providing an attractive target for future studies seeking to characterize the cellular mechanisms underlying mutant mtDNA dynamics in the context of human disease. Overall, the data presented here suggests that exploitation of homeostatic responses may represent a general strategy underlying the proliferation of pathogenic mtDNA mutations.

Acknowledgments

The *uaDf5* heteroplasmic strain, the *pdr-1*(gk448) and *atfs-1*(e15) mutant strains, and the *zcIs9*, *zcIs17*, and *zcIs18* transgenic lines, were kindly provided by the Caenorhabditis Genetics Center (CGC). The *atfs-1*(tm4525) mutant strain was kindly provided by the Mitani Laboratory through the National Bio-Resource Project of the MEXT, Japan. I would like to thank Harmit Malik of the Howard Hughes Medical Institute and the Fred Hutchinson Cancer Research Center for valuable advice and support, and Sarah Sturgeon for technical assistance. Quantification of mtDNA copy number and ∆mtDNA frequency was conducted with the help of the Simon A. Mallal Laboratory

at Vanderbilt University Medical Center, and I especially thank Rama Gangula of the Mallal Laboratory for training on the use of the droplet digital PCR technology.

Funding for this work was provided by a Helen Hay Whitney Foundation Fellowship, by grants from the Mathers Foundation and the Howard Hughes Medical Institute to the Harmit Malik Laboratory, startup funds from Vanderbilt University for the Maulik R. Patel Laboratory, the NIH-sponsored Cellular, Biochemical and Molecular Sciences Training Program (5T32GM008554-18), and the NIH-funded Tennessee Center for AIDS Research (P30 AI110527) to the Mallal Laboratory.

Part III

The multilevel selection dynamics of a selfish mitochondrial genome

Chapter 5

An experimental strategy to measure separate selection forces acting on selfish mitochondrial genomes both within and between hosts

Adapted in part from Gitschlag, B. L., Tate, A. T., Patel, M. R. 2020. Nutrient status shapes selfish mitochondrial genome dynamics across different levels of selection. *eLife*, 9:e56686

Introduction

Mitochondria were hypothesized to experience conflicting evolutionary pressures since as far back as the early 1980s (Leigh, 1983), before the discovery of disease-causing mitochondrial mutations (Holt et al., 1988). Specifically, natural selection favoring selfish genetic elements was proposed to occur within individual hosts, while selection for host fitness was proposed as a form of "group selection," favoring the faithful transmission of a metabolically competent population of mitochondrial genomes (Leigh, 1983). Consistent with this notion, multiple studies in recent years have identified mitochondrial mutations across a wide diversity of life that propagate while inflicting a fitness cost on their hosts (Havird et al., 2019, Klucnika and Ma, 2019). These observations have inspired a widespread interest among mitochondrial geneticists and microbial ecologists in the evolutionary phenomenon of multilevel selection (Dubie et al., 2020, Havird et al., 2019, Klucnika and Ma, 2019, Shou, 2015), which helps to resolve an apparent paradox associated with the adaptive strategy of cheating. In particular, if cheaters gain a fitness advantage over their cooperative counterparts by unilaterally benefiting from the cooperative relationshps without contributing to them, what explains the successful persistence of cooperation across evolutionary time-scales? The theoretical framework of multilevel selection offers some explanatory insight. Since the emergence and survival of higher levels of biological organization—

such as multicellularity or animal societies—is dependent on cooperation at lower levels, the fitness advantage of cheaters can break down at these higher levels (Moreno-Fenoll et al., 2017, Rainey and Rainey, 2003, Wenseleers and Ratnieks, 2004, Wilson and Wilson, 2008). In hierarchically structured populations, where interactions can have unilateral fitness effects in some cases and synergistic fitness effects in others, these conflicting selection pressures can contribute to the coexistence of cooperators and cheaters within the same population.

Consistent with the predictions of conflicting multilevel selection and with previous observation (Liau et al., 2007, Tsang and Lemire, 2002b), I observed that a deleteriously mutated copy of mitochondrial DNA (ΔmtDNA) can stably persist in a population across multiple generations, in spite of inflicting a substantial cost on host fitness (see Chapter 2). Moreover, the stable persistence of mutant mitochondrial genomes in a state of heteroplasmy does not seem to be easily explained by necessity, such as a need to maintain a balance of two or more mutation-burdened genomes that would each be detrimental on its own (Figures 2-4 and 2-5), nor is the stable maintenance of deleterious heteroplasmy easily explained by an intrinsic replication advantage (Figure 2-6). Taken together, these findings raise the interesting possibility that ΔmtDNA likely behaves as a biological cheater, propagating by exploiting interactions with its host. I sought to follow up on this hypothesis in Chapters 3 and 4, by identifying evidence of physiological mechanisms encoded by the host genome that underpin the cheater behavior of ΔmtDNA. However, evolutionary processes do not occur in a vacuum. On the contrary, natural selection—including the question of which trait has adaptive advantage over others—arises as a consequence of interactions between biological systems and their environments. Taking environmental conditions into account should therefore provide deeper insight into the nature of biological cheaters and the competition with their cooperative counterparts.

In heteroplasmic hosts, the selection advantage of one mtDNA variant over another is well understood to be highly context-specific. In one study focusing on the maintenance of a disease-causing mutant mtDNA variant in cultured cells, a shift in favor of the wildtype genome was achieved by subjecting the cells to nutrient conditions that forced them to rely less on glycolysis, and more on aerobic respiration, for energy production (Santra et al., 2004). Importantly, these effects could be observed for a number of reasons. When a condition is found to induce a population-wide shift in mutant mtDNA frequency, is this because the condition alters the impact of the mutation on host fitness, or because it alters the within-host advantage of the mutant versus wildtype genome, or both? By addressing this question, accounting for selection at different levels can uncover a higher-resolution picture of the overall population dynamics of selfish mitochondrial genomes, enabling mechanistic follow-up and potential practical applications, such as the development of therapeutic interventions. Accordingly, I recently sought to develop an approach to separately measure the strength of natural selection at each level in isolation (Gitschlag et al., 2020), namely within hosts (sub-organismal selection) and at the level of overall host fitness (organismal selection). Here, I describe a simple approach for measuring and modeling the multilevel selection dynamics of ΔmtDNA. In the chapters that follow, I apply this approach across different conditions, host genotypes, and mitochondrial mutations, in order to identify and characterize conditions that shape the outcome of competition between the selfish and cooperative mitochondrial genomes, as well as to identify potential similarities and differences in the population dynamics of different mitochondrial mutations.

Methods

Animal husbandry. *C. elegans* strains used in this study were maintained on 60-mm standard nematode growth medium (NGM) plates (for measuring sub-organismal selection), or 100-mm NGM plates (for measuring organismal selection), seeded with live OP50-strain *E. coli* bacteria as a food source. Nematode strains were incubated at 20˚C. Two *C. elegans* strains were used in this study: the Bristol strain of *C. elegans* representing the wildtype animals, and heteroplasmic animals consisting of the *uaDf5* variant (ΔmtDNA) crossed into the nuclear background of the Bristol strain.

Lysate preparation. To prepare animals for quantification of ΔmtDNA frequency, nematodes were transferred to sterile PCR tubes or 96-well PCR plates containing lysis buffer with 100 µg/mL proteinase K. Lysis buffer consisted of 50 mM KCl, 10 mM Tris pH 8.3, 2.5 mM $MgCl_2$, 0.45% Tween 20, 0.45% NP-40 (IGEPAL), and 0.01% gelatin, in deionized water. Volume of lysis buffer varied by worm count: 10 µL for individual adults, pooled larvae, or pooled embryos; 20 µL for pooled adult progeny for measuring sub-organismal selection; and 50 µL for pooled animal lysates from the competition experiments for measuring organismal selection. After transferring worms to lysis buffer, each tube or plate was immediately sealed and incubated at -80˚C for 10 minutes to rupture nematode cuticles, followed by lysis incubation at 60˚C for 60 minutes (90 minutes for pooled nematodes), and then at 95˚C for 15 minutes to inactivate the proteinase K. Nematode lysates were then kept at -20˚C for stable long-term storage until being used for genotyping and quantification.

Detecting presence of the ΔmtDNA variant. To confirm the presence of heteroplasmic ΔmtDNA and wildtype mtDNA, worms were lysed as described above. Next, the presence of ΔmtDNA and wildtype mtDNA was confirmed by PCR using the ΔmtDNA-specific forward primer 5'-

CCATCCGTGCTAGAAGACAA-3' with the wildtype-specific forward primer 5'-TTGGTGTTACAGGGGCAACA-3' (specific to a site within the region spanning the *uaDf5* deletion), and reverse primer 5'-CTTCTACAGTGCATTGACCTAGTC-3', which is common to both ΔmtDNA and wildtype mtDNA.

Quantifying ΔmtDNA levels. Levels of ΔmtDNA were quantified using droplet digital PCR (ddPCR). Nematodes were lysed as described above, then diluted in nuclease-free water, with a dilution factor varying depending on nematode concentration: 20x for embryos, 200x for pooled larvae, 200x for single adults, 1000x for pooled adults (sub-organismal selection experiment), and 20,000x for pooled nematodes of mixed age (organismal selection experiment). Next, 5 µL of each dilute nematode lysate was combined with 0.25 µL of a 10-µM dilution of each primer needed for amplifying wildtype mtDNA, mutant mtDNA, or both, as necessary. The following primers were used for ddPCR amplification.

For amplifying wildtype mtDNA (paired with primers for amplifying ΔmtDNA):
Forward primer: 5'-GTCCTTGTGGAATGGTTGAATTTAC-3'
Reverse primer: 5'-GTACTTAATCACGCTACAGCAGC-3'
For amplifying ΔmtDNA:
Forward primer: 5'-CCATCCGTGCTAGAAGACAAAG-3'
Reverse primer: 5'-CTACAGTGCATTGACCTAGTCATC-3'

Mixtures of dilute nematode lysate and primer were combined with 12.5 µL of Bio-Rad QX200™ ddPCR EvaGreen Supermix and nuclease-free water to a volume of 25 µL in Eppendorf™ 96-well twin.tec™ PCR plates. Droplet generation and PCR amplification were performed according to manufacturer protocol with an annealing temperature of 58˚C. Wildtype and ΔmtDNA primers were combined in the same reaction, and each droplet was scored as containing either wildtype

or mutant template using the 2-dimensional (518 nm and 554 nm dual-wavelength) clustering plot option in the Bio-Rad QuantaSoft™ program.

Sub-organismal selection assay. The strength of sub-organismal (within-host) selection on ΔmtDNA was measured longitudinally across isolated parent-progeny lineages. Multiple L4-stage (late larval) heteroplasmic animals were picked at random under a dissecting microscope from a stock population carrying ΔmtDNA in the Bristol strain (wildtype) nuclear background. These larvae were transferred to a fresh food plate and incubated for 2 days at 20˚C. The day-2 adults were then segregated onto individual plates and incubated for 4 hours at 20˚C to produce age-synchronized progeny. Each parent was then individually lysed. Three embryos from each parent were also lysed at the same time, in one pooled lysate per three same-parent embryos. After 2 days, three L4-stage larvae were pooled and lysed from each parent, similar to the lysis of embryos. After another 2 days, three adult progeny per parent were pooled and lysed as they reached the age at which the parents were lysed, to obtain age-matched pairs consisting of one parent and three of its adult progeny. Each parent-progeny lineage was individually segregated from the rest. Since ΔmtDNA impacts fecundity, the progeny from parents on the lower end of the ΔmtDNA frequency are expected to be overrepresented in the offspring sampled from a mixed cohort of parents. Lineages were therefore segregated to ensure that the ΔmtDNA frequency from each progeny lysate was being compared with that of its own respective parent, to minimize the effect of organismal selection. To reduce the effect of random drift, progeny from each time-point were lysed in pools of three, across multiple independent biological replicates. The ΔmtDNA frequency of parents and progeny was determined using ddPCR as described above.

Experimental evolution (organismal selection). Selection against ΔmtDNA that occurs strictly at the level of organismal fitness was measured using a competition assay. Heteroplasmic nematodes carrying ΔmtDNA in the Bristol nuclear background were combined with Bristol-strain

nematodes on 10-cm NGM plates seeded with live OP50 *E. coli* as a food source. For the first generation, heteroplasmic and Bristol strain nematodes were age-synchronized. Age synchronization was accomplished using a bleaching protocol. Nematodes from a mixed-age stock food plate were washed off the plate and into a sterile 1.7 mL microcentrifuge tube with nuclease-free water. The water was brought to a volume of 750 µL. The volume of each tube was brought to 1 mL by adding 100 µL of 5 N NaOH and 150 µL of 6% bleach. Each nematode tube was incubated at room temperature for 10 minutes with light vortexing every 2 minutes to rupture gravid adults and release embryos. Nematode tubes were centrifuged for 1 minute at 1,000x g to pellet the nematode embryos. To wash the nematode pellets, the supernatant was removed and replaced with 1 mL of nuclease-free water. After a second spin for 1 minute at 1,000x g, the water was removed and the nematode embryos were resuspended in 100 µL M9 buffer. The resuspended embryos were then transferred to glass test tubes containing 500 µL M9 buffer and incubated overnight at room temperature on a gentle shaker to allow hatching and developmental arrest at the L1 larval stage. On the following day, a glass Pasteur pipette was used to transfer approximately equal quantities of heteroplasmic and homoplasmic-wildtype nematodes onto the 10-cm food plates. Approximately 500 nematodes were transferred to each plate. In addition to 8 competing lines, 8 non-competing control lines were established by transferring only heteroplasmic nematodes onto food plates, with no wildtype nematodes to compete against.

Every 3 days, the generation for each experimental line was reset. To do this, nematodes were washed off the plates using sterile M9 buffer into a sterile 1.7 mL collection tube. Approximately 500 nematodes of mixed age from each line were transferred to a fresh food plate. An additional 500 nematodes were lysed together in a single pooled lysate. Every other generation, 48 additional adults randomly selected from each competition line were lysed individually in order to determine the proportion of heteroplasmic animals remaining in each competition line. This experiment was continued for 10 consecutive generations.

Results

To measure the impact of sub-organismal selection on the propagation of ΔmtDNA across generations, ΔmtDNA frequency was quantified longitudinally at successive developmental stages and across multiple parent-progeny lineages. Individual parent-progeny lineages were maintained in isolation from one another to minimize the confounding effect of organismal selection for lower ΔmtDNA levels. Initially, I observed reduced ΔmtDNA frequency in embryos compared to their parents (Figure 5-1A), consistent with the notion of germline purifying selection (Ahier et al., 2018, Hill et al., 2014, Lieber et al., 2019, Ma et al., 2014, Stewart et al., 2008). However, ΔmtDNA proliferates across development, achieving even higher frequency on average in adult progeny than in their respective parents (Figure 5-1A). Moreover, the magnitude of this proliferation declines as a function of increasing initial ΔmtDNA frequency in the parents (Figure 5-1B), consistent with the phenomenon of negative frequency-dependent selection, a common feature of cheater entities (Dobata and Tsuji, 2013, Dugatkin et al., 2005, Pruitt and Riechert, 2009, Riehl and Frederickson, 2016, Ross-Gillespie et al., 2007). Overall, I have successfully isolated and quantitatively measured the impact of selection at the sub-organismal level on ΔmtDNA propagation across generations.

To measure selection against ΔmtDNA strictly at the level of host fitness, I competed heteroplasmic animals carrying ΔmtDNA against their homoplasmic wildtype counterparts on the same food plate (Figure 5-1C). In parallel, I propagated non-competing control lines consisting exclusively of heteroplasmic animals, with no wildtype animals to compete against. Consistent with organismal selection, I observed a decline in the fraction of individuals carrying ΔmtDNA across all 8 replicate lineages (Appendix 2: Supplemental Figure 5-1A and 5-1B). I also quantified ΔmtDNA frequency directly across all competing and non-competing lines using multiplex droplet digital PCR (ddPCR), which revealed a dramatic decline in ΔmtDNA frequency across all 8

competing lines (Appendix 2: Supplemental Figure 5-1C). This decline was not observed in the non-competing lines, which maintained ∆mtDNA frequency near 60 percent despite minor variation (Figure 2-6B, Appendix 2 and Appendix 4). In order to isolate the effect of organismal selection on ∆mtDNA, I controlled for confounding factors such as sub-organismal ∆mtDNA dynamics. To accomplish this, the ∆mtDNA frequencies of the competing lines were normalized to that of the non-competing lines at each generation. This normalizes population-wide frequency to heteroplasmic (sub-organismal) frequency; since non-competing lines contain only heteroplasmic individuals, their population-wide frequency is equal to average heteroplasmic frequency. Moreover, normalizing to ∆mtDNA frequency of non-competing lines sets the slope of those lines to zero (Figure 5-1D, gray lines). Whatever non-zero slope remains for the competing lines can then be attributed to competition with homoplasmic wildtype individuals—the only variable distinguishing the competing from non-competing lines. In conclusion, I have separately measured the effects of selection on ∆mtDNA at the sub-organismal and organismal levels.

I sought to integrate the measurements of sub-organismal and organismal selection into a single theoretical framework describing the overall population dynamics of ∆mtDNA. The Price Equation, which provides such a framework, describes evolution as the covariance between a trait and its reproductive fitness (Frank, 1997, Price, 1972). Since this equation can accommodate more than one source of covariance, including non-linear interactions (Frank, 2012), it can be used to describe selection at different levels simultaneously:

$$w\Delta z = cov(w, z)_{org} + E[cov(w, z)_{sub}]$$

Here, *z* refers to a heritable, quantifiable trait value. Since mitochondrial genotype consists of a heteroplasmic mix of mtDNA variants, this value can be defined as ∆mtDNA frequency. Fitness *w* refers to the replicative success of ∆mtDNA relative to wildtype mtDNA, defined as the ratio of new ∆mtDNA produced per generation to new wildtype mtDNA per generation (see Appendix 5).

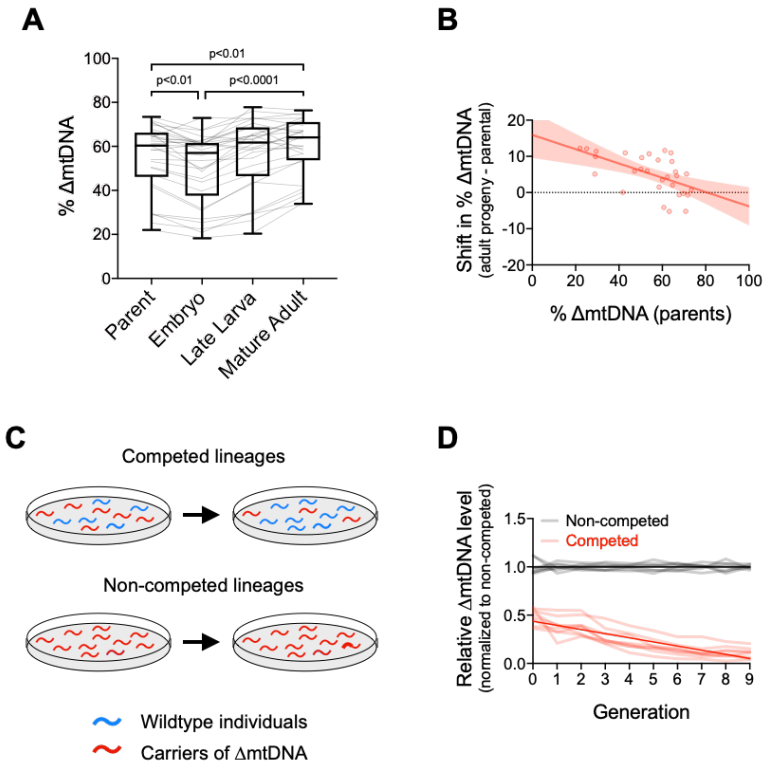

Figure 5-1. Quantification of intergenerational changes in ΔmtDNA frequency due to selection at sub-organismal and organismal levels

(A) ΔmtDNA frequency across parent-progeny lineages, maintained in isolation to minimize the effect of organismal selection. Each light gray line represents a single lineage consisting of a parent lysed individually followed by 3 of its progeny pooled and lysed together at each of 3 developmental time-points. Mature adults were lysed at day 2 of adulthood, the same age at which the parents were lysed, to ensure that parents and their adult progeny were age-matched. Box and whisker plots depict mean heteroplasmic ΔmtDNA frequency and each quartile. N=30 lineages. Friedman test with Dunn's multiple comparisons test.
(B) Shift in ΔmtDNA frequency per generation, obtained by subtracting ΔmtDNA frequency of mature adult progeny in panel (A) from ΔmtDNA frequency of the respective parent, plotted as a function of parental ΔmtDNA frequency. Red shaded region represents 95% confidence interval.
(C) Competition experiment designed to quantify organismal selection against ΔmtDNA.
(D) Population-wide ΔmtDNA frequency across the organismal competition experiment. To isolate the change in ΔmtDNA frequency that occurs strictly due to organismal selection, we controlled for the confounding influence of sub-organismal ΔmtDNA dynamics by normalizing the total population-wide ΔmtDNA frequency of each line to the mean frequency of the non-competed lines at each generation. Because the non-competed lines consist entirely of heteroplasmic individuals, ΔmtDNA frequency across the non-competed populations is equal to mean sub-organismal (heteroplasmic) ΔmtDNA frequency. The overall slope of the non-competing lines is therefore set to zero and the non-zero slope across the competing lines is due to the presence of wildtype animals (see panel C), allowing us to measure the effect of organismal selection by itself. Solid lines represent best-fit regressions across all replicate lineages.
Error bars represent 95% confidence intervals

Subscripts $_{org}$ and $_{sub}$ in this equation (page 93) label covariance between *w* and *z* at organismal and sub-organismal levels, respectively, with covariance defined by the following formula:

$$cov(w,z) = \frac{\sum(w_i - w_{average})(z_i - z_{average})}{n-1}$$

The term *E* in front of the sub-organismal covariance term denotes expected, or average, sub-organismal covariance between *w* and *z*; note that the total sub-organismal change in ∆mtDNA frequency is the average number of replicated copies per template of ∆mtDNA compared to that of wildtype mtDNA. Moreover, since the strength or intensity of selection can be expressed as the selection coefficient *S* (equal to 1-*w*), the change in ∆mtDNA frequency at each respective level of selection can be expressed using the covariance term that relates selection coefficient to ∆mtDNA frequency (see Figure 5-2 for a sample illustration):

$$cov(S, \%\Delta mtDNA) = \frac{\sum(S_i - S_{average})(\%\Delta mtDNA_i - \%\Delta mtDNA_{average})}{n-1}$$

Although the above formula for covariance merely describes how variation in ∆mtDNA frequency relates to variation in selection acting on ∆mtDNA, this relation can be applied to the empirically measured shifts in ∆mtDNA frequency (Figure 5-1 and Appendix 2 to Appendix 4) to derive a function that relates selection to ∆mtDNA frequency, taking both levels of selection into account (for a more detailed derivation of this equation, see Appendix 5):

$$S_{overall} = S_{sub-organismal} + S_{organismal} = (0.01154 * \%\Delta mtDNA - 0.923) + (10^{0.0181 * \%\Delta mtDNA - 1.81})$$

The term shown in the parentheses on the left defines the relationship between ∆mtDNA frequency and sub-organismal selection (plotted in Figure 5-3A). The term shown in the parentheses on the right defines the relationship between heteroplasmic ∆mtDNA frequency and organismal selection (plotted in Figure 5-3B, solid red line), relying on two additional assumptions. The first assumption is that selection coefficient would be zero when ∆mtDNA frequency is 0 percent, since there is no ∆mtDNA to select against. Second, the selection coefficient is assumed to approach 1—in other words, fitness approaches 0, reflecting elimination of ∆mtDNA from the population within a single generation—as ∆mtDNA frequency approaches 100 percent within

hosts. This assumption rests on the fact that the mutation deletes essential genes and should therefore be lethal if present at 100 percent frequency. Summing the organismal and sub-organismal regressions yields the overall, population-wide relationship between heteroplasmic ΔmtDNA frequency and the net selection acting on ΔmtDNA (Figure 5-3C).

This multilevel selection analysis shows that sub-organismal and organismal selection balance—in other words, the overall selection coefficient approaches 0, reflecting no net difference in fitness between ΔmtDNA and wildtype mtDNA—when average heteroplasmic (sub-organismal) ΔmtDNA frequency is near 60 percent (Figure 5-3C). Note that this is the approximate frequency at which ΔmtDNA persists in the non-competing (entirely heteroplasmic) populations, in which the conflicting levels of selection are both in effect (Figure 2-6B and Appendix 2: Supplemental Figure 5-1C). This conclusion is compatible with a range of alternate assumptions regarding the impact of rising heteroplasmic ΔmtDNA frequency on organismal fitness. For example, ΔmtDNA may become lethal before reaching fixation, perhaps at 90 or 95 percent frequency. Consistent with this idea, ΔmtDNA is rarely observed at or above 90 percent frequency (Figures 2-2 and 3-1). Alternatively, the fitness cost of ΔmtDNA might not rise smoothly, as depicted in the non-linear regression in Figure 5-3B. For example, the organismal selection coefficient may rise linearly with increasing heteroplasmic ΔmtDNA frequency up to and beyond the mean of 60 percent, perhaps until reaching a critical threshold before imposing a heavy fitness cost, resulting in an abrupt upward shift in the strength of selection. However, taking these alternative assumptions into account had little effect on my overall conclusions (Figure 5-3B, 5-3C, and Appendix 5). I have thus measured selection on ΔmtDNA at each level separately and integrated them into a unified theoretical framework that robustly predicts the overall, net population dynamics of ΔmtDNA.

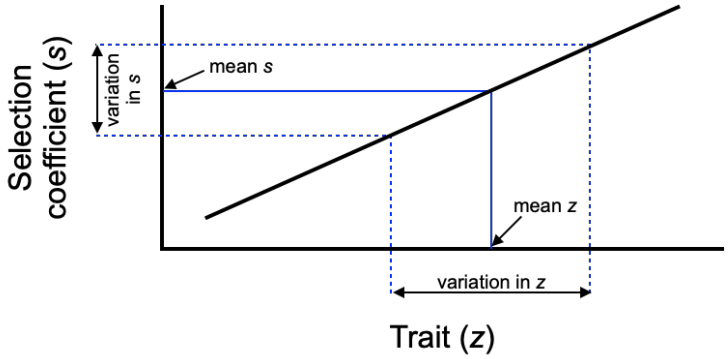

Figure 5-2. Graphical depiction of covariance between a quantifiable trait value and selection coefficient

Covariance implies that variation in a measured trait value *z* (such as ∆mtDNA frequency) corresponds to variation in the selection coefficient *s* (a measure of the strength of the selection force acting to change *z*). A slope of zero indicates that variation in the trait does not correspond to variation in the fitness effects of the trait.

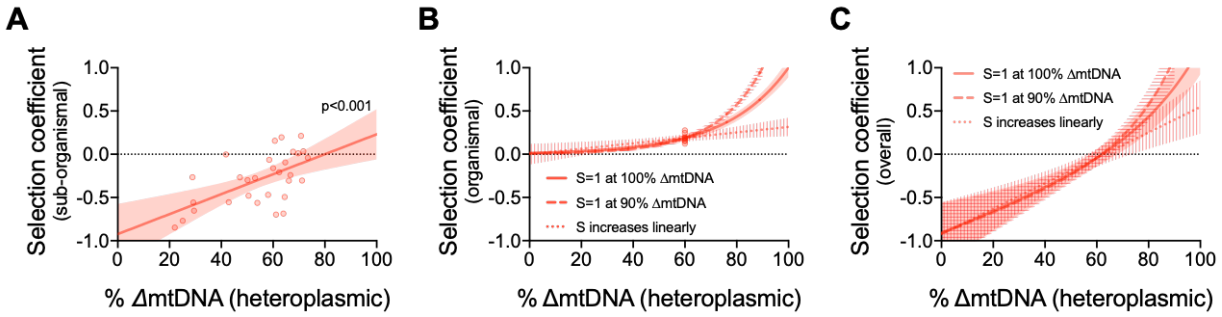

Figure 5-3. Integration of the multilevel selection dynamics of ΔmtDNA using the Price Equation

(A) Sub-organismal selection coefficient plotted as a function of heteroplasmic (sub-organismal) ΔmtDNA frequency. Selection coefficients are calculated from the empirically measured shifts in ΔmtDNA frequency between parents and progeny (Figure 5-1B, Appendix 3 and Appendix 5). Shaded region represents 95% confidence interval.
(B) Organismal selection coefficient plotted as a function of heteroplasmic ΔmtDNA frequency. Selection coefficients are calculated from the population-wide declines in ΔmtDNA frequency during organismal competition (red circles correspond to competing lines in Figure 5-1D; see also Appendix 2: Supplemental Figure 5-1C, Appendix 4 and Appendix 5). However, the selection coefficients are plotted as a function of heteroplasmic (not population-wide) ΔmtDNA frequency. Note that in an entirely heteroplasmic population, as in the non-competing control lines, the overall population-wide ΔmtDNA frequency is equal to the mean heteroplasmic ΔmtDNA frequency. Solid regression and shaded region represents the best fit and 95% confidence interval, respectively, assuming the organismal selection coefficient reaches 1 (lethality) as ΔmtDNA approaches homoplasmic fixation (frequency of 100 percent). Dashed line and horizontally-striped region represents the best fit and 95% confidence interval, respectively, assuming the organismal selection coefficient reaches 1 when heteroplasmic ΔmtDNA frequency is 90 percent. Dotted line and vertically-striped region represents the best fit and 95% confidence interval, respectively, assuming the organismal selection coefficient increases linearly with heteroplasmic ΔmtDNA frequency up to and beyond the mean of 60 percent.
(C) Overall, combined selection coefficient plotted as a function of heteroplasmic ΔmtDNA frequency (summation of plots shown in panels A and B), reflecting the net fitness effects in a heteroplasmic population given each of the alternative organismal covariance models assumed in panel (B).

For each graph shown above, the horizontal dotted line represents no net selection. Above the dotted horizontal line: selection favors wildtype mtDNA. Below the dotted horizontal line: selection favors ΔmtDNA.

Discussion

Multilevel selection offers a powerful explanatory framework to understand cooperator-cheater dynamics. However, investigations of multilevel selection face the challenge of having to account for the confounding influence of selection at one level while trying to estimate the strength of selection at a different level (Goodnight, 2015, Goodnight et al., 1992, Heisler and Damuth, 1987). To overcome these challenges, I developed an approach to empirically quantify selection for cheater mtDNA at the sub-organismal (within-host) level by tracking cheater frequency within isolated parent-progeny lineages. At the organismal (between-host) level, I devised a competition experiment that makes it possible to identify and measure changes in population-wide cheater frequency that occur strictly due to the host fitness cost of the cheater genome. This methodology not only makes it possible to empirically measure selection at different levels, but it also provides a powerful experimental approach that can be applied broadly to future studies seeking mechanistic insight on cooperator-cheater dynamics in hierarchically structured populations.

At the sub-organismal level, I note two trends describing the dynamics of the cheater genome ΔmtDNA. First, ΔmtDNA frequency declines between parent and embryo (Figure 5-1A). This suggests germline purifying selection against deleterious mtDNA, a phenomenon observed across many species (Ahier et al., 2018, Fan et al., 2008, Hill et al., 2014, Lieber et al., 2019, Ma et al., 2014, Stewart et al., 2008). Although the molecular basis for germline purifying selection against ΔmtDNA is unknown, recent work in *Drosophila* has shown that mitochondrial protein synthesis in oocytes is localized around healthy mitochondria, providing a selection advantage for genomes that are free of deleterious mutations (Zhang et al., 2019). Whether similar mechanisms underlie germline purifying selection against ΔmtDNA in *C. elegans* remains to be explored.

Following the initial decline from parent to embryo, ΔmtDNA proliferates across development in a frequency-dependent manner, a common feature of cheater entities (Dobata and Tsuji, 2013, Dugatkin et al., 2005, Pruitt and Riechert, 2009, Riehl and Frederickson, 2016, Ross-Gillespie et al., 2007). Specifically, the sub-organismal advantage of ΔmtDNA declines as its frequency approaches the range of 75-80 percent (Figures 5-1B). One possible explanation for this observation involves resource availability. I previously found that across increasingly higher ΔmtDNA copy number, wildtype mtDNA copy number remains relatively consistent (Figure 3-3). In other words, as ΔmtDNA frequency increases, so does the total size of the mtDNA population. The apparent upper limit observed for sub-organismal ΔmtDNA proliferation could therefore reflect a depletion of resources required for DNA synthesis. Another possibility is the activation of policing mechanisms, a common strategy for enforcing cooperation (Ozkaya et al., 2017, Riehl and Frederickson, 2016). The host genome might prevent ΔmtDNA from rising beyond a certain level by increasing the targeted degradation of underperforming mitochondria via mitophagy. Consistent with this possibility, I find that deletion of the mitochondrial autophagy gene *pdr-1* facilitates an increase in ΔmtDNA frequency (Figure 4-6), suggesting that a cellular policing mechanism encoded by the host genome may limit the extent to which the cheater can proliferate.

Finally, I also explored selection at the organismal level. Consistent with the predictions of multilevel selection, I was able to confirm that ΔmtDNA outcompetes wildtype mtDNA within hosts while the reverse is true at the level of host fitness. The conflicting selection pressures balance when ΔmtDNA is near 60 percent of total mtDNA on average within hosts, enabling ΔmtDNA to stably persist at this level. Remarkably, this conclusion is robust to a range of possible assumptions about how rising ΔmtDNA frequency might impact host fitness (Figure 5-3B and 5-3C). Having separately measured the effects of selection at different levels on a biological cheater, I sought to turn to the question of how environmental factors such as nutrient status influence selection at each of these different levels, which is the primary focus of Chapter 6.

Acknowledgments

The *uaDf5* heteroplasmic strain was kindly provided by the Caenorhabditis Genetics Center (CGC). I would like to thank Ann T. Tate and Allison Hilbun of Vanderbilt University for valuable guidance on experimental design and data analysis. Quantification of mtDNA copy number and ΔmtDNA frequency was accomplished with the help of the Simon A. Mallal Laboratory at Vanderbilt University Medical Center, and I especially thank Rama Gangula of the Mallal Laboratory for training on the use of the droplet digital PCR technology.

Funding for this work was provided by startup funds from Vanderbilt University for the Maulik R. Patel Laboratory, an NIH research project grant (R01 GM123260), the NIH-sponsored Cellular, Biochemical and Molecular Sciences Training Program (5T32GM008554-18), the Ruth L. Kirschstein National Research Service Award Individual Predoctoral Fellowship grant (1F31GM125344), and the NIH-funded Tennessee Center for AIDS Research (P30 AI110527) to the Mallal Laboratory.

Part IV

Environment and the multilevel selection dynamics of a selfish mitochondrial genome

Chapter 6

Diet and host genome interact to shape selfish mitochondrial genome dynamics

Adapted in part from Gitschlag, B. L., Tate, A. T., Patel, M. R. 2020. Nutrient status shapes selfish mitochondrial genome dynamics across different levels of selection. *eLife*, 9:e56686

Introduction

In evolutionary biology, “cheaters” can be defined as entities that benefit at the cost of a cooperative partner (Ghoul et al., 2014). Selfish mitochondrial genomes represent a broad category of biological cheaters, in that they proliferate within hosts at the expense of host fitness (Havird et al., 2019). Given that such a widespread evolutionary adaptive strategy shapes foundational aspects of cell biology in eukaryotic organisms, understanding its basis could have far-reaching implications, potentially yielding valuable insights for both evolutionary and biomedical research. In the preceding chapters, I sought to expand our understanding of selfish mitochondrial genome dynamics by first establishing that the well-characterized selfish mitochondrial DNA (mtDNA) variant *uaDf5* (∆mtDNA) behaves as a genuine selfish genome in the model organism *Caenorhabditis elegans*. This work makes ∆mtDNA ideally suited for follow-up research on the mechanistic basis for the cheating behavior of selfish mitochondrial genomes. Building on this work, I then identify two mechanisms by which ∆mtDNA selfishly proliferates within hosts: the evasion of mtDNA copy-number regulation (see Chapter 3), as well as the evasion of a cellular “policing” mechanism—mitochondrial autophagy, or mitophagy—due to the activation of the mitochondrial unfolded protein response (see Chapter 4). The nucleus encodes numerous mechanisms to maintain a population of mitochondrial genomes that benefit the host, and my findings suggest that evading such mechanisms may represent a general theme in the sub-

organismal (within-host) proliferation of ΔmtDNA. However, natural selection, whether within or between hosts, does not act on genomes in a vacuum. On the contrary, adaptive fitness arises from interactions between biological systems and their environments. I therefore sought to follow up on my previous work by integrating the multilevel selection dynamics of a selfish mitochondrial genome (characterized in Chapter 5) with environmental context (Gitschlag et al., 2020). In this chapter, I describe a genotype-by-environment interaction that plays a crucial role in shaping the outcome of competition between the selfish and cooperative mitochondrial genomes.

Competition over limited resources shapes relative reproductive fitness, and hence Darwinian evolution. Interestingly, some studies have shown that resource abundance can promote the cooperative sharing of public goods, particularly in cases where resource abundance reduces the cost incurred by making cooperative contributions (Brockhurst et al., 2008, Connelly et al., 2017, Sexton and Schuster, 2017). Conversely, resource abundance can also promote selfishness (Chen and Perc, 2014, Ducasse et al., 2015, Velicer et al., 1998). One possible explanation for this apparent discrepancy involves the trade-off between the cost and benefit of cooperation with respect to the use of vital resources. Although resource abundance can promote public-goods cooperation in instances where it reduces the cost of cooperating, resource abundance may also reduce the benefits of cooperating, in which case resource scarcity would be expected to select for cooperation. Indeed, numerous studies have identified resource scarcity as a condition that can promote cooperation (Cao et al., 2015, Chisholm and Firtel, 2004, Koschwanez et al., 2013, Li and Purugganan, 2011, Pereda et al., 2017, Requejo and Camacho, 2011). Consistent with this idea, increased efficiency in resource utilization has been suggested as an adaptive benefit of cooperative groups (Koschwanez et al., 2013, Vanthournout et al., 2016). These studies raise the interesting question of how the environmental variable of resource availability shapes the outcome of competition in a hierarchically structured population, where cooperators and cheaters compete across well-defined levels of selection.

Previous work has shown that the selfish mitochondrial DNA (ΔmtDNA) variant *uaDf5* propagates at the expense of host fitness by exploiting regulatory mechanisms encoded by the host genome. Given the important influence of resource availability on the dynamics of cooperation and selfishness, I sought to expand on my investigation of this biological cheater by integrating genotype with environment, to address the question of how resource availability shapes the multilevel selection dynamics of a selfish mitochondrial genome. In the previous chapter, I describe experiments for isolating and measuring selection on ΔmtDNA separately at the sub-organismal (within-host) level, as well as the organismal level (in other words, selection for host fitness). In this chapter, I adapt the formalized multilevel selection framework to study the effects of food availability and the physiology of nutrient stress tolerance on ΔmtDNA. I find that although diet and nutrient-sensing govern overall mtDNA levels, the preferential proliferation of the selfish genome at the sub-organismal level depends on a key regulator of metabolic stress tolerance, namely the Forkhead box O (FoxO) transcription factor, encoded by the gene *daf-16* in *C. elegans*. Diet restriction strengthens organismal selection against the selfish genome, but only upon deletion of FoxO/DAF-16. I conclude that nutrient availability, and the ability to cope with nutrient scarcity, shape the relative fitness of the cooperators and cheaters both within and between individual hosts.

Methods

Animal husbandry. Except where otherwise indicated, *C. elegans* were maintained on 60-mm standard nematode growth medium (NGM) plates seeded with live OP50-strain *E. coli* bacteria as a food source and incubated at 20˚C. Age-matched nematodes were used in all experiment samples except when tracking heteroplasmy levels across generations in the competition experiments. *C. elegans* stock strains used for this study consisted of the ΔmtDNA heteroplasmy,

insulin receptor mutant *daf-2*(e1370), FoxO mutant *daf-16*(mu86), Parkin mutant *pdr-1*(gk448), mitochondrial fission mutant *drp-1*(tm1108), and apoptosis mutant *ced-3*(ok2734), each crossed into the wildtype (Bristol strain) nuclear background.

Lysate preparation. To prepare nematodes for genotyping and quantification of ΔmtDNA frequency, nematodes were transferred to sterile PCR tubes or 96-well PCR plates containing lysis buffer with 100 µg/mL proteinase K. Lysis buffer consisted of 50 mM KCl, 10 mM Tris pH 8.3, 2.5 mM $MgCl_2$, 0.45% Tween 20, 0.45% NP-40 (IGEPAL), and 0.01% gelatin, in deionized water. Volume of lysis buffer varied by worm count: 10 µL for individual adults or pooled embryos and 20 µL for pooled adult progeny for measuring sub-organismal selection, and 50 µL for pooled animal lysates from the competition experiments for measuring organismal selection. Each tube or plate was then incubated at -80˚C for 10 minutes to rupture nematode cuticles, followed by lysis incubation at 60˚C for 60 minutes (90 minutes for pooled nematodes), and then at 95˚C for 15 minutes to inactivate the proteinase K. Nematode lysates were then stored at -20˚C.

Diet restriction. Diet restriction was accomplished using variable dilutions of UV-inactivated OP50 *E. coli* bacterial lawns on NGM plates. To prepare diet-restricted food plates, 1 L of sterile 2xYT liquid microbial growth medium was inoculated with 1 mL of live OP50 *E. coli* (suspended in liquid LB) using a sterile serological pipette. The inoculated culture was then incubated overnight on a shaker at 37˚C. The following day, the OP50 *E. coli* was pelleted by centrifugation for 6 minutes at 3,900 rpm. The pellet was resuspended to a bacterial concentration of approximately $2x10^{10}$ cells/mL in sterile M9 buffer. This suspension was seeded onto NGM plates (control) or further diluted 100-fold to $2x10^8$ cells/mL in sterile M9 buffer before being seeded onto NGM plates (diet restriction). Plates were incubated upright at room temperature 4 hours to allow the lawns to dry. To inhibit bacterial growth, plates were irradiated with UV radiation using a Stratagene® UV Stratalinker 1800 set to $9.999x10^5$ µJ/cm^2. To confirm inhibition of bacterial growth, UV-treated

plates were incubated overnight at 37˚C. Animals were picked at random under a dissecting microscope onto either control or diet restriction plates.

Genetic crosses and genotyping. To control for nuclear effects on ΔmtDNA proliferation, hermaphroditic nematodes carrying the ΔmtDNA allele *uaDf5* were serially back-crossed into a male stock of the Bristol (N2) *C. elegans* nuclear background for six generations. To investigate the role of insulin signaling in selfish mitochondrial genome dynamics, the alleles *daf-2*(e1370) and *daf-16*(mu86) were introduced to the ΔmtDNA heteroplasmic lineage by classical genetic crosses. To investigate the mechanistic basis by which the insulin signaling pathway regulates mtDNA levels, mutant alleles affecting various putative downstream processes were genetically crossed into the insulin signaling-defective nuclear genotypes. Specifically, the parkin-dependent mitophagy-defective *pdr-1*(gk448), the mitochondrial fission-defective *drp-1*(tm1108), and the apoptosis-defective *ced-3*(ok2734) were each genetically combined with *daf-2*(e1370), both with and without the *daf-16*(mu86) allele. Nuclear genotype was confirmed by PCR using the following oligonucleotide primers:

Mutant and wildtype mtDNA:

Exterior forward: 5’-CCATCCGTGCTAGAAGACAA-3’

Interior forward: 5’-TTGGTGTTACAGGGGCAACA-3’

Reverse: 5’-CTTCTACAGTGCATTGACCTAGTC-3’

daf-2:

Forward: 5’-CATCAAGATCCAGTGCTTCTGAATCGTC-3’

Reverse: 5’-CGGGATGAGACTGTCAAGATTGGAG-3’

daf-16:

Forward: 5’-CACCACGACGCAACACACTAATAGTG-3'

Exterior reverse: 5’-CACGAGACGACGATCCAGGAATCG-3'

Interior reverse: 5’-GGTCTAAACGGAGCAAGTGGTTACTG-3'

pdr-1:

Exterior forward: 5’-GAATCATGTTGAAAATGTGACGCGAG-3'

Interior forward: 5’-CTGACACCTGCAACGTAGGTCAAG-3'

Reverse: 5’-GATTTGACTAGAACAGAGGTTGACGAG-3'

drp-1:

Forward: 5’-CGTCGGATCACAGTCGGC-3'

Reverse: 5’-GCACTGACCGCTCTTTCTCC-3'

ced-3:

Exterior forward: 5’-CAGTACTCCTTAAAGGCGCACACC-3'

Interior forward: 5’-GATTGGTCGCAGTTTTCAGTTTAGAGGG-3'

Reverse: 5’-CGATCCCTGTGATGTCTGAAATCCAC-3'

The insulin signaling receptor allele *daf-2*(e1370) introduces a point mutation that eliminates a *BlpI* restriction endonuclease recognition site. Following PCR amplification, *daf-2* PCR products were incubated with *BlpI* and New England BioLabs CutSmart® buffer at 37˚C for 2 hours prior to gel electrophoresis. Fluorescent reporters used in this study were genotyped by fluorescence microscopy.

Quantifying ΔmtDNA levels. Levels of ΔmtDNA were quantified using droplet digital PCR (ddPCR). Nematodes were lysed as described above, then diluted in nuclease-free water, with a dilution factor varying depending on nematode concentration: 20x for embryos, 200x for single adults, 1000x for pooled adults, 20,000x for pooled nematodes of mixed age from the competition experiments (control diet) or 2,000x for pooled nematodes of mixed age from the competition experiments (restricted diet). The lower dilution factor for the lysates collected from the restricted diet condition was due to the smaller population sizes of nematodes raised on a restricted diet,

which arises from reduced fecundity under diet restriction and was reflected in the number of nematodes present in these lysates. Next, 5 µL of each dilute nematode lysate was combined with 0.25 µL of a 10-µM dilution of the following primers.

For wildtype mtDNA:

Forward primer: 5'-GTCCTTGTGGAATGGTTGAATTTAC-3'

Reverse primer: 5'-GTACTTAATCACGCTACAGCAGC-3'

For ΔmtDNA:

Forward primer: 5'-CCATCCGTGCTAGAAGACAAAG-3'

Reverse primer: 5'-CTACAGTGCATTGACCTAGTCATC-3'

Mixtures of dilute nematode lysate and primer were combined with 12.5 µL of Bio-Rad QX200™ ddPCR EvaGreen Supermix and nuclease-free water to a volume of 25 µL in Eppendorf™ 96-well twin.tec™ PCR plates. Droplet generation and PCR amplification were performed according to manufacturer protocol with an annealing temperature of 58˚C. Wildtype and ΔmtDNA primers were combined in the same reaction, and each droplet was scored as containing either wildtype or mutant template using the 2-dimensional (518 nm and 554 nm dual-wavelength) clustering plot option in the Bio-Rad QuantaSoft™ program.

Insulin signaling inactivation. Insulin signaling was conditionally inactivated using the allele *daf-2*(e1370), encoding a temperature-sensitive variant of the *C. elegans* insulin receptor homolog. Because complete loss of insulin signaling during early larval development results in a stage of developmental arrest (dauer), age-synchronized nematodes were incubated at the permissive temperature of 16˚C until reaching the fourth and final larval stage. L4-stage larvae were then picked at random under a dissecting microscope for either transfer to the restrictive temperature of 25˚C or for continued incubation at 16˚C as a control. After 4 days of incubation, mature adults

were lysed and ddPCR quantification of ∆mtDNA frequency was performed as previously described (see **Quantifying ∆mtDNA levels**). To follow up on the downstream mechanism by which insulin signaling regulates mtDNA dynamics, homoplasmic nematodes were incubated at the restrictive temperature of 25˚C and mtDNA copy number was measured using the same ddPCR primer pair that was used for quantifying the wildtype mtDNA in heteroplasmic worms.

Knockdown of gene expression. Expression knockdown of the *C. elegans* insulin signaling receptor homolog, *daf-2*, was accomplished using feeder plates. Cultures consisting of 2 mL LB and 10 µL ampicillin were inoculated with a bacterial culture obtained from Source BioScience harboring the Y55D5A_391.b (*daf-2*) ORF plasmid clone and incubated overnight on a shaker at 37˚C. Bacteria containing the empty plasmid vector were used to establish a control diet. The following day, 750 µL of culture was transferred to a flask containing 75 mL LB and 375 µL ampicillin and incubated 4-6 hours on a shaker at 37˚C, until $OD_{550\text{-}600}$ >0.8. An additional 75 mL LB was added to the culture along with another 375 µL ampicillin and 600 µL 1 M isopropyl β-D-1-thiogalactopyranoside (IPTG) to induce expression of the small interfering RNA. Cultures were incubated another 4 hours on a shaker at 37˚C. Cultures were then centrifuged for 6 minutes at 3,900 rpm and the resulting bacterial pellets were each resuspended in 6 mL M9 buffer with 8 mM IPTG. Next, 250 µL of resuspension was seeded onto each NGM plate. Plates were allowed to dry at room temperature in the dark and then stored at 4˚C until use. Synchronized L4-stage nematodes were picked at random under a dissecting microscope onto either RNAi knockdown or control plates and incubated at 25˚C until day 4 of adulthood to match the conditions that were used for the *daf-2* mutant allele. Day-4 adults were lysed and their mtDNA copy number was quantified using ddPCR as described above.

Live imaging. Overall mitochondrial content across the wildtype and defective insulin signaling genotypes was measured using the mitochondrial reporter TOMM-20::mCherry. Age-synchronized

nematodes were incubated for 2 days from the L4 stage to mature adulthood at 25˚C, immobilized with 10 mM levamisole, and placed on the center of a 2% agarose pad on a microscope slide. Nematodes were imaged at 10x magnification using a Leica DM6000 B compound fluorescence microscope and mitochondrial fluorescence was quantified using ImageJ. Apoptosis was imaged in *daf-2*(e1370) mutant nematodes and wildtype controls using the CED-1::GFP reporter. Age-synchronized nematodes were incubated for 2 days from the L4 stage to mature adulthood at 25˚C before being immobilized and mounted on microscope slides as described above. Apoptotic cells were imaged using a Zeiss LSM 880 Confocal Laser Scanning microscope at 20x magnification.

Staining and imaging of germline nuclei. Nematode germline nuclei were quantified across age-synchronized mature adults homozygous for *daf-2*(e1370) or *daf-16*(mu86), as well as in double-mutants and wildtype controls. For each genotype, age-synchronized L4-stage nematodes were incubated for 2 days at 25˚C and then placed in a plate containing 3 mL of PBS with 200 µM levamisole. To dissect the nematode gonads, each adult was decapitated using two 25Gx1" hypodermic needles in a scissor-motion under a dissecting microscope. Dissected gonads were fixed for 20 minutes in 3% paraformaldehyde. Fixed gonads were transferred to a glass test tube using a glass Pasteur pipette and the paraformaldehyde was replaced with PBT (PBS buffer with 0.1% Tween 20) and incubated for 15 minutes at room temperature. The PBT was then replaced with PBT containing 100 ng/mL 4',6'-diamidino-2-phenylindole dihydrochloride (DAPI) and the gonads were incubated in darkness for another 15 minutes at room temperature. Gonads were then subjected to 3x consecutive washes, each consisting of a 1-minute centrifugation at 1,000 rpm followed by replacement of the PBT. Gonads were then mounted directly onto a 2% agarose pad on the center of a microscope slide and imaged using a Zeiss LSM 880 Confocal Laser Scanning microscope at 20x magnification.

Measuring sub-organismal selection. Sub-organismal selection for ΔmtDNA was quantified as previously described (see Chapter 5). Briefly, sub-organismal selection was determined by measuring changes in ΔmtDNA frequency as a function of both developmental stage and of initial (parental) ΔmtDNA frequency. Multiple L4-stage heteroplasmic nematodes were picked at random from stocks of nematodes carrying ΔmtDNA in the Bristol strain (wildtype) or *daf-16*(mu86) mutant nuclear background, onto plates seeded with either a control or restricted diet (UV-killed OP50 *E. coli* diluted to approximately $2x10^{10}$ cells/mL or $2x10^{8}$ cells/mL, respectively). After incubating for 2 days at 20˚C, day-2 adults were segregated onto individual plates with the same dietary conditions and incubated for 4 hours at 20˚C to produce age-synchronized progeny. After 4 hours, each parent was individually lysed. Three embryos from each parent were lysed at the same time in one pooled lysate from each parent. After 4 days, three day-2 adult progeny were pooled and lysed from each parent upon reaching the same age at which their respective parents were lysed, to control for the effects of age on ΔmtDNA level. Each parent-progeny lineages was individually segregated from the rest and ΔmtDNA frequency of progeny was compared to that of their own respective parents in order to minimize the confounding influence of organismal selection. Progeny from each time-point were lysed in pools of three to reduce the confounding effect of random drift. The ΔmtDNA frequency of parents and each developmental stage of progeny was determined using ddPCR as described previously (see **Quantifying ΔmtDNA levels**).

Experimental evolution (organismal selection). Selection against ΔmtDNA that occurs strictly at the level of organismal fitness was measured using the competition experiment previously described (see Chapter 5). Briefly, heteroplasmic nematodes carrying ΔmtDNA in the Bristol strain (wildtype) or *daf-16*(mu86) mutant nuclear background were combined with each of their respective homoplasmic (wildtype mtDNA only) counterparts on 10-cm NGM plates seeded with either a control or restricted diet (UV-killed OP50 *E. coli* diluted to approximately $2x10^{10}$ cells/mL

or $2x10^8$ cells/mL, respectively). For the first generation, nematodes were age-synchronized using a bleaching protocol. Nematodes from mixed-age stock food plates were transferred to sterile 1.7 mL microcentrifuge tubes by pipette using nuclease-free water. The water was brought to a volume of 750 µL per tube. The volume of each tube was then brought to 1 mL by adding 100 µL of 5 N NaOH and 150 µL of 6% bleach. Each tube was incubated at room temperature for 10 minutes with light vortexing every 2 minutes to rupture gravid adults and release embryos, followed by centrifugation for 1 minute at 1,000x g to pellet the nematode embryos. To wash the nematode pellets, the supernatant was removed and replaced with 1 mL of nuclease-free water followed by another spin for 1 minute at 1,000x g. The nematode embryos were resuspended in 100 µL M9 buffer and transferred to glass test tubes containing 500 µL M9 buffer for overnight incubation at room temperature on a gentle shaker to allow hatching and developmental arrest at the L1 larval stage. The next day, nematodes were transferred in approximately equal quantities of heteroplasmic and homoplasmic-wildtype nematodes onto the 10-cm food plates containing either a control or restricted diet. Approximately 500 nematodes were transferred to each plate. In addition to 6 replicate competition lines, 6 non-competing control lines were established by transferring only heteroplasmic nematodes randomly selected from the same overnight incubation tubes onto food plates, with no homoplasmic-wildtype nematodes to compete against. Every 3 days, the generation for each experimental line was reset by transferring approximately 200 nematodes of mixed age from each line onto a fresh food plate containing the same dietary condition as in the previous generation (200 nematodes were transferred instead of 500 due to the smaller brood sizes on a restricted diet). An additional 200 nematodes were lysed together in a single pooled lysate per replicate. This experiment was continued for 8 consecutive generations and individual adults from each competition line were lysed to determine the fraction of heteroplasmic nematodes in each competition line after the 8th generation.

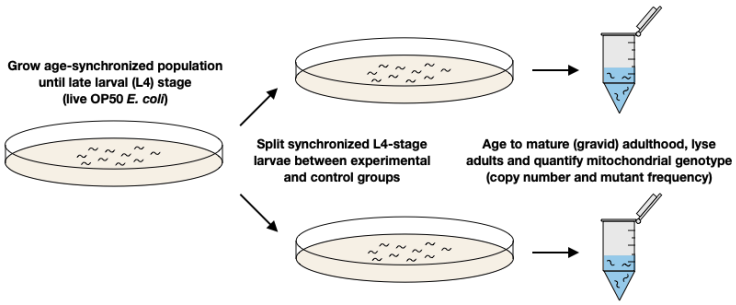

Table 6-1: Experimental conditions under which changes in ∆mtDNA frequency were assayed

Experiment	Food source	Experimental condition	Control
Dietary restriction	UV-inactivated OP50 *E. coli*	Control diet diluted 100-fold in M9 buffer	OP50 *E. coli* resuspended in M9 buffer and UV-inactivated
Insulin signaling inactivation	Live OP50 *E. coli* or RNAi HT115 *E. coli*	25˚C with temperature-sensitive *daf-2*(e1370) or siRNA against wildtype *daf-2*	25˚C with wildtype *daf-2* and live OP50 *E. coli* or control (siRNA-free) HT115 *E. coli*
UV inactivation of bacterial growth	OP50 *E. coli* (live or UV-inactivated)	UV-inactivated OP50 *E. coli*	Live OP50 *E. coli*

Figure 6-1 (Top). Workflow for measuring impact of dietary and metabolic perturbations on ∆mtDNA frequency
Schematic of experimental strategy to assay the impact of dietary and pharmacological approaches to perturb ∆mtDNA frequency.

Table 6-1 (Bottom). Conditions under which changes in ∆mtDNA frequency were explored

Results

Nutrient availability influences sub-organismal ΔmtDNA dynamics. Here I sought to investigate how resource availability affects the multilevel selection dynamics of a selfish mitochondrial genome (ΔmtDNA). Nematodes were raised on food plates seeded with either a high or low concentration of *E. coli* (OP50 strain), which were UV-killed to prevent further bacterial growth (Figure 6-1 and Table 6-1). Although UV-killed OP50 partially mimics diet restriction (Win et al., 2013), I found that animals raised on the more restricted (low concentration) diet harbored significantly lower ΔmtDNA frequency compared to those raised on a more abundant (high concentration) control diet (Figure 6-2A). Moreover, sub-organismal ΔmtDNA frequency is even higher in animals raised on live food (Figure 6-2B). Despite the attenuated ΔmtDNA proliferation on UV-killed food, I still observe noteworthy dietary effects that result simply by varying the concentration of the UV-killed food. First, the initial selection against ΔmtDNA between parent and embryo was abolished by diet restriction, corresponding to a 100-fold dilution of the control diet (Figure 6-2C and 6-2D). Second, ΔmtDNA frequency rose from embryos to adults on a control diet, recovering from the initial purifying selection between parent and embryo (Figure 6-2C), but failed to do so in animals grown on a restricted diet (Figure 6-2D). These observations reveal complex, life-stage-specific effects of diet on ΔmtDNA dynamics: a plentiful diet selects against ΔmtDNA between parent and embryo but selects for ΔmtDNA across development.

ΔmtDNA exploits nutrient sensing to proliferate across development. To better understand the role of nutrient status in the cheating behavior of ΔmtDNA, I focused on sub-organismal ΔmtDNA proliferation across development. In particular, I hypothesized that the insulin-signaling pathway underlies ΔmtDNA proliferation. Insulin acts as a nutrient-dependent growth hormone and regulator of metabolic homeostasis (Figure 6-3A), tailoring the appropriate physiological responses to external nutrient conditions (Badisco et al., 2013, Danielsen et al., 2013, Lee and Dong, 2017,

Lopez et al., 2013, Michaelson et al., 2010, Puig and Tjian, 2006, Shiojima et al., 2002, Das and Arur, 2017, Porte et al., 2005). *C. elegans* expressing a defective allele of the insulin receptor homolog *daf-2* perceive starvation, even in presence of food. However, disrupting insulin signaling in young larvae causes the dauer phenotype, a form of developmental arrest (Gottlieb and Ruvkun, 1994). Thus, I used a temperature-sensitive *daf-2* allele to conditionally inactivate insulin signaling. Animals were incubated at a permissive temperature (16˚C) to preserve insulin signaling during early larval development, thereby preventing developmental arrest. Animals were transferred to the restrictive temperature (25˚C) beginning at the last larval stage (L4) to inactivate insulin signaling during adult maturation, when most mtDNA replication occurs. Compared to animals with intact insulin signaling, I observed lower ΔmtDNA frequency in animals expressing the defective *daf-2* allele (Figure 6-3B). This difference was absent in control lines that were kept exclusively at the permissive temperature of 16˚C (Figure 6-3C), suggesting that loss of insulin signaling limits ΔmtDNA proliferation. Moreover, no overall change in ΔmtDNA frequency occurred across 4 independent lineages of *daf*-2 mutants, even after 4 consecutive generations of alternating between adult maturation at 25˚C and subsequent larval recovery at 16˚C (Figure 6-3D). In contrast, ΔmtDNA frequency increased substantially in insulin signaling-intact controls. These data show that nutrient sensing via the insulin-signaling pathway is involved in sub-organismal proliferation of ΔmtDNA.

The insulin receptor communicates nutrient status to the cell largely through the negative regulation of the Forkhead box O (FoxO) family of transcription factors (O-Sullivan et al., 2015), encoded by the gene *daf-16* in *C. elegans* (Figure 6-3A). Nutrient limitation or inactivation of the receptor activates FoxO/DAF-16, resulting in altered expression of its target genes. Interestingly, deletion of *daf-16* restores the proliferation of ΔmtDNA in animals defective for *daf-2* function (Figure 6-3B). Based on these results, I conclude that insulin signaling promotes sub-organismal ΔmtDNA proliferation by inhibiting the function of the protein FoxO/DAF-16.

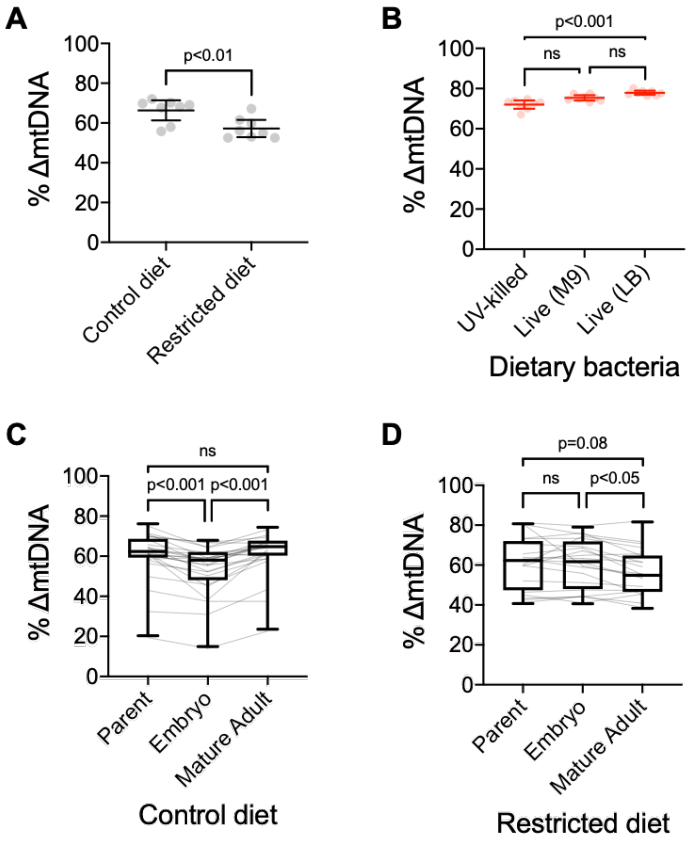

Figure 6-2. Nutrient abundance promotes preferential proliferation of the selfish genome

(A) ΔmtDNA frequency on restricted versus control diet. Nematodes were maintained at 20˚C on a diet of UV-killed OP50 *E. coli*. N=8 pooled lysates of 5 age-synchronized day-4 adults each. Mann-Whitney test.
(B) ΔmtDNA frequency in age-synchronized adults maintained at 20˚C on one of three food plates: UV-killed OP50 *E. coli*, live OP50 suspended in M9 buffer, and live OP50 suspended in LB medium. N=8 pooled lysates of 10 animals each. One-way ANOVA with Dunnett's multiple comparisons test.
(C-D) ΔmtDNA frequency across parent-progeny lineages raised on control (C) or restricted (D) diet. Each light gray line represents a single lineage consisting of a parent lysed individually followed by 3 of its progeny pooled and lysed together at each of 2 developmental time-points. Animals were maintained at 20˚C on a diet of UV-killed OP50 *E. coli*. Mature adults were lysed at day 2 of adulthood, the same age at which the parents were lysed, to ensure that parents and their adult progeny were age-matched. Box and whisker plots depict mean ΔmtDNA frequency and each quartile. N=24 lineages (control diet); N=20 lineages (restricted diet). Friedman test with Dunn's multiple comparisons test.
Error bars represent 95% confidence intervals.

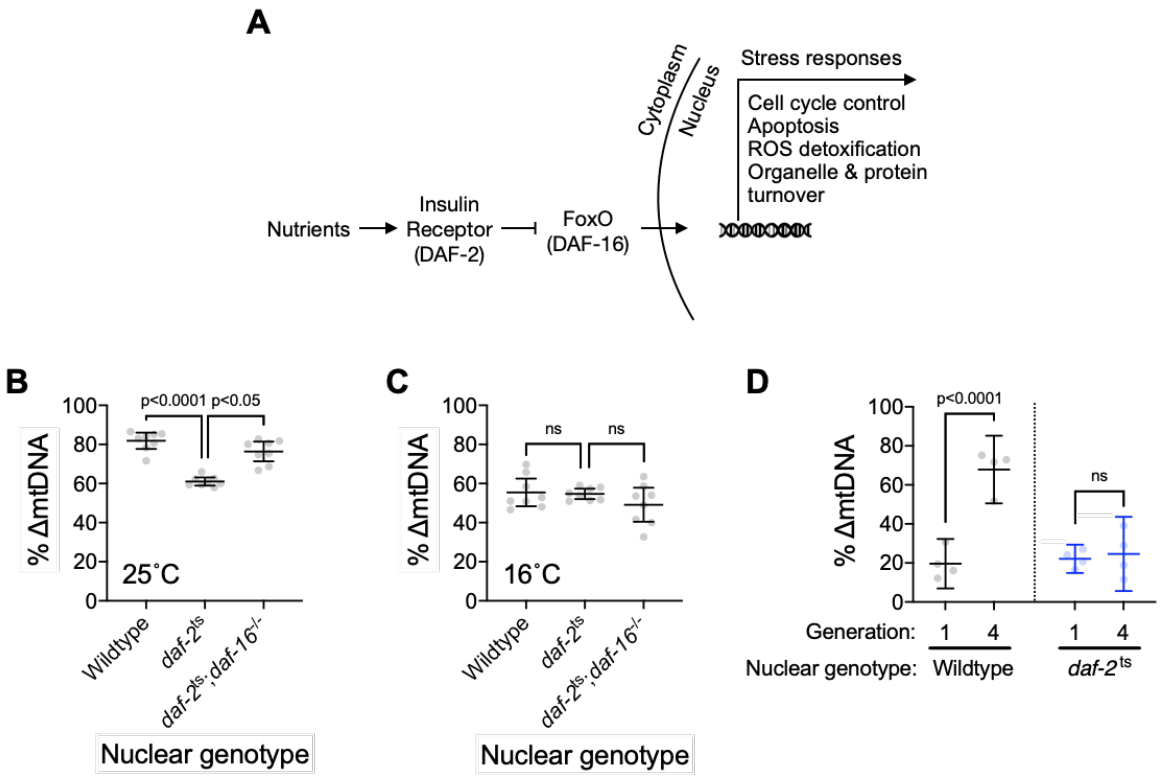

Figure 6-3. The insulin signaling pathway modulates ΔmtDNA frequency by inhibiting FoxO/DAF-16

(A) FoxO-dependent insulin signaling cascade with *C. elegans* homologs in parentheses.
(B) ΔmtDNA frequency among wildtype, *daf-2*(e1370) mutant, and *daf-2*(e1370);*daf-16*(mu86) double-mutant host genotypes, incubated at 16˚C until L4 larval stage and then transferred to 25˚C (the restrictive temperature for the *daf-2* mutant allele) for adult maturation. Animals were maintained on a plentiful diet consisting of live OP50 *E. coli*. N=8 pooled lysates of 5 age-synchronized day-4 adults each. Kruskal-Wallis ANOVA with Dunn's multiple comparisons test.
(C) ΔmtDNA frequency among wildtype, *daf-2*(e1370) mutant, and *daf-2*(e1370);*daf-16*(mu86) double-mutant genotypes maintained at 16˚C (the permissive temperature for the *daf-2* mutant allele), on a plentiful diet consisting of live OP50 *E. coli*. N=8 pooled lysates of 5 age-synchronized adults each. Kruskal-Wallis ANOVA with Dunn's multiple comparisons test.
(D) ΔmtDNA frequency in generation 1 versus generation 4, between wildtype and the temperature-sensitive allele *daf-2*(e1370). Starting with heteroplasmic animals carrying ΔmtDNA at low frequency, embryos from each of four consecutive generations were incubated at the permissive temperature of 16˚C to preserve DAF-2 function during larval development and prevent developmental arrest, followed by transfer of L4-stage larvae to 25˚C, the restrictive temperature of the *daf-2*(e1370) allele, to inactivate DAF-2 during progression to adulthood and the production of progeny. N=4 lysates containing 5 pooled age-synchronized adults each. Two-way ANOVA with Sidak's multiple comparisons test.
All experiments featured in this figure used nematodes that were lysed at day 4 of adulthood. Error bars represent 95% confidence intervals.

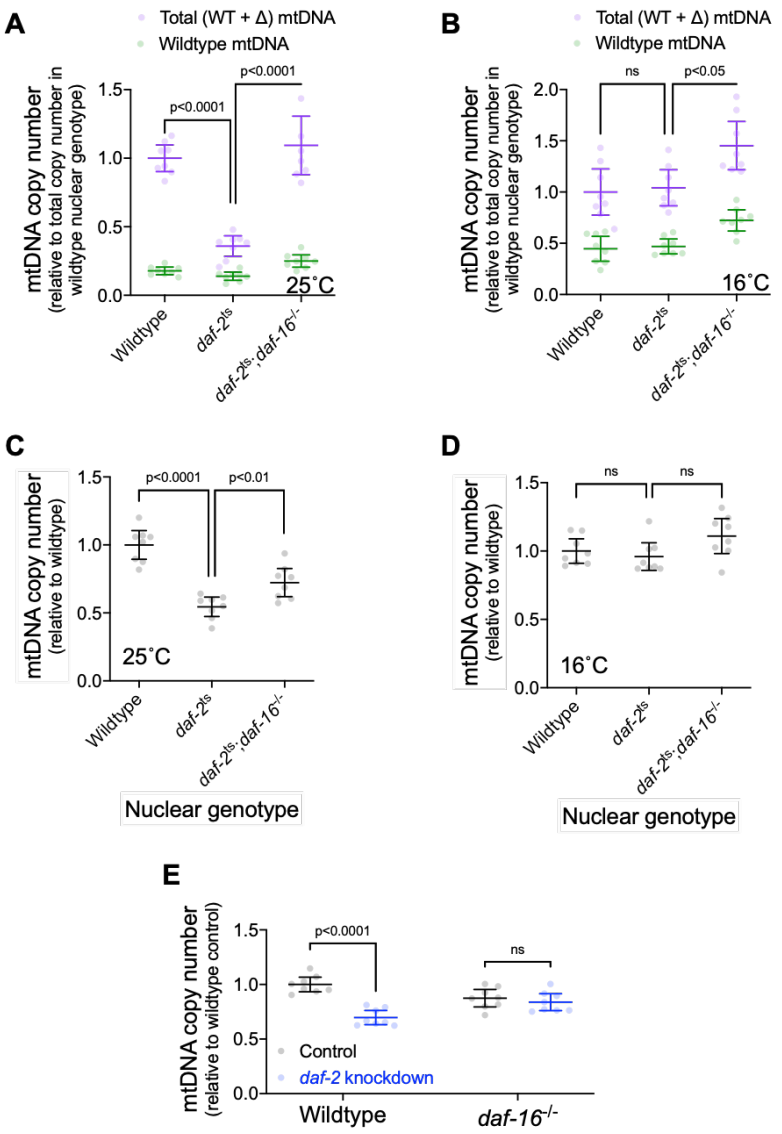

Figure 6-4. FoxO/DAF-16 inhibition by the insulin receptor DAF-2 increases overall mtDNA copy number in a manner that preferentially drives up ΔmtDNA frequency

(A) mtDNA copy number of individuals in Figure 6-3B, incubated from L4 larval stage to adulthood at 25˚C, normalized to total mtDNA from wildtype nuclear background. Green and purple represent wildtype and total mtDNA copy number, respectively, with the vertical distance between green and purple representing ΔmtDNA copy number. N=8 pooled lysates of 5 age-synchronized adults each. Two-way ANOVA with Sidak's multiple comparisons test; p-values reflect comparisons of total mtDNA copy number.
(B) mtDNA copy number of individuals in Figure 6-3C, maintained at 16˚C (the permissive temperature for the *daf-2* mutant allele), normalized to total mtDNA from wildtype nuclear background. Green and purple represent wildtype and total mtDNA copy number, respectively, with the vertical distance between green and purple representing ΔmtDNA copy number. N=8 pooled lysates of 5 age-synchronized adults each. Two-way ANOVA with Sidak's multiple comparisons test; p-values reflect comparisons of total mtDNA copy number.
(C) mtDNA copy number in homoplasmic adults of wildtype, *daf-2*(e1370) mutant, and *daf-2*(e1370);*daf-16*(mu86) double-mutant host genotypes, incubated from L4 larval stage to adulthood at 25˚C. Animals were maintained on a plentiful diet consisting of live OP50 *E. coli*. N=8 pooled lysates of 5 age-synchronized day-4 adults each. One-way ANOVA with Dunnett's multiple comparisons test.

(D) mtDNA copy number in homoplasmic adults of wildtype, *daf-2*(e1370) mutant, and *daf-2*(e1370);*daf-16*(mu86) double-mutant genotypes, maintained at 16˚C (the permissive temperature for the *daf-2* mutant allele), on a plentiful diet consisting of live OP50 *E. coli*. N=8 pooled lysates of 5 age-synchronized adults each. One-way ANOVA with Dunnett's multiple comparisons test.
(E) mtDNA copy number in homoplasmic adults (lacking ∆mtDNA) of either wildtype or null *daf-16*(mu86) host genotype, on either *daf-2* RNAi knockdown or empty-vector control conditions. N=8 lysates containing 5 pooled age-synchronized day-4 adults each. Two-way ANOVA with Sidak's multiple comparisons test.
Experiments depicted in panels (A) and (C) used nematodes that were maintained at 16˚C during larval development and transferred at the L4 stage to 25˚C for adult maturation, corresponding to the permissive and restrictive temperatures for the *daf-2*(e1370) allele, respectively.
All experiments featured in this figure used nematodes that were lysed at day 4 of adulthood. Error bars represent 95% confidence intervals.

How does DAF-16-dependent insulin signaling affect ΔmtDNA proliferation? The reduction of ΔmtDNA frequency by DAF-2 inactivation, and the rescue of ΔmtDNA frequency by loss of DAF-16, are almost entirely attributable to large differences in the copy number of the mutant genome alone (Figure 6-4A and 6-4B). In other words, insulin signaling promotes elevated total mtDNA copy number, perhaps as a driver of ΔmtDNA proliferation or as a consequence of it. To distinguish between these possibilities, I quantified copy number in animals lacking ΔmtDNA. Homoplasmic wildtype mtDNA copy number was quantified using the multiplex droplet digital PCR (ddPCR) method. To obtain relative copy number, raw mtDNA copy number across each nuclear genotype was normalized to that of the wildtype controls. In homoplasmic animals (lacking ΔmtDNA), I observed lower mtDNA copy number upon loss of insulin signaling, whether by *daf-2* mutation (Figure 6-4C and 6-4D) or by knockdown of *daf-2* gene expression (Figure 6-4E), consistent with previous work in *Drosophila* (Wang et al., 2019). Loss of DAF-16 partially but significantly rescued copy number (Figure 6-4C to 6-4E). Together, these data suggest that DAF-2 signaling inhibits DAF-16 to allow high mtDNA copy number, which permits sub-organismal ΔmtDNA proliferation.

How does DAF-16 suppress mtDNA copy number? This suppression could be achieved via mechanisms that result in the elimination of mitochondria, either at the organelle level through increased mitochondrial autophagy (mitophagy) or at the cellular level through increased apoptosis. Consistent with these possibilities, previous studies have identified FoxO/DAF-16 as a regulator of genes involved in autophagy and apoptosis (Murtaza et al., 2017, Webb and Brunet, 2014, Webb et al., 2016). I therefore reasoned that loss of insulin signaling might lead DAF-16 to suppress mtDNA copy number, by upregulating either the direct destruction of mitochondria or cell death in the female germline. To test this idea, I genetically targeted PINK1/Parkin-dependent mitophagy using a deletion of *pdr-1*, encoding the *C. elegans* Parkin homolog. I genetically targeted apoptosis with a deletion of *ced-3*, encoding the terminator caspase in *C. elegans*. I observed no increase in germline apoptosis in *daf-2* mutants (Figure 6-5A and 6-5B).

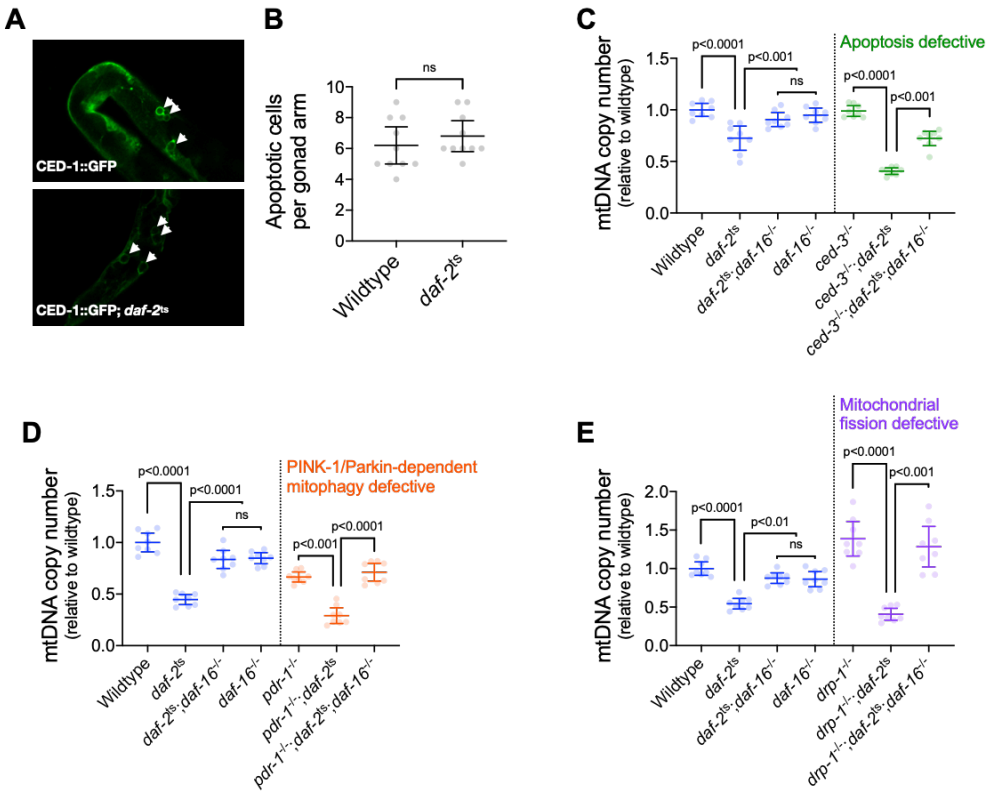

Figure 6-5. Inactivation of DAF-2 suppresses mtDNA copy number in a FoxO/DAF-16-dependent manner but not through apoptosis, Parkin-dependent mitophagy, or mitochondrial fission

(A and B) Images (A) and quantification (B) of apoptosis as indicated by the engulfment of apoptotic cells by the reporter CED-1::GFP (white arrows in panel A), between age-synchronized adults of wildtype or temperature-sensitive *daf-2*(e1370) mutant genotype. Nematodes were maintained on a diet of live OP50 *E. coli* at 16˚C during larval development and transferred at the L4 stage to 25˚C for adult maturation, corresponding to the permissive and restrictive temperatures for the *daf-2*(e1370) allele, respectively, and were imaged at day 2 of adulthood. N=10 age-synchronized adults. Mann-Whitney test.
(C-E) mtDNA copy number in age-synchronized adults of wildtype, temperature-sensitive *daf-2*(e1370) mutant, null *daf-16*(mu86) mutant, or double-mutant genotype. Copy number is also shown in wildtype, *daf-2*(e1370), and *daf-2*(e1370);*daf-16*(mu86) double-mutant adults each paired with *ced-3*(ok2734) (C), *pdr-1*(gk448) (D), or *drp-1*(tm1108) (E), representing loss-of-function alleles of the terminator caspase CED-3, the Parkin homolog, or dynamin-related protein, respectively. Copy number in *daf-16*(mu86) single-mutants is also shown. N=8 lysates containing 5 pooled age-synchronized day-4 adults each. One-way ANOVA with Sidak's multiple comparisons test.
Error bars represent 95% confidence intervals

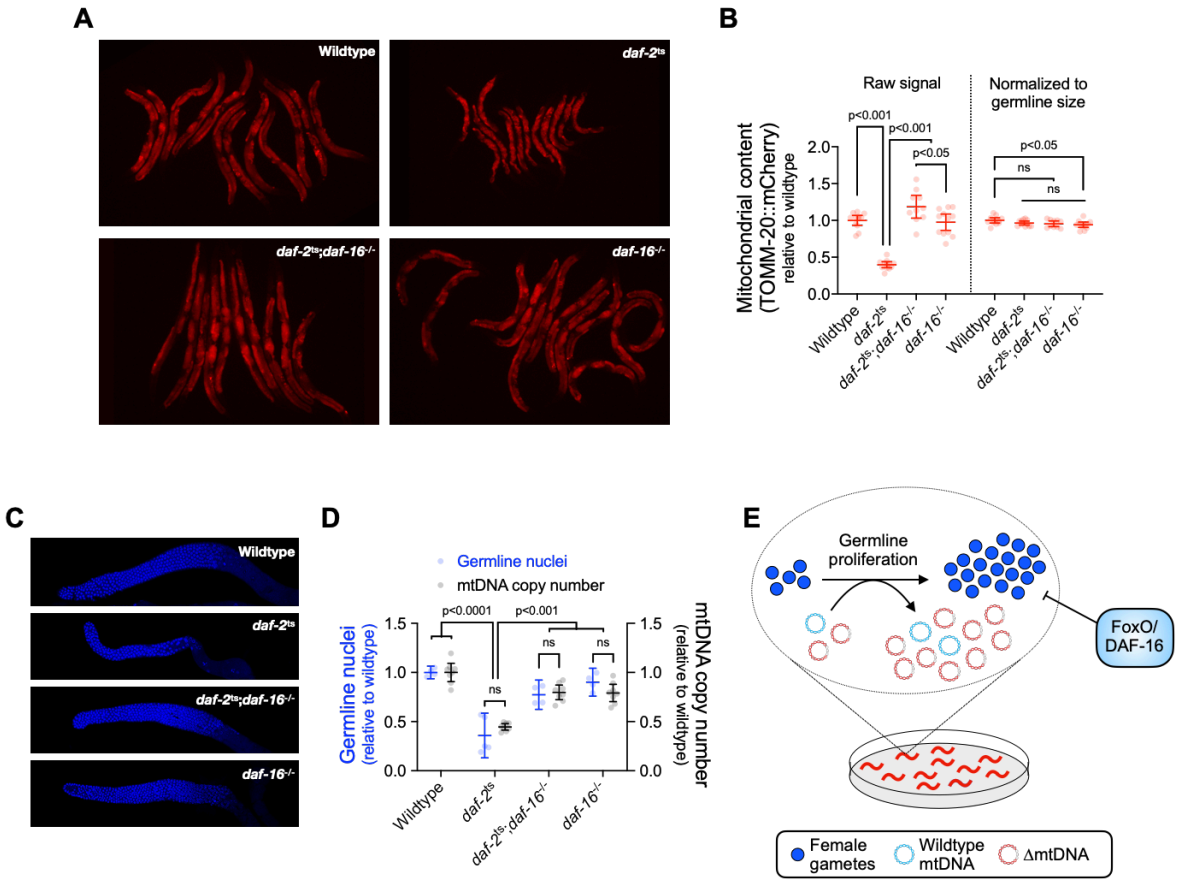

Figure 6-6. FoxO/DAF-16 activation upon loss of insulin signaling suppresses mtDNA content via regulation of germline proliferation

(A-B) Images (A) and quantification (B) of germline mitochondria labeled with TOMM-20::mCherry across wildtype, *daf-2*(e1370), *daf-16*(mu86), or double-mutant genotype. Each data point in (B) represents one adult visualized in (A). One-way ANOVA with Sidak's multiple comparisons test.
(C-D) Representative images (C) and quantification (D) of DAPI-stained nuclei with mtDNA copy number across wildtype, *daf-2*(e1370), *daf-16*(mu86), or double-mutant genotype. Each gray data point represents one adult female gonad. For mtDNA copy number, N=8 pooled lysates of 5 age-synchronized adults each. Two-way ANOVA with Sidak's multiple comparisons test.
(H) Schematic showing that upon loss of insulin signaling, FoxO/DAF-16 limits ΔmtDNA proliferation by restricting germline development.
All experiments featured in this figure used nematodes that were maintained on a diet of live OP50 *E. coli* at 16˚C during larval development and transferred at the L4 stage to 25˚C for adult maturation, corresponding to the permissive and restrictive temperatures for the *daf-2*(e1370) allele, respectively. Imaging was conducted on day-2 adults to visualize germlines at peak fecundity (Hughes et al., 2007).
Error bars represent 95% confidence intervals

Moreover, mtDNA copy number in *daf-2* mutants was not rescued by loss of apoptosis nor PINK-1/Parkin-dependent mitophagy (Figure 6-5C and 6-5D). Because mitochondrial degradation can occur in a PINK1/Parkin-independent manner (Allen et al., 2013, Di Rita et al., 2018, Hibshman et al., 2018), I therefore also tested for a potential role of mitochondrial fission, a common precursor of mitophagy, using a deletion in the gene *drp-1*, which encodes a dynamin-related protein important for mitochondrial fission. Although I observe an increase in mtDNA copy number when mitochondrial fission is disrupted in animals with intact insulin signaling (Figure 6-5E), consistent with reduced mitophagy, I did not observe a rescue of mtDNA copy number in *daf-2*;*drp-1* double-mutants. These data suggest that the suppression of mtDNA content upon loss of insulin signaling is not mediated through the elimination of mitochondria by PINK1/Parkin-dependent mitophagy, mitochondrial fission, or apoptosis.

Alternatively, DAF-16 might restrict mtDNA biogenesis. Nutrient availability and insulin signaling each promote development of the female germline (Angelo and Van Gilst, 2009, Drummond-Barbosa and Spradling, 2001, Michaelson et al., 2010, Narbonne and Roy, 2006, Shim et al., 2002), which harbors the vast majority of mtDNA in the adult nematode (Bratic et al., 2009, Tsang and Lemire, 2002a). I observed that mitochondrial organelle quantity and mtDNA copy number are proportional to gonad size and cell count, respectively, across wildtype, *daf-2* mutant, and *daf-2*;*daf-16* double-mutants (Figure 6-6A to 6-6D). I therefore conclude that suppression of germline development by DAF-16 accounts for the reduced mtDNA content in insulin-signaling mutants (Figure 6-6E).

Because DAF-16 is required for mtDNA copy-number suppression upon loss of insulin signaling, I reasoned that DAF-16 should also be required for copy-number suppression in response to diet restriction. However, while diet restriction suppresses mtDNA copy number, this occurs independently of DAF-16 (Figure 6-7A). Given that ∆mtDNA frequency is sensitive to changes in

total mtDNA copy number (Figures 6-3 to 6-4), the effect of diet on total copy number suggests that diet might also modulate ΔmtDNA frequency independently of DAF-16. Remarkably, I only observed diet-dependent elevation in ΔmtDNA frequency when DAF-16 was present (Figure 6-7B). Moreover, while total mtDNA copy number and ΔmtDNA frequency each rose significantly across development on a control relative to restricted diet (Figure 6-7C), copy number rose by itself, with no accompanying change in ΔmtDNA frequency, in *daf-16* mutants (Figure 6-7D). Because diet restriction and loss of DAF-16 were each found to attenuate ΔmtDNA proliferation, I conclude that nutrient abundance and DAF-16 are each necessary (Figure 6-7E), but not sufficient individually, for ΔmtDNA to maintain a sub-organismal selection advantage.

Nutrient status governs selection on ΔmtDNA at different levels. FoxO/DAF-16 regulates numerous genes involved in stress tolerance (Klotz et al., 2015, Martins et al., 2016, Murphy et al., 2003, Tepper et al., 2013, Webb et al., 2016) and promotes organismal survival during nutrient scarcity (Greer et al., 2007, Hibshman et al., 2017, Kramer et al., 2008). I therefore asked whether nutrient availability and DAF-16 affect selection on ΔmtDNA at both the organismal and sub-organismal levels. Sub-organismal selection was quantified as before (see Chapter 5), on restricted versus control diets, in the presence versus absence of DAF-16 (Figure 6-8A and 6-8D). Organismal selection was quantified under each of these same conditions, using the competition method previously described (see Chapter 5). In populations expressing wildtype DAF-16, diet restriction did not significantly affect organismal selection against ΔmtDNA (Figure 6-8B and 6-8C). However, diet restriction intensified organismal selection against ΔmtDNA among *daf-16* mutants (Figure 6-8E and 6-8F). These data indicate that although food scarcity can accelerate selection against ΔmtDNA at the organismal level, DAF-16 protects ΔmtDNA from this effect (Figure 6-8G).

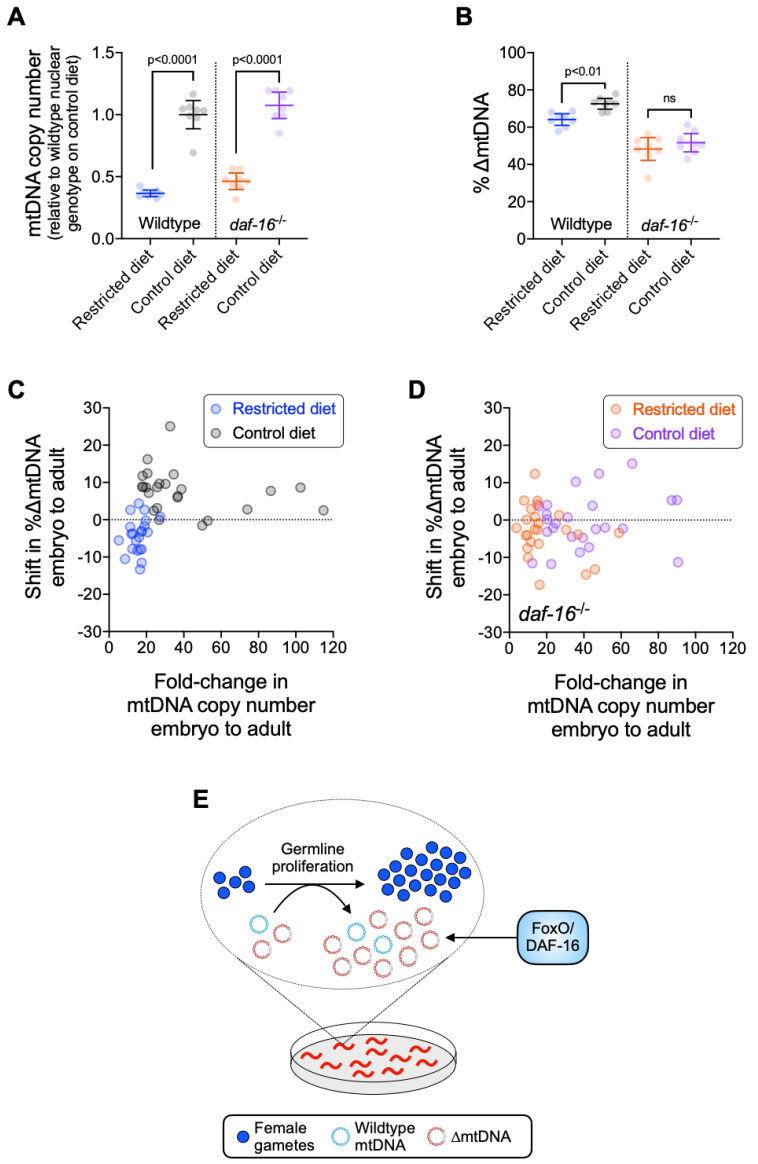

Figure 6-7. The sub-organismal selection advantage of ΔmtDNA requires both nutrient abundance and FoxO/DAF-16

(A) Total mtDNA copy number in heteroplasmic individuals, wildtype versus null *daf-16*(mu86) host genotype, restricted versus control diet. N=8 pooled lysates of 5 age-synchronized day-4 adults each. One-way ANOVA with Sidak's multiple comparisons test.
(B) ΔmtDNA frequency of individuals in (A). One-way ANOVA with Sidak's multiple comparisons test.
(C-D) Change in mtDNA copy number and ΔmtDNA frequency across development, with wildtype (C) versus null *daf-16*(mu86) (D) host genotype, on restricted versus control diet. Each data point represents the difference in copy number (horizontal axis) and ΔmtDNA frequency (vertical axis) between 3 pooled day-2 adults (age-matched to their respective parents) and 3 pooled embryos of the same brood. N=22 wildtype, restricted diet; N=24 wildtype, control diet; N=24 *daf-16*(mu86), restricted diet; N=24 *daf-16*(mu86), control diet. Mann-Whitney tests with Bonferroni corrections.
(E) Schematic showing that FoxO/DAF-16 is required in order for ΔmtDNA to take advantage of the increased mtDNA replication on an abundant diet.
All experiments featured in this figure used animals maintained on a diet of UV-killed OP50 *E. coli* at 20˚C. Error bars represent 95% confidence intervals

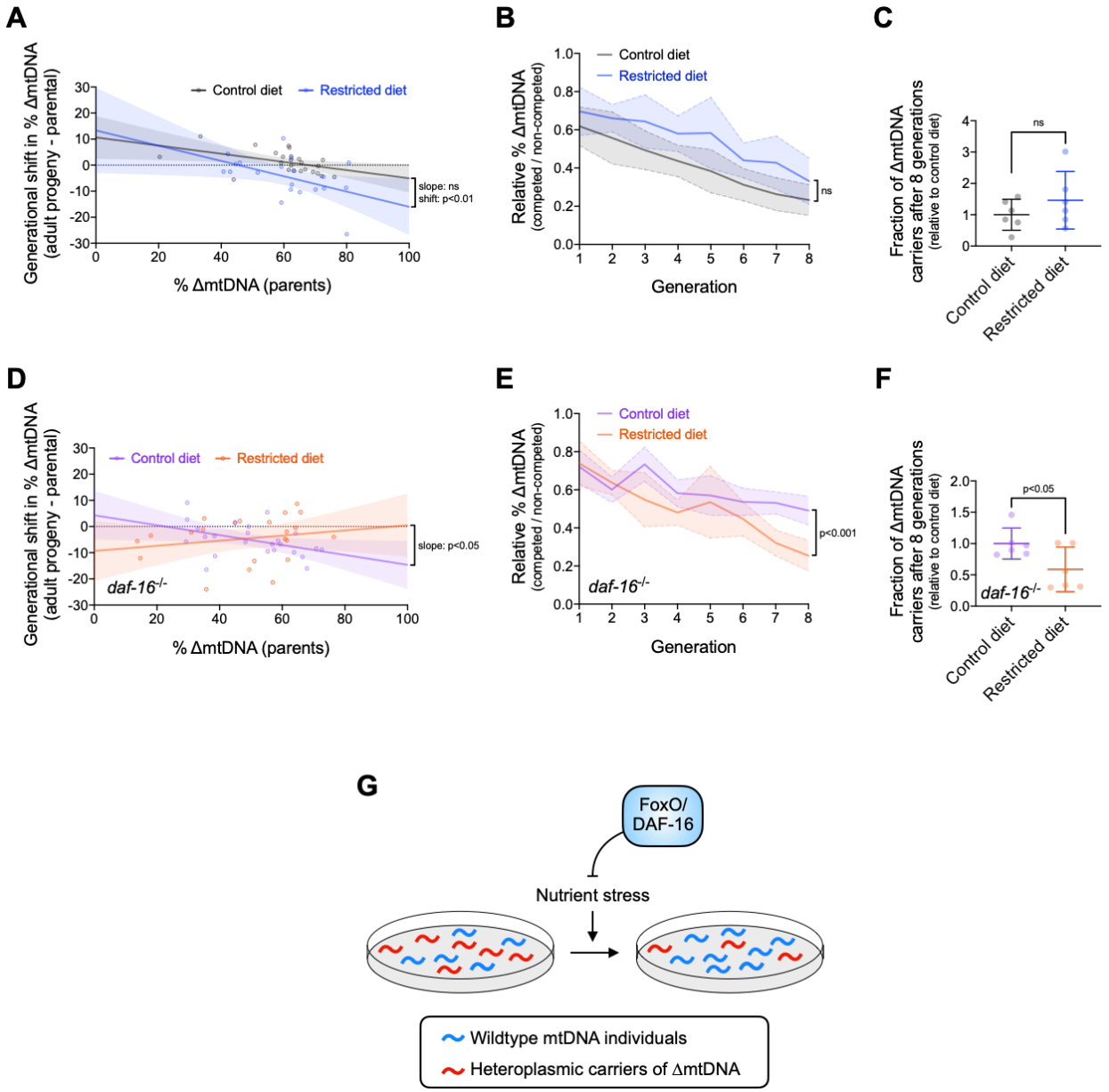

Figure 6-8. Nutrient status impacts multilevel selection dynamics of ΔmtDNA

(A) Sub-organismal shift in ΔmtDNA frequency per generation, similar to Figure 5-1B, in the background of the wildtype host genotype, on restricted versus control diets. Adult progeny were lysed at day 2 of adulthood, the same age at which the parents were lysed, to ensure that parents and their adult progeny were age-matched. Regressions were compared using analysis of covariance.
(B) Organismal selection against ΔmtDNA as measured by population-wide (not heteroplasmic) ΔmtDNA frequency, relative to average frequency across non-competing populations, in competing lines of wildtype nuclear background, similar to Figure 5-1D but in populations maintained on restricted or control diet (non-competed lines omitted for visual simplicity). To isolate the change in ΔmtDNA frequency that occurs strictly due to organismal selection, I controlled for the confounding influence of sub-organismal ΔmtDNA dynamics by normalizing overall ΔmtDNA across each population to that of the non-competed lines at each generation. Because all individuals within the non-competed lines contain ΔmtDNA, the frequency across a non-competing population is equal to the average sub-organismal ΔmtDNA. Hence, normalizing ΔmtDNA to the non-competing lines accounts for sub-organismal ΔmtDNA dynamics and reveals the decline in

∆mtDNA that occurs strictly due to selection at the level of organismal fitness. Solid lines reflect mean normalized ∆mtDNA frequency. Non-competed lines not shown for visual simplicity. Linear regression analysis.
(C) Fraction of ∆mtDNA-carrying individuals at generation 8 of the competition experiment shown in (B), normalized to control-diet lines. Two-tailed Welch's t-test.
(D) Sub-organismal shift in ∆mtDNA frequency per generation in the background of the null *daf-16*(mu86) mutant host genotype, on restricted versus control diets. Adult progeny were lysed at day 2 of adulthood, the same age at which the parents were lysed, to ensure that parents and their adult progeny were age-matched. Regressions were compared using analysis of covariance.
(E) Organismal selection against ∆mtDNA as measured by population-wide ∆mtDNA frequency relative to average heteroplasmic (non-competed) frequency, similar to panel (B), in competing lines of *daf-16*(mu86) mutant nuclear background, maintained on restricted or control diet. The ∆mtDNA frequency of each line, at each generation, was normalized to that of the non-competed lines in order to control for the confounding influence of sub-organismal ∆mtDNA dynamics, as was done in (B). Solid lines reflect mean normalized ∆mtDNA frequency. Non-competed lines not shown for visual simplicity. Linear regression analysis.
(F) Fraction of ∆mtDNA-carrying individuals with *daf-16*(mu86) nuclear background at generation 8 of the competition experiment shown in (E), normalized to control-diet lines. Two-tailed Welch's t-test.
(G) Schematic showing the influence of FoxO/DAF-16 on organismal selection against ∆mtDNA. Specifically, FoxO/DAF-16 protects ∆mtDNA from greater organismal selection during nutrient stress.
All experiments featured in this figure used nematodes maintained on a diet of UV-killed OP50 *E. coli* at 20˚C.
Error bars and shaded regions represent 95% confidence intervals.

Finally, I sought to integrate these observations of sub-organismal and organismal selection for each of the conditions tested (Figure 6-9A to 6-9F), using the Price Equation framework described in Chapter 5. The sub-organismal selection advantage of ΔmtDNA is compromised by diet restriction, loss of DAF-16, or both (Figures 6-7, 6-8A, 6-8D, 6-9A, and 6-9D). Furthermore, diet restriction was observed to accelerate organismal selection against ΔmtDNA, but only in the absence of DAF-16 (Figures 6-8B and 6-8C, 6-8E and 6-8F, 6-9B and 6-9E, and Appendices 6, 8, and 10). The combined covariances predict that the weakest overall selection occurs in populations with DAF-16 and experiencing food abundance (Figure 6-9C), while the strongest net selection against ΔmtDNA occurs in populations lacking DAF-16 and experiencing food scarcity (Figure 6-9F), with the remaining conditions each corresponding to an intermediate magnitude of selection. Measuring ΔmtDNA frequency across non-competing heteroplasmic populations afforded the opportunity to test this prediction. Remarkably, this prediction is consistent with observation (Figure 6-9G), even though UV-killed food compromises ΔmtDNA propagation even in the control diet (Figure 6-9G, compare gray to dotted brown line). Combined, these findings reveal numerous ways in which diet and host genome interact to shape the multilevel selection dynamics of a cheater genome (Figure 6-10).

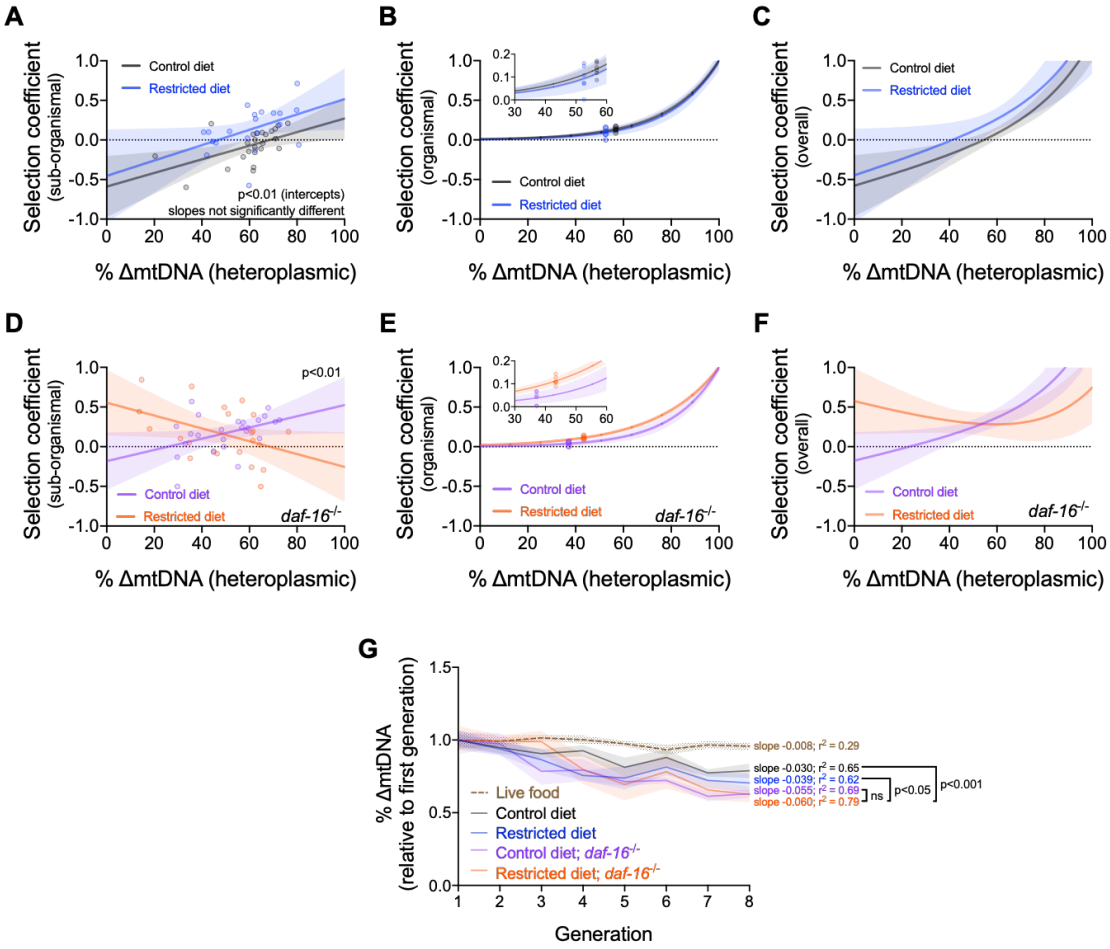

Figure 6-9. Separately measuring, and then summing, the effects of diet and host FoxO/DAF-16 genotype on sub-organismal and organismal selection accurately predict the combined effects of these conditions on ΔmtDNA

(A) Sub-organismal selection coefficient plotted as a function of heteroplasmic (sub-organismal) ΔmtDNA frequency, on control and restricted diets. Selection coefficients are calculated similarly to Figure 5-3A, using the empirically measured shifts in ΔmtDNA frequency between parents and progeny under variable diet conditions (Figure 6-8A). Regressions were compared using analysis of covariance.
(B) Organismal selection coefficient plotted as a function of heteroplasmic ΔmtDNA frequency, on control and restricted diets. Selection coefficients are calculated similarly to Figure 5-3B, from the population-wide declines in ΔmtDNA frequency during organismal competition under variable diet conditions (Figure 6-8B). For visual simplicity, the regressions assume the organismal selection coefficient reaches 1 (lethality) as ΔmtDNA approaches homoplasmic fixation (frequency of 100 percent), omitting the effect of the alternate assumptions featured in Figure 5-3B. Inset: magnification of the regressions around the range of mean heteroplasmic frequencies observed in these experiments.
(C) Overall, combined selection coefficient plotted as a function of heteroplasmic ΔmtDNA frequency (summation of plots shown in panels A and B), reflecting the net fitness effects in a heteroplasmic population.
(D-F) Similar to panels A-C but in the background of host genotypes homozygous for the null *daf-16*(mu86) mutant allele, obtained from the sub-organismal and organismal shifts in ΔmtDNA shown in Figures 6-8D and 6-8E. Regressions in panel (D) were compared using analysis of covariance.
(G) ΔmtDNA frequency, normalized to starting frequency, in non-competing lines from the organismal competition experiment (Figure 6-8B and 6-8E). For reference, dotted brown line represents data of non-

competing lines from the competition experiment on live OP50 *E. coli* (see Chapter 5). Linear regression analyses with Bonferroni correction for multiple comparisons.
Shaded regions represent 95% confidence intervals.
For panels A-F, the horizontal dotted line represents no net selection. Above the dotted horizontal line: selection favors wildtype mtDNA. Below the dotted horizontal line: selection favors ΔmtDNA.

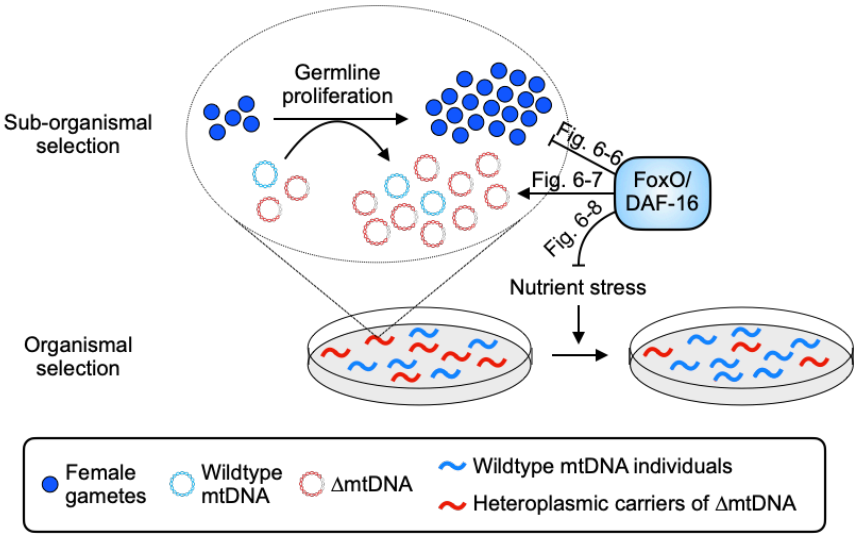

Figure 6-10. Summary of influence of diet and nutrient stress tolerance on multilevel selection dynamics of ΔmtDNA

At the sub-organismal level, FoxO/DAF-16 influences ΔmtDNA dynamics via two separate functions. On one hand, loss of insulin signaling results in activation of FoxO/DAF-16, which inhibits germline development (Figure 6-6). On the other hand, ΔmtDNA preferentially propagates by taking advantage of dietary nutrients but only when FoxO/DAF-16 is present (Figure 6-7), indicating that nutrient supply and FoxO/DAF-16-dependent nutrient sensing are each necessary, but not sufficient individually, for ΔmtDNA proliferation. During conditions of food scarcity, FoxO/DAF-16 partially shields ΔmtDNA from organismal selection (Figures 6-8 and 6-9), suggesting that nutrient supply and FoxO/DAF-16 promote ΔmtDNA propagation across organismal and sub-organismal selection levels.

Discussion

The role of nutrient status in shaping cooperator-cheater dynamics is not well understood. I first characterized the effect of maternal diet and nutrient sensing on sub-organismal cheater mtDNA dynamics, which revealed that nutrient abundance and insulin signaling promote mtDNA biogenesis in the germline, thereby providing the niche space for cheater proliferation. I further found that the stress-response transcription factor FoxO/DAF-16 is necessary for the cheater to take advantage of the nutrient supply and proliferate. These findings reveal that while nutrient abundance may be necessary, it is not sufficient to promote selfish mtDNA proliferation.

Interestingly, while I find that nutrient scarcity promotes the cooperative over cheater genotype, nutrient abundance is known to select for cooperation in other contexts. I propose that the impact of nutrient availability depends on whether the cost or the benefit of cooperation is the predominant effect. Nutrient abundance can promote public-goods cooperation by reducing the cost of making a cooperative contribution (Brockhurst et al., 2008, Connelly et al., 2017, Sexton and Schuster, 2017). Alternatively, scarcity can increase the benefit of cooperating, a phenomenon I observe in heteroplasmy dynamics. Since heteroplasmic animals exhibit lower rates of respiration despite increased mtDNA copy number and overall mitochondrial content (see Chapters 2 to 4), the wildtype mtDNA achieves a greater bioenergetic payoff per quantity of nutrients invested. When nutrients are scarce, a shift occurs within hosts in favor of the more metabolically efficient wildtype genome. In conclusion, I find that the benefit of cooperation, as indicated by net cooperator (wildtype)-biased replication, increases during nutrient scarcity and decreases during abundance.

In addition to nutrient abundance, DAF-16 is also required for sub-organismal selfish mtDNA proliferation. This could occur through compensatory biogenesis that favors underperforming mitochondria, inadvertently biasing replication toward the cheater genotype. Consistent with this

possibility, FoxO/DAF-16 has been identified as a regulator of genes associated with mitochondrial biogenesis (Tepper et al., 2013, Webb et al., 2016). Alternatively, DAF-16 might passively permit proliferation of the cheater genome by alleviating stress. DAF-16 up-regulates the expression of multiple genes involved in energy metabolism and antioxidant defense (Depuydt et al., 2014, Tepper et al., 2013, Webb et al., 2016). By seeking to rescue energy production and protect against cellular damage, DAF-16 may passively permit the spread of deleterious mtDNA mutants by relaxing the sub-organismal selection pressure to maintain optimal mitochondrial genome function.

How does resource availability affect selection on cooperators and cheaters at the level of competing groups? Note that the female germline harbors the entire population of mtDNA molecules that compete for transmission to the next generation. Selection on mtDNA genotype at the organismal level can thus be viewed as a group-level phenomenon, insofar as host fitness is determined by the cumulative effects of its mtDNA population. Accordingly, sub-organismal selection could be viewed as selection at the within-group level. On one hand, if resource scarcity selects for cooperation, groups with a higher proportion of cooperators should gain an extra fitness advantage over other groups during times of scarcity. On the other hand, exposure to cheating can lead to an evolutionary arms race whereby cooperators acquire resistance to cheaters, a phenomenon observed in bacteria and social amoebae (Hollis, 2012, O'Brien et al., 2017, Khare et al., 2009). Could food scarcity select for adaptations that reduce the impact of cheaters on group fitness? I propose that DAF-16 functions as an example of this type of stress tolerance. Although diet restriction compromised the sub-organismal advantage of ΔmtDNA, it had no effect on the organismal disadvantage—that is, no effect on the host fitness cost of carrying ΔmtDNA—provided DAF-16 is present. However, in *daf-16* mutants, diet restriction intensified organismal selection against ΔmtDNA. I therefore conclude that FoxO/DAF-16, which is known to prolong organismal survival during nutrient deprivation (Greer et al., 2007, Hibshman et al., 2017, Kramer et al., 2008), prevents food scarcity from exposing the cheater to stronger negative selection at the organismal

level. Broadly, these findings suggest that the ability to cope with resource scarcity can promote group-level tolerance to cheating, inadvertently prolonging cheater persistence.

Acknowledgments

The *uaDf5* heteroplasmic strain was kindly provided by the Caenorhabditis Genetics Center (CGC). I would like to thank Ann T. Tate and Allison Hilbun of Vanderbilt University for valuable guidance on experimental design and data analysis. Quantification of mtDNA copy number and ∆mtDNA frequency was accomplished with the help of the Simon A. Mallal Laboratory at Vanderbilt University Medical Center, and I especially thank Rama Gangula of the Mallal Laboratory for training on the use of the droplet digital PCR technology. I thank the members of the Patel Laboratory, past and present (especially James P Held, Cait S Kirby, Nikita Tsyba, Benjamin R Saunders, and Cassidy A Johnson), as well as Janet M Young, Mia T Levine, Sarah E Zanders, Harmit Malik, and Antonis Rokas for their valuable feedback on this work.

Funding for this work was provided by startup funds from Vanderbilt University for the Maulik R. Patel Laboratory, an NIH research project grant (R01 GM123260), the NIH-sponsored Cellular, Biochemical and Molecular Sciences Training Program (5T32GM008554-18), the Ruth L. Kirschstein National Research Service Award Individual Predoctoral Fellowship grant (1F31GM125344), Vanderbilt University Medical Center Diabetes Research and Training Center Pilot and Feasibility Grant to the Patel Laboratory, and the NIH-funded Tennessee Center for AIDS Research (P30 AI110527) to the Mallal Laboratory. Confocal microscopy imaging was performed through the use of the Vanderbilt Cell Imaging Shared Resource (supported by NIH grants CA68485, DK20593, DK58404, DK59637 and EY08126).

Part V

Themes and differences in selfish mitochondrial genome dynamics

Chapter 7

Comparison of multilevel selection dynamics across a collection of mutant mitochondrial genomes

Based on data not yet published

Introduction

Mutant mitochondrial genomes that propagate selfishly at the expense of host fitness have been observed to arise spontaneously in laboratory populations of yeast (Bernardi, 2005) and *Caenorhabditis elegans* (Dubie et al., 2020, Konrad et al., 2017), indicating that cheating may represent a relatively common theme in the population dynamics of mitochondrial mutations. On the other hand, the phenotypic manifestations of mitochondrial mutations vary considerably, not only between different individuals but also between different mutant mitochondrial DNA (mtDNA) variants (Taylor and Turnbull, 2005). Moreover, since mtDNA is a high-copy-number genome, mutations generally become pathogenic only when they proliferate to relatively high heteroplasmic frequency (Stewart and Chinnery, 2015, Wallace and Chalkia, 2013). Their proliferation and phenotypic diversity together suggest that mutant mitochondrial genomes may interact with their host through a variety of mechanisms—depending on the nature of the mutation—to reach and maintain high frequency.

In the preceding chapters, I identified a bona fide selfish mitochondrial genome. I then proceeded to identify and characterize mechanisms by which this genome propagates at the expense of host fitness. However, this progress was achieved by focusing on the mutant mtDNA variant *uaDf5*. Given the phenotypic diversity of mtDNA mutations, I sought to expand the scope of my

investigation to include other heteroplasmies. In Chapter 5, I describe experiments designed to isolate and quantitatively measure sub-organismal and organismal selection, since the defining feature of a "cheater" mitochondrial genome involves both of these levels: mitochondrial cheaters, or selfish mitochondrial genomes, are those that propagate within hosts at the expense of host fitness, giving rise to conflicting multilevel selection. In Chapter 6, I apply these experiments under conditions of variable diet and host genotype to investigate a key way in which the host genome interfaces with its environment to shape the dynamics of its resident mitochondrial population. Here, I apply the same experiments across a range of heteroplasmies that consist of deletions affecting enzyme complexes I, III, and IV of the electron transport chain (ETC). These experiments reveal that although cheating is evidently a common feature among deleterious mitochondrial mutations, the specific nature of the cheating "strategy" varies between mutant mtDNA variants.

Methods

Animal husbandry. *C. elegans* strains used in this study were maintained on 60-mm standard nematode growth medium (NGM) plates (for measuring sub-organismal selection), or 100-mm NGM plates (for measuring organismal selection), seeded with live OP50-strain *E. coli* bacteria as a food source. Nematode strains were incubated at 20˚C. In addition to the Bristol wildtype strain and the heteroplasmic *uaDf5* strain characterized in previous chapters, five additional *C. elegans* strains were used in this study. These consisted of heteroplasmic mutant genomes *mpt1*, *mpt2*, *mptDf3*, *mptDf2*, and *mpt4*, each crossed into the nuclear background of the Bristol strain.

Lysate preparation. To prepare animals for quantification of ∆mtDNA frequency, nematodes were transferred to sterile PCR tubes or 96-well PCR plates containing lysis buffer with 100 µg/mL

proteinase K. Lysis buffer consisted of 50 mM KCl, 10 mM Tris pH 8.3, 2.5 mM $MgCl_2$, 0.45% Tween 20, 0.45% NP-40 (IGEPAL), and 0.01% gelatin, in deionized water. Volume of lysis buffer varied by worm count: 10 µL for individual adults of the parent generation and 20 µL for pooled adult progeny for measuring sub-organismal selection, and 50 µL for pooled animal lysates from the competition experiments for measuring organismal selection. After transferring worms to lysis buffer, each tube or plate was immediately sealed and incubated at -80˚C for 10 minutes to rupture nematode cuticles, followed by lysis incubation at 60˚C for 60 minutes (90 minutes for pooled nematodes), and then at 95˚C for 15 minutes to inactivate the proteinase K. Nematode lysates were then kept at -20˚C for stable long-term storage until being used for genotyping and quantification.

Quantifying mutant mtDNA levels. Levels of each mutant mtDNA variant were quantified as described previously for *uaDf5*, using droplet digital PCR (ddPCR). In particular, nematodes were lysed as described above, then diluted in nuclease-free water, with a dilution factor varying depending on nematode concentration: 200x for single adults, 1000x for pooled adults (sub-organismal selection experiment), and 20,000x for pooled nematodes of mixed age (organismal selection experiment). Next, 5 µL of each dilute nematode lysate was combined with 0.25 µL of a 10-µM dilution of each primer needed for amplifying each mtDNA variant. The following primers were used for ddPCR amplification of each mutant variant as necessary.

mpt1:

Forward primer 1: 5’-TTCTGAAGGTGAAAGGGAGTTAG-3’

Reverse primer 1: 5’-ACTGACCTTAATGGTAAAGTATTTG-3’

Forward primer 2: 5’-GGGTACTTTCTTCTGCTATAT-3’

Reverse primer 2: 5’-CGATAACGAGGGTATGAACTACG-3’

mpt2:

Forward primer 1: 5'-GAAGAAGGTGGTAGCCTTGAGGAC-3'

Reverse primer 1: 5'-CGTATAAGAAAAGTCTTGGGATGTTAAG-3'

Forward primer 2: 5'-GGATTAATTTTCTCAAGGGGTGCTG-3'

Reverse primer 2: 5'-CTTTTTCAAAGACGAAAACTGTAACC-3'

mptDf3:

Forward primer 1: 5'-CCCTGAAGAGGCTAAGAATATTAGG-3'

Reverse primer 1: 5'-GGCAATGTCACCAACATCC-3'

Reverse primer 2: 5'-CCCAATACAATAACTAGAATAGCTCACG-3'

mptDf2:

Forward primer 1: 5'-GGATTGGCAGTTTGATTAGAGAG-3'

Reverse primer 1: 5'-AAGTAACAAACACTAAAACTCCCAAC-3'

Forward primer 2: 5'-CGTGCTTATTTTTCGGCTGC-3'

Reverse primer 2: 5'-CTTTAACACCTGTTGGCACTG-3'

mpt4:

Forward primer 1: 5'-CGGTGGTTTTGGTAACTG-3'

Reverse primer 1: 5'-TCATAGTGTAACACCCGTGAAAATCC-3'

Forward primer 2: 5'-TGATCCAAGAACTGGAGGTAATC-3'

Reverse primer 2: 5'-CCTGTTGGCACTGCAATAAC-3'

Mixtures of dilute nematode lysate and primer were combined with 12.5 µL of Bio-Rad QX200™ ddPCR EvaGreen Supermix and nuclease-free water to a volume of 25 µL in Eppendorf™ 96-well twin.tec™ PCR plates. Droplet generation and PCR amplification were performed according to manufacturer protocol. Wildtype and mutant-specific primers were combined in the same reaction, and each droplet was scored as containing either wildtype or mutant mtDNA using the

2-dimensional (518 nm and 554 nm dual-wavelength) clustering plot option in the Bio-Rad QuantaSoft™ program.

Sub-organismal selection assay. The strength of sub-organismal (within-host) selection on mutant mtDNA was measured longitudinally across isolated parent-progeny lineages, as described in the case of *uaDf5* (see Chapter 5). Multiple L4-stage (late larval) heteroplasmic animals were picked at random under a dissecting microscope from a stock population carrying ∆mtDNA in the Bristol strain (wildtype) nuclear background. These larvae were transferred to a fresh food plate and incubated for 2 days at 20˚C. The day-2 adults were then segregated onto individual plates and incubated for 4 hours at 20˚C to produce age-synchronized progeny. Each parent was then individually lysed. Three embryos from each parent were also lysed at the same time, in one pooled lysate per three same-parent embryos. After 2 days, three L4-stage larvae were pooled and lysed from each parent, similarly to the lysis of embryos. After another 2 days, three adult progeny per parent were pooled and lysed as they reached the age at which the parents were lysed, to obtain age-matched pairs consisting of one parent and three of its adult progeny. Each parent-progeny lineage was individually segregated from the rest. Lineages were segregated to ensure that mutant mtDNA frequency from each progeny lysate was being compared with that of its own respective parent, to minimize the effect of confounding factors such as organismal selection. To reduce the effect of random drift, progeny from each time-point were lysed in pools of three, across multiple independent biological replicates. Mutant mtDNA frequency of parents and progeny was determined for each heteroplasmy using ddPCR as described (see **Quantifying mutant mtDNA levels**).

Experimental evolution (organismal selection). Selection against mutant mtDNA that occurs strictly at the level of organismal fitness was measured using a competition assay similar to the one described for *uaDf5* (see Chapter 5). Briefly, for each mutant mtDNA variant, heteroplasmic

nematodes carrying mutant mtDNA in the Bristol nuclear background were combined with Bristol-strain nematodes on 10-cm NGM plates seeded with live OP50 *E. coli* as a food source. Approximately 500 nematodes were transferred to each plate. In addition to 4 replicate competition lines for each heteroplasmy, 4 non-competing control lines were established by transferring only heteroplasmic nematodes onto food plates, with no homoplasmic-wildtype nematodes to compete against. Every 3 days, the generation for each experimental line was reset; nematodes were washed off the plates using M9 buffer into a sterile 1.7 mL collection tube. Approximately 500 animals of mixed age from each line were transferred to a fresh food plate. Another 500 nematodes were lysed together in a single pooled lysate. This experiment was continued for 6 consecutive generations.

Results

I sought to identify broad themes and notable differences between different stably propagating heteroplasmic mtDNA variants. I elected to use the mutant mtDNA variants *mpt1*, *mpt2*, *mptDf3*, *mptDf2*, and *mpt4* (Figure 7-1). These encompass mutations in ETC complex I (*mpt1* and *mpt2*), complex III (*mptDf3*), and complex IV (*mpt4* and *mptDf2*). See Figure 1-1 for an ETC diagram. Although the mutations in *mpt1*, *mpt2*, and *mpt4* are each confined to a single protein-coding gene, the *mptDf2* deletion also deletes transfer RNA (tRNA) genes, indicating that it may disrupt ETC function beyond complex IV by also impacting protein synthesis. Moreover, the complex III mutation in *mptDf3* deletes the last 5 nucleotides on the 3' end of the isoleucine tRNA gene, although it is not clear whether this affects protein synthesis.

By tracking levels in parent-progeny lineages, as well as competing heteroplasmic hosts against their wildtype counterparts, I was able to isolate changes in mutant mtDNA frequency in a manner

specific to each level of selection (Figure 7-2). Since each mtDNA variant stably persists in a heteroplasmic population, despite harboring a deleterious mutation in at least one essential gene, they could all be predicted to undergo conflicting multilevel selection similarly to *uaDf5* (see Chapter 5, Figure 5-3). Surprisingly, however, the capacity for within-host proliferation, as well as the host-level fitness costs, vary considerably between mutant mitochondrial genomes.

Neither of the ETC complex I deletions show a significant effect on host fitness. It should be noted, however, that the two complex I mutations stably persist at different frequencies (Figure 7-2C, 7-2E and Appendix 11: Supplemental Figure 7-1A and 7-1B). Consistent with a lack of host fitness effects, these mutations appear to undergo neither within-host proliferation nor negative organismal selection, remaining at similar frequencies across generations in both sub-organismal and organismal experiments (Figure 7-2C to 7-2F). The same is true for the complex III mutation in *mptDf3* (Figure 7-2G and 7-2H). Interestingly, the population-wide frequency of *mptDf3* rose dramatically in only one of the competition lines (Figure 7-2H), consistent with random drift toward higher population-wide fraction of heteroplasmic animals. The complex IV mutations, on the other hand, inflict dramatic fitness effects, being almost entirely outcompeted by homoplasmic (wildtype) animals within six generations (Figure 7-2J and 7-2L). This was true for *mptDf2*, which affects both complex IV and tRNA genes, as well as *mpt4*, which only affects the complex IV gene *CO1*. Consistent with these findings, mutations in human *CO1* are associated with a number of clinical pathologies (Brown et al., 1992, Namslauer and Brzezinski, 2009, Varlamov et al., 2002). Based on these severe host fitness costs, I predict that if these mutations are to persist in a population, they must undergo significant within-host proliferation, sufficient to overcome the strong negative selection at the organismal level. Indeed, this prediction is remarkably consistent with my observations based on the measurement of sub-organismal selection (Figure 7-2I and 7-2K). I therefore have identified mutations that behave similarly to *uaDf5*, and some that differ, from among a collection of five heteroplasmic mtDNA mutations.

As with *uaDf5*, I sought to integrate these findings into the same theoretical framework of the Price Equation (see Chapter 5), by summing the covariance between mutant mtDNA frequency and the strength of selection at the sub-organismal and organismal levels (Figure 7-3). Not surprisingly, when the levels of selection are combined into a single overarching description of their respective population dynamics, there is no overall (population-level) covariance between mutant frequency and selection, at least for *mpt1*, *mpt2*, and *mptDf3* (Figure 7-3D to 7-3L). In other words, the frequency of these mutations does not seem to correlate with their fitness effects, at least within the frequency ranges at which these heteroplasmies were observed to persist. In contrast, the combined covariance for the mutant genome *mptDf2* (Figure 7-3O) predicts that this genome stably persists at very high frequency—near 80 percent—due to a balance between a strong sub-organismal proliferative advantage and a strong host fitness cost. As with *uaDf5*, this prediction is highly consistent with the empirical observation that *mptDf2* stably propagates at very high frequency across multiple generations in non-competing lines, where the forces of sub-organismal and organismal selection are both in effect (Appendix 11: Supplemental Figure 7-1D, non-competing lines). Finally, although *mpt4* undergoes robust sub-organismal proliferation (Figure 7-2K), the magnitude of proliferation does not appear to co-vary with *mpt4* frequency (Figure 7-3P), indicating that the combined population-level covariance fails to predict the level at which this mutant genome persists (Figure 7-3R). However, the substantial host fitness cost of this genome (Figures 7-2L and 7-3Q) implies a strong selection pressure that acts in opposition to the sub-organismal proliferation, similarly to *uaDf5* and *mptDf2*. In conclusion, I have identified notable similarities and differences in the population dynamics of selfish mitochondrial genomes.

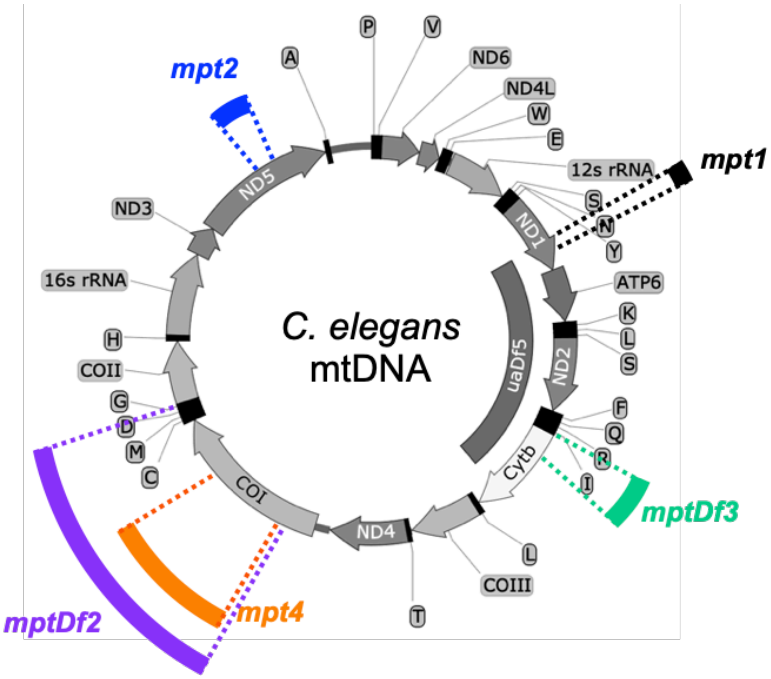

Figure 7-1. Map of mitochondrial genome in *Caenorhabditis elegans* showing locations and sizes of heteroplasmic mutations featured in this chapter

The *uaDf5* deletion, comprising the majority focus of chapters 2 through 6, and the genome itself are decolorized to more easily visualize the mutations. Proteins and ribosomal RNA genes are in gray; the locations of transfer RNA genes are shown in black. Colored bars around the perimeter of the genome represent approximate locations and sizes of the mtDNA deletions used in this study. Coloring corresponds to the visualization of data in Figures 7-2 and 7-3.

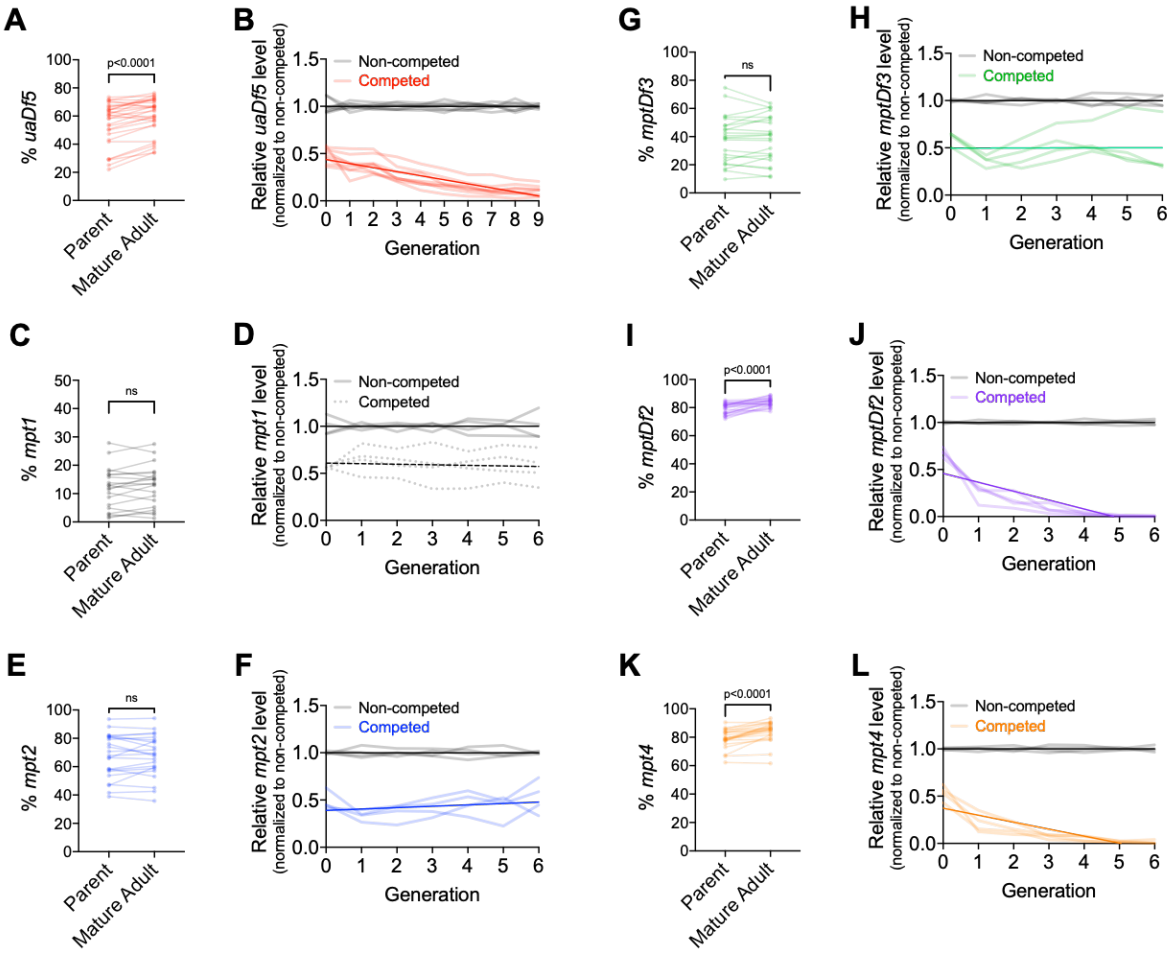

Figure 7-2. Data from experiments designed to measure possible changes in frequency at the sub-organismal and organismal levels, carried out across the collection of heteroplasmic mutations featured in Figure 7-1

(A-B) For reference, shifts in *uaDf5* frequency at the levels of sub-organismal (A) and organismal (B) selection, using data from Figures 5-1A and 5-1D, respectively. Embryo and larval time-points are omitted from panel (A), otherwise this data is the same as in Figure 5-1A. Wilcoxon matched-pairs signed-rank test (A).
(C-D) Data obtained from experiments to measure possible changes in *mpt1* frequency at the levels of sub-organismal (C) and organismal (D) selection. Wilcoxon matched-pairs signed-rank test (C).
(E-F) Data obtained from experiments to measure possible changes in *mpt2* frequency at the levels of sub-organismal (E) and organismal (F) selection. Wilcoxon matched-pairs signed-rank test (E).
(G-H) Data obtained from experiments to measure possible changes in *mptDf3* frequency at the levels of sub-organismal (G) and organismal (H) selection. Wilcoxon matched-pairs signed-rank test (G).
(I-J) Data obtained from experiments to measure possible changes in *mptDf2* frequency at the levels of sub-organismal (I) and organismal (J) selection. Wilcoxon matched-pairs signed-rank test (I).
(K-L) Data obtained from experiments to measure possible changes in *mpt4* frequency at the levels of sub-organismal (K) and organismal (L) selection. Wilcoxon matched-pairs signed-rank test (K).

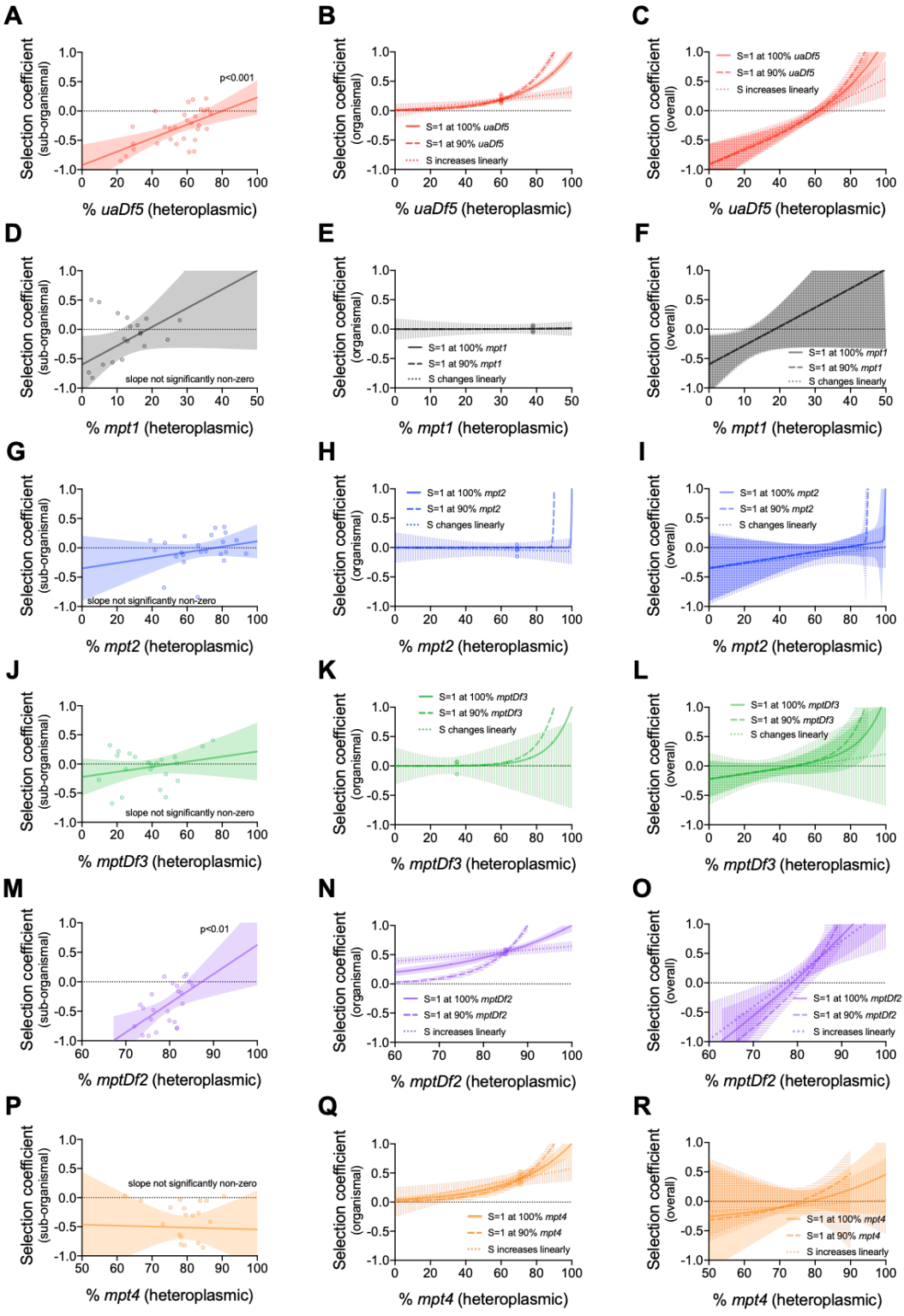

Figure 7-3. Integration of the multilevel selection dynamics of all six heteroplasmies using the Price Equation

For each graph shown above, the horizontal dotted line represents no net selection. Above the dotted horizontal line: selection favors wildtype mtDNA. Below the dotted horizontal line: selection favors ΔmtDNA.

(A-C) For reference, the plots showing selection coefficients as functions of heteroplasmic *uaDf5* frequency (from Figure 5-3) are once again shown here.
(D-F) Similar to (A-C) but for *mpt1*, using data obtained from Figure 7-2C and 7-2D.
(G-I) Similar to (A-C) but for *mpt2*, using data obtained from Figure 7-2E and 7-2F.
(J-L) Similar to (A-C) but for *mptDf3*, using data obtained from Figure 7-2G and 7-2H.
(M-O) Similar to (A-C) but for *mptDf2*, using data obtained from Figure 7-2I and 7-2J.
(P-R) Similar to (A-C), but for *mpt4*, using data obtained from Figure 7-2K and 7-2L.
As before (see Figure 5-3), shaded, horizontally-striped, and vertically-striped regions on the organismal and combined ("overall") plots respectively represent the 95% confidence ranges that result from assuming the selection coefficient reaches 1 (lethality) when the mutant is at 100 percent frequency, or when the mutant is at 90 percent heteroplasmic frequency, or assuming the selection coefficient increases linearly with heteroplasmic mutant frequency. Note that confidence ranges capable of accommodating a horizontal regression indicate a slope that is not significantly non-zero, implying no significant relationship between heteroplasmic mutant mtDNA frequency and natural selection, at least within the mutant frequency range in which the data were collected.

Discussion

The mutant mtDNA variant *uaDf5* is an excellent model for the study of selfish mitochondrial genome dynamics, for a number of reasons. For example, this mutant rises in frequency across animal development at the expense of inflicting a fitness cost (see Chapter 2). The proliferation of *uaDf5* is also frequency-dependent, a common feature of cheater entities (Dobata and Tsuji, 2013, Dugatkin et al., 2005, Pruitt and Riechert, 2009, Riehl and Frederickson, 2016, Ross-Gillespie et al., 2007). Moreover, *uaDf5* proliferates by exploiting interactions with the host genome that exist to minimize the harmful effects of metabolic and nutrient stress (see Chapters 3, 4, and 6), for which reason it can be viewed as a bona fide cheater entity. However, mitochondrial mutations are not all alike with respect to their fitness effects. How generalizable are the findings from the study of *uaDf5*? I sought to address this question here by identifying noteworthy trends and differences in the population dynamics of mitochondrial mutations.

Variation in selfish mitochondrial genome dynamics. By quantitatively measuring the strength of selection acting on mutant mtDNA at the sub-organismal and organismal levels, across a collection of mitochondrial mutations, I identified two interesting themes. On one hand, like *uaDf5*, some mutant mtDNA variants propagate in spite of inflicting a heavy fitness burden on their hosts. As expected, their seemingly paradoxical persistence—in other words, their ability to avoid extinction in the face of strong negative organismal selection—appears to coincide with strong positive sub-organismal selection. I observe these conflicting multilevel selection dynamics in three of the six ΔmtDNA variants featured here: *uaDf5*, *mptDf2*, and *mpt4*. Although the molecular basis of these dynamics are not clear, the only thing that all three mutations have in common is a disruption to ETC complex IV. Consistent with these findings, mutations in the complex IV gene *CO1*, whose *C. elegans* homolog is deleted in *mptDf2* and *mpt4*, are associated with a number of clinical pathologies in humans (Brown et al., 1992, Namslauer and Brzezinski, 2009, Varlamov

et al., 2002). In any case, the canonical cheater dynamics, whereby mutant genomes survive negative organismal selection by outcompeting wildtype mtDNA within individual hosts, appears to be a relatively common, albeit not universal, theme among mutant mitochondrial genomes.

In addition to these conflicting multilevel selection dynamics, a second general theme emerges from tracking the levels of some of the mutant genomes featured here. In contrast to *uaDf5*, *mptDf2*, and *mpt4*, not all mutant mitochondrial genomes persist by rising in frequency across development at the expense of a strong host fitness cost. On the contrary, despite carrying deletions in essential metabolic genes, some mutant genomes appear to undergo neutral drift, even when the heteroplasmic animals compete for several generations against their wildtype counterparts on the same food. This is true for both mutations in ETC complex I—the *mpt1* deletion in *ND1* and the *mpt2* deletion in *ND5*—as well as for *mptDf3*, which affects the complex III gene for Cytochrome b. Taken together, these observations suggest that mtDNA variants can persist in a manner consistent with neutral drift, despite carrying mutations that deleteriously affect essential ETC components.

Comparison with previous findings. Interestingly, *mptDf3*, which carries a deletion affecting the only mtDNA-encoded protein in ETC complex III, namely Cytochrome b, does not appear to inflict a significant host fitness cost, at least not within the frequency range at which *mptDf3* is observed to persist. This may be difficult to reconcile with previous work showing that an mtDNA variant labeled Δ*ctb-1*—owing to a Cytochrome b mutation—behaves much more like *uaDf5*, by proliferating within hosts while imposing a host fitness cost (Dubie et al., 2020). One possible explanation for this apparent discrepancy between the dynamics of Δ*ctb-1* and *mptDf3* is that Δ*ctb-1* contains other mutations in addition to the deletion in Cytochrome b, which may contribute to the observed selfish proliferation of Δ*ctb-1*, or its host fitness consequences, or both (Dubie et al., 2020).

Hypotheses and future directions. What might explain the apparent neutral persistence of a deletion-bearing mitochondrial genome? One conceivable explanation for these observations invokes the misidentification of discarded mtDNA. In other words, perhaps these mutant genomes do indeed severely impact mitochondrial function and consequently elicit mitochondrial autophagy (mitophagy). If mitophagy is accompanied by the release of partially-degraded mtDNA fragments into the rest of the cell, those fragments could potentially be detected and interpreted as genomes residing within mitochondria and undergoing neutral drift. Although conceivably possible, this explanation seems highly unlikely for two reasons. First, I previously observed a mitophagy gene, *pdr-1*, to measurably affect mutant mtDNA frequency (see Chapter 4, Figure 4-6), suggesting that mitophagy does not release detectable genome fragments from the degradation of mitochondria. Second, if free-floating mutant mtDNA were showing up in the droplet digital PCR (ddPCR) data, these molecules would likely not have access to replication machinery, such as the mtDNA polymerase enzyme POLG, whose localization to intact mitochondria is evidently important for mtDNA synthesis (Zhang et al., 2016). I would therefore expect the mutant mtDNA levels to rapidly dwindle, being diluted through successive rounds of cell division and organismal reproduction in the absence of sustained replication. In contrast to this expectation, each mutant mtDNA variant featured in this study was observed to stably persist across generations (Figure 7-2). This suggests that the mitochondrial genomes detected by ddPCR undergo sustained replication within their hosts and therefore likely reside at least within structurally—if not functionally—intact mitochondria.

If mutant mtDNA levels are free to randomly drift within their hosts, *de novo* homoplasmic animals might be expected to regularly occur within their respective heteroplasmic stock populations. Given this expectation, how might a genome that lacks an essential gene manage to stably persist with no measurable fitness effect at either level of selection (organismal or sub-organismal)?

Although the explanation is not known, these observations raise the interesting possibility that some mutant genomes propagate, not in spite of a deleterious host fitness cost, but rather because of what could be considered a “flying under the radar” strategy. In other words, some mutant genomes seem to successfully persist by maintaining a frequency range that enables them to avoid exposure to negative organismal selection. One possible basis for this phenomenon would invoke a balance between positive and negative selection at the sub-organismal level. For example, these mutant genomes might affect mitochondrial function in a manner that elicits a combination of cellular mechanisms that simultaneously favor and disfavor the mutant genome within individual hosts. If this balance is achieved within a frequency range that is too low to significantly impact host fitness, the mutant mtDNA could undergo neutral drift at the organismal level while maintaining a steady-state heteroplasmy.

This possibility could be explored in future research by testing host genes for their effect on heteroplasmy dynamics within hosts. For example, the gene *clk-1*, which encodes the *C. elegans* homolog of the mammalian enzyme COQ7, has been identified as a candidate regulator of mtDNA copy number via compensatory (stress-induced) mtDNA replication (Cristina et al., 2009, Gorbunova and Seluanov, 2002, Kirby and Patel, 2021). Accordingly, *clk-1* might mediate the preferential replication of genomes residing in defective regions of the mitochondrial network, thereby favoring the replication of mutant mtDNA (see Chapter 3 for a description of a model and mtDNA copy-number data consistent with this hypothesis). Moreover, previous work has shown that mtDNA replication can be biased in favor of either a mutant or wildtype genome depending on the expression level of POLG (Chiang et al., 2019, Lin et al., 2016). This raises the possibility that physiological stress-response mechanisms might bias replication in favor of the mutant genome by influencing the expression or localization of mtDNA replication machinery. For example, the gene *daf-16* encodes a Forkhead box O (FoxO) transcription factor that functions as a master regulator of metabolic homeostasis. Although *daf-16* does not appear to directly

regulate POLG expression (Tepper et al., 2013), it nevertheless regulates other aspects of mitochondrial function, including the expression of proteins involved in energy metabolism and stress response (Depuydt et al., 2014, Tepper et al., 2013, Webb et al., 2016). If its attempt to rescue metabolic integrity influences mtDNA replication, even indirectly, then a compensatory effect could result that favors underperforming regions of the mitochondrial network, inadvertently promoting replication of mutant genomes. Consistent with this possibility, *daf-16* mediates rising ∆mtDNA frequency across organismal development (see Chapter 6, Figure 6-7). Like *daf-16*, the gene *atfs-1* also regulates a transcriptional response to metabolic stress, in this case by activating the mitochondrial unfolded protein response (UPR^{mt}) (Nargund et al., 2012). Importantly, *atfs-1* gain-of-function mutations are associated with elevations in both *uaDf5* frequency (see Chapter 4, Figure 4-4C) and expression of *polg-1*, the gene encoding POLG (Lin et al., 2016). Together, these considerations highlight *clk-1*, *daf-16*, and *atfs-1* as attractive candidate genes underlying positive sub-organismal selection for the mutant mitochondrial genomes featured in this study. Conversely, *drp-1* is involved in mitochondrial fission, while *pink-1* and *pdr-1* play central roles in PINK1/Parkin-dependent mitophagy, and both of these processes have been implicated in selection against mutant mtDNA at the sub-organismal level (Gitschlag et al., 2016, Kandul et al., 2016, Lieber et al., 2019, Lin et al., 2016, Suen et al., 2010, Valenci et al., 2015). Does the combined activity—and corresponding influence—of each such pathway vary depending on the mitochondrial mutation? This could be addressed by future research, for example by comparing UPR^{mt} activation, or mitochondrial localization of the mitophagy machinery, across different heteroplasmies. It would also be informative to determine how different heteroplasmies compare in their sensitivity to the disruption of these pathways.

Following up on these questions would provide valuable clarification on the various ways in which selfish mitochondrial genomes interact with their hosts. In the mean time, I conclude by noting that the tendency to “cheat” per se, by rising in frequency across development at the expense of

host fitness, has been observed among three of the six mutant mitochondrial genomes featured in the research described here. This implies that cheating is a relatively common strategy when mitochondrial genomes compete within the maternal germline for transmission to the next generation. On the other hand, all six mtDNA variants stably persist despite carrying mutations that disrupt essential genes. Taken together, these findings suggest a more general form of selfish propagation, characterized by the persistence of a mutation with no accompanying host fitness advantage, with “cheating” constituting a special case of a broader phenomenon.

Acknowledgments

I would like to recognize O. Thompson and R. Waterston at University of Washington for identifying the *mpt1*, *mpt2*, *mptDf3*, *mptDf2*, and *mpt4* deletions from the Million Mutation Project worm collection. I would like to thank Ann T. Tate and Allison Hilbun of Vanderbilt University for valuable guidance on experimental design and data analysis. I would like to thank James P. Held and Claudia V. Pereira of the Patel Laboratory for their valuable contributions by carrying out the genetic crosses featured in this chapter. Quantification of mtDNA copy number and ΔmtDNA frequency was accomplished with the help of the Simon A. Mallal Laboratory at Vanderbilt University Medical Center, and I especially thank Rama Gangula of the Mallal Laboratory for training on the use of the droplet digital PCR technology.

Funding for this work was provided by startup funds from Vanderbilt University for the Maulik R. Patel Laboratory, the NIH-sponsored Cellular, Biochemical and Molecular Sciences Training Program (5T32GM008554-18), the Ruth L. Kirschstein National Research Service Award Individual Predoctoral Fellowship (1F31GM125344), and the NIH-funded Tennessee Center for AIDS Research (P30 AI110527) to the Mallal Laboratory.

Chapter 8

Summary and discussion of findings, future directions, and concluding remarks

Background and goals: the nature of cheating among mutant mitochondrial genomes

I sought to explore how a foundational aspect of the biology of complex life, specifically the relationship between the two genomes that give rise to the eukaryotic cell, can be better understood in light of the evolutionary forces shaping it. I focused in particular on the implications of the symbiotic origin of eukaryotes. Symbiosis can be a double-edged sword. On one hand, a cooperative relationship provides an opportunity for an entity to outsource some of the functions required for survival and reproduction to another entity, as in the case of the eukaryotic cell relying on a bacteria-derived endosymbiont for the majority of its energy production. On the other hand, the outsourcing of vital functions to another entity—a host—also represents a key defining feature of parasites. The key difference is who benefits: both parties, or one at the expense of the other?

By providing adaptive benefits such as a division of labor, sharing of resources, and protection against threats, cooperation plays a central role in the evolution of more complex life forms (Fisher and Regenberg, 2019, Gulli et al., 2019, Michod et al., 2006, West et al., 2015, Hammerschmidt et al., 2014). In spite of these benefits, cooperation comes with a noteworthy vulnerability: the risk of being exploited by defectors, or cheaters, which reap the benefit of having cooperative partners without incurring the cost of contributing any payoff in return for the cooperative contributions of the partners. Just as eukaryotic life arose from a mutually beneficial symbiosis between a bacterium and a larger host cell (Lang et al., 1999, Sagan, 1967, Wang and Wu, 2015), it likewise remains vulnerable to the occasional emergence of genetic elements that selfishly propagate at the expense of host fitness. In addition to being taxonomically widespread (Havird et al., 2019),

mitochondrial mutations conferring a tendency to propagate selfishly, at a cost to host fitness, have been observed to occur spontaneously in laboratory populations of yeast (Bernardi, 2005) and *Caenorhabditis elegans* (Dubie et al., 2020, Konrad et al., 2017), indicating that cheating likely represents a relatively common phenomenon among mutant mitochondrial genomes.

"Cheating" can be defined as a pattern of interaction with a fitness asymmetry that arises from an entity making a costly cooperative contribution toward the benefit of another entity, without the recipient facilitating any fitness payoff for the benefactor (Ghoul et al., 2014). This relatively broad characterization applies across many levels of scale and in many taxa, including individual genes (Bravo Nunez et al., 2018, Hammond et al., 2012, Hu et al., 2017, Larracuente and Presgraves, 2012, Schimenti, 2000), bacteria (Fiegna and Velicer, 2003, Hammerschmidt et al., 2014, Sexton and Schuster, 2017), amoebae (Khare et al., 2009, Strassmann et al., 2000), and animals (Aumer et al., 2019, Dobata et al., 2009, Riehl and Frederickson, 2016, Wenseleers and Ratnieks, 2004). Understanding cheating, in terms of the mechanisms and conditions underlying its success as an adaptive strategy, could therefore have broad implications for both biomedical science and evolutionary biology.

In addition to cooperation, which characterizes the mito-nuclear interactions that benefit both genomes, the adaptive strategy of cheating also frequently characterizes mutant mitochondrial genomes. To understand how such a genome can cheat, I first sought to identify a selfish mitochondrial DNA (mtDNA) variant within an experimentally tractable organism for use as a model cheater. The mutant mtDNA variant *uaDf5* in *C. elegans* represented an excellent candidate, due to the versatile experimental tools available with this animal species, in addition to the prior observations that this genome stably propagates across generations (Tsang and Lemire, 2002b) in spite of deleterious phenotypic effects (Liau et al., 2007). These findings raise the possibility that *uaDf5* behaves as a cheater. To further test this hypothesis, I used a

combination of droplet digital PCR (ddPCR) and fitness assays to replicate and confirm prior observations that *uaDf5* proliferates at the expense of host fitness (see Chapter 2). I then addressed alternative hypotheses, including the idea that *uaDf5* proliferates out of necessity for host viability—for example by genetically complementing other mutant genomes within the same host—as well as the idea that *uaDf5* merely proliferates due to the intrinsic replication advantage of being a smaller genome than wildtype mtDNA (see Chapter 2). Having identified *uaDf5* as a selfish mitochondrial genome, I then proceeded to investigate mechanisms underlying its cheating behavior, as well as conditions influencing the relative fitness of the selfish and cooperative (wildtype) genomes at the respective levels where they each have a selection advantage.

How it cheats: mechanisms underlying proliferation of a selfish mitochondrial genome

Having identified a genuine selfish mitochondrial genome in *C. elegans*, I endeavored to follow up on the question of how this genome behaves as a cheater, as well as the conditions shaping its fitness relative to its cooperative, wildtype counterparts. Using ddPCR, I found that variation in copy number of the mutant and wildtype genomes is consistent with mtDNA copy-number regulation, which the mutant genome manages to evade (see Chapter 3). Although I found the copy-number data to be consistent with the predictions of a model that invokes drift to higher mutant frequency (Capps et al., 2003, Durham et al., 2007), it remains unclear whether the escape from copy-number regulation and the associated elevation in mutant frequency occur via drift or selection per se. Interestingly, a recent study showed that the protein CLK-1 influences mtDNA copy number through a mechanism that is evidently independent of its function in ubiquinone synthesis (Kirby and Patel, 2021). Together with previous *in vitro* work showing that CLK-1 binds to an mtDNA origin-of-replication sequence in a manner that is inhibited by ADP (Gorbunova and Seluanov, 2002), these findings raise the possibility that compensatory mtDNA replication occurs

in response to local energy depletion in the vicinity of deleteriously mutated mtDNA, predisposing the mutant genomes to positive selection. This scenario predicts that in heteroplasmic animals carrying a deleterious mitochondrial mutation, CLK-1 should bind to the wildtype genome at higher rates than the mutant genome, which could be tested using a CLK-1 antibody. Moreover, this scenario also predicts that the proliferative advantage of the mutant genome should decrease upon deletion of the gene encoding CLK-1. Future studies seeking to test these predictions will yield valuable insights on the nature of mtDNA copy-number homeostasis and its role in selfish mitochondrial genome dynamics.

Separately, using a combination of ddPCR, microscopy, classical and molecular genetic techniques, I found that *uaDf5* perturbs mitochondrial function in a manner that activates a stress-response mechanism, the mitochondrial unfolded protein response (UPR^{mt}). Upon activation, UPR^{mt} promotes the propagation of the mutant genome, at least in part by protecting the mutant from a cellular policing mechanism, namely mitochondrial autophagy or mitophagy, which would otherwise selective against copies of the mutant genome (see Chapter 4). Interestingly, recent work suggests that mitochondrial localization of the UPR^{mt}-activating transcription factor ATFS-1 promotes the propagation of *uaDf5* (Yang, 2021). Moreover, mitophagy appeared to play a very limited role in the reduction of *uaDf5* frequency upon loss of ATFS-1. Although I found loss of the mitophagy gene *pdr-1* to restore *uaDf5* proliferation in UPR^{mt}-defective mutants (see Chapter 4), the influence of ATFS-1 on the dynamics of mutant mtDNA may involve multiple mechanisms. It should also be noted that my work utilized a hypomorph allele of the encoding gene, *atfs-1*(tm4525), resulting in a considerable but not complete loss of gene function. Accordingly, one potential explanation for the apparent differences in the effect of mitophagy is the differences in the magnitude of UPR^{mt} deficiency; perhaps mitophagy plays a bigger role in the elimination of *uaDf5* in animals with a partial but not complete absence of ATFS-1 function. This possibility is consistent with the observation that constitutive UPR^{mt} activation via the *atfs-1* gain-of-function

allele promotes a robust rise in *uaDf5* frequency. Taken together, these observations suggest that ATFS-1 may promote selfish mitochondrial genome proliferation in more than one way, involving both nuclear and mitochondrial localization of ATFS-1. Moreover, I observe even greater *uaDf5* levels in mitophagy-defective *pdr-1* mutants than in hosts with a wildtype genome, suggesting that physiological stress-responses likely represent a general category of mechanisms that similarly promote selfish mtDNA proliferation, at least in cases where such mechanisms interfere with the mitophagy pathway.

The evidence of wildtype-specific copy-number regulation and UPR^{mt}-dependent mutant mtDNA proliferation together indicate that efforts by the host genome to preserve mitochondrial function can inadvertently amplify the numbers of mutant mtDNA. The observation that mitochondrial stress-response mechanisms enable the persistence of mutant mtDNA variants is not particularly surprising per se. After all, these mechanisms evolved to preserve host viability in the event of physiological stressors. Remarkably, however, mitochondrial stress-response mechanisms do not promote the propagation of mutant mtDNA merely by shielding the host against the deleterious effects of the mutant mtDNA. On the contrary, perhaps the most noteworthy finding of my research is that host stress-response mechanisms are actually responsible for facilitating the selective advantage—the "cheating" behavior—of the mutant genomes within the host germline and across generations.

Conditions shaping the population dynamics of a selfish mitochondrial genome

Because selfish mitochondrial genomes are defined by proliferation or positive selection within hosts at the expense of host fitness, selfish mitochondrial genomes are frequently characterized by conflicting multilevel selection (Dubie et al., 2020, Havird et al., 2019, Klucnika and Ma, 2019,

Shou, 2015). Specifically, the selfish genomes outcompete cooperative genomes within hosts while the cooperative genomes simultaneously retain an advantage at the level of selection for host fitness. Given the high intracellular copy number and relaxed replication of the mitochondrial genome, the relative levels of mutant and wildtype mtDNA can fluctuate within a host. Moreover, since high mutant mtDNA levels tend to be more deleterious, hosts in which the mutant genome has drifted to lower frequency should be at a fitness advantage over hosts with a higher mutant load. The stable heteroplasmic persistence of a deleterious mitochondrial mutation therefore likely reflects a balance between opposing selection pressures favoring each mtDNA variant over the other depending on the level of selection. By conducting experiments designed to quantitatively measure each of these selection pressure in isolation, under varying conditions and host genotypes, it is possible to identify environmental conditions and host genes that interact to determine the proliferative capacity of the mutant genome within hosts, as well as the magnitude of the impact of the mitochondrial mutation on host fitness (see Chapters 5-6). Using this approach, I identified important roles for dietary nutrient availability and a key regulator of metabolic homeostasis, namely FoxO (DAF-16 in *C. elegans*). Dietary nutrient abundance and FoxO/DAF-16 are each necessary, but not sufficient individually, for the selfish proliferation of the mutant mitochondrial genome within individual hosts. At the same time, dietary nutrient availability and the function of FoxO/DAF-16 are each able to mitigate the cost that the mutant genome inflicts on host fitness. Taken together, these findings reveal an important way in which the host interfaces with its environment to influence both sides of cheating: selfish proliferation and the negative fitness cost.

How does FoxO/DAF-16 accomplish these effects? The molecular details become unclear downstream of FoxO/DAF-16, mostly due to the fact that this protein regulates the expression of several hundred genes (Martins et al., 2016, Murphy et al., 2003, Tepper et al., 2013, Webb et al., 2016), and its effect on the dynamics of mutant mitochondrial genomes may involve a

concerted effort of many genes or pathways. However, some previous studies hint at a possible link between the different functions of FoxO/DAF-16 identified in my work. For example, FoxO/DAF-16 is especially well-known for its role in the link between nutrition and longevity, prolonging organismal survival during nutrient deprivation (Greer et al., 2007, Hibshman et al., 2017, Kramer et al., 2008). Moreover, FoxO/DAF-16 has been reported to regulate the expression of genes associated with mitochondrial function and stress response (Depuydt et al., 2014, Tepper et al., 2013, Webb et al., 2016). Together with my findings, these studies suggest that in the presence of deleterious mitochondrial mutations, FoxO/DAF-16 likely functions to rescue energy production and protect against physiological stress, enabling the mutant mtDNA to proliferate while simultaneously mitigating its deleterious host fitness effects. Interestingly, FoxO/DAF-16 promotes proliferation of the mutant genome only in the presence of nutrient abundance (see Chapter 6), while it robustly mitigates the host fitness cost of the mutant genome especially in the presence of nutrient scarcity. These results raise the intriguing possibility that FoxO/DAF-16 mitigates the fitness cost of mutant mtDNA through a function that is related to its role in diet restriction-mediated longevity.

By fueling germline development, nutrient abundance creates the niche space for mitochondrial genomes to multiply within hosts. However, the preferential amplification of the mutant genome also requires FoxO/DAF-16, suggesting that FoxO/DAF-16 may mediate a compensatory mechanism that inadvertently contributes to proliferation of the mutant mtDNA, similarly to UPR^{mt}. Is it possible to decouple these functions of FoxO/DAF-16 across the different levels of selection, so that its role in mutant mtDNA proliferation can be disabled while preserving its role in mitigating the harmful effects of the mtDNA mutation? Future studies that address this question by clarifying the details downstream of FoxO/DAF-16 could potentially lead to therapeutic applications.

Generalizability of my findings

The vast majority of my work described thus far focuses on the cheating behavior of *uaDf5*. While such a focus enabled a deep exploration of mechanisms underlying the proliferation of this genome, mtDNA encodes subunits of several electron transport chain (ETC) complexes, as well as transfer RNA (tRNA) and ribosomal RNA. The phenotypic effects and corresponding population dynamics of mitochondrial mutations can therefore be predicted to vary. I sought to identify common themes and notable differences in the propensity for cheating—including both within-host proliferation and host fitness cost—by examining a wider collection of mitochondrial mutations. By repeating the experiments designed to measure within-host and host-level selection across a collection of five additional heteroplasmic mtDNA variants, representing mutations in ETC complexes I, III, and IV, as well as deletions affecting both protein-coding and tRNA genes, I found that some but not all mutant genomes behave similarly to *uaDf5*. In particular, some mtDNA mutations persist without inflicting a significant fitness cost on their host. Since all six heteroplasmies included in this study feature deletions in at least one essential ETC component, the lack of observable host fitness cost among some heteroplasmies is presumably because these genomes persist in a frequency range below the threshold at which the deleterious fitness effects would become manifest. On the other hand, some mutations, particularly those affecting *CO1* (a central catalytic subunit of ETC complex IV), were observed to inflict a severe host fitness cost. Their persistence within their respective host populations therefore predicts that these two mutations would behave most selfishly, having the strongest tendency to rise in frequency within individual hosts. Indeed, this prediction is consistent with my observations. In conclusion, although I observe variation in the propensity for selfish proliferation, the proliferation and host fitness consequences among three of the six mutant mtDNA variants in my research—*uaDf5*, *mptDf2*, and *mpt4*—implies that cheating likely represents a common strategy of mitochondrial genomes, particularly with respect to competition within the germline for transmission to future generations.

Concluding remarks

I initially set out to design experiments to assess natural selection at different levels, within and between hosts, in response to preliminary observations of nuclear genotypes that affect mutant mtDNA frequency (see Chapters 4 and 6). Knowing the level(s) at which such an effect occurs is important for the sake of follow-up research and potential biomedical applications. For example, if an experimental condition results in a shift to lower mutant mtDNA frequency across a population of *C. elegans*, does this shift arise from changes in organismal or sub-organismal selection? Perhaps the experimental condition makes animals with high levels of mutant mtDNA less viable, in which case the observed population-wide shift toward lower mutant frequency results from stronger selection against the mutant at the organismal level—that is, by altering selection for host fitness. Alternatively, the shift to lower mutant mtDNA frequency may be due to an effect on the physiology of the organism that alters the within-host competition between mutant and wildtype mtDNA. Although either possibility would be insightful, since a deeper understanding of both the propagation and phenotypic effects of a mutant genome hang in the balance, the ability to follow up on these findings with detailed mechanistic characterization nevertheless requires the ability to parse the magnitude that each level of selection contributes toward the overall population dynamics of the mutant genome. By taking this into consideration, I was able to identify an interesting interaction between host genome and an environmental condition—dietary nutrient availability—that shapes the outcome of competition between the selfish and cooperative mitochondrial genomes. In future research, the experiments to quantitatively measure the multilevel selection forces acting on mitochondrial genomes could be applied to additional heteroplasmies, environmental conditions, and host genotypes, to uncover any number of hitherto unidentified ways in which evolutionary forces shape the complex interactions at the foundation of the eukaryotic cell.

References

ADAMS, K. L. & PALMER, J. D. 2003. Evolution of mitochondrial gene content: gene loss and transfer to the nucleus. *Mol Phylogenet Evol,* 29**,** 380-95.

AGREN, J. A. & CLARK, A. G. 2018. Selfish genetic elements. *PLoS Genet,* 14**,** e1007700.

AHIER, A., DAI, C. Y., TWEEDIE, A., BEZAWORK-GELETA, A., KIRMES, I. & ZURYN, S. 2018. Affinity purification of cell-specific mitochondria from whole animals resolves patterns of genetic mosaicism. *Nat Cell Biol,* 20**,** 352-360.

AKTIPIS, C. A., BODDY, A. M., JANSEN, G., HIBNER, U., HOCHBERG, M. E., MALEY, C. C. & WILKINSON, G. S. 2015. Cancer across the tree of life: cooperation and cheating in multicellularity. *Philos Trans R Soc Lond B Biol Sci,* 370.

AL RAWI, S., LOUVET-VALLEE, S., DJEDDI, A., SACHSE, M., CULETTO, E., HAJJAR, C., BOYD, L., LEGOUIS, R. & GALY, V. 2011. Postfertilization autophagy of sperm organelles prevents paternal mitochondrial DNA transmission. *Science,* 334**,** 1144-7.

ALLEN, G. F., TOTH, R., JAMES, J. & GANLEY, I. G. 2013. Loss of iron triggers PINK1/Parkin-independent mitophagy. *EMBO Rep,* 14**,** 1127-35.

ALLEN, J. F. 1993. Control of gene expression by redox potential and the requirement for chloroplast and mitochondrial genomes. *J Theor Biol,* 165**,** 609-31.

ALLEN, J. F. 2015. Why chloroplasts and mitochondria retain their own genomes and genetic systems: Colocation for redox regulation of gene expression. *Proc Natl Acad Sci U S A,* 112**,** 10231-8.

ANDERSON, J. A., GILLILAND, W. D. & LANGLEY, C. H. 2009. Molecular population genetics and evolution of Drosophila meiosis genes. *Genetics,* 181**,** 177-85.

ANGELO, G. & VAN GILST, M. R. 2009. Starvation protects germline stem cells and extends reproductive longevity in C. elegans. *Science,* 326**,** 954-8.

AUMER, D., STOLLE, E., ALLSOPP, M., MUMOKI, F., PIRK, C. W. W. & MORITZ, R. F. A. 2019. A Single SNP Turns a Social Honey Bee (Apis mellifera) Worker into a Selfish Parasite. *Molecular Biology and Evolution,* 36**,** 516-526.

BADISCO, L., VAN WIELENDAELE, P. & VANDEN BROECK, J. 2013. Eat to reproduce: a key role for the insulin signaling pathway in adult insects. *Front Physiol,* 4**,** 202.

BAKER, B. M., NARGUND, A. M., SUN, T. & HAYNES, C. M. 2012. Protective coupling of mitochondrial function and protein synthesis via the eIF2alpha kinase GCN-2. *PLoS Genet,* 8**,** e1002760.

BENEDETTI, C., HAYNES, C. M., YANG, Y., HARDING, H. P. & RON, D. 2006. Ubiquitin-like protein 5 positively regulates chaperone gene expression in the mitochondrial unfolded protein response. *Genetics,* 174**,** 229-39.

BERG, O. G. & KURLAND, C. G. 2000. Why mitochondrial genes are most often found in nuclei. *Mol Biol Evol,* 17**,** 951-61.

BERNARDI, G. 2005. Lessons from a small, dispensable genome: the mitochondrial genome of yeast. *Gene,* 354**,** 189-200.

BILLING, O., KAO, G. & NAREDI, P. 2011. Mitochondrial function is required for secretion of DAF-28/insulin in C. elegans. *PLoS One,* 6**,** e14507.

BJORKHOLM, P., HARISH, A., HAGSTROM, E., ERNST, A. M. & ANDERSSON, S. G. 2015. Mitochondrial genomes are retained by selective constraints on protein targeting. *Proc Natl Acad Sci U S A,* 112**,** 10154-61.

BLANCHARD, J. L. & LYNCH, M. 2000. Organellar genes: why do they end up in the nucleus? *Trends Genet,* 16**,** 315-20.

BOGENHAGEN, D. & CLAYTON, D. A. 1977. Mouse L cell mitochondrial DNA molecules are selected randomly for replication throughout the cell cycle. *Cell,* 11**,** 719-27.

BRANDVAIN, Y. & WADE, M. J. 2009. The functional transfer of genes from the mitochondria to the nucleus: the effects of selection, mutation, population size and rate of self-fertilization. *Genetics,* 182**,** 1129-39.

BRATIC, I., HENCH, J., HENRIKSSON, J., ANTEBI, A., BURGLIN, T. R. & TRIFUNOVIC, A. 2009. Mitochondrial DNA level, but not active replicase, is essential for Caenorhabditis elegans development. *Nucleic Acids Res,* 37**,** 1817-28.

BRAVO NUNEZ, M. A., NUCKOLLS, N. L. & ZANDERS, S. E. 2018. Genetic Villains: Killer Meiotic Drivers. *Trends Genet,* 34**,** 424-433.

BROCKHURST, M. A., BUCKLING, A., RACEY, D. & GARDNER, A. 2008. Resource supply and the evolution of public-goods cooperation in bacteria. *BMC Biol,* 6**,** 20.

BROWN, M. D., YANG, C. C., TROUNCE, I., TORRONI, A., LOTT, M. T. & WALLACE, D. C. 1992. A mitochondrial DNA variant, identified in Leber hereditary optic neuropathy patients, which extends the amino acid sequence of cytochrome c oxidase subunit I. *Am J Hum Genet,* 51**,** 378-85.

CAO, P., DEY, A., VASSALLO, C. N. & WALL, D. 2015. How Myxobacteria Cooperate. *J Mol Biol,* 427**,** 3709-21.

CAPPS, G. J., SAMUELS, D. C. & CHINNERY, P. F. 2003. A model of the nuclear control of mitochondrial DNA replication. *J Theor Biol,* 221**,** 565-83.

CARABALLO, H. & KING, K. 2014. Emergency department management of mosquito-borne illness: malaria, dengue, and West Nile virus. *Emerg Med Pract,* 16**,** 1-23; quiz 23-4.

CHATRE, L. & RICCHETTI, M. 2013. Prevalent coordination of mitochondrial DNA transcription and initiation of replication with the cell cycle. *Nucleic Acids Res,* 41**,** 3068-78.

CHEN, X. & PERC, M. 2014. Excessive abundance of common resources deters social responsibility. *Sci Rep,* 4**,** 4161.

CHEN, X. J. & CLARK-WALKER, G. D. 2000. The petite mutation in yeasts: 50 years on. *Int Rev Cytol,* 194**,** 197-238.

CHIANG, A. C., MCCARTNEY, E., O'FARRELL, P. H. & MA, H. 2019. A Genome-wide Screen Reveals that Reducing Mitochondrial DNA Polymerase Can Promote Elimination of Deleterious Mitochondrial Mutations. *Curr Biol,* 29**,** 4330-4336 e3.

CHINNERY, P. F. & SAMUELS, D. C. 1999. Relaxed replication of mtDNA: A model with implications for the expression of disease. *Am J Hum Genet,* 64**,** 1158-65.

CHISHOLM, R. L. & FIRTEL, R. A. 2004. Insights into morphogenesis from a simple developmental system. *Nat Rev Mol Cell Biol,* 5**,** 531-41.

CHRISTIE, J. R., SCHAERF, T. M. & BEEKMAN, M. 2015. Selection against heteroplasmy explains the evolution of uniparental inheritance of mitochondria. *PLoS Genet,* 11**,** e1005112.

CLARK, K. A., HOWE, D. K., GAFNER, K., KUSUMA, D., PING, S., ESTES, S. & DENVER, D. R. 2012. Selfish little circles: transmission bias and evolution of large deletion-bearing mitochondrial DNA in Caenorhabditis briggsae nematodes. *PLoS One,* 7**,** e41433.

CLAY MONTIER, L. L., DENG, J. J. & BAI, Y. 2009. Number matters: control of mammalian mitochondrial DNA copy number. *J Genet Genomics,* 36**,** 125-31.

CONNELLY, B. D., BRUGER, E. L., MCKINLEY, P. K. & WATERS, C. M. 2017. Resource abundance and the critical transition to cooperation. *J Evol Biol,* 30**,** 750-761.

CONSORTIUM, C. E. S. 1998. Genome sequence of the nematode C. elegans: a platform for investigating biology. *Science,* 282**,** 2012-8.

CRISTINA, D., CARY, M., LUNCEFORD, A., CLARKE, C. & KENYON, C. 2009. A regulated response to impaired respiration slows behavioral rates and increases lifespan in Caenorhabditis elegans. *PLoS Genet,* 5**,** e1000450.

DANIELSEN, E. T., MOELLER, M. E. & REWITZ, K. F. 2013. Nutrient signaling and developmental timing of maturation. *Curr Top Dev Biol,* 105**,** 37-67.

DAS, D. & ARUR, S. 2017. Conserved insulin signaling in the regulation of oocyte growth, development, and maturation. *Mol Reprod Dev,* 84**,** 444-459.

DE VARGAS RODITI, L., BOYLE, K. E. & XAVIER, J. B. 2013. Multilevel selection analysis of a microbial social trait. *Mol Syst Biol,* 9**,** 684.

DEPUYDT, G., XIE, F., PETYUK, V. A., SMOLDERS, A., BREWER, H. M., CAMP, D. G., 2ND, SMITH, R. D. & BRAECKMAN, B. P. 2014. LC-MS proteomics analysis of the insulin/IGF-1-deficient Caenorhabditis elegans daf-2(e1370) mutant reveals extensive restructuring of intermediary metabolism. *J Proteome Res,* 13**,** 1938-56.

DI RITA, A., PESCHIAROLI, A., P, D. A., STROBBE, D., HU, Z., GRUBER, J., NYGAARD, M., LAMBRUGHI, M., MELINO, G., PAPALEO, E., DENGJEL, J., EL ALAOUI, S., CAMPANELLA, M., DOTSCH, V., ROGOV, V. V., STRAPPAZZON, F. & CECCONI, F. 2018. HUWE1 E3 ligase promotes PINK1/PARKIN-independent mitophagy by regulating AMBRA1 activation via IKKalpha. *Nat Commun,* 9**,** 3755.

DIAZ, F., BAYONA-BAFALUY, M. P., RANA, M., MORA, M., HAO, H. & MORAES, C. T. 2002. Human mitochondrial DNA with large deletions repopulates organelles faster than full-length genomes under relaxed copy number control. *Nucleic Acids Res,* 30**,** 4626-33.

DILLIN, A., HSU, A. L., ARANTES-OLIVEIRA, N., LEHRER-GRAIWER, J., HSIN, H., FRASER, A. G., KAMATH, R. S., AHRINGER, J. & KENYON, C. 2002. Rates of behavior and aging specified by mitochondrial function during development. *Science,* 298**,** 2398-401.

DINGLEY, S. D., POLYAK, E., OSTROVSKY, J., SRINIVASAN, S., LEE, I., ROSENFELD, A. B., TSUKIKAWA, M., XIAO, R., SELAK, M. A., COON, J. J., HEBERT, A. S., GRIMSRUD, P. A., KWON, Y. J., PAGLIARINI, D. J., GAI, X., SCHURR, T. G., HUTTEMANN, M., NAKAMARU-OGISO, E. & FALK, M. J. 2014. Mitochondrial DNA variant in COX1 subunit significantly alters energy metabolism of geographically divergent wild isolates in Caenorhabditis elegans. *J Mol Biol,* 426**,** 2199-216.

DOBATA, S., SASAKI, T., MORI, H., HASEGAWA, E., SHIMADA, M. & TSUJI, K. 2009. Cheater genotypes in the parthenogenetic ant Pristomyrmex punctatus. *Proc Biol Sci,* 276**,** 567-74.

DOBATA, S. & TSUJI, K. 2013. Public goods dilemma in asexual ant societies. *Proc Natl Acad Sci U S A,* 110**,** 16056-60.

DRUMMOND-BARBOSA, D. & SPRADLING, A. C. 2001. Stem cells and their progeny respond to nutritional changes during Drosophila oogenesis. *Dev Biol,* 231**,** 265-78.

DUBIE, J. J., CARAWAY, A. R., STOUT, M. M., KATJU, V. & BERGTHORSSON, U. 2020. The conflict within: origin, proliferation and persistence of a spontaneously arising selfish mitochondrial genome. *Philos Trans R Soc Lond B Biol Sci,* 375**,** 20190174.

DUCASSE, H., ARNAL, A., VITTECOQ, M., DAOUST, S. P., UJVARI, B., JACQUELINE, C., TISSOT, T., EWALD, P., GATENBY, R. A., KING, K. C., BONHOMME, F., BRODEUR, J., RENAUD, F., SOLARY, E., ROCHE, B. & THOMAS, F. 2015. Cancer: an emergent property of disturbed resource-rich environments? Ecology meets personalized medicine. *Evolutionary Applications,* 8**,** 527-540.

DUGATKIN, L. A., PERLIN, M., LUCAS, J. S. & ATLAS, R. 2005. Group-beneficial traits, frequency-dependent selection and genotypic diversity: an antibiotic resistance paradigm. *Proc Biol Sci,* 272**,** 79-83.

DUNBAR, D. R., MOONIE, P. A., JACOBS, H. T. & HOLT, I. J. 1995. Different cellular backgrounds confer a marked advantage to either mutant or wild-type mitochondrial genomes. *Proc Natl Acad Sci U S A,* 92**,** 6562-6.

DURHAM, S. E., SAMUELS, D. C., CREE, L. M. & CHINNERY, P. F. 2007. Normal levels of wild-type mitochondrial DNA maintain cytochrome c oxidase activity for two pathogenic mitochondrial DNA mutations but not for m.3243A-->G. *Am J Hum Genet,* 81**,** 189-95.

DURIEUX, J., WOLFF, S. & DILLIN, A. 2011. The cell-non-autonomous nature of electron transport chain-mediated longevity. *Cell,* 144**,** 79-91.

DUTRA, H. L., ROCHA, M. N., DIAS, F. B., MANSUR, S. B., CARAGATA, E. P. & MOREIRA, L. A. 2016. Wolbachia Blocks Currently Circulating Zika Virus Isolates in Brazilian Aedes aegypti Mosquitoes. *Cell Host Microbe,* 19**,** 771-4.

ECKL, E. M., ZIEGEMANN, O., KRUMWIEDE, L., FESSLER, E. & JAE, L. T. 2021. Sensing, signaling and surviving mitochondrial stress. *Cell Mol Life Sci*.

ESTES, S., COLEMAN-HULBERT, A. L., HICKS, K. A., DE HAAN, G., MARTHA, S. R., KNAPP, J. B., SMITH, S. W., STEIN, K. C. & DENVER, D. R. 2011. Natural variation in life history and aging phenotypes is associated with mitochondrial DNA deletion frequency in Caenorhabditis briggsae. *BMC Evol Biol,* 11**,** 11.

FAN, W., WAYMIRE, K. G., NARULA, N., LI, P., ROCHER, C., COSKUN, P. E., VANNAN, M. A., NARULA, J., MACGREGOR, G. R. & WALLACE, D. C. 2008. A mouse model of mitochondrial disease reveals germline selection against severe mtDNA mutations. *Science,* 319**,** 958-62.

FIEGNA, F. & VELICER, G. J. 2003. Competitive fates of bacterial social parasites: persistence and self-induced extinction of Myxococcus xanthus cheaters. *Proc Biol Sci,* 270**,** 1527-34.

FIORESE, C. J., SCHULZ, A. M., LIN, Y. F., ROSIN, N., PELLEGRINO, M. W. & HAYNES, C. M. 2016. The Transcription Factor ATF5 Mediates a Mammalian Mitochondrial UPR. *Curr Biol,* 26**,** 2037-2043.

FIRE, A., XU, S., MONTGOMERY, M. K., KOSTAS, S. A., DRIVER, S. E. & MELLO, C. C. 1998. Potent and specific genetic interference by double-stranded RNA in Caenorhabditis elegans. *Nature,* 391**,** 806-11.

FISHER, R. M. & REGENBERG, B. 2019. Multicellular group formation in Saccharomyces cerevisiae. *Proc Biol Sci,* 286**,** 20191098.

FRANK, S. A. 1997. The Price Equation, Fisher's fundamental theorem, kin selection, and causal analysis. *Evolution,* 51**,** 1712-1729.

FRANK, S. A. 2012. Natural selection. IV. The Price equation. *J Evol Biol,* 25**,** 1002-19.

GHOUL, M., GRIFFIN, A. S. & WEST, S. A. 2014. Toward an evolutionary definition of cheating. *Evolution,* 68**,** 318-31.

GITSCHLAG, B. L., KIRBY, C. S., SAMUELS, D. C., GANGULA, R. D., MALLAL, S. A. & PATEL, M. R. 2016. Homeostatic Responses Regulate Selfish Mitochondrial Genome Dynamics in C. elegans. *Cell Metab,* 24**,** 91-103.

GITSCHLAG, B. L., TATE, A. T. & PATEL, M. R. 2020. Nutrient status shapes selfish mitochondrial genome dynamics across different levels of selection. *Elife,* 9.

GOODNIGHT, C. J. 2015. Multilevel selection theory and evidence: a critique of Gardner, 2015. *Journal of Evolutionary Biology,* 28**,** 1734-1746.

GOODNIGHT, C. J., SCHWARTZ, J. M. & STEVENS, L. 1992. Contextual Analysis of Models of Group Selection, Soft Selection, Hard Selection, and the Evolution of Altruism. *American Naturalist,* 140**,** 743-761.

GORBUNOVA, V. & SELUANOV, A. 2002. CLK-1 protein has DNA binding activity specific to O(L) region of mitochondrial DNA. *FEBS Lett,* 516**,** 279-84.

GOTTLIEB, S. & RUVKUN, G. 1994. daf-2, daf-16 and daf-23: genetically interacting genes controlling Dauer formation in Caenorhabditis elegans. *Genetics,* 137**,** 107-20.

GRANDHI, S., BOSWORTH, C., MADDOX, W., SENSIBA, C., AKHAVANFARD, S., NI, Y. & LAFRAMBOISE, T. 2017. Heteroplasmic shifts in tumor mitochondrial genomes reveal tissue-specific signals of relaxed and positive selection. *Hum Mol Genet,* 26**,** 2912-2922.

GREER, E. L., DOWLATSHAHI, D., BANKO, M. R., VILLEN, J., HOANG, K., BLANCHARD, D., GYGI, S. P. & BRUNET, A. 2007. An AMPK-FOXO pathway mediates longevity induced by a novel method of dietary restriction in C. elegans. *Curr Biol,* 17**,** 1646-56.

GULLI, J. G., HERRON, M. D. & RATCLIFF, W. C. 2019. Evolution of altruistic cooperation among nascent multicellular organisms. *Evolution,* 73**,** 1012-1024.

HADJIVASILIOU, Z., POMIANKOWSKI, A., SEYMOUR, R. M. & LANE, N. 2012. Selection for mitonuclear co-adaptation could favour the evolution of two sexes. *Proc Biol Sci,* 279**,** 1865-72.

HAMMERSCHMIDT, K., LANDAN, G., DOMINGUES KUMMEL TRIA, F., ALCORTA, J. & DAGAN, T. 2021. The Order of Trait Emergence in the Evolution of Cyanobacterial Multicellularity. *Genome Biol Evol,* 13.

HAMMERSCHMIDT, K., ROSE, C. J., KERR, B. & RAINEY, P. B. 2014. Life cycles, fitness decoupling and the evolution of multicellularity. *Nature,* 515**,** 75-9.

HAMMOND, T. M., REHARD, D. G., XIAO, H. & SHIU, P. K. 2012. Molecular dissection of Neurospora Spore killer meiotic drive elements. *Proc Natl Acad Sci U S A,* 109**,** 12093-8.

HARRISON, E., MACLEAN, R. C., KOUFOPANOU, V. & BURT, A. 2014. Sex drives intracellular conflict in yeast. *J Evol Biol,* 27**,** 1757-63.

HAVIRD, J. C., FORSYTHE, E. S., WILLIAMS, A. M., WERREN, J. H., DOWLING, D. K. & SLOAN, D. B. 2019. Selfish Mitonuclear Conflict. *Curr Biol,* 29**,** R496-R511.

HAYNES, C. M. & RON, D. 2010. The mitochondrial UPR - protecting organelle protein homeostasis. *J Cell Sci,* 123**,** 3849-55.

HEISLER, I. L. & DAMUTH, J. 1987. A Method for Analyzing Selection in Hierarchically Structured Populations. *American Naturalist,* 130**,** 582-602.

HENIKOFF, S., AHMAD, K. & MALIK, H. S. 2001. The centromere paradox: stable inheritance with rapidly evolving DNA. *Science,* 293**,** 1098-102.

HERBST, A., JOHNSON, C. J., HYNES, K., MCKENZIE, D. & AIKEN, J. M. 2013. Mitochondrial biogenesis drives a vicious cycle of metabolic insufficiency and mitochondrial DNA deletion mutation accumulation in aged rat skeletal muscle fibers. *PLoS One,* 8**,** e59006.

HIBSHMAN, J. D., DOAN, A. E., MOORE, B. T., KAPLAN, R. E., HUNG, A., WEBSTER, A. K., BHATT, D. P., CHITRAKAR, R., HIRSCHEY, M. D. & BAUGH, L. R. 2017. daf-16/FoxO promotes gluconeogenesis and trehalose synthesis during starvation to support survival. *Elife,* 6.

HIBSHMAN, J. D., LEUTHNER, T. C., SHOBEN, C., MELLO, D. F., SHERWOOD, D. R., MEYER, J. N. & BAUGH, L. R. 2018. Nonselective autophagy reduces mitochondrial content during starvation in Caenorhabditis elegans. *Am J Physiol Cell Physiol,* 315**,** C781-C792.

HICKS, K. A., HOWE, D. K., LEUNG, A., DENVER, D. R. & ESTES, S. 2012. In vivo quantification reveals extensive natural variation in mitochondrial form and function in Caenorhabditis briggsae. *PLoS One,* 7**,** e43837.

HILGENBOECKER, K., HAMMERSTEIN, P., SCHLATTMANN, P., TELSCHOW, A. & WERREN, J. H. 2008. How many species are infected with Wolbachia?--A statistical analysis of current data. *FEMS Microbiol Lett,* 281**,** 215-20.

HILL, J. H., CHEN, Z. & XU, H. 2014. Selective propagation of functional mitochondrial DNA during oogenesis restricts the transmission of a deleterious mitochondrial variant. *Nat Genet,* 46**,** 389-92.

HINDSON, B. J., NESS, K. D., MASQUELIER, D. A., BELGRADER, P., HEREDIA, N. J., MAKAREWICZ, A. J., BRIGHT, I. J., LUCERO, M. Y., HIDDESSEN, A. L., LEGLER, T. C., KITANO, T. K., HODEL, M. R., PETERSEN, J. F., WYATT, P. W., STEENBLOCK, E. R., SHAH, P. H., BOUSSE, L. J., TROUP, C. B., MELLEN, J. C., WITTMANN, D. K., ERNDT, N. G., CAULEY, T. H., KOEHLER, R. T., SO, A. P., DUBE, S., ROSE, K. A., MONTESCLAROS, L., WANG, S., STUMBO, D. P., HODGES, S. P., ROMINE, S., MILANOVICH, F. P., WHITE, H. E., REGAN, J. F., KARLIN-NEUMANN, G. A., HINDSON, C. M., SAXONOV, S. & COLSTON, B. W. 2011. High-throughput droplet digital PCR system for absolute quantitation of DNA copy number. *Anal Chem,* 83**,** 8604-10.

HOLLIS, B. 2012. Rapid antagonistic coevolution between strains of the social amoeba Dictyostelium discoideum. *Proc Biol Sci,* 279**,** 3565-71.

HOLT, I. J., DUNBAR, D. R. & JACOBS, H. T. 1997. Behaviour of a population of partially duplicated mitochondrial DNA molecules in cell culture: segregation, maintenance and recombination dependent upon nuclear background. *Hum Mol Genet,* 6**,** 1251-60.

HOLT, I. J., HARDING, A. E. & MORGAN-HUGHES, J. A. 1988. Deletions of muscle mitochondrial DNA in patients with mitochondrial myopathies. *Nature,* 331**,** 717-9.

HOLT, I. J., SPEIJER, D. & KIRKWOOD, T. B. 2014. The road to rack and ruin: selecting deleterious mitochondrial DNA variants. *Philos Trans R Soc Lond B Biol Sci,* 369**,** 20130451.

HORNETT, E. A., DUPLOUY, A. M., DAVIES, N., RODERICK, G. K., WEDELL, N., HURST, G. D. & CHARLAT, S. 2008. You can't keep a good parasite down: evolution of a male-killer suppressor uncovers cytoplasmic incompatibility. *Evolution,* 62**,** 1258-63.

HOUTKOOPER, R. H., MOUCHIROUD, L., RYU, D., MOULLAN, N., KATSYUBA, E., KNOTT, G., WILLIAMS, R. W. & AUWERX, J. 2013. Mitonuclear protein imbalance as a conserved longevity mechanism. *Nature,* 497**,** 451-7.

HOWE, D. K. & DENVER, D. R. 2008. Muller's Ratchet and compensatory mutation in Caenorhabditis briggsae mitochondrial genome evolution. *BMC Evol Biol,* 8**,** 62.

HU, W., JIANG, Z. D., SUO, F., ZHENG, J. X., HE, W. Z. & DU, L. L. 2017. A large gene family in fission yeast encodes spore killers that subvert Mendel's law. *Elife,* 6.

HUGHES, S. E., EVASON, K., XIONG, C. & KORNFELD, K. 2007. Genetic and pharmacological factors that influence reproductive aging in nematodes. *PLoS Genet,* 3**,** e25.

JAENIKE, J. 2007. Spontaneous emergence of a new Wolbachia phenotype. *Evolution,* 61**,** 2244-52.

JASMIN, J. N. & ZEYL, C. 2014. Rapid evolution of cheating mitochondrial genomes in small yeast populations. *Evolution,* 68**,** 269-75.

JENSEN, M. B. & JASPER, H. 2014. Mitochondrial proteostasis in the control of aging and longevity. *Cell Metab,* 20**,** 214-25.

KANDUL, N. P., ZHANG, T., HAY, B. A. & GUO, M. 2016. Selective removal of deletion-bearing mitochondrial DNA in heteroplasmic Drosophila. *Nat Commun,* 7**,** 13100.

KHARE, A., SANTORELLI, L. A., STRASSMANN, J. E., QUELLER, D. C., KUSPA, A. & SHAULSKY, G. 2009. Cheater-resistance is not futile. *Nature,* 461**,** 980-2.

KIRBY, C. S. & PATEL, M. R. 2021. Elevated mitochondrial DNA copy number found in ubiquinone-deficient clk-1 mutants is not rescued by ubiquinone precursor 2-4-dihydroxybenzoate. *Mitochondrion,* 58**,** 38-48.

KLOTZ, L. O., SANCHEZ-RAMOS, C., PRIETO-ARROYO, I., URBANEK, P., STEINBRENNER, H. & MONSALVE, M. 2015. Redox regulation of FoxO transcription factors. *Redox Biology,* 6**,** 51-72.

KLUCNIKA, A. & MA, H. 2019. A battle for transmission: the cooperative and selfish animal mitochondrial genomes. *Open Biol,* 9**,** 180267.

KONRAD, A., THOMPSON, O., WATERSTON, R. H., MOERMAN, D. G., KEIGHTLEY, P. D., BERGTHORSSON, U. & KATJU, V. 2017. Mitochondrial Mutation Rate, Spectrum and Heteroplasmy in Caenorhabditis elegans Spontaneous Mutation Accumulation Lines of Differing Population Size. *Mol Biol Evol,* 34**,** 1319-1334.

KOSCHWANEZ, J. H., FOSTER, K. R. & MURRAY, A. W. 2013. Improved use of a public good selects for the evolution of undifferentiated multicellularity. *Elife,* 2**,** e00367.

KRAMER, J. M., SLADE, J. D. & STAVELEY, B. E. 2008. foxo is required for resistance to amino acid starvation in Drosophila. *Genome,* 51**,** 668-72.

LAMELZA, P. & AILION, M. 2017. Cytoplasmic-Nuclear Incompatibility Between Wild Isolates of Caenorhabditis nouraguensis. *G3 (Bethesda),* 7**,** 823-834.

LANE, N. 2014. Bioenergetic constraints on the evolution of complex life. *Cold Spring Harb Perspect Biol,* 6**,** a015982.

LANG, B. F., SEIF, E., GRAY, M. W., O'KELLY, C. J. & BURGER, G. 1999. A comparative genomics approach to the evolution of eukaryotes and their mitochondria. *J Eukaryot Microbiol,* 46**,** 320-6.

LARRACUENTE, A. M. & PRESGRAVES, D. C. 2012. The selfish Segregation Distorter gene complex of Drosophila melanogaster. *Genetics,* 192**,** 33-53.

LARSSON, N. G., HOLME, E., KRISTIANSSON, B., OLDFORS, A. & TULINIUS, M. 1990. Progressive increase of the mutated mitochondrial DNA fraction in Kearns-Sayre syndrome. *Pediatr Res,* 28**,** 131-6.

LEE, S. & DONG, H. H. 2017. FoxO integration of insulin signaling with glucose and lipid metabolism. *Journal of Endocrinology,* 233**,** R67-R79.

LEE, Y. C., LEEK, C. & LEVINE, M. T. 2017. Recurrent Innovation at Genes Required for Telomere Integrity in Drosophila. *Mol Biol Evol,* 34**,** 467-482.

LEIGH, E. G. 1983. When does the good of the group override the advantage of the individual? *Proc Natl Acad Sci U S A,* 80**,** 2985-9.

LEPAGE, D. P., METCALF, J. A., BORDENSTEIN, S. R., ON, J., PERLMUTTER, J. I., SHROPSHIRE, J. D., LAYTON, E. M., FUNKHOUSER-JONES, L. J., BECKMANN, J. F. & BORDENSTEIN, S. R. 2017. Prophage WO genes recapitulate and enhance Wolbachia-induced cytoplasmic incompatibility. *Nature,* 543**,** 243-247.

LI, S. I. & PURUGGANAN, M. D. 2011. The cooperative amoeba: Dictyostelium as a model for social evolution. *Trends Genet,* 27**,** 48-54.

LIAU, W. S., GONZALEZ-SERRICCHIO, A. S., DESHOMMES, C., CHIN, K. & LAMUNYON, C. W. 2007. A persistent mitochondrial deletion reduces fitness and sperm performance in heteroplasmic populations of C. elegans. *BMC Genet,* 8**,** 8.

LIEBER, T., JEEDIGUNTA, S. P., PALOZZI, J. M., LEHMANN, R. & HURD, T. R. 2019. Mitochondrial fragmentation drives selective removal of deleterious mtDNA in the germline. *Nature,* 570**,** 380-384.

LIN, Y. F., SCHULZ, A. M., PELLEGRINO, M. W., LU, Y., SHAHAM, S. & HAYNES, C. M. 2016. Maintenance and propagation of a deleterious mitochondrial genome by the mitochondrial unfolded protein response. *Nature,* 533**,** 416-9.

LIU, W., ACIN-PEREZ, R., GEGHMAN, K. D., MANFREDI, G., LU, B. & LI, C. 2011. Pink1 regulates the oxidative phosphorylation machinery via mitochondrial fission. *Proc Natl Acad Sci U S A,* 108**,** 12920-4.

LOPEZ, A. L., 3RD, CHEN, J., JOO, H. J., DRAKE, M., SHIDATE, M., KSEIB, C. & ARUR, S. 2013. DAF-2 and ERK couple nutrient availability to meiotic progression during Caenorhabditis elegans oogenesis. *Dev Cell,* 27**,** 227-240.

MA, H., XU, H. & O'FARRELL, P. H. 2014. Transmission of mitochondrial mutations and action of purifying selection in Drosophila melanogaster. *Nat Genet,* 46**,** 393-7.

MACALPINE, D. M., KOLESAR, J., OKAMOTO, K., BUTOW, R. A. & PERLMAN, P. S. 2001. Replication and preferential inheritance of hypersuppressive petite mitochondrial DNA. *EMBO J,* 20**,** 1807-17.

MANHES, P. & VELICER, G. J. 2011. Experimental evolution of selfish policing in social bacteria. *Proc Natl Acad Sci U S A,* 108**,** 8357-62.

MARTINS, R., LITHGOW, G. J. & LINK, W. 2016. Long live FOXO: unraveling the role of FOXO proteins in aging and longevity. *Aging Cell,* 15**,** 196-207.

MATSUDA, N., SATO, S., SHIBA, K., OKATSU, K., SAISHO, K., GAUTIER, C. A., SOU, Y. S., SAIKI, S., KAWAJIRI, S., SATO, F., KIMURA, M., KOMATSU, M., HATTORI, N. & TANAKA, K. 2010. PINK1 stabilized by mitochondrial depolarization recruits Parkin to damaged mitochondria and activates latent Parkin for mitophagy. *J Cell Biol,* 189**,** 211-21.

MCLAUGHLIN, R. N., JR. & MALIK, H. S. 2017. Genetic conflicts: the usual suspects and beyond. *J Exp Biol,* 220**,** 6-17.

MICHAELSON, D., KORTA, D. Z., CAPUA, Y. & HUBBARD, E. J. A. 2010. Insulin signaling promotes germline proliferation in C. elegans. *Development,* 137**,** 671-680.

MICHOD, R. E. 2006. The group covariance effect and fitness trade-offs during evolutionary transitions in individuality. *Proc Natl Acad Sci U S A,* 103**,** 9113-7.

MICHOD, R. E. & ROZE, D. 1997. Transitions in individuality. *Proc Biol Sci,* 264**,** 853-7.

MICHOD, R. E., VIOSSAT, Y., SOLARI, C. A., HURAND, M. & NEDELCU, A. M. 2006. Life-history evolution and the origin of multicellularity. *J Theor Biol,* 239**,** 257-72.

MORAES, C. T., KENYON, L. & HAO, H. 1999. Mechanisms of human mitochondrial DNA maintenance: the determining role of primary sequence and length over function. *Mol Biol Cell,* 10**,** 3345-56.

MORAES, C. T., SCIACCO, M., RICCI, E., TENGAN, C. H., HAO, H., BONILLA, E., SCHON, E. A. & DIMAURO, S. 1995. Phenotype-genotype correlations in skeletal muscle of patients with mtDNA deletions. *Muscle Nerve Suppl,* 3**,** S150-3.

MORENO-FENOLL, C., CAVALIERE, M., MARTINEZ-GARCIA, E. & POYATOS, J. F. 2017. Eco-evolutionary feedbacks can rescue cooperation in microbial populations. *Sci Rep,* 7**,** 42561.

MOUCHIROUD, L., HOUTKOOPER, R. H., MOULLAN, N., KATSYUBA, E., RYU, D., CANTO, C., MOTTIS, A., JO, Y. S., VISWANATHAN, M., SCHOONJANS, K., GUARENTE, L. & AUWERX, J. 2013. The NAD(+)/Sirtuin Pathway Modulates Longevity through Activation of Mitochondrial UPR and FOXO Signaling. *Cell,* 154**,** 430-41.

MURPHY, C. T., MCCARROLL, S. A., BARGMANN, C. I., FRASER, A., KAMATH, R. S., AHRINGER, J., LI, H. & KENYON, C. 2003. Genes that act downstream of DAF-16 to influence the lifespan of Caenorhabditis elegans. *Nature,* 424**,** 277-83.

MURTAZA, G., KHAN, A. K., RASHID, R., MUNEER, S., HASAN, S. M. F. & CHEN, J. 2017. FOXO Transcriptional Factors and Long-Term Living. *Oxid Med Cell Longev,* 2017**,** 3494289.

NAMSLAUER, I. & BRZEZINSKI, P. 2009. A mitochondrial DNA mutation linked to colon cancer results in proton leaks in cytochrome c oxidase. *Proc Natl Acad Sci U S A,* 106**,** 3402-7.

NARBONNE, P. & ROY, R. 2006. Regulation of germline stem cell proliferation downstream of nutrient sensing. *Cell Division,* 1.

NARENDRA, D., TANAKA, A., SUEN, D. F. & YOULE, R. J. 2008. Parkin is recruited selectively to impaired mitochondria and promotes their autophagy. *J Cell Biol,* 183**,** 795-803.

NARENDRA, D., WALKER, J. E. & YOULE, R. 2012. Mitochondrial quality control mediated by PINK1 and Parkin: links to parkinsonism. *Cold Spring Harb Perspect Biol,* 4.

NARGUND, A. M., FIORESE, C. J., PELLEGRINO, M. W., DENG, P. & HAYNES, C. M. 2015. Mitochondrial and nuclear accumulation of the transcription factor ATFS-1 promotes OXPHOS recovery during the UPR(mt). *Mol Cell,* 58**,** 123-33.

NARGUND, A. M., PELLEGRINO, M. W., FIORESE, C. J., BAKER, B. M. & HAYNES, C. M. 2012. Mitochondrial import efficiency of ATFS-1 regulates mitochondrial UPR activation. *Science,* 337**,** 587-90.

NEWLON, C. S. & FANGMAN, W. L. 1975. Mitochondrial DNA synthesis in cell cycle mutants of Saccharomyces cerevisiae. *Cell,* 5**,** 423-8.

O-SULLIVAN, I., ZHANG, W. W., WASSERMAN, D. H., LIEW, C. W., LIU, J., PAIK, J., DEPINHO, R. A., STOLZ, D. B., KAHN, C. R., SCHWARTZ, M. W. & UNTERMAN, T. G. 2015. FoxO1 integrates direct and indirect effects of insulin on hepatic glucose production and glucose utilization (vol 6, 7079, 2015). *Nature Communications,* 6.

O'BRIEN, S., LUJAN, A. M., PATERSON, S., CANT, M. A. & BUCKLING, A. 2017. Adaptation to public goods cheats in Pseudomonas aeruginosa. *Proc Biol Sci,* 284.

O'HARA, R., TEDONE, E., LUDLOW, A., HUANG, E., AROSIO, B., MARI, D. & SHAY, J. W. 2019. Quantitative mitochondrial DNA copy number determination using droplet digital PCR with single-cell resolution. *Genome Res,* 29**,** 1878-1888.

OKIMOTO, R., MACFARLANE, J. L., CLARY, D. O. & WOLSTENHOLME, D. R. 1992. The mitochondrial genomes of two nematodes, Caenorhabditis elegans and Ascaris suum. *Genetics,* 130**,** 471-98.

OZKAYA, O., XAVIER, K. B., DIONISIO, F. & BALBONTIN, R. 2017. Maintenance of Microbial Cooperation Mediated by Public Goods in Single- and Multiple-Trait Scenarios. *J Bacteriol,* 199.

PALIKARAS, K., LIONAKI, E. & TAVERNARAKIS, N. 2015. Coordination of mitophagy and mitochondrial biogenesis during ageing in C. elegans. *Nature,* 521**,** 525-8.

PAZDERNIK, N. & SCHEDL, T. 2013. Introduction to germ cell development in Caenorhabditis elegans. *Adv Exp Med Biol,* 757**,** 1-16.

PEREDA, M., ZURRO, D., SANTOS, J. I., BRIZ, I. G. I., ALVAREZ, M., CARO, J. & GALAN, J. M. 2017. Emergence and Evolution of Cooperation Under Resource Pressure. *Sci Rep,* 7**,** 45574.

PERLMUTTER, J. I., BORDENSTEIN, S. R., UNCKLESS, R. L., LEPAGE, D. P., METCALF, J. A., HILL, T., MARTINEZ, J., JIGGINS, F. M. & BORDENSTEIN, S. R. 2019. The phage gene wmk is a candidate for male killing by a bacterial endosymbiont. *PLoS Pathog,* 15**,** e1007936.

PERLMUTTER, J. I., MEYERS, J. E. & BORDENSTEIN, S. R. 2020. Transgenic Testing Does Not Support a Role for Additional Candidate Genes in Wolbachia Male Killing or Cytoplasmic Incompatibility. *mSystems,* 5.

PHILLIPS, W. S., COLEMAN-HULBERT, A. L., WEISS, E. S., HOWE, D. K., PING, S., WERNICK, R. I., ESTES, S. & DENVER, D. R. 2015. Selfish Mitochondrial DNA Proliferates and Diversifies in Small, but not Large, Experimental Populations of Caenorhabditis briggsae. *Genome Biol Evol,* 7**,** 2023-37.

PICARD, M., ZHANG, J., HANCOCK, S., DERBENEVA, O., GOLHAR, R., GOLIK, P., O'HEARN, S., LEVY, S., POTLURI, P., LVOVA, M., DAVILA, A., LIN, C. S., PERIN, J. C., RAPPAPORT, E. F., HAKONARSON, H., TROUNCE, I. A., PROCACCIO, V. & WALLACE, D. C. 2014. Progressive increase in mtDNA 3243A>G heteroplasmy causes abrupt transcriptional reprogramming. *Proc Natl Acad Sci U S A,* 111**,** E4033-42.

POOLE, A. C., THOMAS, R. E., ANDREWS, L. A., MCBRIDE, H. M., WHITWORTH, A. J. & PALLANCK, L. J. 2008. The PINK1/Parkin pathway regulates mitochondrial morphology. *Proc Natl Acad Sci U S A,* 105**,** 1638-43.

PORTE, D., BASKIN, D. G. & SCHWARTZ, M. W. 2005. Perspectives in diabetes - Insulin signaling in the central nervous system - A critical role in metabolic homeostasis and disease from C-elegans to humans. *Diabetes,* 54**,** 1264-1276.

PRICE, G. R. 1972. Extension of Covariance Selection Mathematics. *Annals of Human Genetics,* 35**,** 485-&.

PRUITT, J. N. & RIECHERT, S. E. 2009. Frequency-dependent success of cheaters during foraging bouts might limit their spread within colonies of a socially polymorphic spider. *Evolution,* 63**,** 2966-73.

PUIG, O. & TJIAN, R. 2006. Nutrient availability and growth: regulation of insulin signaling by dFOXO/FOXO1. *Cell Cycle,* 5**,** 503-5.

RADZVILAVICIUS, A. 2021. Beyond the "selfish mitochondrion" theory of uniparental inheritance: A unified theory based on mutational variance redistribution. *Bioessays,* 43**,** e2100009.

RADZVILAVICIUS, A. L., HADJIVASILIOU, Z., POMIANKOWSKI, A. & LANE, N. 2016. Selection for Mitochondrial Quality Drives Evolution of the Germline. *PLoS Biol,* 14**,** e2000410.

RAIDERS, S. A., EASTWOOD, M. D., BACHER, M. & PRIESS, J. R. 2018. Binucleate germ cells in Caenorhabditis elegans are removed by physiological apoptosis. *PLoS Genet,* 14**,** e1007417.

RAINEY, P. B. & RAINEY, K. 2003. Evolution of cooperation and conflict in experimental bacterial populations. *Nature,* 425**,** 72-4.

RANDOW, F. & YOULE, R. J. 2014. Self and nonself: how autophagy targets mitochondria and bacteria. *Cell Host Microbe,* 15**,** 403-11.

RATNIEKS, F. L., FOSTER, K. R. & WENSELEERS, T. 2006. Conflict resolution in insect societies. *Annu Rev Entomol,* 51**,** 581-608.

RAUTHAN, M., RANJI, P., AGUILERA PRADENAS, N., PITOT, C. & PILON, M. 2013. The mitochondrial unfolded protein response activator ATFS-1 protects cells from inhibition of the mevalonate pathway. *Proc Natl Acad Sci U S A,* 110**,** 5981-6.

REA, S. L., VENTURA, N. & JOHNSON, T. E. 2007. Relationship between mitochondrial electron transport chain dysfunction, development, and life extension in Caenorhabditis elegans. *PLoS Biol,* 5**,** e259.

REQUEJO, R. J. & CAMACHO, J. 2011. Evolution of cooperation mediated by limiting resources: connecting resource based models and evolutionary game theory. *J Theor Biol,* 272**,** 35-41.

REZNIK, E., MILLER, M. L., SENBABAOGLU, Y., RIAZ, N., SARUNGBAM, J., TICKOO, S. K., AL-AHMADIE, H. A., LEE, W., SESHAN, V. E., HAKIMI, A. A. & SANDER, C. 2016. Mitochondrial DNA copy number variation across human cancers. *Elife,* 5.

RIEHL, C. & FREDERICKSON, M. E. 2016. Cheating and punishment in cooperative animal societies. *Philos Trans R Soc Lond B Biol Sci,* 371**,** 20150090.

ROBIN, E. D. & WONG, R. 1988. Mitochondrial DNA molecules and virtual number of mitochondria per cell in mammalian cells. *J Cell Physiol,* 136**,** 507-13.

ROSS-GILLESPIE, A., GARDNER, A., WEST, S. A. & GRIFFIN, A. S. 2007. Frequency dependence and cooperation: theory and a test with bacteria. *Am Nat,* 170**,** 331-42.

RUNKEL, E. D., LIU, S., BAUMEISTER, R. & SCHULZE, E. 2013. Surveillance-activated defenses block the ROS-induced mitochondrial unfolded protein response. *PLoS Genet,* 9**,** e1003346.

SAGAN, L. 1967. On the origin of mitosing cells. *J Theor Biol,* 14**,** 255-74.

SAMUELS, D. C., LI, C., LI, B., SONG, Z., TORSTENSON, E., BOYD CLAY, H., ROKAS, A., THORNTON-WELLS, T. A., MOORE, J. H., HUGHES, T. M., HOFFMAN, R. D., HAINES, J. L., MURDOCK, D. G., MORTLOCK, D. P. & WILLIAMS, S. M. 2013. Recurrent tissue-specific mtDNA mutations are common in humans. *PLoS Genet,* 9**,** e1003929.

SANTRA, S., GILKERSON, R. W., DAVIDSON, M. & SCHON, E. A. 2004. Ketogenic treatment reduces deleted mitochondrial DNAs in cultured human cells. *Ann Neurol,* 56**,** 662-9.

SASAKI, T., SATO, Y., HIGASHIYAMA, T. & SASAKI, N. 2017. Live imaging reveals the dynamics and regulation of mitochondrial nucleoids during the cell cycle in Fucci2-HeLa cells. *Sci Rep,* 7**,** 11257.

SCHIMENTI, J. 2000. Segregation distortion of mouse t haplotypes the molecular basis emerges. *Trends Genet,* 16**,** 240-3.

SCHULZ, A. M. & HAYNES, C. M. 2015. UPR(mt)-mediated cytoprotection and organismal aging. *Biochim Biophys Acta,* 1847**,** 1448-56.

SENA, E. P., WELCH, J. W., HALVORSON, H. O. & FOGEL, S. 1975. Nuclear and mitochondrial deoxyribonucleic acid replication during mitosis in Saccharomyces cerevisiae. *J Bacteriol,* 123**,** 497-504.

SEXTON, D. J. & SCHUSTER, M. 2017. Nutrient limitation determines the fitness of cheaters in bacterial siderophore cooperation. *Nat Commun,* 8**,** 230.

SHAFFER, Z., SASAKI, T., HANEY, B., JANSSEN, M., PRATT, S. C. & FEWELL, J. H. 2016. The foundress's dilemma: group selection for cooperation among queens of the harvester ant, Pogonomyrmex californicus. *Sci Rep,* 6**,** 29828.

SHARPLEY, M. S., MARCINIAK, C., ECKEL-MAHAN, K., MCMANUS, M., CRIMI, M., WAYMIRE, K., LIN, C. S., MASUBUCHI, S., FRIEND, N., KOIKE, M., CHALKIA, D., MACGREGOR, G., SASSONE-CORSI, P. & WALLACE, D. C. 2012. Heteroplasmy of mouse mtDNA is genetically unstable and results in altered behavior and cognition. *Cell,* 151**,** 333-343.

SHAY, J. W., PIERCE, D. J. & WERBIN, H. 1990. Mitochondrial DNA copy number is proportional to total cell DNA under a variety of growth conditions. *J Biol Chem,* 265**,** 14802-7.

SHIDARA, Y., YAMAGATA, K., KANAMORI, T., NAKANO, K., KWONG, J. Q., MANFREDI, G., ODA, H. & OHTA, S. 2005. Positive contribution of pathogenic mutations in the mitochondrial genome to the promotion of cancer by prevention from apoptosis. *Cancer Res,* 65**,** 1655-63.

SHIM, Y. H., CHUN, J. H., LEE, E. Y. & PAIK, Y. K. 2002. Role of cholesterol in germ-line development of Caenorhabditis elegans. *Mol Reprod Dev,* 61**,** 358-66.

SHIOJIMA, I., YEFREMASHVILI, M., LUO, Z., KUREISHI, Y., TAKAHASHI, A., TAO, J., ROSENZWEIG, A., KAHN, C. R., ABEL, E. D. & WALSH, K. 2002. Akt signaling mediates postnatal heart growth in response to insulin and nutritional status. *J Biol Chem,* 277**,** 37670-7.

SHOU, W. 2015. Acknowledging selection at sub-organismal levels resolves controversy on pro-cooperation mechanisms. *Elife,* 4.

STEWART, J. B. & CHINNERY, P. F. 2015. The dynamics of mitochondrial DNA heteroplasmy: implications for human health and disease. *Nat Rev Genet,* 16**,** 530-42.

STEWART, J. B., FREYER, C., ELSON, J. L., WREDENBERG, A., CANSU, Z., TRIFUNOVIC, A. & LARSSON, N. G. 2008. Strong purifying selection in transmission of mammalian mitochondrial DNA. *PLoS Biol,* 6**,** e10.

STRASSMANN, J. E., ZHU, Y. & QUELLER, D. C. 2000. Altruism and social cheating in the social amoeba Dictyostelium discoideum. *Nature,* 408**,** 965-7.

SUEN, D. F., NARENDRA, D. P., TANAKA, A., MANFREDI, G. & YOULE, R. J. 2010. Parkin overexpression selects against a deleterious mtDNA mutation in heteroplasmic cybrid cells. *Proc Natl Acad Sci U S A,* 107**,** 11835-40.

SZATHMARY, E. 2015. Toward major evolutionary transitions theory 2.0. *Proc Natl Acad Sci U S A,* 112**,** 10104-11.

TAKEUCHI, N. & KANEKO, K. 2019. The origin of the central dogma through conflicting multilevel selection. *Proc Biol Sci,* 286**,** 20191359.

TAM, Z. Y., GRUBER, J., HALLIWELL, B. & GUNAWAN, R. 2015. Context-Dependent Role of Mitochondrial Fusion-Fission in Clonal Expansion of mtDNA Mutations. *PLoS Comput Biol,* 11**,** e1004183.

TANG, Y., MANFREDI, G., HIRANO, M. & SCHON, E. A. 2000a. Maintenance of human rearranged mitochondrial DNAs in long-term cultured transmitochondrial cell lines. *Mol Biol Cell,* 11**,** 2349-58.

TANG, Y., SCHON, E. A., WILICHOWSKI, E., VAZQUEZ-MEMIJE, M. E., DAVIDSON, E. & KING, M. P. 2000b. Rearrangements of human mitochondrial DNA (mtDNA): new insights into the regulation of mtDNA copy number and gene expression. *Mol Biol Cell,* 11**,** 1471-85.

TAYLOR, D. R., ZEYL, C. & COOKE, E. 2002. Conflicting levels of selection in the accumulation of mitochondrial defects in Saccharomyces cerevisiae. *Proc Natl Acad Sci U S A,* 99**,** 3690-4.

TAYLOR, R. C. & DILLIN, A. 2011. Aging as an event of proteostasis collapse. *Cold Spring Harb Perspect Biol,* 3.

TAYLOR, R. W. & TURNBULL, D. M. 2005. Mitochondrial DNA mutations in human disease. *Nat Rev Genet,* 6**,** 389-402.

TEPPER, R. G., ASHRAF, J., KALETSKY, R., KLEEMANN, G., MURPHY, C. T. & BUSSEMAKER, H. J. 2013. PQM-1 complements DAF-16 as a key transcriptional regulator of DAF-2-mediated development and longevity. *Cell,* 154**,** 676-690.

TRIFUNOV, S., PYLE, A., VALENTINO, M. L., LIGUORI, R., YU-WAI-MAN, P., BURTE, F., DUFF, J., KLEINLE, S., DIEBOLD, I., RUGOLO, M., HORVATH, R. & CARELLI, V. 2018. Clonal expansion of mtDNA deletions: different disease models assessed by digital droplet PCR in single muscle cells. *Sci Rep,* 8**,** 11682.

TSANG, W. Y. & LEMIRE, B. D. 2002a. Mitochondrial genome content is regulated during nematode development. *Biochem Biophys Res Commun,* 291**,** 8-16.

TSANG, W. Y. & LEMIRE, B. D. 2002b. Stable heteroplasmy but differential inheritance of a large mitochondrial DNA deletion in nematodes. *Biochem Cell Biol,* 80**,** 645-54.

VALENCI, I., YONAI, L., BAR-YAACOV, D., MISHMAR, D. & BEN-ZVI, A. 2015. Parkin modulates heteroplasmy of truncated mtDNA in Caenorhabditis elegans. *Mitochondrion,* 20**,** 64-70.

VAN DER BLIEK, A. M., SEDENSKY, M. M. & MORGAN, P. G. 2017. Cell Biology of the Mitochondrion. *Genetics,* 207**,** 843-871.

VAN VALEN, L. 1973. A new evolutionary law. *Evolutionary Theory,* 1**,** 1-30.

VANTHOURNOUT, B., GREVE, M., BRUUN, A., BECHSGAARD, J., OVERGAARD, J. & BILDE, T. 2016. Benefits of Group Living Include Increased Feeding Efficiency and Lower Mass Loss during Desiccation in the Social and Inbreeding Spider Stegodyphus dumicola. *Front Physiol,* 7**,** 18.

VARLAMOV, D. A., KUDIN, A. P., VIELHABER, S., SCHRODER, R., SASSEN, R., BECKER, A., KUNZ, D., HAUG, K., REBSTOCK, J., HEILS, A., ELGER, C. E. & KUNZ, W. S. 2002. Metabolic consequences of a novel missense mutation of the mtDNA CO I gene. *Hum Mol Genet,* 11**,** 1797-805.

VELICER, G. J., KROOS, L. & LENSKI, R. E. 1998. Loss of social behaviors by myxococcus xanthus during evolution in an unstructured habitat. *Proc Natl Acad Sci U S A,* 95**,** 12376-80.

WALKER, T., JOHNSON, P. H., MOREIRA, L. A., ITURBE-ORMAETXE, I., FRENTIU, F. D., MCMENIMAN, C. J., LEONG, Y. S., DONG, Y., AXFORD, J., KRIESNER, P., LLOYD, A. L., RITCHIE, S. A., O'NEILL, S. L. & HOFFMANN, A. A. 2011. The wMel Wolbachia strain blocks dengue and invades caged Aedes aegypti populations. *Nature,* 476**,** 450-3.

WALKER, T., QUEK, S., JEFFRIES, C. L., BANDIBABONE, J., DHOKIYA, V., BAMOU, R., KRISTAN, M., MESSENGER, L. A., GIDLEY, A., HORNETT, E. A., ANDERSON, E. R., CANSADO-UTRILLA, C., HEGDE, S., BANTUZEKO, C., STEVENSON, J. C., LOBO, N. F., WAGSTAFF, S. C., NKONDJIO, C. A., IRISH, S. R., HEINZ, E. & HUGHES, G. L. 2021. Stable high-density and maternally inherited Wolbachia infections in Anopheles moucheti and Anopheles demeilloni mosquitoes. *Curr Biol,* 31**,** 2310-2320 e5.

WALLACE, D. C. 1992. Mitochondrial genetics: a paradigm for aging and degenerative diseases? *Science,* 256**,** 628-32.

WALLACE, D. C. & CHALKIA, D. 2013. Mitochondrial DNA genetics and the heteroplasmy conundrum in evolution and disease. *Cold Spring Harb Perspect Biol,* 5**,** a021220.

WANG, Z. & WU, M. 2015. An integrated phylogenomic approach toward pinpointing the origin of mitochondria. *Sci Rep,* 5**,** 7949.

WANG, Z. H., LIU, Y., CHAITANKAR, V., PIROOZNIA, M. & XU, H. 2019. Electron transport chain biogenesis activated by a JNK-insulin-Myc relay primes mitochondrial inheritance in Drosophila. *Elife,* 8.

WATERS, K. A. & REINKE, V. 2011. Extrinsic and intrinsic control of germ cell proliferation in Caenorhabditis elegans. *Mol Reprod Dev,* 78**,** 151-60.

WEBB, A. E. & BRUNET, A. 2014. FOXO transcription factors: key regulators of cellular quality control. *Trends Biochem Sci,* 39**,** 159-69.

WEBB, A. E., KUNDAJE, A. & BRUNET, A. 2016. Characterization of the direct targets of FOXO transcription factors throughout evolution. *Aging Cell,* 15**,** 673-85.

WENSELEERS, T. & RATNIEKS, F. L. 2004. Tragedy of the commons in Melipona bees. *Proc Biol Sci,* 271 Suppl 5**,** S310-2.

WERREN, J. H., BALDO, L. & CLARK, M. E. 2008. Wolbachia: master manipulators of invertebrate biology. *Nat Rev Microbiol,* 6**,** 741-51.

WERREN, J. H., NUR, U. & WU, C. I. 1988. Selfish genetic elements. *Trends Ecol Evol,* 3**,** 297-302.

WEST, S. A., FISHER, R. M., GARDNER, A. & KIERS, E. T. 2015. Major evolutionary transitions in individuality. *Proc Natl Acad Sci U S A,* 112**,** 10112-9.

WILLIAMSON, D. 2002. The curious history of yeast mitochondrial DNA. *Nat Rev Genet,* 3**,** 475-81.

WILSON, D. S. & WILSON, E. O. 2007. Rethinking the theoretical foundation of sociobiology. *Quarterly Review of Biology,* 82**,** 327-348.

WILSON, D. S. & WILSON, E. O. 2008. Evolution "for the good of the group". *American Scientist,* 96**,** 380-389.

WIN, M. T., YAMAMOTO, Y., MUNESUE, S., HAN, D., HARADA, S. & YAMAMOTO, H. 2013. Validated Liquid Culture Monitoring System for Lifespan Extension of Caenorhabditis elegans through Genetic and Dietary Manipulations. *Aging Dis,* 4**,** 178-85.

YANG, Q., LIU, P, ANDERSON, N. S., SHPILKA, T., DU, Y., NARESH, N. U., LUK, K., LAVELLE, J., ZEINERT, R. D., CHIEN, P., WOLFE, S. A., HAYNES, C. M. 2021. mtDNA replication in dysfunctional mitochondria promotes deleterious heteroplasmy via the UPRmt. *BioRxiv*.

YONEDA, M., CHOMYN, A., MARTINUZZI, A., HURKO, O. & ATTARDI, G. 1992. Marked replicative advantage of human mtDNA carrying a point mutation that causes the MELAS encephalomyopathy. *Proc Natl Acad Sci U S A,* 89**,** 11164-8.

YONEDA, T., BENEDETTI, C., URANO, F., CLARK, S. G., HARDING, H. P. & RON, D. 2004. Compartment-specific perturbation of protein handling activates genes encoding mitochondrial chaperones. *J Cell Sci,* 117**,** 4055-66.

ZANDERS, S. E. & UNCKLESS, R. L. 2019. Fertility Costs of Meiotic Drivers. *Curr Biol,* 29**,** R512-R520.

ZHANG, Y., CHEN, Y., GUCEK, M. & XU, H. 2016. The mitochondrial outer membrane protein MDI promotes local protein synthesis and mtDNA replication. *EMBO J,* 35**,** 1045-57.

ZHANG, Y., WANG, Z. H., LIU, Y., CHEN, Y., SUN, N., GUCEK, M., ZHANG, F. & XU, H. 2019. PINK1 Inhibits Local Protein Synthesis to Limit Transmission of Deleterious Mitochondrial DNA Mutations. *Mol Cell,* 73**,** 1127-1137 e5.

ZHAO, Q., WANG, J., LEVICHKIN, I. V., STASINOPOULOS, S., RYAN, M. T. & HOOGENRAAD, N. J. 2002. A mitochondrial specific stress response in mammalian cells. *EMBO J,* 21**,** 4411-9.

Appendix 1: Droplet Digital PCR Protocol for Quantification of Nematode DNA

STEP 1: PREPARE TEMPLATE-PRIMER MIX

Ingredient:	Volume:
Diluted lysate with template DNA	Variable (2-5 µL depending on DNA concentration)*
Forward primer (10 µM aliquot)	0.25 µL
Reverse primer (10 µM aliquot)	0.25 µL
Additional primers or fluorescent probes as necessary	
Nuclease-free water	To 8 µL total volume

*I generally aim for triple-digit positive-droplet counts (between 5% and 20% of the total droplet count, which is generally close to 20,000 per reaction well); this may require scaling up or down the dilution factors recommended above, depending on worm age and number of worms per volume of lysate.

Prepare the above mixture for each reaction in a well of an Eppendorf twin.tec™ 96-well semi-skirted plates (catalog number 951020303).

STEP 2: COMBINE DNA PRIMER MIX WITH REACTION MASTER MIX

Combine 4.5 µL nuclease-free water with 12.5 µL supermix (EvaGreen or probes) per reaction, with ~10% extra volume (for example combine 49.5 µL water with 137.5 µL supermix for 10x reactions). Add 17 µL of water+supermix to each well, bringing the total volume to 25 µL. Spin the plate in a centrifuge for a few seconds to ensure sample is collected in the basin of each well.

STEP 3: GENERATE DROPLETS

Add fresh Bio-Rad cartridges, filter tips, the 96-well twin.tec PCR plate containing the ddPCR samples, and a fresh 96-well twin.tec PCR plate (nested in a 96-well freezer block, which is in the black tray that fits on the front-right platform of the droplet generator robot) to the Bio-Rad Droplet Generator robot. Make sure the appropriate droplet generator oil (EvaGreen or probes) is loaded and the robot is equipped with the necessary number of fresh tips and the instructions on which columns in the Twin Tec plates contain sample using the touchscreen prompts.

Alternatively, utilize the Bio-Rad manual droplet generator with cartridges and gaskets manufactured for the manual droplet generator. Using a multichannel pipette to slowly dispense the sample into the sample-well of the manual droplet generation cartridge. Add 70 µL of appropriate droplet generator oil (EvaGreen or probes) into the oil-wells of the cartridge. Load the gasket onto the cartridge and load the cartridge into the manual droplet generator within two minutes of adding the samples and oil to the cartridge. After droplet generation, using a multichannel pipette again, angle the pipette tips into the row of wells containing the droplets (the pipette should be held at an angle to allow the droplets an unobstructed path into the tips), and slowly draw 40 µL of samples+droplets into the multichannel (this should take about five seconds) so as not to disturb the droplets. Slowly load the samples+droplets into a fresh 96-well twin.tec plate, being careful to not generate bubbles. Refer to pages 17-19 of the Bio-Rad ddPCR Application Guide for further detail.

STEP 4: SEAL THE PLATE

Use an automated plate sealer and foil plate seals. Set the plate sealer to 180˚C and a seal time of 4 seconds.

STEP 5: PCR

Immediately following plate sealing, start the PCR. For ddPCR with EvaGreen, use the protocol recommended in the Bio-Rad QX200 ddPCR EvaGreen product sheet (included with EvaGreen shipment):

Cycle step:	Temperature:	Time:
Enzyme activation	95˚C	5 min
Denaturation	95˚C	30 sec
*Annleaing/Extension	60˚C	1 min
Signal stabilization	4˚C	5 min
Signal stabilization	90˚C	5 min
Hold	10˚C	Infinite

*Annealing/Extension temperature may need to be adjusted depending on the primers

STEP 6: DROPLET READING

Load the plate into the Bio-Rad droplet reader and ensure the waste is sufficiently empty and droplet reader oil is sufficiently full to read the plate. Read the droplets in the plate using using the 2-dimensional (518 nm and 554 nm dual-wavelength) clustering plot option in the Bio-Rad QuantaSoft™ program.

Appendix 2

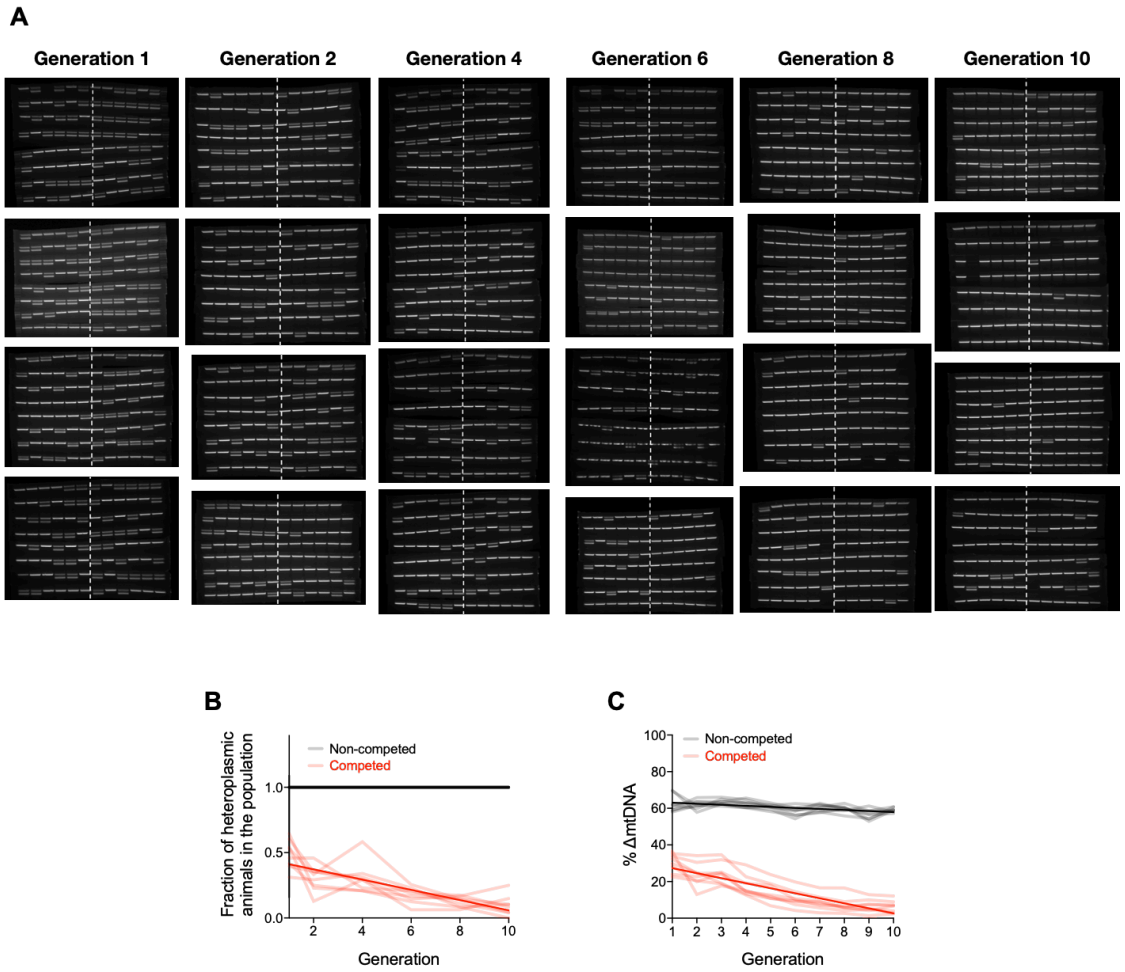

Supplemental Figure 5-1. Raw measurements of decline in both prevalence of heteroplasmic hosts and overall *uaDf5* frequency upon competition with wildtype animals

(A) PCR gel images reflecting individual adult nematodes sampled from the competition lines in the organism-level selection experiment (Figure 5-1C). Approximately 48 adults were individually lysed from the first generation and every other generation thereafter. A single PCR band reflects Bristol strain nematodes (homoplasmic for wildtype mtDNA), whereas double bands reflect heteroplasmic animals carrying the ΔmtDNA variant. Vertical dashed white lines separate cohorts obtained from different replicate competition lines.
(B) Quantification of panel (A).
(C) ΔmtDNA frequency across 8 replicate competed (red) and non-competed (black) lineages. Same experiment as shown in Figure 5-1D, but with y-axis expressing raw, non-normalized ΔmtDNA frequency measurements. Dark lines reflect best-fit regression across all replicate lines.
Nematodes were maintained on a diet of live OP50 *E. coli* at 20˚C.

Appendix 3

Table 5-1: Empirically derived ΔmtDNA frequencies and selection coefficients at the sub-organismal level

Replicate	Parents		Mature adult progeny		S	Predicted S	Residual
	% ΔmtDNA	% Wildtype mtDNA	% ΔmtDNA	% Wildtype mtDNA			
1	64.47	35.53	73.06	26.94	-0.494	-0.179	-0.315
2	47.22	52.78	53.13	46.87	-0.267	-0.378	0.111
3	71.71	28.29	71.00	29.00	0.034	-0.095	0.130
4	58.06	41.94	67.05	32.95	-0.470	-0.253	-0.217
5	64.71	35.29	66.76	33.24	-0.095	-0.176	0.081
6	73.44	26.56	74.20	25.80	-0.040	-0.075	0.035
7	42.89	57.11	53.85	46.15	-0.554	-0.428	-0.126
8	29.47	70.53	40.85	59.15	-0.653	-0.583	-0.070
9	62.35	37.65	66.67	33.33	-0.208	-0.203	-0.004
10	60.03	39.97	63.57	36.43	-0.162	-0.230	0.068
11	67.76	32.24	67.12	32.88	0.029	-0.141	0.170
12	29.20	70.80	39.10	60.90	-0.557	-0.586	0.029
13	71.21	28.79	76.34	23.66	-0.304	-0.101	-0.204
14	63.25	36.75	58.05	41.95	0.196	-0.193	0.389
15	66.70	33.30	71.31	28.69	-0.241	-0.153	-0.088
16	69.69	30.31	69.44	30.56	0.012	-0.119	0.130
17	63.95	36.05	74.94	25.06	-0.686	-0.185	-0.501
18	28.85	71.15	33.92	66.08	-0.266	-0.590	0.324
19	53.94	46.06	64.65	35.35	-0.562	-0.300	-0.261
20	66.08	33.92	71.79	28.21	-0.306	-0.160	-0.146
21	60.68	39.32	56.57	43.43	0.156	-0.223	0.378
22	61.14	38.86	72.75	27.25	-0.697	-0.217	-0.480
23	53.04	46.96	59.02	40.98	-0.275	-0.311	0.036
24	50.51	49.49	60.14	39.86	-0.479	-0.340	-0.139
25	50.15	49.85	56.65	43.35	-0.299	-0.344	0.045
26	25.09	74.91	37.20	62.80	-0.769	-0.633	-0.136
27	22.01	77.99	34.26	65.74	-0.847	-0.669	-0.178
28	58.50	41.50	60.02	39.98	-0.065	-0.248	0.183
29	70.81	29.19	65.63	34.37	0.213	-0.106	0.318
30	41.81	58.19	41.86	58.14	-0.002	-0.440	0.438
Average	54.96	45.04	60.03	39.97	-0.289	-0.289	6.52*10-6

Appendix 4

Table 5-2: Empirically derived ΔmtDNA frequencies and selection coefficients at the organismal level

Population type	Measured value	Generation	Replicate line 1	2	3	4	5	6	7	8
Competing	% ΔmtDNA (population-wide)	1	36.56	23.95	32.38	28.24	29.76	22.60	35.26	33.80
		2	12.97	22.64	24.47	20.03	24.82	20.43	34.16	30.45
		3	17.66	25.06	24.64	24.13	19.09	18.73	34.67	31.96
		4	15.12	19.03	14.70	14.53	13.23	12.61	22.64	29.08
		5	10.75	18.03	11.89	12.67	10.89	6.81	18.86	23.86
		6	9.25	10.12	7.44	10.61	9.34	4.20	14.46	19.80
		7	7.75	7.05	5.71	9.32	8.93	2.89	11.43	16.58
		8	5.82	6.73	4.12	5.85	5.73	2.66	9.09	16.52
		9	7.69	7.29	4.79	5.21	4.14	1.35	9.96	12.87
		10	6.72	7.28	2.79	3.91	6.73	2.39	8.94	12.15
	% Wildtype mtDNA (100 - %ΔmtDNA)	1	63.44	76.05	67.62	71.76	70.24	77.40	64.74	66.20
		2	87.03	77.36	75.53	79.97	75.18	79.57	65.84	69.55
		3	82.34	74.94	75.36	75.87	80.91	81.27	65.33	68.04
		4	84.88	80.97	85.30	85.47	86.77	87.39	77.36	70.92
		5	89.25	81.97	88.11	87.33	89.11	93.19	81.14	76.14
		6	90.75	89.88	92.56	89.39	90.66	95.80	85.54	80.20
		7	92.25	92.95	94.29	90.68	91.07	97.11	88.57	83.42
		8	94.18	93.27	95.88	94.15	94.27	97.34	90.91	83.48
		9	92.31	92.71	95.21	94.79	95.86	98.65	90.04	87.13
		10	93.28	92.72	97.21	96.09	93.27	97.61	91.06	87.85
Non-competing	% ΔmtDNA (population-wide)	1	61.88	69.39	59.09	69.88	57.94	60.19	62.03	58.72
		2	59.86	61.50	61.60	57.77	61.52	65.82	63.67	63.59
		3	65.06	62.12	61.13	62.34	63.50	66.07	63.69	62.65
		4	62.76	60.48	60.25	60.37	65.65	64.76	62.68	63.25
		5	60.50	59.42	58.16	61.09	62.97	60.79	61.57	61.95
		6	58.40	54.27	56.25	56.15	60.23	59.29	62.57	58.92
		7	62.80	60.45	57.56	57.97	61.91	58.82	61.93	60.75
		8	59.66	60.69	59.83	55.86	60.45	58.66	59.80	62.71
		9	56.90	52.86	58.55	54.43	54.03	61.30	56.52	58.62
		10	59.19	58.94	60.84	59.27	60.71	58.03	57.12	58.51
	% Wildtype mtDNA (100 - %ΔmtDNA)	1	38.13	30.61	40.91	30.12	42.06	39.81	37.97	41.28
		2	40.14	38.50	38.40	42.23	38.48	34.18	36.33	36.41
		3	34.94	37.88	38.87	37.66	36.50	33.93	36.31	37.35
		4	37.24	39.52	39.75	39.63	34.35	35.24	37.32	36.75
		5	39.50	40.58	41.84	38.91	37.03	39.21	38.43	38.05
		6	41.60	45.73	43.75	43.85	39.77	40.71	37.43	41.08
		7	37.20	39.55	42.44	42.03	38.09	41.18	38.07	39.25
		8	40.34	39.31	40.17	44.14	39.55	41.34	40.20	37.29
		9	43.10	47.14	41.45	45.57	45.97	38.70	43.48	41.38
		10	40.81	41.06	39.16	40.73	39.29	41.97	42.88	41.49
	Mean $\%\Delta mtDNA_{non\text{-}competed}$					60				
Selection coefficients										
$S_{competed}$ at 60% ΔmtDNA			0.1735	0.1834	0.2710	0.2196	0.2079	0.2995	0.2026	0.1463
$S_{non\text{-}competed}$ at 60% ΔmtDNA						0.0237				
$S_{organismal}$ ($S_{competed}$ - $S_{non\text{-}competed}$) at 60% ΔmtDNA			0.1497	0.1597	0.2473	0.1958	0.1841	0.2757	0.1788	0.1225
Assumption	**Variable**									
***S*=1 at 100% ΔmtDNA**	Best fit					$S = 10^{0.0181 * \%\Delta mtDNA - 1.81}$				
	Derivative					$dS = 6.455*10^{-4} * e^{0.0417 * \%\Delta mtDNA}$				
	| Covariance Matrix |					0.9837				
***S*=1 at 90% ΔmtDNA**	Best fit					$S = 10^{0.0241 * \%\Delta mtDNA - 2.17}$				
	Derivative					$dS = 3.753*10^{-4} * e^{0.0555 * \%\Delta mtDNA}$				
	| Covariance Matrix |					0.9890				
***S* increases linearly**	Predicted *S*					0.1892				
	Residual		$-3.95*10^{-2}$	$-2.95*10^{-2}$	$5.81*10^{-2}$	$6.67*10^{-3}$	$-5.06*10^{-3}$	$8.65*10^{-2}$	$-1.04*10^{-2}$	$-6.67*10^{-2}$
	$Residual^2$		$1.56*10^{-3}$	$8.72*10^{-4}$	$3.37*10^{-3}$	$4.44*10^{-5}$	$2.56*10^{-5}$	$7.49*10^{-3}$	$1.07*10^{-4}$	$4.44*10^{-3}$

Appendix 5: Mathematical analysis of multilevel selection dynamics of ∆mtDNA

Here, the regressions shown in Chapter 5, Figure 5-3, are derived using data obtained from the measurements of organismal and sub-organismal selection (see Chapter 5, Methods, and Appendix 2 to Appendix 4), together with the general framework of the Price Equation:

$$w\Delta z = cov(w,z)_{org} + E[cov(w,z)_{sub}]$$

Where:
w = reproductive fitness, or number of replication events per generation, for one trait relative to another
z = measurable value of a trait (in this case, ∆mtDNA frequency)
$cov(w,z)_{org}$ = covariance between w and z contributed by selection at the organismal level
$E[cov(w,z)_{sub}]$ = expected or average covariance between w and z contributed by sub-organismal selection

Note that the version of the Price Equation shown above is equivalent to the form shown as equation (A17) in Price, 1972. At each level of selection, organismal and sub-organismal, the term for the covariance between w and z can be defined as follows:

$$cov(w,z) = \frac{\sum(w_i - w_{average})(z_i - z_{average})}{n-1}$$

Where:
w_i = fitness w of trait z in the ith replicate parent-progeny lineage from the sample or population
$w_{average}$ = average w across the sample or population
z_i = value of trait z in the parent of the ith replicate parent-progeny lineage from the sample or population
$z_{average}$ = average value of z across the sample or population
n = number of parent-progeny lineages sampled

Since the selection coefficient, which measures the strength of selection acting on a trait, is directly to fitness, the Price Equation can be expressed using covariance terms between selection coefficient, S, and the value of a trait, z. Defining trait-value as the heteroplasmic (sub-organismal or within-host) frequency of ∆mtDNA ($\%\Delta mtDNA$) yields the following form of the Price Equation:

$$Change\ in\ \%\Delta mtDNA = cov(S, \%\Delta mtDNA)_{org} + E[cov(S, \%\Delta mtDNA)_{sub}]$$

Replacing w and z in the Price Equation with S and $\%\Delta mtDNA$ yields the following formula for covariance:

$$cov(S, \%\Delta mtDNA) = \frac{\sum(S_i - S_{average})(\%\Delta mtDNA_i - \%\Delta mtDNA_{average})}{n-1}$$

Where:
S_i = selection coefficient of ∆mtDNA in the ith replicate of each experiment (sub-organismal and organismal)
$S_{average}$ = average S across the sample or population of each experiment
$\%\Delta mtDNA_i$ = heteroplasmic ∆mtDNA frequency from the ith parent (sub-organismal) or line (organismal)
$\%\Delta mtDNA_{average}$ = average heteroplasmic ∆mtDNA frequency across all replicates

In the sub-sections that follow, the individual regressions are derived for the strength of sub-organismal and organismal selection as a function of heteroplasmic ∆mtDNA frequency, shown using the data from Chapter 5 and Appendix 2 to Appendix 4. The multilevel selection analyses in Chapter 6 (Figure 6-9) and Chapter 7 (Figure 7-3) are performed using the same approach.

Sub-organismal regression (Chapter 5, Figure 5-3A):

For selection acting on ∆mtDNA at the sub-organismal level, selection coefficient, *S*, is calculated for a given change in ∆mtDNA frequency between parent and progeny using the following equation:

$$S = 1 - w = 1 - \frac{\%\Delta mtDNA_{g+1}/\%\Delta mtDNA_g}{\%wildtype\ mtDNA_{g+1}/\%wildtype\ mtDNA_g}$$

Where:
w = average replicative fitness of ∆mtDNA relative to wildtype mtDNA
g = parental generation

The following regression, relating selection coefficient to heteroplasmic ∆mtDNA frequency, can be derived using the covariance relationship defined on the previous page and the data shown in Appendix 3:

$$S = slope(S, \%\Delta mtDNA) * \%\Delta mtDNA + intercept(S, \%\Delta mtDNA)$$

Note that this equation takes the form of the slope-intercept equation, *y=mx+b*, in which *y* corresponds to selection coefficient, *S*, and *x* corresponds to heteroplasmic ∆mtDNA frequency, denoted *%∆mtDNA*. The slope, *m*, can be calculated from its relationship to covariance and variance. In particular, the covariance between *S* and *%∆mtDNA* is equal to the variance of *%∆mtDNA* multiplied by the slope of the regression (Price, 1970):

$$cov(S, \%\Delta mtDNA) = var(\%\Delta mtDNA) * slope(S, \%\Delta mtDNA)$$

Here, the term *var*(*S,%∆mtDNA*) represents the variance of *%∆mtDNA*, calculated as follows:

$$var(\%\Delta mtDNA) = \frac{\sum(\%\Delta mtDNA_i - \%\Delta mtDNA_{average})^2}{n-1}$$

Note that the formula for variance is similar to the formula for covariance, with one exception: the errors or residuals in *S* (S_i - $S_{average}$) are replaced by the errors in *%∆mtDNA* ($\%\Delta mtDNA_i$ - $\%\Delta mtDNA_{average}$). In other words, in contrast to the covariance of *S* and *%∆mtDNA*, the variance of *%∆mtDNA* is equivalent to the covariance of *%∆mtDNA* with itself. The term *slope*(*S,%∆mtDNA*), shown above, represents the slope of the regression obtained by plotting *S* as a function of *%∆mtDNA*. The slope can be calculated by rearranging the relation between covariance, variance, and slope, as follows:

$$slope(S, \%\Delta mtDNA) = \frac{cov(S, \%\Delta mtDNA)}{var(\%\Delta mtDNA)} = \frac{\sum(S_i - S_{average})(\%\Delta mtDNA_i - \%\Delta mtDNA_{average})}{\sum(\%\Delta mtDNA_i - \%\Delta mtDNA_{average})^2}$$

Entering the empirically derived values for *S* and *%∆mtDNA* in Appendix 3 yields a slope of 0.01154. Next, the slope-intercept equation can be rearranged to solve for the intercept, as follows:

$$intercept(S, \%\Delta mtDNA) = S - slope(S, \%\Delta mtDNA) * \%\Delta mtDNA$$

By entering the slope, together with any pair of corresponding values of *S* and *%∆mtDNA* that fall on the regression line (such as $S_{average}$ and $\%\Delta mtDNA_{average}$, taken from Appendix 3), the intercept is calculated to be -0.923 as follows:

$$intercept(S, \%\Delta mtDNA) = S - slope(S, \%\Delta mtDNA) * \%\Delta mtDNA = -0.289 - 0.01154 * 54.96 = -0.923$$

Accordingly, the covariance between selection coefficient and ∆mtDNA frequency at the sub-organismal level yields the following relation:

$$S = 0.01154 * \%\Delta mtDNA - 0.923$$

This equation defines the regression line shown in Figure 5-3A. The confidence interval surrounding the regression (defining the shaded region) is calculated for each value of ΔmtDNA frequency, from 0 to 100, using the following formula:

$$95\%\ confidence\ interval = t_{n-2} * \sigma_R \sqrt{\frac{1}{n} + \frac{(\%\Delta mtDNA^* - \%\Delta mtDNA_{ave})^2}{{\sigma_{RS}}^2 (n-1)}}$$

Where:
t_{n-2} = critical value from Student's t-table for *n-2*, two-tailed, α=0.05
σ_R = standard deviation of the residuals for selection coefficient *S*
n = sample size
$\%\Delta mtDNA^*$ = each value of ΔmtDNA frequency at which confidence interval is being calculated
$\%\Delta mtDNA_{ave}$ = average ΔmtDNA frequency across all samples
σ_{RS} = standard deviation of the residuals of *S*, with each residual defined as $S_{actual} - S_{predicted}$

Organismal regression (Chapter 5, Figure 5-3B):

For selection acting on ΔmtDNA at the organismal level, in other words the selection against ΔmtDNA that arises strictly from the cost that ΔmtDNA imposes on host fitness, the selection coefficient, *S*, is calculated from the change in ΔmtDNA frequency across a population consisting of heteroplasmic hosts (carrying ΔmtDNA) competed against their wildtype counterparts on the same food plate. In contrast to the sub-organismal selection experiment, where *S* is calculated from the change in ΔmtDNA frequency between parents and their immediate progeny, the organismal competition experiment involved measuring the change in ΔmtDNA frequency across multiple successive generations. Accordingly, the selection coefficient can be calculated as follows:

$$S = 1 - w = 1 - e^{slope[g, LN(\%\Delta mtDNA/\%WT\ mtDNA)]}$$

Where:
LN = natural logarithm
%ΔmtDNA = population-wide (not heteroplasmic) ΔmtDNA frequency
%WT mtDNA = population-wide wildtype mtDNA frequency (equal to 100 – *%ΔmtDNA*)
g = time, measured in number of generations
LN(*%ΔmtDNA* / *%WT mtDNA*)] = natural logarithm of the ratio of *%ΔmtDNA* to *%WT mtDNA*
slope[*g*,*LN*(*%ΔmtDNA* / *%WT mtDNA*)] = slope of *LN*(*%ΔmtDNA* / *%WT mtDNA*)] versus time, as follows:

$$slope[g, LN(\%\Delta mtDNA/\%WT\ mtDNA)] = \frac{\sum \left[LN\left(\frac{\Delta}{W}\right)_i - LN\left(\frac{\Delta}{W}\right)_{average} \right] (g_i - g_{average})}{\sum (g_i - g_{average})^2}$$

Where:
$LN(\Delta/W)_i$ = *LN*(*%ΔmtDNA* / *%WT mtDNA*) for the *i*th generation
$LN(\Delta/W)_{average}$ = average value of $LN(\%\Delta mtDNA_I$ / *%WT mtDNA*) across all generations
g_i = the *i*th generation
$g_{average}$ = average g_i value across all generations (equal to 5.5 for generations 1 to 10)

The selection coefficient of ΔmtDNA is calculated for both the competed and non-competed populations in the organismal competition experiment. Although ΔmtDNA persists within a stable frequency range in non-competed populations, ΔmtDNA undergoes slight variation in frequency, perhaps due to drift, variations in sub-organismal selection, and population structure (during population expansion at the onset of each new generation, adults become rapidly outnumbered by embryos and larvae, which tend to carry lower ΔmtDNA than adults, see Figures 2-2 and 5-1A). In any case, to control for sources other than organismal selection (that is, variation in ΔmtDNA frequency occurring for reasons other than the fitness differences between

heteroplasmic animals and their wildtype counterparts), the average selection coefficient across all replicate non-competed populations (containing exclusively heteroplasmic animals) is subtracted from the selection coefficient of each replicate competed population, yielding the selection coefficient for organismal selection against ∆mtDNA:

$$S_{organismal} = S_{competed} - \bar{S}_{non-competed}$$

Where:
$S_{organismal}$ = selection coefficient, S, strictly at the level of organismal selection
$S_{competed}$ = S across a competed line
$\bar{S}_{non-competed}$ = average S across all non-competed lines

Deriving a regression between selection coefficient and heteroplasmic ∆mtDNA frequency is trickier at the organismal level, since the relationship is non-linear. In particular, a large deletion such as in ∆mtDNA results in the loss of essential genes and is therefore expected to be lethal when present at very high frequency (fitness w = 0, or S = 1). However, the organismal selection coefficient is approximately only 0.1892 at a heteroplasmic frequency of 60% ∆mtDNA. Moreover, S is expected to be 0 when ∆mtDNA frequency is zero, since no selection is occurring against ∆mtDNA among hosts that lack ∆mtDNA. The appropriate regression will therefore constitute a non-linear trend-line that rises sharply at progressively higher ∆mtDNA frequency, passing through S=0 when $\%\Delta mtDNA$=0, S=0.189 when $\%\Delta mtDNA$=60, and S=1 when $\%\Delta mtDNA$=100. An ideal candidate regression would therefore be logarithmic, in which rather than being directly proportional to ∆mtDNA frequency, S is equal to some quantity raised to the power of an exponent (which itself is proportional to ∆mtDNA frequency). The least-squares regression method can be used to fit a non-linear regression. As the name suggests, this method seeks to minimize the square of the errors, or residuals, along the dependent variable (in this case S), which can be calculated as shown:

$$SSQ = \sum [S_i - f(\%\Delta mtDNA)]^2$$

Where:
SSQ = sum of the squares of residuals
S_i = organismal selection coefficient for replicate line i in the organismal competition experiment
$f(\%\Delta mtDNA)$ = predicted value of S, defined as a function of $\%\Delta mtDNA$
$S_i - f(\%\Delta mtDNA)$ = error, or residual, between actual and predicted values of S

The least-squares method, computed here using the GraphPad Prism software package, fits a regression by finding the curve with a shape that minimizes the value of SSQ. When assuming S=0 at 0% ∆mtDNA and S=1 at 100% ∆mtDNA, together with the empirically derived value of S=0.1892 at 60% ∆mtDNA, the least-squares method identifies the following regression to minimize SSQ:

$$S = 10^{0.0181 * \%\Delta mtDNA - 1.81}$$

However, S may approach 1 at a ∆mtDNA frequency lower than 100%. Consistent with this possibility, hosts are almost never observed to carry ∆mtDNA at or above 90% frequency (Figures 2-2 and 3-1). To account for the uncertainty in how the fitness cost of ∆mtDNA scales with ∆mtDNA frequency, the following regression was obtained using the least-squares method when assuming that S=1 at 90% instead of 100% ∆mtDNA:

$$S = 10^{0.0241 * \%\Delta mtDNA - 2.17}$$

Finally, S might rise modestly until reaching a particular (albeit unknown) ∆mtDNA frequency threshold, followed by an abrupt shift to higher S in a sort of stepwise fashion. To account for this uncertainty, the assumption that S reaches 1 at a given ∆mtDNA frequency was eliminated, enabling a standard linear regression between S=0 at 0% ∆mtDNA and S=0.1892 at 60% ∆mtDNA:

$$S = 0.003153 * \%\Delta mtDNA$$

The confidence interval for the non-linear regressions can be calculated using the following formula:

$$95\%\ confidence\ interval = t_{n-1}\sqrt{CM * dS^2}$$

Where:
t_{n-1} = critical value from student's t-table for *n-1*
CM = covariance matrix value (Appendix 4, Table 5-2)
dS = derivative of the non-linear regression *S* = *f*(*%∆mtDNA*) (Appendix 4, Table 5-2)
n = sample size

The confidence interval for the linear regressions can be calculated in a similar manner as in the case of the linear regressions between *S* and *%∆mtDNA* at the sub-organismal level (see the previous sub-section):

$$95\%\ confidence\ interval = t_{n-2} * \sigma_R \sqrt{\frac{1}{n} + \frac{(\%\Delta mtDNA^* - \%\Delta mtDNA_{ave})^2}{\sigma_{\%\Delta mtDNA}{}^2 (n-1)}}$$

Where:
n = sample size
t_{n-2} = critical value from student's t-table for *n-2*
σ_R = standard deviation of the residuals for selection coefficient *S* (Appendix 4, Table 5-2)
$\%\Delta mtDNA^*$ = each value of ∆mtDNA frequency at which the confidence interval is being calculated
$\%\Delta mtDNA_{ave}$ = average ∆mtDNA frequency across input values (*S*=0.1892 at 60% and *S*=0 at 0% ∆mtDNA)
$\sigma_{\%\Delta mtDNA}$ = standard deviation of ∆mtDNA frequency

Overall (combined) regression (Chapter 5, Figure 5-3C):

According to the general framework of the Price Equation, the overall relationship between ∆mtDNA frequency and the strength of selection—when both the sub-organismal and organismal levels are taken into account—results from summing the regressions as well as their confidence intervals. The overall relationship is therefore defined as the following (assuming $S_{organismal}$=1 at 100% ∆mtDNA):

$$S_{overall} = S_{sub-organismal} + S_{organismal} = (0.01154 * \%\Delta mtDNA - 0.923) + (10^{0.0181 * \%\Delta mtDNA - 1.81})$$

Assuming $S_{organismal}$=1 at 90% ∆mtDNA:

$$S_{overall} = S_{sub-organismal} + S_{organismal} = (0.01154 * \%\Delta mtDNA - 0.923) + (10^{0.0241 * \%\Delta mtDNA - 2.17})$$

Assuming $S_{organismal}$ rises linearly from 0% ∆mtDNA to 60% ∆mtDNA and beyond:

$$S_{overall} = S_{sub-organismal} + S_{organismal} = (0.01154 * \%\Delta mtDNA - 0.923) + (0.003153 * \%\Delta mtDNA)$$

Finally, for each regression, the combined confidence interval can be calculated as follows:

$$95\%\ confidence\ interval_{overall} = \frac{1}{2} * \sqrt{(2 * 95\%CI_{sub-org})^2 + (2 * 95\%CI_{org})^2}$$

Where:
$95\%CI_{sub\text{-}org}$ = confidence interval for the regression of *S* and *%∆mtDNA* at the sub-organismal level
$95\%CI_{org}$ = confidence interval for the regression of *S* and *%∆mtDNA* at the organismal level

Appendix 6

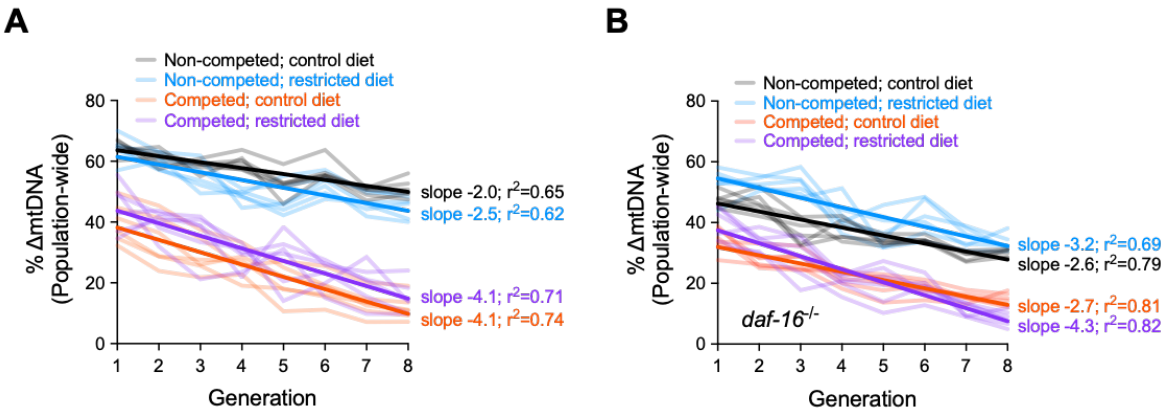

Supplemental Figure 6-1. Raw measurements of decline in ΔmtDNA frequency upon competition with homoplasmic counterparts (lacking ΔmtDNA) under variable diets and host genotypes

(A) Same data presented in Figure 6-8B showing raw Δ**mtDNA** frequency measurements, with non-competing control lines included (omitted from Figure 6-8B for visual simplicity). Solid lines represent best-fit regressions.
(B) Same data presented in Figure 6-8E showing raw Δ**mtDNA** frequency measurements, similar to panel (A) but in the background of host genomes homozygous for the null *daf-16*(mu86) mutation. Non-competing control lines are once again included (omitted from Figure 6-8E for visual simplicity). Solid lines represent best-fit regressions.

Appendix 7

Table 6-2: Summary statistics for change in ΔmtDNA frequency at sub-organismal level by diet and host genotype

Genotype	Wildtype		*daf-16*$^{-/-}$	
Diet	Control (*ad libitum*)	Restricted	Control (*ad libitum*)	Restricted
Units				
X-axis	% ΔmtDNA (parents)	% ΔmtDNA (parents)	% ΔmtDNA (parents)	% ΔmtDNA (parents)
Y-axis	Shift in % ΔmtDNA (progeny - parent)	Shift in % ΔmtDNA (progeny - parent)	Shift in % ΔmtDNA (progeny - parent)	Shift in % ΔmtDNA (progeny - parent)
Best-fit values				
Slope	-0.157	-0.294	-0.189	0.0978
Intercept	10.66	13.34	4.301	-9.319
Standard Error				
Slope	0.064	0.125	0.086	0.107
Intercept	3.971	7.78	4.494	5.5
Goodness of Fit				
R square	0.214	0.234	0.181	0.0402
Sy.x	3.889	7.063	5.772	8.734
Linear regression statistics				
N	24	20	24	22
F	5.992	5.5	4.845	0.8378
P (non-zero slope)	0.0228	0.0307	0.0385	0.3709

Appendix 8

Table 6-3: Summary statistics for change in ΔmtDNA frequency at organismal level by diet and host genotype

Genotype	Wildtype		*daf-16*$^{-/-}$	
Diet	Control (*ad libitum*)	Restricted	Control (*ad libitum*)	Restricted
Units				
X-axis	Time (generations)	Time (generations)	Time (generations)	Time (generations)
Y-axis	Relative % ΔmtDNA (population / individual)	Relative % ΔmtDNA (population / individual)	Relative % ΔmtDNA (population / individual)	Relative % ΔmtDNA (population / individual)
Best-fit values				
Slope	-0.0568	-0.0515	-0.0306	-0.0623
Intercept	0.668	0.777	0.733	0.776
Standard Error				
Slope	0.0059	0.0076	0.0052	0.0067
Intercept	0.0298	0.0386	0.0265	0.0336
Goodness of Fit				
R square	0.668	0.497	0.424	0.656
Sy.x	0.094	0.121	0.083	0.106
Linear regression statistics				
N	48	48	48	48
F	92.65	45.44	33.88	87.55
P (non-zero slope)	<0.0001	<0.0001	<0.0001	<0.0001
P (effect of diet)	0.59		0.0003	

Appendix 9

Table 6-4: Summary statistics for selection coefficient at sub-organismal level, by diet and host genotype

Genotype	Wildtype		*daf-16*$^{-/-}$	
Diet	Control (*ad libitum*)	Restricted	Control (*ad libitum*)	Restricted
Units				
X-axis	% ΔmtDNA (parents)	% ΔmtDNA (parents)	% ΔmtDNA (parents)	% ΔmtDNA (parents)
Y-axis	Selection coefficient	Selection coefficient	Selection coefficient	Selection coefficient
Best-fit values				
Slope	0.0086	0.0097	0.0071	-0.0081
Intercept	-0.59	-0.45	-0.18	0.55
95% C.I.				
Slope	0.0062	0.0094	0.0069	0.0081
Horizontal intercept (%ΔmtDNA)	59 to 95	0 to 59	0 to 42	51 to 100
Goodness of Fit				
R square	0.27	0.21	0.17	0.18
Sy.x	0.18	0.25	0.22	0.32
Linear regression statistics				
N	24	20	24	20
F	8.16	4.66	4.48	4.36
P (non-zero slope)	<0.01	<0.05	<0.05	<0.05

Appendix 10

Table 6-5: Summary statistics for selection coefficient at organismal level, by diet and host genotype

Genotype	Wildtype		*daf-16*$^{-/-}$	
Diet	Control (*ad libitum*)	Restricted diet	Control (*ad libitum*)	Restricted diet
Units				
X-axis	Mean heteroplasmic %	Mean heteroplasmic %	Mean heteroplasmic %	Mean heteroplasmic %
Y-axis	Selection coefficient	Selection coefficient	Selection coefficient	Selection coefficient
Best-fit values				
Slope	0.02015	0.0149	0.0145	0.0112
Intercept	-2.015	-1.49	-1.45	-1.115
95% C.I.				
Slope	0.0023	0.0060	0.0059	0.0014
Intercept	0.2175	0.594	0.584	0.133
Goodness of Fit				
R square	0.993	0.978	0.995	0.997
Sy.x	0.028	0.053	0.026	0.019

Appendix 11

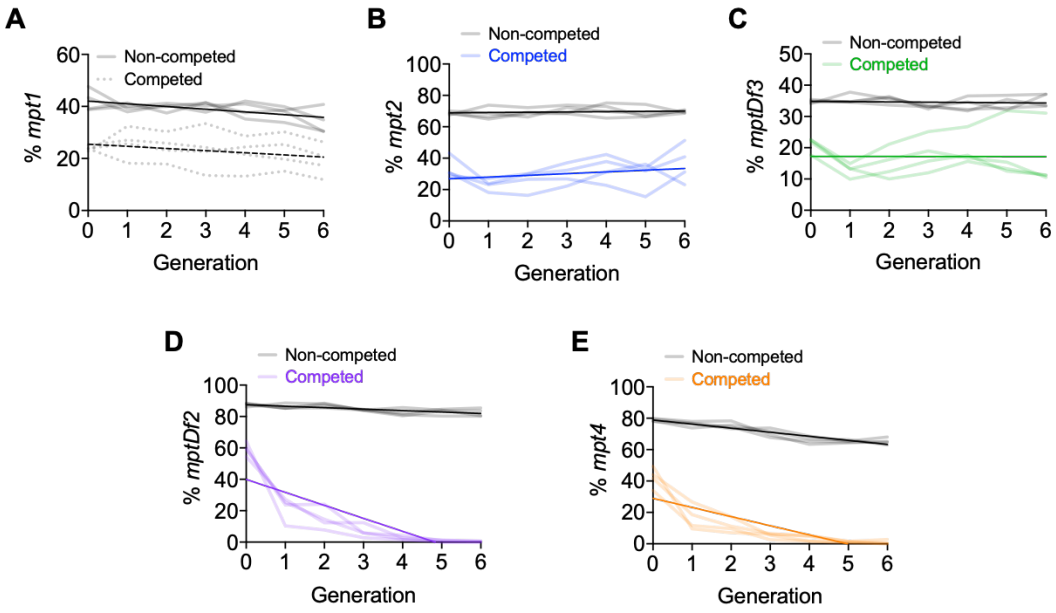

Supplemental Figure 7-1. Raw measurements of decline in mutant frequency upon competition with homoplasmic counterparts (lacking ∆mtDNA), across the collection of heteroplasmies featured in Figure 7-1

(A) Same experiment as shown in Figure 7-2D, but with vertical axis expressed in raw (non-normalized) *mpt1* frequency.
(B) Same experiment as shown in Figure 7-2F, but with vertical axis expressed in raw *mpt2* frequency.
(C) Same experiment as shown in Figure 7-2H, but with vertical axis expressed in raw *mptDf3* frequency.
(D) Same experiment as shown in Figure 7-2J, but with vertical axis expressed in raw *mptDf2* frequency.
(E) Same experiment as shown in Figure 7-2L, but with vertical axis expressed in raw *mpt4* frequency.
Straight lines represent best-fit regression across all replicates.